Chemical kinetics modelling of combustion processes in SI engines

by

Ahmed Faraz Khan
B.Sc., M.S.

Submitted in accordance with the requirements for the degree of
Doctor of Philosophy

The University of Leeds

School of Mechanical Engineering

May 2014

The candidate confirms that the work submitted is his own, except where work which has formed part of jointly authored publications has been included. The contribution of the candidate and the other authors to this work has been explicitly indicated below. The candidate confirms that appropriate credit has been given within the thesis where reference has been made to the work of others.

The Figure 2.5 in Chapter 2 has been published in a jointly authored publication:

A.F.Khan and A.A.Burluka. *An Investigation of Various Chemical Kinetic Models for the Prediction of Autoignition in HCCI Engine.* ASME 2012 Internal Combustion Engine Division Fall Technical Conference, Vancouver, BC, Canada, September 23 – 26, 2012. Paper No. ICEF2012-92057, pp. 737-745; doi:10.1115/ICEF2012-92057

The content taken from the above publication for use in this thesis was solely generated by the author. The co-author is credited to technical discussion on the results produced in the publication.

Acknowledgements

The completion of this work owes a lot to the contribution and support of so many people in my professional and personal life. This is where I show my gratitude and acknowledge their support which is certainly immeasurable in words.

First and foremost, my supervisor Dr Alexey Burluka, my utmost thanks for the guidance all through the years – you have always been there. In addition to all-things-combustion, conversations on world politics were indeed enlightening. I also enjoyed the crash course on how to appreciate opera while driving down to Northampton – I have seen a couple of them after that with tremendous enjoyment. But above all, many thanks for giving me the opportunity to do this PhD.

Unfortunately, I did not have much interaction with Prof Chris Sheppard due to his retirement but his spirit was certainly present in the form of a plethora of SAE papers and titbits from Alex.

My utmost gratitude to a bunch of brilliant engineers and fantastic human beings at Mahle Powertrain. Without any exaggeration, working with you guys was one of the most enjoyable aspects of my PhD. I have to name some names here: Jens Neumeister, Dave Oudenijeweme and Paul Freeland, many many thanks for helping me on so many things. I certainly learned a lot from you guys. Thanks for keeping me on track too, those weekly teleconferences were very useful, not sure about the Gantt charts though. A special thanks must also go to John Mitcalf for taking the time out for all the CFD work, thanks to David Gurney and Andre Bisordi for tips on GT-Power.

I must acknowledge Prof Jeffrey Cash at Imperial College London for the numerical library MEBDFI, Prof Valeri Golovitchev at Chalmers Institute of Technology for kindly providing the gasoline mechanism

and Dr Youngchul Ra at University of Wisconsin-Madison for the Reitz/MultiChem mechanism. Due thanks to Dr Phil Roberts for the permission to use LUPOE2-D experimental data.

Colleagues in combustion group at Leeds University, who are (in no particular order) Tawfiq, Navanshu, Ahmed, Dominic, Zhengyang, Nini, Daniel, it was a great pleasure working with you all – my best wishes for your future. I must pay a special tribute to Dr Graham Conway who always took the time out to attend to my questions, many thanks for all those discussions on LUSIE and other things in general. Your presence made things a lot easier for me in the early days.

Thanks to the IT staff at the School, in particular, John Hodrien, whose help always came with words of wisdom on all-things-LINUX.

My housemates over the years who became my BFFs, Sabina, Lubka, Eva, Danny, Julian, Sandra and Beta, I could not have asked for better friends – thank you! BTW I wouldn't have to do a PhD if I had a penny for every time you asked me, *"when do you finish?"*.

Lastly, because it's the most important one, my family. I have no words to thank you with for the limitless love and support you have given me over the years. Ami, Abu, Khurram, Ambreen, Babar, Aleezah, thank you all!

Abstract

The need for improving the efficiency and reducing emissions is a constant challenge in combustion engine design. For spark ignition engines, these challenges have been targeted in the past decade or so, through 'engine downsizing' which refers to a reduction in engine displacement accompanied by turbocharging. Besides the benefits of this, it is expected to aggravate the already serious issue of engine knock owing to increased cylinder pressure. Engine knock which is a consequence of an abnormal mode of combustion in SI engines, is a performance limiting phenomenon and potentially damaging to the engine parts. It is therefore of great interest to develop capability to predict autoignition which leads to engine knock. Traditionally, rather rudimentary skeletal chemical kinetics models have been used for autoignition modelling, however, they either produce incorrect predictions or are only limited to certain fuels. In this work, realistic chemical kinetics of gasoline surrogate oxidation has been employed to address these issues.

A holistic modelling approach has been employed to predict combustion, cyclic variability, end gas autoignition and knock propensity of a turbocharged SI engine. This was achieved by first developing a Fortran code for chemical kinetics calculations which was then coupled with a quasi-dimensional thermodynamic combustion modelling code called LUSIE and the commercial package, GT-Power. The resulting code allowed fast and appreciably accurate predictions of the effects of operating condition on autoignition. Modelling was validated through comparisons with engine experimental data at all stages.

Constant volume chemical kinetics modelling of the autoignition of various gasoline surrogate components, i.e. iso-octane, n-heptane, toluene and ethanol, by using three reduced mechanisms revealed how the conversion rate of relatively less reactive blend components,

toluene and ethanol, is accelerated as they scavenge active radical formed during the oxidation of n-heptane and iso-octane. Autoignition modelling in engines offered an insight into the fuel-engine interactions and that how the composition of a gasoline surrogate should be selected. The simulations also demonstrated the reduced relevance of research and motor octane numbers to the determination of gasoline surrogates and that it is crucial for a gasoline surrogate to reflect the composition of the target gasoline and that optimising its physicochemical properties and octane numbers to match those of the gasoline does not guarantee that the surrogate will mimic the autoignition behaviour of gasoline.

During combustion modelling, possible deficiencies in in-cylinder turbulence predictions and possible inaccuracies in turbulent entrainment velocity model required an optimisation of the turbulent length scale in the eddy burn-up model to achieve the correct combustion rate. After the prediction of a correct mean cycle at a certain engine speed, effects of variation in intake air temperature and spark timing were studied without the need for any model adjustment. Autoignition predictions at various conditions of a downsized, turbocharged engine agreed remarkably well with experimental values. When coupled with a simple cyclic variability model, the autoignition predictions for the full spectrum of cylinder pressures allowed determination of a percentage of the severely autoigniting cycles at any given spark timing or intake temperature. Based on that, a knock-limited spark advance was predicted within an accuracy of 2° of crank angle.

Contents

List of Figures

List of Tables

Nomenclature

Roman and Greek Symbols

Symbol	Units	Description
A	m^2,	Area
C_z	–	Zimont burning velocity model constant
a	m/sec	Speed of sound in a gas
α	1/sec	Stretch rate
B	m	Engine bore
C_λ	-	Taylor microscale multiplier
δ_l	m	Laminar flame thickness
D	m^2/sec	Mass diffusivity
Da	–	Damkhöler number
Ka	–	Karlovitz number
k	m^2/s^2	Turbulent kinetic energy
κ	m^2/s	Thermal diffusivity
Le	–	Lewis number
L	m	Turbulent integral length scale
λ	m	Turbulent Taylor microscale
η	m	Turbulent Kolmogorov length scale
p	Pa	Pressure
ϕ	–	Equivalence Ratio
m	kg	Mass
$\dot{m}$	kg/sec	Mass flow rate
ρ	kg / m^3	Density
r	m	Radius
Re	-	Reynolds Number
T	K	Temperature
t	sec	Time
τ_{ign}	ms	Ignition delay time

u	m/sec	Burning Velocity
u'	m/sec	Rms turbulent velocity

Abbreviations

aTDC	After top dead centre
bTDC	Before top dead centre
^{o}CA	Degrees of crank angle rotation
CR	Compression ratio
DNS	Direct numerical simulation
ECU	Electronic control unit
EGR	Exhaust gas recirculation
EPC/EVC	Exhaust port closure / exhaust valve closure
HCCI	Homogeneous charge compression ignition
IMEP	Indicated mean effective pressure
IPC/IVC	Intake port closure / intake valve closure
K	Kalghatgi octane index correction factor
LDV	Laser doppler velocimetry
LES	Large eddy simulation
LUPOE1/2-D	Leeds university ported optical engine (Mk I/II) disc configuration
LUSIE	Leeds university spark ignition engine (simulation software)
LUSIEDA	Leeds university spark ignition engine data analysis
MATLAB	Matrix Laboratory
MBT	Maximum Brake Torque
MON	Motor octane number
NTC	Negative temperature coefficient
OI	Octane index
ON	Octane Number
PIV	Particle image velocimetry
PRF	Primary reference fuel
rms	Root mean square
rpm	Revolutions per minute
RON	Research octane number
S	Fuel sensitivity

SI	Spark ignition
TDC	Top dead centre
TDCF	Firing, top dead centre
TKE	Turbulent kinetic energy
VVT	Variable valve timing
VVL	Variable vale lift
WOT	Wide open throttle

Subscripts

b	Burned
i	Intake
l	Laminar
t	Turbulent
r	Reaction (burnt)
u	Unburned

Chapter 1

Introduction to topic and terminologies

1.1 Introduction and motivation

Combustion engines had a tremendous impact on society at the time of their first use and to this day are one of the most important energy conversion devices and see wide usage in transport sector and electric power generation. Internal combustion engines, or ICEs, have come a long way since their inception and modern day spark ignition (SI) engines are able to reach thermal efficiency around 35% and compression ignition (CI) engines reaching slightly higher figures. The most important factors in the development of new engine technologies are the emission legislation, fuel efficiency and viability of renewable fuels for engine use.

Taylor [2008] in his ICE technology review predicted an improvement in fuel efficiency of about 6 to 15 $\pm$2% for gasoline and compressed natural gas engines using port fuel injection and direct injection; and an improvement of 7% for CI engines reaching efficiency levels of 52%, owing to pressure charging, reduced frictional losses and improved combustion control. SI engine development in the past decade or so has already incorporated ideas such as direct injection, heavy turbocharging and 'downsizing' which is brought about by a reduction in engine displacement. This is achieved by either cylinder deactivation which is popular in USA or reduction in number of cylinders and/or reduction in cylinder capacity, an approach taken by both American and European car makers. Engine

downsizing thus exploits the advantages of reduced frictional losses, no pumping losses due to turbocharging which improves part-load performance while maintaining peak performance. Some examples of downsizing report considerable improvements of drive cycle fuel consumption in comparison to the baseline engine while maintaining similar level of performance, e.g. 25-30% fuel consumption improvement for a 50% downsized engine [Lumsden et al., 2009], 20% for a 60% downsized engine [Attard et al., 2010] and 17% for a 40% downsized engine [Han et al., 2007]. Fuel efficiency advantages also reflect in lower CO_2 emissions per mile, however, the usual challenges of controlling other regulated emissions remain.

One of the key challenges faced in engine downsizing is of the increased likelihood of engine knock caused by the higher in-cylinder pressures associated with turbocharging. Knock is caused by the autoignition of the unburned air-fuel mixture or the so-called 'end gas' resulting in oscillating pressure waves in the combustion chamber. These high energy pressure waves when resonate with the metallic components in the engine, set them to vibrate resulting in a signature noise known as *knock*. Engine knock, where severely undermines engine performance and emissions may also cause serious damage to the engine parts and therefore is unwanted [Heywood, 1988]. The effects of high pressures on the nature of 'pre-autoignition' reactions of gasoline in the end gas leading up to its autoignition are not properly understood ([Kalghatgi, 2014], p. 149). This is because of the lack of information on reaction rates and ignition delay times at high pressures for gasoline-like fuels. As a result the chemical kinetics mechanisms available, have an inherent uncertainty when applied to such engine conditions. Some of the earlier explanations of the chemical origins of engine autoignition were presented in the classical works of Halstead et al. [1977], Leppard [1990] and Westbrook et al. [1991], among others.

Application of chemical kinetics to investigate autoignition in engines is not new, however, most of the recent chemistry based investigations into the gasoline autoignition have been in HCCI[1] engine framework which have undoubtedly helped better understand autoignition in the end gas of a SI engine. Coupling of detailed chemical kinetics with 3-D computational fluid dynamics (CFD) has also been demonstrated for autoignition prediction in HCCI engines, e.g. [Liu and Karim, 2008] and [Bedoya et al., 2012]. Same has been demonstrated for SI

[1]HCCI stands for homogeneous charge compression ignition. The combustion in such engines is spatially distributed without a propagating flame, and its start is controlled by the fuel reactivity rather than an external spark as in a SI engine.

engine autoignition but with rather simpler chemical mechanisms, e.g. [Nishiwaki et al., 2000] and [Zhen et al., 2013] for a methanol fuelled SI engine which used a 21 species and 84 reactions mechanism. One can easily imagine the computational costs associated with CFD modelling of combustion using a gasoline surrogate mechanism which comprise a large number of species and reactions. Therefore, modelling of SI engine autoignition has mostly been carried out using simpler mechanisms, e.g. [Cowart et al., 1991] and [Bozza et al., 2009], in a multi-zone modelling approach as described later in Section 4.5.3. Although, application of detailed chemical kinetics mechanisms has been demonstrated such as in [Mehl et al., 2005], where a mechanisms comprising 5000 reactions and 250 chemical species was used with a 0-D quasi-dimensional combustion model for CFR engine; the attempts to couple detailed chemical kinetics coupled with a predictive multi-zone thermodynamic combustion model are few and far between. This has been achieved in this work and has been applied to a turbocharged SI engine.

An important prerequisite to autoignition modelling is the knowledge of the thermodynamic state of the unburned charge. It is therefore that a significant amount of this work is focused on the use of quasi-dimensional thermodynamic combustion modelling approach (described in Chapter 4) which has previously been successfully applied to naturally aspirated and turbocharged engines. Thus, the ultimate objective of this work was to develop tools for the modelling of combustion and autoignition of gasoline-like fuels i.e. gasoline surrogates in downsized turbocharged engines. Before some basic concepts used in this work are described, an overall scope and the organisation of thesis is presented.

1.2 Scope of this work

Through the preceding discussion on the topic of knock and autoignition, it is emphasised that the ability to predict autoignition of complex gasoline fuels in modern turbocharged engines of which operate at much higher pressures is of utmost importance. It offers to predict reliably those engine design parameters, operating conditions and fuels which would offer a knock free operation. Chemical kinetics studies allow also to understand better the autoignition chemistry of gasoline surrogate fuels at conditions relevant to engine autoignition. Present work aims primarily at the development of such modelling tools as well as their testing and validation. The scope of this work is summarised below.

- Development of a computer code for chemical kinetics calculations.
- Assessment of various chemical kinetics mechanisms for PRFs (iso-octane and n-heptane) and other gasoline surrogates through ignition delay time calculations and comparisons with shock tube and RCM measurements.
- Testing of the existing well developed legacy code, LUSIE (Leeds University Spark Ignition Engine [Code]) at conditions of a turbocharged engine.
- Application of selected chemical kinetics mechanisms to autoignition modelling in SI engines.
- Study of the autoignition behaviour of gasoline surrogate fuels.

1.3 Thesis organisation

The thesis is organised into seven chapters, a brief introduction to their content is given below.

- **Chapter 2** This chapter covers fundamentals of chemical reaction kinetics, knowledge of which was mandatory for the development of the chemical kinetics solver. The structure of the Fortran code is discussed highlighting how computational efficiency was achieved by structuring the code in modules and subroutines. The third-party solver for stiff type ordinary differential equations, MEBDFI has also been introduced. Various types of chemical kinetics mechanisms are discussed followed by the three mechanisms which have been used in this work and reasons for their use.
- **Chapter 3** This chapter starts with a discussion of the established oxidation pathways of major gasoline surrogate fuels i.e. iso-octane, n-heptane, ethanol and toluene followed by chemical kinetics modelling of oxidation reactions using the three selected mechanisms. The purpose of this work is to assess the fidelity of reduced chemical kinetics mechanisms to the established understanding. Simulations are also presented on the basis of which the interactions of different surrogate components are studied.
- **Chapter 4** This chapter covers the fundamentals of SI combustion and turbulence in engines. A description of the combustion modelling code (LUSIE) is presented and also its coupling with the commercial engine modelling

software GT-Power which done by the author. The two engines studied in this work are also described in this chapter.

- **Chapter 5** This chapter exclusively deals with autoignition modelling in a bespoke Leeds University research engine using the chemical kinetics solver described in Chapter 2. The chapter deals with the study of fuel engine interaction i.e. how the autoignition characteristics of a fuel, its RON and MON relate to the thermodynamic state of the end gas and also how relevant these quantities are in deciding a surrogate for gasoline.

- **Chapter 6** This chapter deals with combined combustion and autoignition modelling in a downsized turbocharged engine and is the culmination of the modelling tools developed and tested during the course of this work. Simulations in this chapter deal with the study of effect of pressure charging and engine speed on the flame structure; relationship of engine cyclic variability and knock and its modelling. Predictions of the knock limited spark advance have also been made.

- **Chapter 7** This chapter concludes this work by summarising various inferences which can be made as well as recommendations for the future work which will attempt to broaden the scope of this work.

1.4 Autoignition and knock

End gas autoignition and knock phenomena, although related, are different such that the autoignition is determined by the thermodynamic state of the end gas i.e. the temperature and pressure, and its composition. Whereas, knock depends on the detonability of the end gas i.e. likelihood of the superposition of a high pressure wave and a reaction front which turns into a detonation wave causing a very high rate of heat release characteristic of knock [Dahnz and Spicher, 2010]. Modelling of knock phenomenon itself warrants a dedicated study, however, owing to its complexity, the current work has only been limited to the prediction of autoignition and empirical knock indices have rather been employed to gauge the severity of predicted autoignition.

In this work, the term autoignition is used to imply the ignition which is known to take place due to a low temperature chemical activity causing self-heating, added to it by compression due to an oncoming flame which eventually

causes a thermal runaway. This precludes surface ignition which is caused by an overheated surface or due to the presence of a glowing deposit on the chamber surface. Such abnormalities can be eliminated by better engine design, e.g. adequate cooling of valves and spark plug, deposit control additives, such as detergents in fuel which prevent deposit formation by maintaining a thin layer of hydrocarbon on the chamber surfaces; and dispersants in lubricant which react with the deposits to prevent deposition, (see [Kalghatgi, 2014] for details on deposits).

1.4.1 Factors affecting engine knock

Some fuels have a greater innate propensity to autoignite at a given pressure and temperature ($p - T$) than other fuels owing to the molecular size and structure; this will be discussed further in Chapter 3. However, for a given fuel, an engine operating condition which results in a higher end gas pressure and temperature would in most cases cause an earlier knock onset. Such fuel and engine related factor which affect knock are discussed below.

1.4.1.1 Engine design and operating conditions

Engine knock is performance limiting even during the design phase as it restricts the compression ratio to lower values thereby limiting the thermal efficiency of the engine. A higher compression ratio would result in higher in-cylinder pressure and temperature increasing the knock propensity. Reliable autoignition predictions can therefore help in deciding the basic geometry of the engine during the development phase for which the engine performance will not be knock limited.

Knock is more likely to occur and with greater intensity when the spark timing is advanced. An advanced (sooner) timing will initiate combustion earlier when piston is closer to the top dead center (TDC). The resulting pressure is much higher as compared to when the spark is retarded (delayed) for which combustion for most part occurs during the expansion stroke. The spark timing at which knock becomes considerable is known as the knock limited spark advance or KLSA for short. This relationship between knock tendency and spark timing has implications on the maximum brake torque (MBT) which can be achieved at that speed. The spark timing needed for such combustion phasing with respect to the piston movement which produces the maximum brake torque at those condi-

tions is called MBT timing. If MBT timing is sooner than KLSA then the engine is said to be knock limited as it cannot achieve the best possible performance due to knock. Most engines are knock limited at some parts of their operating map; it is generally the low speed and high load conditions.

An increased intake air temperature increases knocking tendency by accelerating the autoignition reactions, however, the air temperature is typically controlled to prevent volumetric efficiency losses and it is therefore not a major factor in knock occurrence. However, exhaust gas recirculation (EGR) which is a strategy to control NOx emissions as well as knock, affects the end gas temperature and its reactivity in a complex way. It is well established that EGR decreases the flame temperature and burning rate [Stone, 1999], which substantially decreases the NOx formation. Moreover, a reduced burning rate also has an equivalent effect of spark retard i.e. the peak pressure decreases, consequentially the knock tendency decreases as well. With EGR, an earlier KLSA can be achieved or in other words the range of knock free spark advance is expanded. In addition to this combustion phasing effect of EGR, it also decreases the peak unburned gas temperature and its reactivity as it *"increases the extent of quenching reactions"* [Hoepke et al., 2012].

For near stoichiometric operation, generally the composition of EGR is simplistically thought to be of the complete combustion products i.e. CO_2, H_2O, N_2 and occasionally minute amounts of O_2. However, combustion is almost invariably incomplete and even in lean HCCI operation, the EGR has been found to be composed of CO, NO, NO_2, O_2 and unburned hydrocarbons (HC) such as aldehydes, ketones and polycyclic aromatic hydrocarbons (PAH), concentrations of which change along the EGR pipe [Piperel et al., 2007]. Major constituents of EGR do not dissociate at the temperatures which the end gas is typically subjected to (less than 900 K) and therefore are inert. Their effect on the autoignition is mainly through their heat capacity. However, contradictory findings have been reported on the effects of NO on engine knock, (see [Roberts and Sheppard, 2013] and references therein), as in it may suppress or promote knock. Some clarity has been reached through the aforementioned works and through [Burluka et al., 2004] which show that the effect of NO on knock is of promoting it when present in low concentrations (about 500 ppm) and of delaying it when increased to higher values (about 1400 ppm) [Stenls et al., 2002]; where this switch in NO effect at specific concentration levels is also temperature dependant. Roberts and Sheppard [2013] assert that the role of NO is influenced by the ignition behaviour

of the fuel i.e. whether it ignites through a single stage or exhibits a negative temperature coefficient (NTC) phase of reduced reactivity. However, they mostly observed experimentally, the knock promoting effect of NO for fuels such as iso-octane, primary and toluene reference fuels and a commercial unleaded gasoline (ULG). In the present work, internal burned gas residuals are accounted for in the initial composition of the air-fuel charge and their effect on the autoignition is predicted by the elementary reactions in the chemical kinetic mechanisms used; no dedicated NO formation mechanism has been used.

1.4.1.2 Fuel effects

Oxidation behaviour of a fuel tremendously affects its knocking tendency. Fuels which are more reactive exhibit shorter ignition delays and are more likely to autoignite in an engine. In the field of engines, the so called octane number of a fuel which signifies its resistance to autoignition is quantified by two standard tests carried out on a single cylinder variable compression ratio engine called Cooperative Fuel Research (CFR) engine. The Research octane number or RON[1] test was devised first in 1930 and the Motor octane number or MON[2] test was proposed later and these are still in use. In these tests the knock intensity of a given fuel is compared to the knock intensity of a number of reference fuels which are blends of n-heptane and iso-octane, arbitrarily given octane numbers of 0 and 100 respectively. The octane number of the fuel is then taken to be equal to the volumetric proportion of iso-octane in that blend which had the same knock intensity at the same compression ratio and test conditions of the CFR engine.

The octane quality of a gasoline is dependant on its constituents i.e. various hydrocarbon compounds which are blended to make it. Gasoline is produced from light fraction of the crude oil known as naphtha with a boiling range of roughly 20 - 160°C. Typically, 70% by weight of a gasoline is made up of 20 or so compounds and the rest is composed of more than a hundred different compounds which are less than 1% by weight each [Kalghatgi, 2014]. Further processing of naphtha and blending with other production streams of the refinery is done to improve various properties of gasoline, in particular the octane quality. The antiknock quality of gasoline has its origins in the molecular size and structure of its constituents, which in turn determines the nature of oxidation reactions

[1]RON test is standardised as ASTM D-2699. The operating conditions are: engine speed 600 rpm, intake temperature 52°C, spark advance 13° bTDC.

[2]MON test is standardised as ASTM D-2700. The operating conditions are: engine speed 900 rpm, intake temperature 149°C, spark advance 19-26° bTDC.

which the fuel undergoes. These will be discussed in Chapter 3 in more detail for representative hydrocarbon compounds.

During oxidation process, the conversion of fuel molecules into intermediate species depends on the bond energies involved. Typically, the oxidation of a long chained hydrocarbon initiates much more easily than a more compact short branched hydrocarbon with the same number of hydrogen and carbon atoms. A straight chained molecule has more secondary carbon-hydrogen bonds which offer a lower bond energy barrier as compared to primary bonds[1] whose number increases as the degree of branching increases. For most of hydrocarbons, a correlation can be seen between their RON and MON and the number of branches. For example, n-heptane has a RON of 0 whereas, 2,2,3-trimethylbutane has a RON of 112.1 albeit a formula of $\mathrm{C_7H_{16}}$, (see Westbrook et al. [1991] for more examples).

Primary reference fuels have the same RON and MON by definition. On the contrary, gasoline and other non-PRF pure compounds do not necessarily have same RON and MON because their autoignition behaviour can be different from a PRF and therefore two different PRFs would match their autoignition characteristics at the two RON and MON tests. Since the operating conditions of the MON test are more vigorous than the RON test, a PRF of lower octane number would match the gasoline, therefore, the MON for non-PRFs tends to be lower than the RON. The difference of RON and MON represents the extent to which the octane quality of a fuel depreciates as the end gas temperature increases; this difference is referred to as the sensitivity, S, of the fuel. The sensitivity of the fuel purely arises from its varying reactivity at different $p - T$ conditions. When the engine operating conditions are such that the end gas $p - T$ conditions are neither of the RON or MON tests, the autoignition characteristics of the fuel may not match those of RON-PRF or MON-PRF. An effective octane index, OI, can therefore be defined which represents the octane quality of a fuel at a given operating condition. This notion has been extensively researched by G.T.Kalghatgi who showed that the effective octane index of a fuel embodies not only its sensitivity but difference of the end gas $p - T$ conditions from those of the RON and MON tests given as,

[1] A primary site is the bonding site on a carbon atom which is bonded to only one other carbon atom. A secondary site is the site at a carbon atom which is bonded to two other carbon atoms and similarly the bonding site available on a carbon atom which is bonded to three other carbon atoms is a tertiary site. The energy barrier for the removal of a H atom from a secondary bonding site is lower than the primary site and so forth for the tertiary site.

$$OI = (1 - \mathrm{K})\mathrm{RON} + \mathrm{KMON} \tag{1.1}$$

since $\mathrm{RON} - \mathrm{MON} = S$, Equation 1.1 can be written as,

$$OI = \mathrm{RON} - \mathrm{K}S \tag{1.2}$$

where, K is shown to be an engine dependant factor, see [Kalghatgi, 2001] for details. It follows from the definition that the K-value is 1 for the MON test and 0 for the RON test. Kalghatgi has shown that the K-value is dependant on the unburned zone temperature and based on numerous experiments has been correlated to the unburned zone temperature at 15 bar for stoichiometric mixtures and is given as,

$$\mathrm{K} = 0.00497 \cdot T_{comp15} - 3.67 \tag{1.3}$$

Modern engines operate with unburned gas temperatures lower than the RON test at same pressures which yields from Equation 1.3 that the K-value is negative for such engines. This has an effect of enhancing the effective octane rating (OI) of gasoline as compared to their rated RON and MON. This has implications on the relevance of RON and MON to modern fuels and engines. This notion is further discussed in Chapters 5 and 6.

1.5 Ignition delay time measurements

A more fundamental property of a fuel which quantifies its ease of ignition is simply the duration of time to ignition taken by a mixture of fuel and an oxidiser, usually air, at a specific pressure, temperature and composition. This time, commonly known as ignition delay or induction time, τ_{ign}, is determined using a rapid compression machine (RCM) or a shock tube (ST); such experiments are a cornerstone of the science of autoignition and chemical reaction kinetics.

A RCM is a piston cylinder arrangement which is mostly pneumatically driven. Some designs may have two horizontally opposing pistons. In all variations of RCMs, a cushioning mechanism is incorporated to suddenly stop the piston achieving a constant volume at the end of the compression. The working principle is to adiabatically compress an air fuel mixture to a small near constant volume and allow it to autoignite. The ignition event is observed as a sudden increase in pressure as illustrated in Figure 1.1, which may be accompanies by

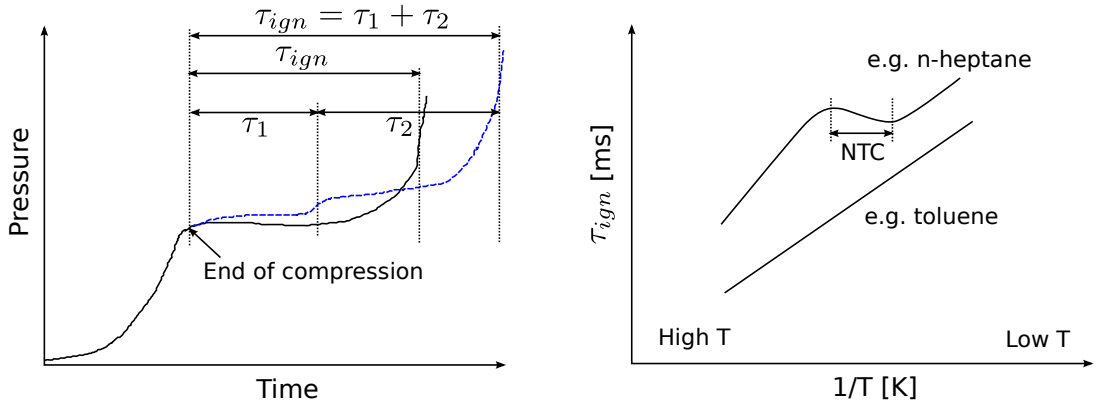

Figure 1.1: Illustrations of a typical pressure trace observed in a RCM (a) showing stages of ignition and the definition of ignition delay time. Shown in (b) is a generic Arrhenius plot.

recording the light emission from the ignition event, if possible. The ignition delay is the duration of time between the end of compression and the pressure rise and is characteristic of the end of compression $p - T$ conditions and the mixture composition. The reacting mixture may also be analysed by means of gas chromatography or mass spectrometry – by extracting a portion of it into a cold chamber. A wealth of information on chemical reaction rates has been collected by various researchers through such studies which have particularly been crucial in the understanding of low temperature oxidation chemistry of hydrocarbon fuels.

Typically, RCMs are used at low pressures, roughly up to 20 bar, and low temperatures, less than 1000 K. Measurements made in different RCMs tend to disagree due to differences in combustion chamber design, heat loss, formation of boundary layers and turbulent vortices resulting in temperature inhomogeneities in the bulk of the gas.

Shock tubes eliminate some of the issues such as heat loss and temperature inhomogeneities, as the charge heating is achieved through a high pressure shock wave. The charge temperature increase is brought about in times of the order of less than 10^{-7} s [Fernandes, 2010]; as opposed to about 30 ms in the case of a typical RCM. The construction of a typical shock tube has two chambers separated by a diaphragm. The charge is kept in the low pressure chamber, whereas, a driver gas is brought to a very high pressure in the second chamber. Upon reaching a certain pressure, the gas ruptures the diaphragm and creates a shock wave which travels through the charge while heating it. Further heating of the charge takes

places as the wave reflects from a flat plate at the end of the test chamber. The ignition delay time is determined from the recorded pressure trace in a similar way as for a RCM or from the onset of CH* emission.

The ignition delay time measurements are typically presented on so called Arrhenius plot as $\log(\tau_{ign})$ vs. the reciprocal of temperature (Figure 1.1). Such plots reveal if a fuel exhibits a range of temperature increase during which the ignition delay time increase too, known as the negative temperature coefficient or NTC, shown by the S-shaped curve. Such fuels typically autoignite through two distinct stages of ignition with different types of chemical pathways dominant before the two stages e.g. n-heptane. On the contrary fuels such as toluene autoignite through a single stage of chemical activity and lack the NTC behaviour, shown by the straight line.

1.6 Autoignition modelling

The autoignition event can be attributed to the accumulation of a critical intermediate specie and it can be marked either by it achieving a certain concentration level or by an associated heat release and temperature rise. This can be modelled by detailed reaction kinetics which comprises at least the important if not all of the elementary steps involved in the global reaction. Long ignition delay times of hydrocarbons, peculiar ignition behaviours such as cool flames and two stage ignitions are explained by these intermediate elementary reactions which proceed at different rates until they give way to rapid exothermic reactions, causing a thermal runaway thereby inducing ignition – hence the terminology of induction time. The rate of a reaction, as will be discussed in detail in Chapter 2, depends on the reactant concentrations and the system temperature embodied in a reaction coefficient, k_r. The rate coefficient and the temperature are related exponentially by the Arrhenius equation,

$$k_r = A\exp^{(-E/RT)} \tag{1.4}$$

where, A is a frequency factor, E is the activation energy, R is the universal gas constant and T is the temperature. Similarly, an empirical relation can be developed for a global reaction rate and ignition delay in terms of a global activation energy with dependencies on the pressure and temperature. Such relations take the form,

$$\tau_{ign} = Ap^{-n}\exp^{(B/T)} \tag{1.5}$$

where, n, A and B are determined by means of regression analyses of measured induction times, such relations are fuel specific and limited to narrow pressure and temperature ranges. However, such models offer computational advantage and accuracy when fitted to a set of conditions. Perhaps one of the most important of such models is of Douaud and Eyzat [1978], given as,

$$\tau_{ign} = 17.68\left(\frac{ON}{100}\right)^{3.402} p^{-1.7}\exp^{(3800/T)} \tag{1.6}$$

The Douaud and Eyzat model, or simply the D&E model, has been widely used, tested and modified to fit different experimental datasets. It offers a dependency on not only on the state of the charge but its octane number, however, the original model was developed for PRFs and since their autoignition behaviour differs from gasoline at conditions other than those of RON and MON tests, the D&E model is expected to make incorrect engine autoignition predictions. Previously at Leeds University, D&E model has been used with some success for autoignition predictions mostly with the optimisation of the model constants [Roberts, 2010]. Severe discrepancies in model results have been reported in [Conway, 2013], where the D&E model mostly wrongly predicted autoignition for boosted engines running on gasoline, when no autoignition was observed in experiments and it generally did not predict autoignition for naturally aspirated engines which ran on PRFs. When autoignition was predicted as well as observed in experiments, the errors was of the order of 10° of crank angle for a boosted engine and about 2° of crank angle for a naturally aspirated engine.

Equation 1.6 calculates induction time at a given $p - T$ condition, however, the unburned gas pressure and temperature continuously changes with time and therefore the individual induction times have to be converted to an aggregate induction time for the changing $p-T$ history. Livengood and Wu [1955] postulated that the extent of chemical activity required for a thermal ignition at constantly changing pressure and temperature is achieved when the integral, I, of the inverse of induction times reach unity. Their integral is given as,

$$I = \int_0^{t_i} \frac{1}{\tau(p,T)} dt \tag{1.7}$$

where, t_i is the elapsed time. Autoignition is said to have occurred when the

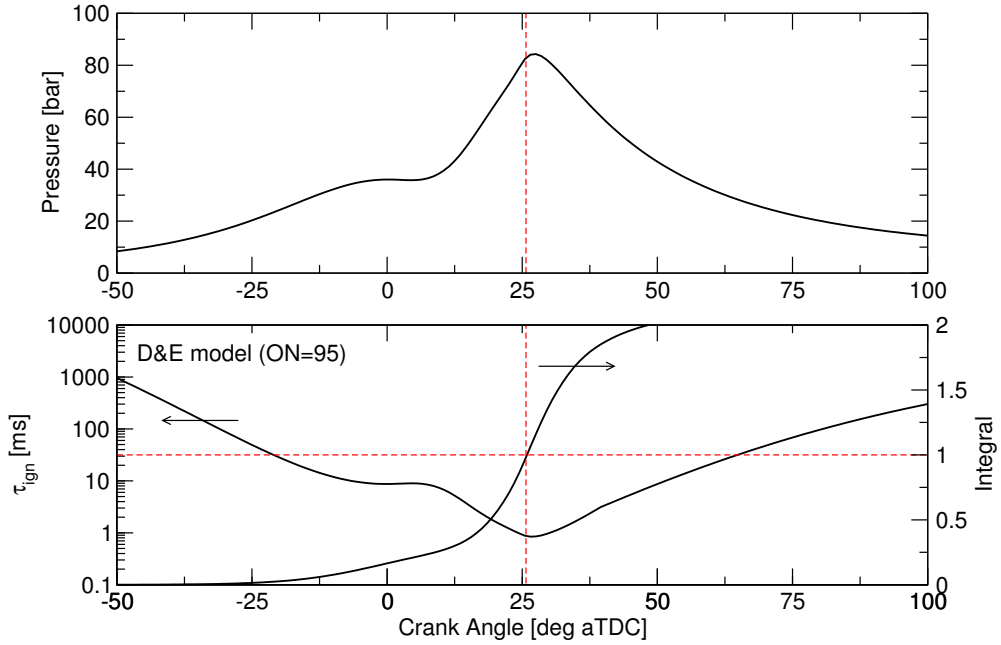

Figure 1.2: Autoignition prediction using the D&E model and Livengood-Wu integral for the in-cylinder pressure of the Di3 engine (see Section 4.10.2) recorded at 2000 rpm.

integral reaches unity as shown in Figure 1.2 which also illustrates that it is the shorter ignition delay times obtained at hight $p-T$ conditions which contribute the most to the integral. This implies that the autoignition onset prediction by Livengood-Wu integral is relatively insensitive to the ignition delays of low $p-T$ conditions. However, this may not be true when detailed reaction kinetics is used to predict autoignition; this will be explored in the later chapters.

As demonstrated, the D&E model and the Livengood-Wu integral offer a fast and powerful means of predicting engine autoignition and are widely used in the automotive industry, however, they suffer from an inflexibility of application to gasoline with much different autoigniton behaviour than PRFs and are not fully predictive in nature. Chemical kinetics modelling offers to eliminate these problems and therefore has been employed in this work.

Chapter 2

Principles and modelling of chemical kinetics

2.1 Introduction

As outlined in the scope of this work in Chapter 1, one of the main tasks was the development of a Fortran code to model the gas phase chemical kinetics of the autoignition of hydrocarbon fuels. Chemical kinetics deals with the calculation of elementary[1] reaction rates and since the reaction rate is dependant on the reactant concentration and the thermodynamic state of the reacting system, an accurate chemical kinetic mechanism can predict the autoignition event in an engine at a wide range of pressure - temperature ($p-T$) conditions and any composition of the fuel blend, equivalence ratio and burned residual fraction without the need for any beforehand optimisation of autoignition model. The chemical kinetic mechanisms in the so called Chemkin format were employed in this work as most of the mechanisms in the literature are available in such a format. This chapter deals with the principles of the gas phase chemical kinetics which have been implemented in the development of the chemical kinetics code.

[1] An elementary reaction is a reaction which involves only one or two molecules and only one activated complex, effectively it is a transformation event related to a single event of molecular or atomic collision.

2.2 Chemical kinetics fundamentals

The rate of an elementary reaction is as H.E.Avery [1974] states, the change in time of a measurable quantity related to the reaction system. The concentration of any of the reactants or the products can be monitored in time to determine the rate of reaction. Consider for example, a bimolecular reaction i.e. a reaction which involves the collision of two reactant molecules, A and B,

$$\mathrm{n_A A} + \mathrm{n_B B} \longleftrightarrow \mathrm{n_P P} + \mathrm{n_Q Q} \tag{2.1}$$

the rate of reaction in terms of the specie concentrations can be given as,

$$\text{rate} = \frac{-1}{n_A}\frac{d[A]}{dt} = \frac{-1}{n_B}\frac{d[B]}{dt} = \frac{1}{n_P}\frac{d[P]}{dt} = \frac{1}{n_Q}\frac{d[Q]}{dt} \tag{2.2}$$

The rate of a reaction is empirically found to be proportional to the concentration of its reactants, this is unsurprising as the collision theory dictates a higher rate of reaction when the likelihood of collisions between particles is greater. This even holds for unimolecular reactions which need to be activated through collision before undergoing a dissociation or isomerisation. We may therefore write,

$$\text{rate} \propto [A]^i[B]^j \tag{2.3}$$

where, i and j are constants which indicate that the reaction is of the order i with respect to A and of the order j with respect to B and the overall order of the reaction is $i + j$. The order of reaction can only be determined experimentally and for some reactions, it may be different at different pressures as for Fall-off reactions discussed later; its value may be fractional but typically in gas phase reactions these values are equal to the stoichiometric coefficients. A constant of proportionality known as reaction coefficient can be introduced in the above relation which embodies the effects of temperature and collision frequency on the reaction rate. The reaction rate equation can therefore be written as,

$$\frac{-1}{n_A}\frac{d[A]}{dt} = k_f[A]^{n_A}[B]^{n_B} \tag{2.4}$$

Based on the van't Hoff's isochore equation which relates the equilibrium constant with the temperature, Arrhenius showed that the rate of a reaction is related to the temperature as,

$$k_f = A\exp\left(\frac{-E_a}{RT}\right) \tag{2.5}$$

where, the pre-exponential factor A is the collision frequency factor which is the product of the frequency factor Z and the steric factor ω, E_a is the activation energy, R is the universal gas constant and T is the temperature. The term $\exp\left(\frac{-E_a}{RT}\right)$ represents the fraction of molecules which have sufficient kinetic energy to undergo chemical reactions. At very high temperature the exponential term equals unity and the reaction coefficient is equal to the collision frequency factor meaning that all the molecules are able to react, a near impossibility. Chemical reaction kinetics is typically studied at temperature much lower than that. More recently, the Arrhenius equation is written with an explicit dependence of the collision frequency on temperature by introducing a parameter b. The equation thus takes the form,

$$k_f = AT^b\exp\left(\frac{-E_a}{RT}\right) \tag{2.6}$$

The reaction coefficient for an elementary reaction increases with temperature as shown in Figure 2.1 which also shows the sensitivity of the reaction coefficient to changes in the Arrhenius parameters. The effect of pressure is also to increase the rate of reaction as it essentially increases the molar concentration of the reactants thereby increasing the likelihood of collisions in the system.

Arrhenius parameters are extensively researched for numerous elementary reactions of hydrocarbons and constitute the various chemical kinetic mechanisms. Mechanisms may differ from each other in terms of the chemical pathways and or just the Arrhenius parameters. For example, Arrhenius parameters for an elementary reaction, $\mathrm{H_2O_2 + OH \longrightarrow H_2O + HO_2}$, have been shown in Figure 2.1, see bottom graph, for three chemical kinetic mechanisms for gasoline surrogates, described in later sections. The reaction coefficient is considerably different considering that the reactions involving hydrogen peroxide and hydroxyl have been found to be crucial in hydrocarbon oxidation and have been extensively studied and yet considerable difference can been seen among different mechanisms. This may arise due to differences in the measurements of reaction rates or as in most cases because of an *ad hoc* optimisation of the mechanism to agree with a given experimental dataset of ignition delay times or laminar burning velocities.

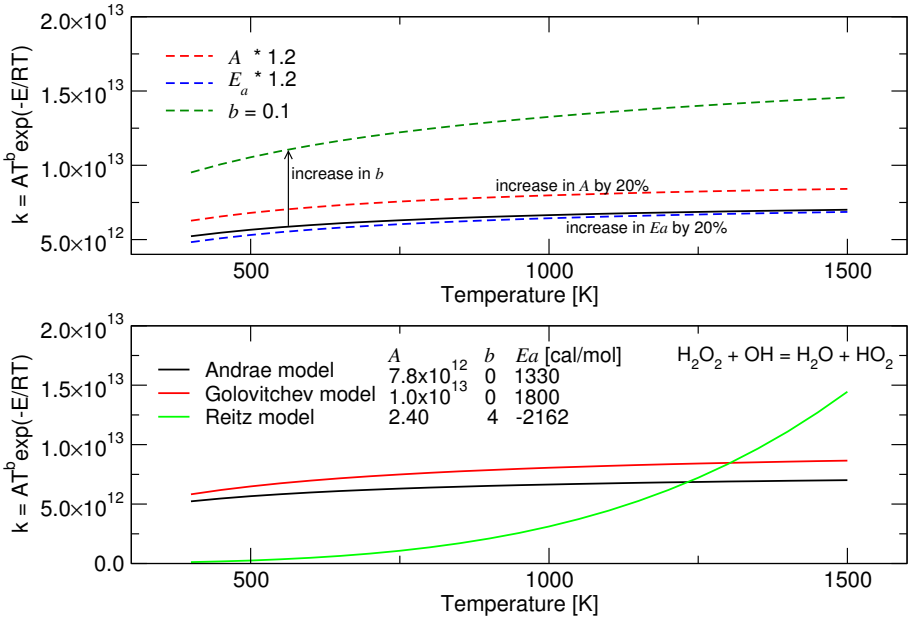

Figure 2.1: Temperature dependence of the Arrhenius parameters, A, b and E_a in the Andrae model for the reaction shown (*top*); reaction coefficient for an elementary reactions in three different chemical kinetic mechanisms (*bottom*).

2.2.1 Rate of formation or depletion of species

The rate equations presented earlier determine only the rate of change in the concentration of a given species, say k, in a given elementary reaction i out of I number of reactions. However, in order to determine the global rate of change of a specie concentration, the reaction rates of all the reactions which involve that particular specie need to be considered. Elementary reactions also proceed in the backward direction but in some cases the reactions may be irreversible. For an elementary reaction such as 2.1, the net rate can be written as,

$$q_i = k_{f_i}[A]^{n_A}[B]^{n_B} - k_{r_i}[P]^{n_P}[Q]^{n_Q} \tag{2.7}$$

where, k_{r_i} is the reverse reaction coefficient and it may be calculated using Arrhenius parameters for the reverse reaction or through the relation with equilibrium constant,

$$k_{r_i} = \frac{k_{f_i}}{K_{c_i}} \tag{2.8}$$

and the equilibrium constant can be determined as,

$$K_{c_i} = K_{p_i} \exp\left(\frac{P_{atm}}{RT}\right)^{\sum_{k=1}^{K} n_{ki}} \tag{2.9}$$

where, n_{ki} is essentially the change in number of moles as the reaction completes and K_{p_i}, the equilibrium constant in terms of pressure, is obtained by the relation,

$$K_{p_i} = \exp\left(\frac{\Delta S_i^\circ}{R} - \frac{\Delta H_i^\circ}{RT}\right) \tag{2.10}$$

The calculation of change in entropy and enthalpy for a given reaction will be presented in Section 2.2.3. The net rate given by Equation 2.7 of all the reactions which involve any given species k, cumulatively determines the rate of change of concentration of specie k as following,

$$\frac{d[k]}{dt} = \sum_{i=1}^{I} n_{ki} q_i \tag{2.11}$$

For systems in which the wall-termination reactions are also considered, a loss term quantifying the net rate of termination reactions is also subtracted from the net rate in Equation 2.11, however, wall-termination has not been considered in this work. Equation 2.11 is an ordinary differential equation (ODE) and for any chemical mechanism, there are an equal number of such equations as there are species. The whole system of equations is integrated simultaneously to determine the state of the system at each time step. This has been discussed in further detail in later sections. In addition to the ODEs for rate of concentration change, an energy balance equation for the system temperature is also required. Since the ignition delay time calculations in this work have been made for a constant volume adiabatic system, no heat loss term is employed and the equation takes the form,

$$C_v \frac{dT}{dt} = \sum_{i=1}^{I} \Delta H_i^\circ q_i \tag{2.12}$$

2.2.1.1 Three-body collision reactions

Lindemann et al. [1922] theorised that for even the unimolecular dissociation reactions, the molecules collide with themselves or another inert molecule to acquire the necessary energy to reach an activated state followed by the dissociation. In the bimolecular combination reactions, the energy liberated during the bond formation and the collision energy is sufficient to dissociate the new

molecule back unless a *third* molecule (M) collides with the newly formed activated complex to absorb the excess energy which stabilises the reaction product [Lewis and von Elbe, 1987], e.g.

$$\mathrm{A} + \mathrm{M} \longrightarrow \mathrm{B} + \mathrm{C} + \mathrm{M} \tag{2.13}$$

in which the third body, M, is not consumed or formed, however, its concentration affects the reaction rate which is given as,

$$q_i = \left(\sum_{k=1}^{K} \epsilon_{ki}[Y_k] \right) (k_{f_i}[A]^{n_A} - k_{r_i}[B]^{n_b}[C]^{n_c}) \tag{2.14}$$

where, the ϵ is a weighting or an enhancement factor, it is equal to one if all the molecules present in the system participate equally in the reaction and the total molar concentration of all the species is used to calculate the reaction rate. However, some third bodies may participate more efficiently than others, in such cases the enhancements factors for each third body are used to determine a weighted total concentration to be used in Equation 2.14.

2.2.2 Pressure dependant or fall-off reactions

Reactions involving a third body may have pressure dependant reaction coefficient due to different orders of reaction at different pressures. Lindemann showed that the unimolecular dissociation reactions take place in steps, first, a bimolecular collision forming an active or energised molecule which is followed by a time delay in which the energised molecule may deactivate if another collision occurs or dissociate forming the products [H.E.Avery, 1974]. Consider the sequence of reactions,

$$\mathrm{A} + \mathrm{M} \longrightarrow \mathrm{A}^* + \mathrm{M} \tag{2.15}$$

$$\mathrm{A}^* + \mathrm{M} \longrightarrow \mathrm{A} + \mathrm{M} \tag{2.16}$$

$$\mathrm{A}^* \longrightarrow \mathrm{products} \tag{2.17}$$

The pressure dependence of the rate of formation of products comes from the increase or decrease in number of collisions between A^* and M as the pressure changes. These collision cause the energised molecules to deactivate and when

the rate of deactivation is high enough i.e. at high pressures, an equilibrium is established between the activation and deactivation reactions. Owing to this equilibrium, the rate of product formation which is proportional to the concentration of energised molecules is now only dependant on the concentration of the inactive molecules. Therefore, the reaction is first order at high pressures, i.e. $\text{rate} = k_\infty[A]$. But at low pressures the deactivating collisions are fewer and the rate of conversion of A^* into products is higher than its deactivation. As a result the product formation is proportional to the rate at which the activation occurs which is a bimolecular process, hence the product formation is second order at low pressures i.e. $\text{rate} = k_0[A]^2$.

The coefficients k_∞ and k_0 are the limiting rate coefficients at high and low pressures and can be determined using the Arrhenius equation and two separate sets of Arrhenius parameters which as shown earlier to embody only the temperature dependence. However, between the two ranges the rate coefficient is not only temperature dependent but strongly pressure dependent as well. The reaction coefficient which varies with $p - T$ conditions is given as,

$$k = k_\infty \left(\frac{k_0[M]}{k_\infty + k_0[M]} \right) F \tag{2.18}$$

which is a mathematical result due to [Lindemann et al., 1922] and a derivation can be found in [H.E.Avery, 1974]. The concentration [M] is determined as discussed earlier. In the treatment due to Lindemann, the function F is equal to one however, in other more complicated formulations such as due to Troe [1974] and Stewart et al. [1989] it is calculated using the following expressions which require reaction specific parameters. The Troe treatment of the reaction coefficient in the fall-off region involves the calculation of the function F as,

$$\log F = \left[1 + \left(\frac{log P_r + c}{n - d(log P_r + c)} \right)^2 \right]^{-1} \log F_{cent} \tag{2.19}$$

where, P_r is the reduced pressure given as,

$$P_r = \frac{K_0[M]}{K_\infty} \tag{2.20}$$

various other parameters are given as,

$$c = -0.4 - 0.67 \log F_{cent} \tag{2.21}$$

$$n = 0.75 - 1.27 \log F_{cent} \tag{2.22}$$

$$d = 0.14 \tag{2.23}$$

$$F_{cent} = (1-\alpha)\exp\left(\frac{-T}{T'''}\right) + \alpha\exp\left(\frac{-T}{T'}\right) + \exp\left(\frac{-T''}{T}\right) \tag{2.24}$$

The parameters in Equation 2.24, α, T', T'' and T''' are reaction specific and are specified in the chemical kinetics mechanism.

2.2.3 Thermodynamic properties

The knowledge of thermodynamic properties of the chemical species is necessary to calculate the heat of reactions, equilibrium constants and the rate of temperature change of the system. These property calculations have been made by using the so-called NASA polynomials. These polynomials are the linear least squares fit to the thermodynamic data of species which were based on the works of Gordon and BcBride [1971] at NASA, hence the name NASA polynomials. The thermodynamic properties have been calculated by different researchers using various theoretical methods, e.g. electronic structure calculations or bond additivity rules.

The thermodynamic data usually refers to the two sets of 7 polynomial coefficients each, one set for low temperatures, usually from 300 to 1000 K and a second set of coefficients for temperature higher than 1000 K up to 5000 K, but these ranges may slightly be different for different species. The two sets of coefficients allow better capturing of the temperature dependence of heat capacity mainly but also of the other two properties. The polynomials for heat capacity at constant pressure, C_p, sensible enthalpy, H° and standard entropy, S° at 1 atm are given as following,

$$\frac{C_p}{R} = a_1 + a_2 T + a_3 T^2 + a_4 T^3 + a_5 T^4 \tag{2.25}$$

$$\frac{H^\circ}{RT} = a_1 + \frac{a_2}{2}T + \frac{a_3}{3}T^2 + \frac{a_4}{4}T^3 + \frac{a_5}{5}T^4 + \frac{a_6}{T} \tag{2.26}$$

$$\frac{S^\circ}{R} = a_1 \ln T + a_2 T + \frac{a_3}{2}T^2 + \frac{a_4}{3}T^3 + \frac{a_5}{4}T^4 + a_7 \tag{2.27}$$

2.3 Numerical integration

The differential equations (2.11) contain reaction rate terms which may be orders of magnitude different from each other. The rates for some reactions may change quickly in time and may have high values forcing the integration time step to be very small and on the other hand some reactions may have slower rates causing the overall computation time to be long. Such systems of equations are *stiff* and require special numerical methods for integration to achieve optimum accuracy in feasible computational times. A brief list of such algorithms can be found in [Gardiner, 2000].

The stiff ODEs for the rate of change of species concentrations in this work have been integrated by using the numerical library MEBDFI[1], an implementation of a backward differential formula by Cash [1983].

2.4 Code development

Various computational chemistry packages are commercially available, notable example of which are Chemkin[2] and COSILAB[3]. The development of a chemistry solver at Leeds University was intended to allow for a greater flexibility of coupling the code with other modelling tools, ease of future enhancements in the code and for the benefits of a licence free use.

The chemical kinetics principles discussed in preceding sections were implemented in a Fortran code which is split in two separate routines namely, kinreader.f and KineticModule.f. The code was developed while keeping modularity in mind to allow ease of modifications and coupling with other packages. The overall collection of routines which have been employed in this work can be divided into three parts as shown in Figure 2.2. The initial parsing of the mechanism files (chem.inp and therm.dat) was done by using the Chemkin II

[1]The name MEBDFI is short for (M)odified (E)xtended (B)ackward (D)ifferentiation (F)ormula for fully (I)mplicit equations. The first version of the numerical library was authored by T.J. Abdullah and J.R. Cash in 2003 at Imperial College London. The version used in this work is a later Fortran 95 translation made by Bill Paxton.

[2]The earlier versions of Chemkin developed at Sandia National Laboratories were distributed by the laboratory and US Department of Energy for academic use. Current version of Chemkin has been considerably enhanced by Reaction Design and are licensed and distributed by the said company. In this work an earlier Sandia release of the Chemkin interpreter, ckinterp.f, has been used under the terms of academic use as described on the webpage http://www.sandia.gov/chemkin/FAQs.html accessed on 29 April 2014.

[3]COSILAB is a computational chemistry package developed and distributed by Rotexo GmbH & Co. KG. More details can be found at www.rotexo.com

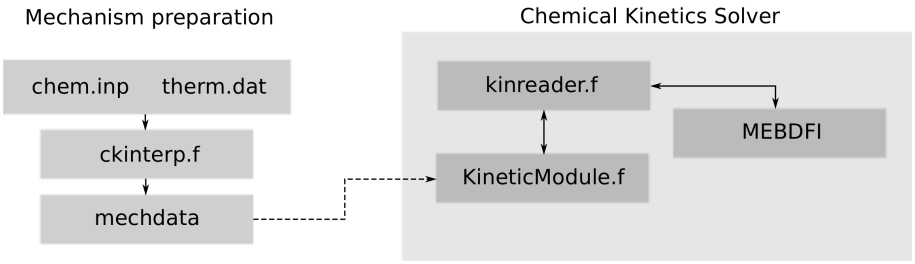

Figure 2.2: Block diagram showing various routines which comprise the chemical kinetics solver. The routines developed in this work are kinreader.f and KineticModule.f.

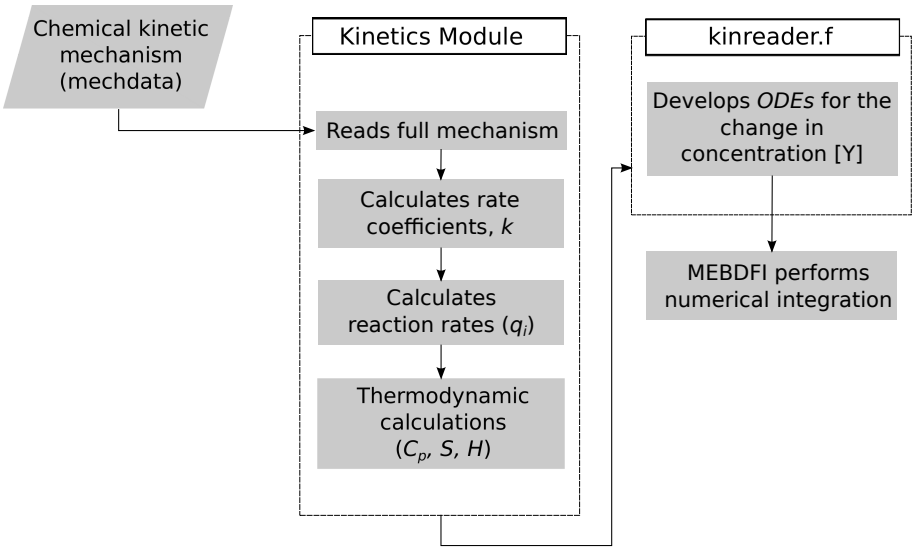

Figure 2.3: Block diagram showing parts of the chemical kinetics code where various calculations are done.

interpreter package called 'ckinterp.f' whose output was modified to reformat the mechanism parameters and the polynomial coefficients into a text file named 'mechdata' which was used as an input to the chemical kinetics code developed in this work which forms the second part of the overall code. The third part is the numerical library MEBDFI used for numerical integration and was presented earlier in Section 2.3.

The code developed in this work, was structured to allow for efficient computations. This was achieved by the use of 'modules' and 'subroutines' in Fortran 95. The tasks such as the reading of the mechanism information, calculation of thermodynamic properties and the reaction coefficient were done minimally and this information was made available to the other relevant parts of the code by declaring them global in their respective modules, see Figure 2.3. This prevented the use of rather obsolete and cumbersome 'common blocks' and having to pass

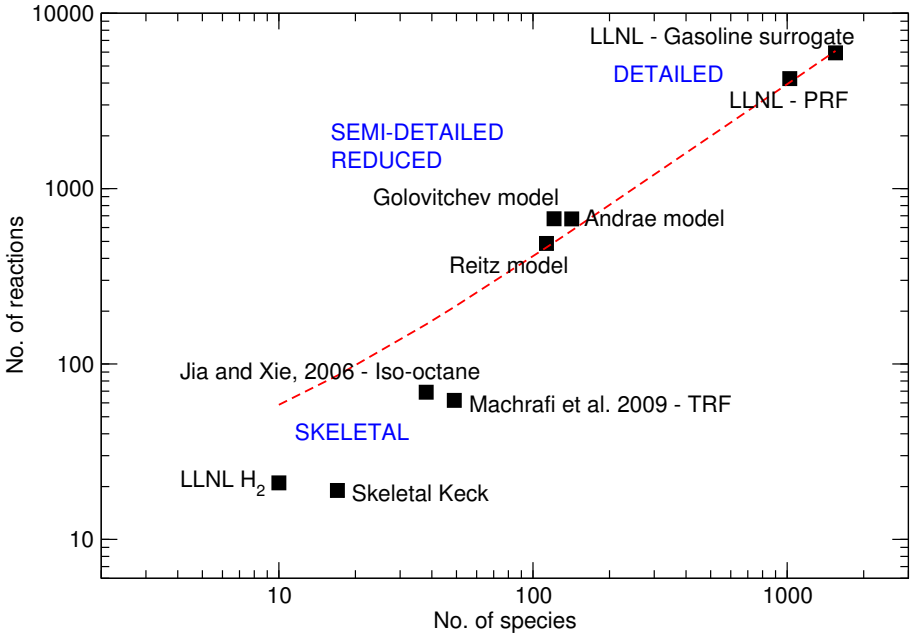

Figure 2.4: Plot showing relative sizes of various mechanisms from the literature in terms of their number of species and elementary reactions, some of these mechanisms have been studied in this work.

the information as arguments to the subroutines, thus increasing computational efficiency. It is however, stated that further enhancements can still be made to increase the computation efficiency of the code. Further discussion of the computation times will be presented in later sections.

2.5 Chemical kinetics mechanisms

A size of a detailed chemical kinetics mechanism which comprises all the known elementary reactions depends on the size and complexity of the fuel molecule. For hydrocarbon molecules with 7 or more carbon atoms, detailed mechanisms may have upto a few thousand of such reactions and about a thousand intermediate species. Such mechanisms however, can be reduced in size by only considering the most important reactions and species which are sufficient to predict the key peculiarities of the combustion reaction. One way of simplifying chemical kinetics is the development of mathematical models which comprise of generalised species and reactions, such models are also referred to as skeletal mechanisms. A well renowned example of skeletal mechanism is the 'Shell model' developed by Halstead et al. [1977] which assumed five generalised species which participated in eight generalised reactions representing chain/degenerate branching

and termination reactions. Separate sets of fitted Arrhenius parameters for PRFs of RON 70, 90 and 100, TRFs of RON 89.5 and 99.6 and 2-methyl-2hex-2-ene were provided. This mechanism formed the foundation for numerous important skeletal mechanisms for alkanes. One of the important work on skeletal hydrocarbon mechanisms is of Cox and Cole [1985] who developed on the earlier works of Knox [1967] and also the Shell model and proposed an alkane mechanism with 15 reactions and 10 species. This model was further extended by Hu and Keck [1987] specifically for iso-octane, comprising of 18 reactions for low to high temperature chemistry in temperature range of 700 - 1300 K. Later extensions of Hu and Keck model have long been used at Leeds University for autoignition prediction and are referred to as Skeletal Keck models. These extensions of the Keck model are [Chun et al., 1989], [Cowart et al., 1991] and [Nishiwaki et al., 2000]. Examples of various mechanisms from the literature have been presented in Figure 2.4 which shows a relative comparison of the complexity of these mechanisms which can be arbitrarily grouped as detailed, semi-detailed or reduced and skeletal mechanisms.

A comparison of the autoignition delay times predicted using these mechanisms is presented in Figure 2.5. It should be noted that these preliminary simulations in Figure 2.5 were done using Cosilab for the detailed and semi-detailed mechanisms; earlier Fortran implementations of the Skeletal Keck models were used and the models [Machrafi et al., 2009] and [Jia and Xie, 2006] were explicitly implemented in a Fortran code. The ignition delays for iso-octane shown in the figure indicate that simpler skeletal and heavily reduced mechanisms deviate substantially from the shock tube measurements. The Skeletal Keck mechanisms are only reasonable in predicting at the lowest temperatures which are more relevant to engine autoignition, however, model inaccuracies have been found to result in unreliable autoignition predictions as demonstrated in Chapter 6. Moreover, such skeletal mechanisms are optimised for a specific fuel and it is not possible to account for different RON and MON of the fuels. The most detailed mechanism in this comparison, the PRF mechanism proposed in [Curran et al., 1998b] and named as LLNL - PRF in Figure 2.4 performs well but no better than the three reduced mechanisms. These are the Andrae [Andrae and Head, 2009] model which comprises 144 species and 673 reactions, the Golovitchev [Huang et al., 2010] model comprising 121 species and 681 reactions and the Reitz [Ra and Reitz, 2011] model also known as MultiChem model which comprises 113 species and 487 reactions.

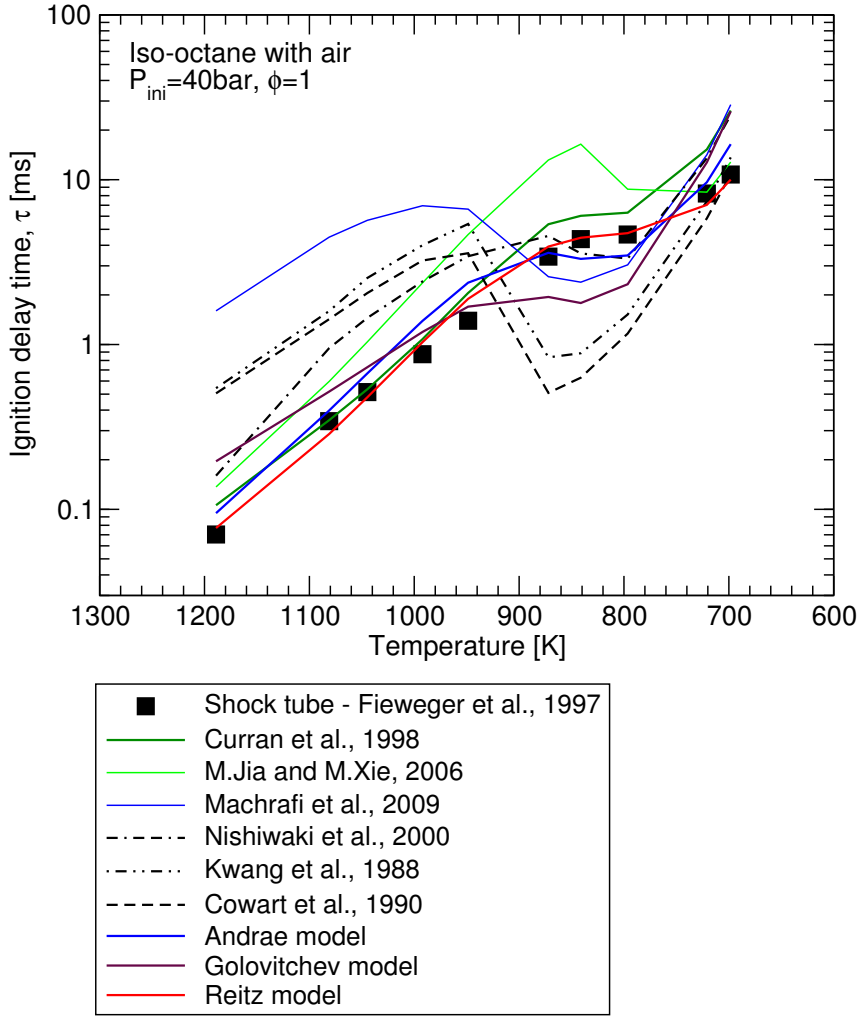

Figure 2.5: Ignition delay time predictions of 9 different mechanisms of different orders of complexity. Simulations for detailed and semi-detailed mechanisms were done in Cosilab, whereas, reduced and skeletal models were implemented in Fortran.

It was found that the three reduced mechanisms are a better choice over more detailed or simpler Skeletal mechanisms because they comprise pathways for key gasoline surrogate components which can be used as representatives of the major constituent hydrocarbon families of the gasoline. These mechanisms are also appropriately sized which results in feasible computational times. Most importantly, these mechanisms are able to predict ignition delay times with appreciable accuracy for a variety of operating conditions and equivalence ratios, as will be demonstrated through comparisons with experimental measurements from the literature in later sections. A brief introduction of these mechanisms is given here.

2.5.1 Andrae model

The mechanism used in this work can be obtained as supplementary material to the paper [Andrae and Head, 2009]. Andrae and partners developed their gasoline surrogate mechanism by extending an earlier tri-component TRF mechanism, [Andrae et al., 2007]; the resulting multi-component mechanism was first introduced in [Andrae, 2008]. Andrae's TRF mechanism was essentially a coupling of highly reduced PRF submechanisms with a relatively detailed toluene mechanism and expectedly, his extension work to produce the gasoline surrogate mechanism involved further addition to the toluene mechanism of the key reactions of phenyl (C_6H_5) whose participant species were observed at lean conditions in shock tube experiments, see [Andrae, 2008] and references therein. This allowed improvements in lean combustion predictions demonstrated by HCCI predictions. Andrae considered diisobutylene[1] (DIB) to be an important olefin and a suitable surrogate component and included its reaction pathways and rate data from the work of Metcalfe et al. [2007] who studied DIB as a candidate for diesel surrogate. DIB was given importance because of its similar structure to that of iso-octane which means it can be an important intermediary to iso-octane oxidation. It was therefore, proposed to be formed in the reaction,

$$C_8H_{17} + O_2 \longleftrightarrow C_8H_{16} + HO_2 \tag{2.28}$$

and decomposed irreversibly to form iso-butene (IC_4H_8), an important olefin. The submechanism for ethanol was based on the works of Marinov [1999] as do most

[1]Diisobutylene is a mixture of two conjugate olefins of iso-octane, which are 2,4,4-trimethyl-1-(and-2)-pentene with a molecular formula of C_8H_{16}.

of the ethanol mechanisms as limited reaction rate data is available for its oxidation.

Although various works report good agreement predictions of autoignition delays of DIB and its blends, however, one drawback for choosing DIB as an olefin representative for gasoline is its high molecular weight. Majority of olefin content in gasoline is composed of smaller molecules and as a result surrogate formulation becomes challenging if matching the hydrogen to carbon ratio (H/C) and molecular weights of the surrogate and gasoline is desired. Moreover, the octane numbers of DIB are:

2,4,4-trimethyl-1-pentene	106 RON	86.5 MON
2,4,4-trimethyl-2-pentene	103.5 RON	86.2 MON

which are considerably high compared to smaller olefins. This notion will be further explored in sections covering gasoline surrogate formulation. But it is worth mentioning it here because, even though Andrae model performs well and it has acted as basis for a number of recent reduced gasoline surrogates with similar constituents, e.g. [Wang et al., 2013] and [Zhong and Zheng, 2014], it appears that original thinking on prioritising olefins for specifically gasoline surrogates, is lacking.

2.5.2 Golovitchev model

The Golovitchev mechanism is also a multicomponent gasoline surrogate mechanism which was developed hierarchically by building on submechanisms for H_2, CH_3, CH_2O, CH_3CHO, CO, larger alkanes, alkenes and finally incorporating pathways for toluene. That resulting mechanism was without ethanol and it was extensively validated for the autoigniton predictions of the submechanisms on their own as well as for blends of the main components i.e. the gasoline surrogates at different conditions which can be found in [Ogink and Golovitchev, 2002] and [Ogink, 2004]. The mechanism was further extended by the addition of ethanol pathways which also consisted of reactions for dimethyl-ether (DME) and revalidated against a large set of ignition delay time data and laminar burning velocities as well [Huang et al., 2010].

2.5.3 Reitz model

The Reitz model otherwise known as MultiChem is a reduced multicomponent mechanism which has submechanisms for a number of species which qualify as both gasoline and diesel surrogates, e.g. dimethyl-ether, methyl butanoate and n-tetradecane which are present in addition to the usual components. The mechanism development rather seems to follow a top-down reduction approach from more detailed mechanisms, resulting in a small mechanism of 113 species and 487 reactions, smaller than the Andrae and the Golovitchev models.

MultiChem evolved from their earlier PRF mechanism [Ra and Reitz, 2008] which was reduced from the detailed works of [Curran et al., 1998a] and [Curran et al., 2002]. The mechanism was reported to perform remarkably well for PRFs for their 0-D autoignition delays and CFD modelling of HCCI and this also been seen in this work that the PRF predictions of the Reitz model are superior with some exceptions. The pathways for PRF oxidation are not greatly different for the three mechanisms, the difference is mostly in the reaction coefficients which are optimised in each mechanism, however, more so in Reitz model than others. The mechanism for toluene in the Reitz model is based on the works of [Bounaceur et al., 2005] and [Andrae et al., 2007]. The ethanol mechanism is based on the detailed mechanism of Marinov [1999] which was reduced through sensitivity and flux analyses. Ra and Reitz [2011] also included submechanism for cyclo-hexane, an important naphthene component of gasoline, although not as abundant as cyclo-pentane [Pera and Knop, 2012].

2.6 Code validation

The chemistry solver developed as part of this work was first compared to two other packages, Chemkin II and Cosilab. Some of the comparisons of ignition delay times of iso-octane, n-heptane and toluene obtained by the three reduced mechanisms have been presented in Figures 2.6 to 2.8 which show that the ignition delay times calculated using the Leeds Chemistry Solver are very close to the calculations of other two packages. Minute differences can be seen which can be attributed to the different numerical schemes used by these packages, rounding of the digits and possibly interpolation of thermodynamic data instead of recalculation at each time-step by Chemkin II and Cosilab which was not done in Leeds Chemistry Solver as it did not offer any perceptible computational benefit.

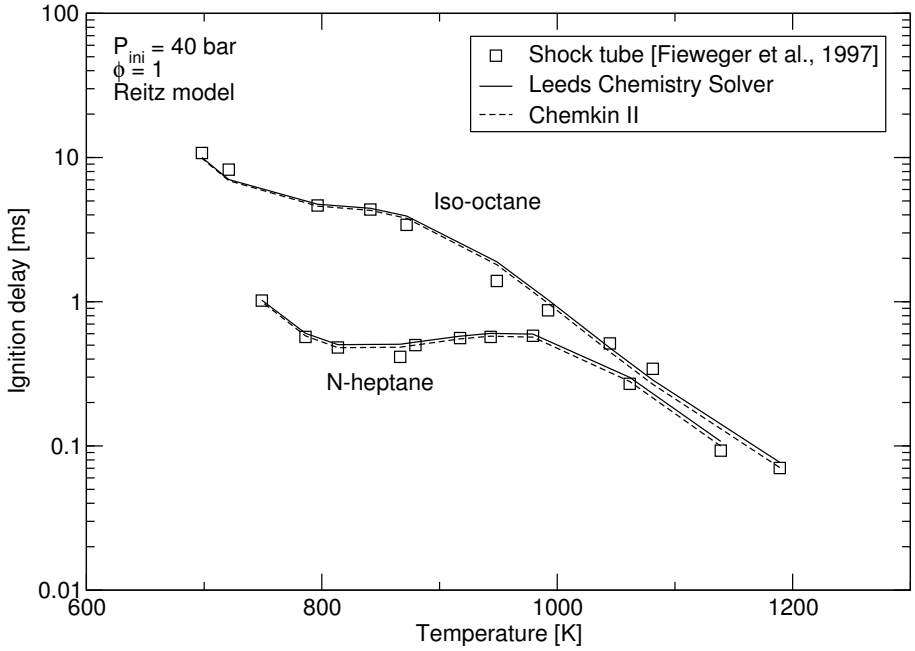

Figure 2.6: Comparison of ignition delay predictions made by the Leeds Chemistry Solver and Chemkin II for n-heptane and iso-octane using the Reitz model.

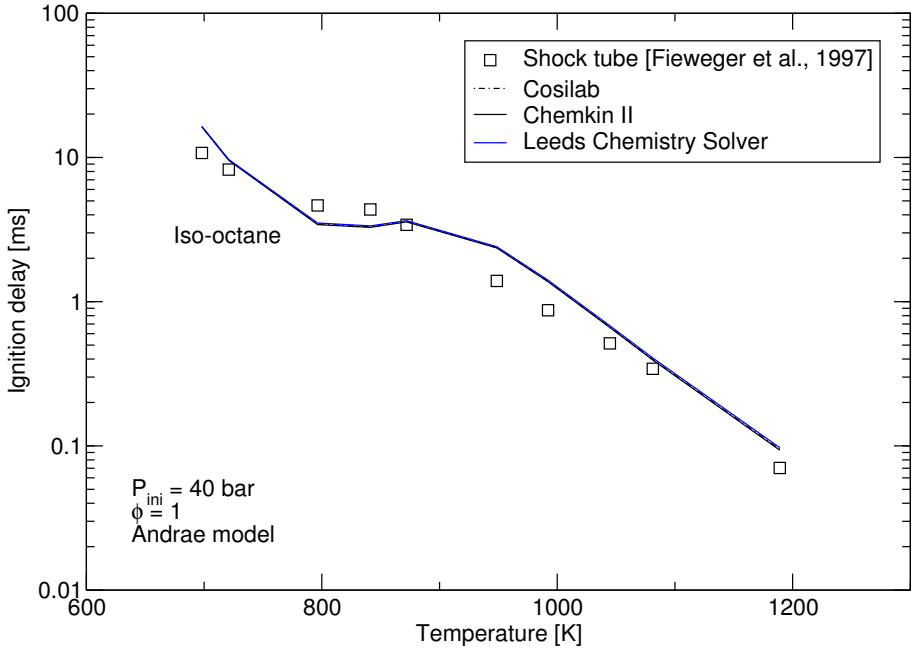

Figure 2.7: Comparison of ignition delay predictions made by the Leeds Chemistry Solver, Cosilab and Chemkin II for iso-octane using the Andrae model.

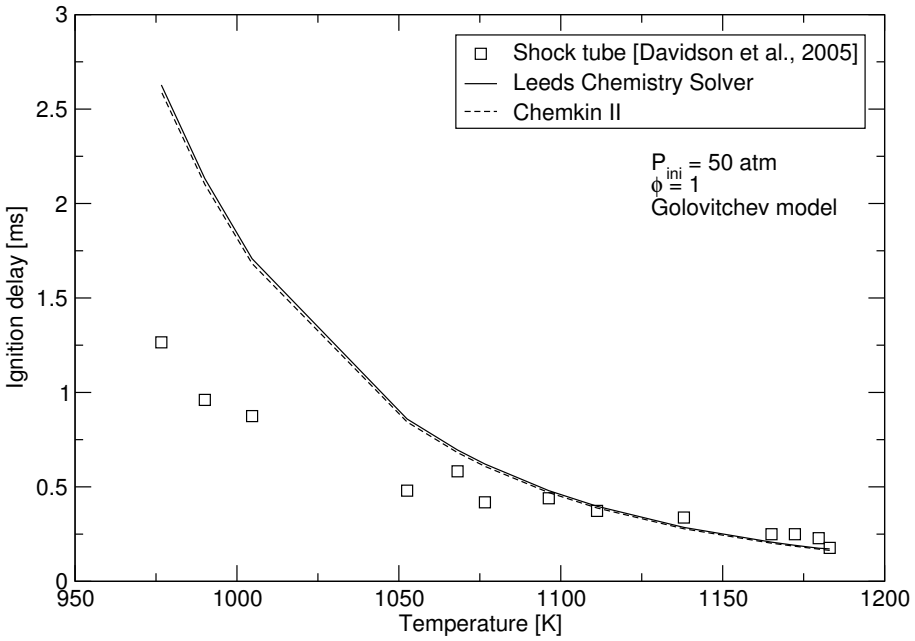

Figure 2.8: Comparison of ignition delay predictions made by the Leeds Chemistry Solver and Chemkin II for toluene using the Golovitchev model.

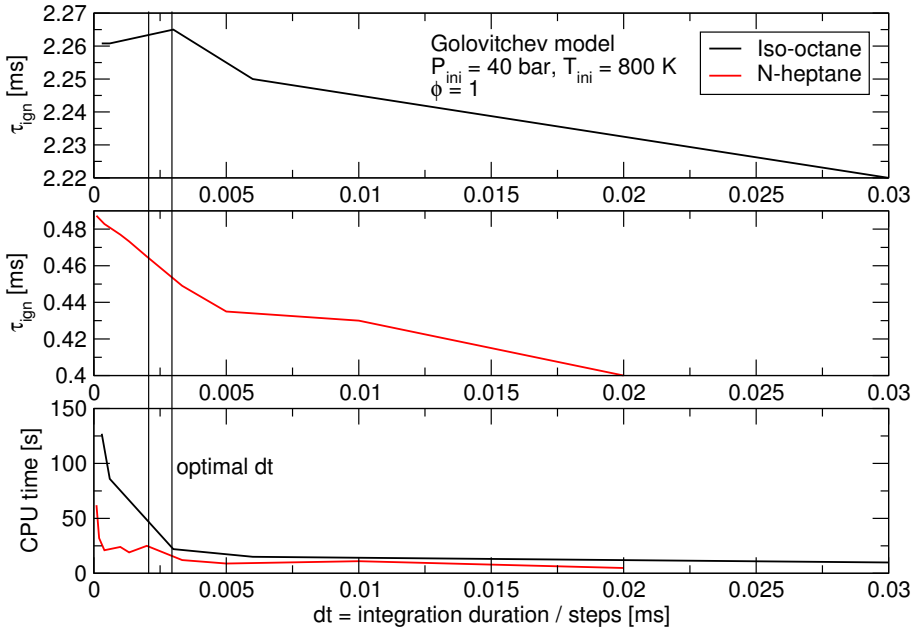

Figure 2.9: Effect of the integration time step on ignition delay time and computational time.

The time duration of a simulation was found to be dependant on the integration time step and also the stiffness of the mechanism. The numerical library, MEBDFI, uses an internal dynamic time step, however, the duration of integration and the integration interval or the step size must be specified. A smaller time step, dt, increases the computational time and a too coarse a time step causes larger truncation errors. A compromise must therefore be reached between accuracy and computational time. The stiffness of the mechanism plays a role when all or a large number of reactions have a non-zero net reaction rate which forces the internal dynamic stepping to be refined which increases the computational time. Simulations of blends are therefore expected to be longer than neat fuels as presence of difference species right from the beginning would initiate reactions earlier on increasing stiffness. Figure 2.9 shows ignition delay times, τ_{ign}, for iso-octane and n-heptane at same initial $p - T$ condition but the time step has been changed. As the time step is decreased, τ_{ign} starts to stabilise, see iso-octane curve specifically, however, correspondingly the computation time increases manifolds. A time step of roughly 0.025 ms appears to be a feasible value at which the computational times are between 20 to 30 s acceptable for a single constant volume autoignition simulation. When coupled with engine modelling, the computational time will also depend on engine speed and in this work is found to be of the order of 1 minute per cycle.

2.7 Autoignition simulation results

It was of an obvious interest to first study the autoignition predictions of the three reduced mechanisms. Constant volume, 0-D, autoignition simulations were carried out by using the Leeds Chemistry Solver for the four main gasoline surrogate components, iso-octane, n-heptane, toluene and ethanol. Simulations done for a range of temperatures, were compared to shock tube measurements at low pressures (10 - 13 bar) and high pressures (40 - 50 bar) for stoichiometric air-fuel mixtures as these are of relevance to SI engines. The low pressure comparisons have been presented in Figure 2.10 and high pressure comparisons in Figure 2.11. For SI engine autoignition, the temperatures upto about 850 K or $1000/\mathrm{T} > 1.15$ are important. The model accuracy at these temperatures is indeed of great significance, however, accurate predictions at higher temperatures are crucial too as blending may cause the otherwise high temperature channels for certain components to become active at lower temperatures, e.g. for toluene and ethanol when

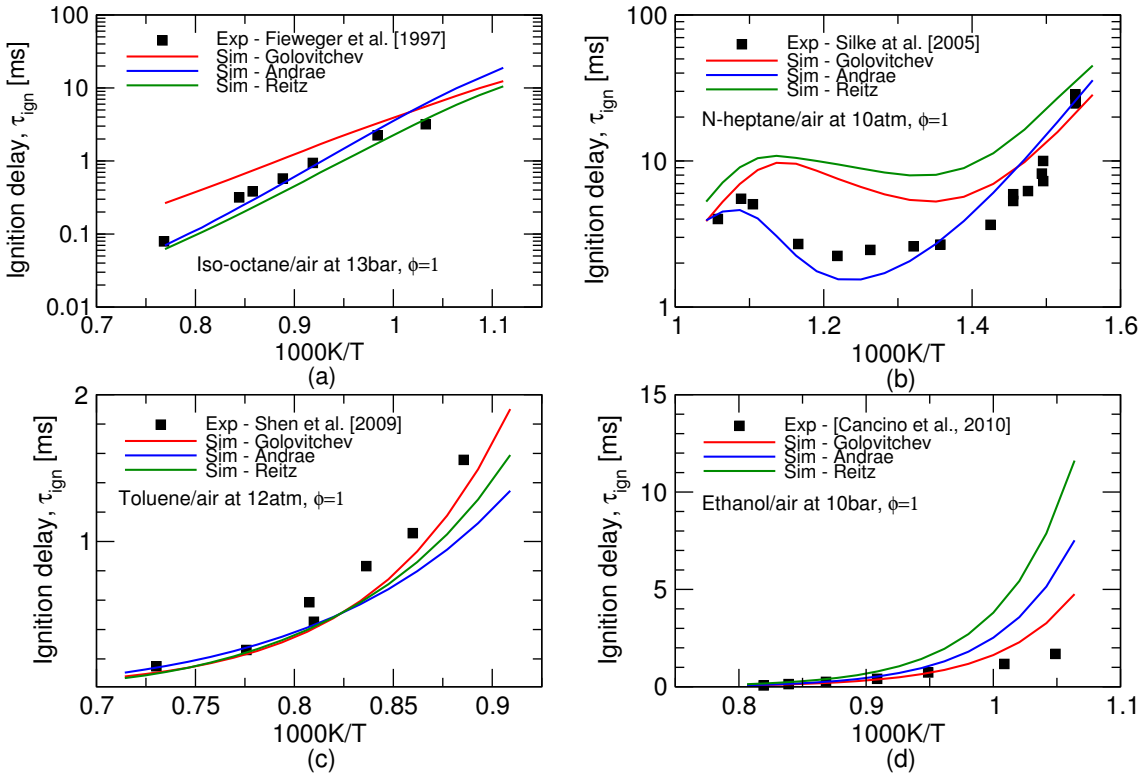

Figure 2.10: Low pressure ignition delay time predictions (lines) made by the three reduced chemical kinetic mechanisms for four key gasoline surrogate components. Symbols represent shock tube measurements; (a) [Fieweger et al., 1997] (b) [Silke et al., 2005] (c) [Shen et al., 2009] (d) [Cancino et al., 2010].

blended with PRFs as discussed in Chapter 3. High octane number fuels, particularly toluene and ethanol are difficult to ignite on their own at such engine relevant conditions and that is why comparisons with shock tube measurements are at higher temperatures. The autoignition predictions for each fuel are discussed below.

- **Iso-octane**, all three models predict reasonably well the ignition delay times at both low and high pressure conditions, however, the Golovitchev model tends to deviate the most and the Reitz model seems to be most closest to the shock tube measurements.
- **N-heptane**, the Andrae model is the most consistent in its predictions at low and high pressures and the other two models predict considerably long ignition delays for most of the NTC phase, however, the agreement with measurements is much better at high pressure.
- **Toluene**, the only good agreement is of the Andrae model at high pressure.

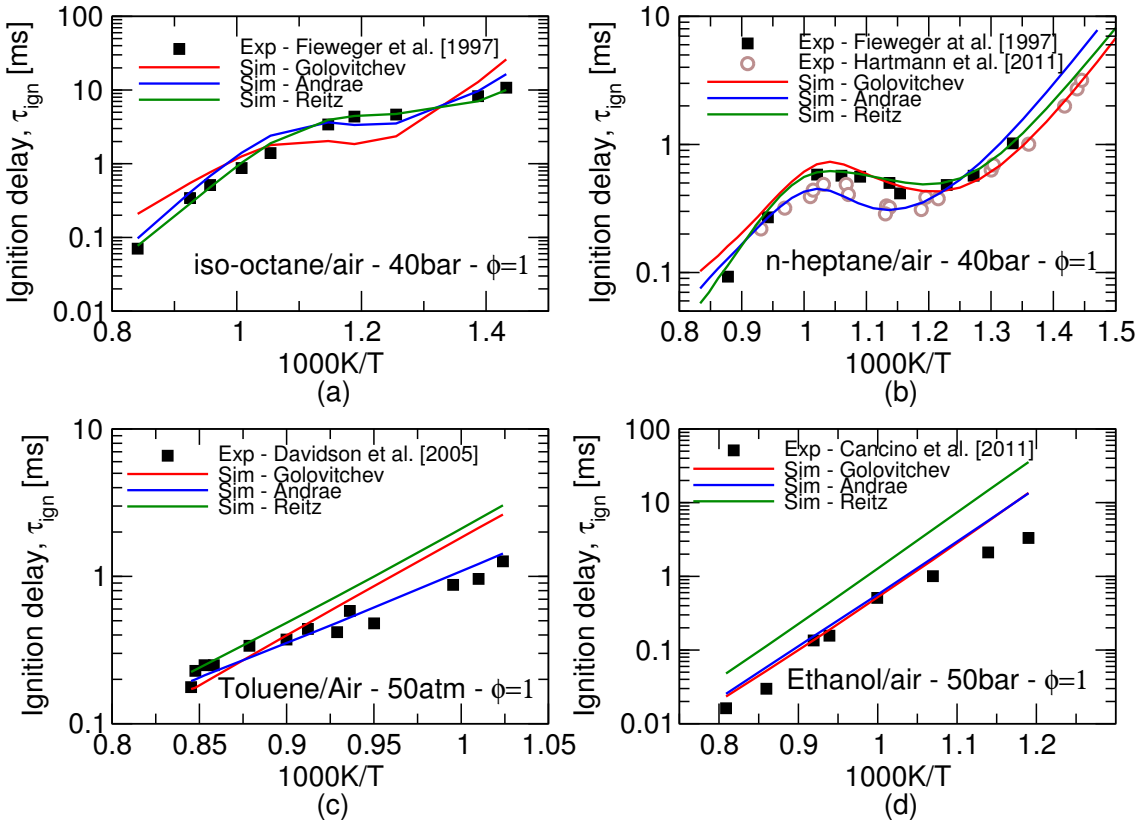

Figure 2.11: High pressure ignition delay times predictions (lines) made by the three reduced chemical kinetic mechanisms for four key gasoline surrogate components. Symbols represent shock tube measurements; (a) [Fieweger et al., 1997] (b) [Fieweger et al., 1997; Hartmann et al., 2011] (c) [Davidson et al., 2005] (d) [Cancino et al., 2011].

All models predict shorter delays at low pressure, the Andrea model deviating the most. At higher temperatures, the agreement of the three models is appreciably good with the measurements.

- **Ethanol**, just as for toluene, all models only agree well with the measurements at higher temperatures. The deviation from experiments is considerable at lower temperature at both low and high pressure. The Reitz model predicts excessively long ignition delay times. Similar ethanol pathways in Golovitchev and Andrae model result in similar predictions at high pressure.

Among the three mechanisms, the PRF submechanism in the Reitz model seems to agree the best with the measurements at 40 bar initial pressure, see Figures 2.12. The predictions of the Andrae model are fairly accurate for the medium to high temperatures but disagreement of the bi-component blends at low temperatures is considerable possibly due to deficiencies in the cross reactions of iso-octane and n-heptane. The Golovitchev model appears to disagree with measurements for high RON PRFs possibly due to deficiencies in the iso-octane reaction rates.

2.8 Practical gasoline surrogates

The simplest surrogates i.e. PRFs are used in the well known RON and MON tests to quantify the knock resistance of a gasoline by matching their knock intensities in a standard engine. Compared to RON test, at the same pressure, in a MON test the end gas in the engine cylinder is subject to higher temperatures and therefore, unless the gasoline exhibits a NTC phase at those temperatures, the MON tends to be lower than RON. The sensitivity S, i.e the difference of octane numbers ($S = \mathrm{RON} - \mathrm{MON}$) is a measure of the fuel response to lower pressures and higher temperatures. PRFs have zero sensitivity by definition, however, a gasoline is expected to exhibit different anti-knock properties in a MON test from those of a PRF of equivalent RON. This gives gasolines a non-zero sensitivity. Blends of iso-octane and n-heptane with toluene (TRF) have an advantage of non-zero sensitivity and offer to recreate the anti-knock properties at both RON and MON test $p - T$ conditions. Binary blends of toluene with iso-octane and n-heptane have been studied in order to isolate their cross-oxidation chemistry, however, such blends have found little application as gasoline surrogates.

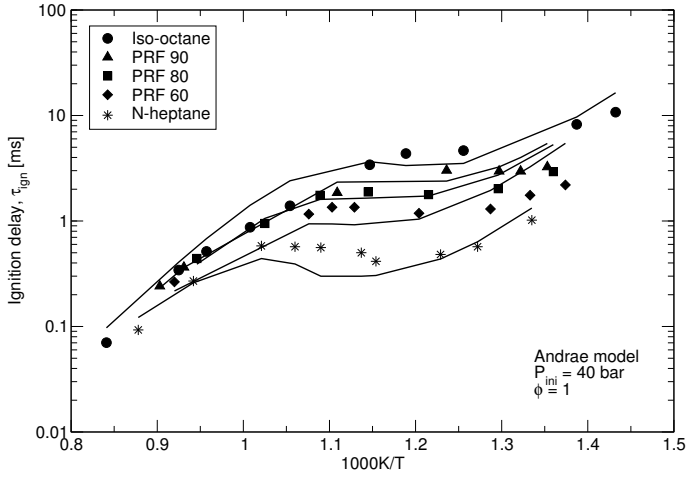

(a)

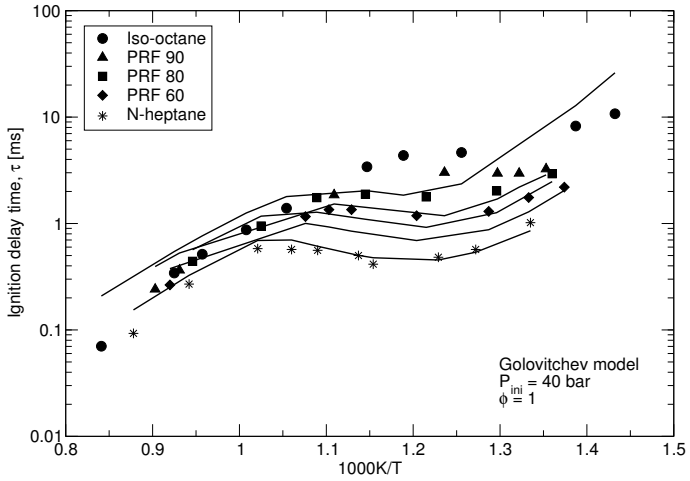

(b)

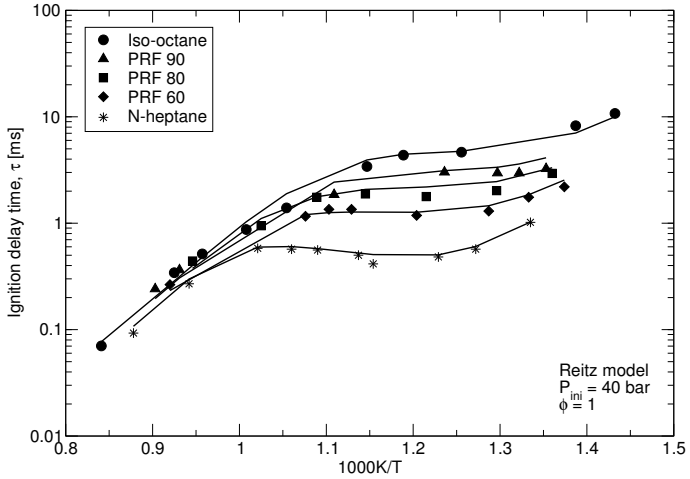

(c)

Figure 2.12: Comparisons of ignition delay time measurements by Fieweger et al. [1997] and predictions by using the Andrae model (a), Golovitchev model (b) and Reitz model (c).

Iso-octane	n-heptane	Toluene	Ethanol	Olefin	RON/MON	Reference
% by volume						
63	17	20	-	-	86.6/84.2*	Gauthier et al. [2004]
69	17	14	-	-	85.7/84.6*	Gauthier et al. [2004]
62	18	-	20	-	95.1/89.5	Fikri et al. [2008]
25	20	45.0	-	10 (DIB**)	94.6/85	Fikri et al. [2008]
37.8	10.2	12	40	-	98.75§	Cancino et al. [2009]
30	22	25	10	13 (DIB)	-	Cancino et al. [2009]
57	16	23	-	4 ($C_5H_{10}-2$)	91/83$^{est.}$	Mehl et al. [2011]

* determined by Knop et al. [2014]
** diisobutylene (C_8H_{16})
$^{est.}$ estimated values
§ estimated value, see Cancino et al. [2009]

Table 2.1: Volumetric composition of various gasoline surrogate blends found in the literature for which extensive shock tube and RCM measurements have been made.

Use of iso-octane and n-heptane as components of a surrogate is hardly avoidable as they represent linear and branched alkanes which are major gasoline components. Besides, the chemistry leading to their auto-ignition is relatively well understood. However, gasoline does not consists only of alkanes. Thus, EN228, the European standard for gasoline specifies aromatic content of up to 35% by volume, it also allows 5% ethanol by volume. Therefore, it seems natural to seek gasoline surrogates going beyond PRFs and TRFs which contain compounds approximating various families of hydrocarbons present in the gasoline.

Various surrogates, TRFs as well as blends containing olefins and oxygenates, particularly ethanol, have been studied for their autoigntion properties in rapid compression machines, shock tubes and HCCI engines and list of such surrogates is presented in Table 2.1. Gauthier et al. [2004] performed a fairly comprehensive shock tube study of two TRFs for $p-T$ conditions of 12 - 25 atm and 45 - 60 atm at 850 - 1280 K temperatures. The two TRFs were proposed to approximate a standard research gasoline, RD387; with an anti knock index ($AKI = \frac{\text{RON+MON}}{2}$) of 87. The measurements demonstrated similarities between the autoignition characteristics of the surrogates and their gasoline. Kukkadapu et al. [2013] further investigated one of the TRF formulation proposed in [Gauthier et al., 2004]; this surrogate is referred to as Gauthier TRF-A (iso-octane 63%, n-heptane 17%, toluene 20% by volume). Using Mehl et al. [2011] approach (described in subsequent paragraph) they also over-estimated the sensitivity of the Gauthier-A TRF to be 6 points with RON/MON of 89.5/83.5. However, the RON and MON of the two Gauthier TRFs were later determined by Knop et al. [2014] and the AKI of the surrogates were found to be lower than 87, see Table 2.1. But, even more importantly, the sensitivity S of the two TRFs was found to be much lower than the usual gaso-

line range of $S \sim 8 - 12$ points, 2.4 points for Gauthier-A TRF. Although, such blends cannot be used as surrogates for a regular commercial gasoline which has a higher RON and sensitivity, but such studies offer invaluable source of chemical kinetics validation.

Since, the composition of a gasoline may vary, it would be helpful if bespoke surrogates can be formulated to recreate the autoignition behaviour of a given gasoline. Mehl et al. [2011] demonstrated that the sensitivity of a surrogate can be correlated to the slope of the NTC region $dlog(\tau_{ign})/dT$ while the values of the autoignition delay time τ_{ign} in the NTC region depend on the AKI of the surrogate. The two correlations thus obtained and the knowledge of the gasoline composition provided constraints for the aromatic and olefinic content of the surrogate which are key to achieving a realistic NTC behaviour and thus the sensitivity. The PRF content can then be varied to achieve the correct H/C ratio and the octane numbers. This approach was applied to a RD387 gasoline for which a 4-component surrogate was proposed (Table 2.1), however, as said earlier, their approach yielded inaccurate estimate of the surrogate sensitivity. The theoretical estimate of the octane numbers of a mixture of different fuels is a difficult task as the octane number is not a property which can simply be summed, weighed by the proportion of a given constituent.

In order to cater to the modern high ON gasolines which typically contain up to 5 - 10% ethanol, Fikri et al. [2008] and Cancino et al. [2009] performed shock tube measurements of gasoline surrogates including ethanol as a component, see Table 2.1. To the best of the author's knowledge, at the time of this work their blends are the only ethanol containing surrogates for which ignition delay times have been measured. The EN 228 gasoline standard also specifies a maximum olefin content of 18% by volume. Most European gasolines have olefin content between 5 and 9% by volume, mostly branched rather than straight or cyclic compounds, e.g. see details on a French gasoline in [Pera and Knop, 2012]. Oxidation characteristics of some olefins, such as 1-hexene, cyclohexene and 1-pentene have been studied, however, other very common ones, e.g. 2-methyl-2-butene are little studied. It is because of this lack of understanding of common gasoline olefins that chemical kinetic mechanisms for gasoline surrogate differ significantly in terms of olefins.

The three reduced mechanisms studied in this work were originally validated against some of the measurements for the surrogates in Table 2.1. Presently, a comparison of the ignition delay time predictions of these mechanisms for $\phi = 1$

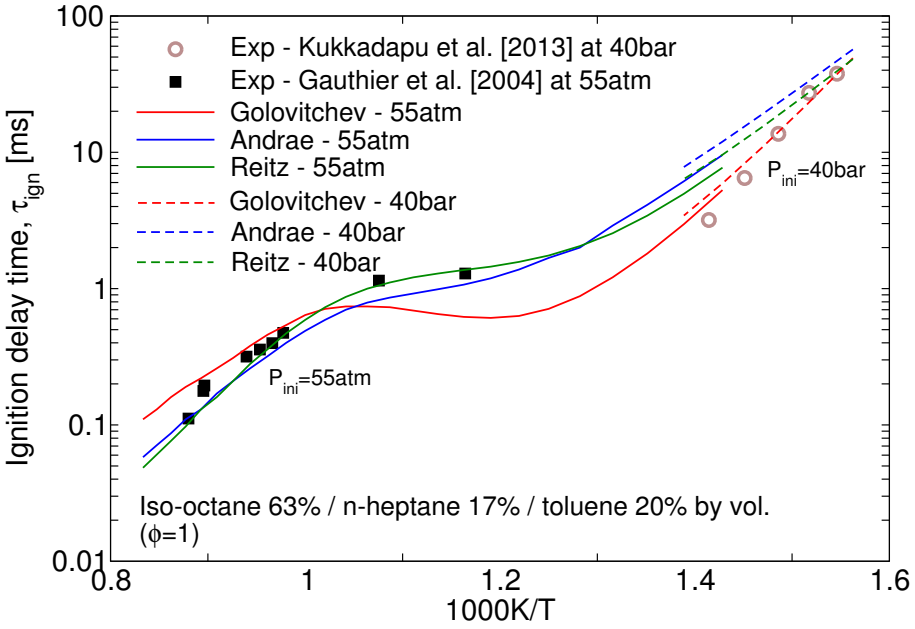

(a)

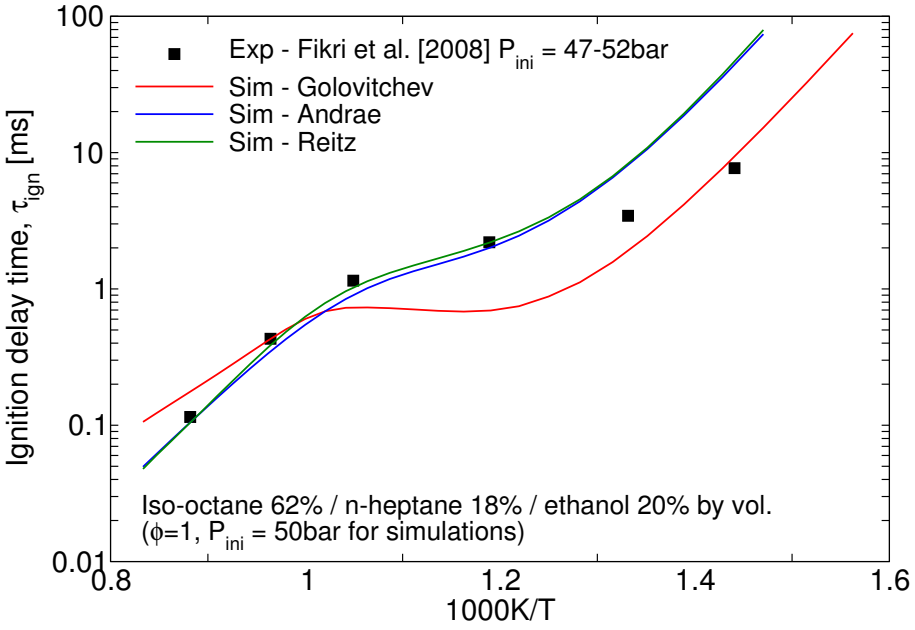

(b)

Figure 2.13: Comparison of predicted Ignition delay times of the Gauthier-A TRF and a gasoline surrogate by Fikri et al. [2008] to the shock tube and RCM measurements.

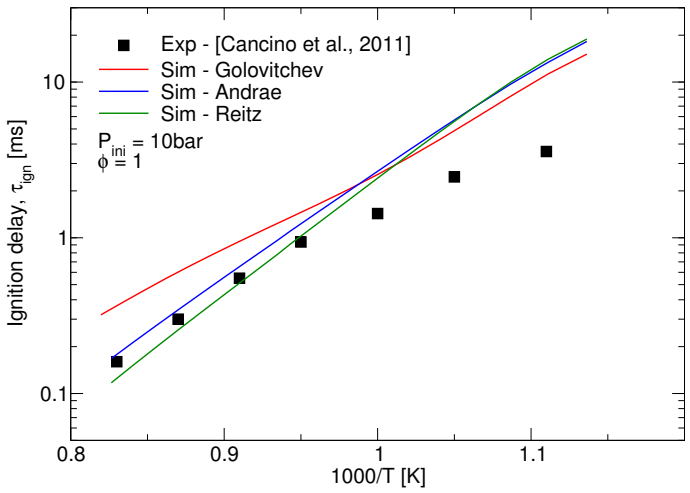

(a)

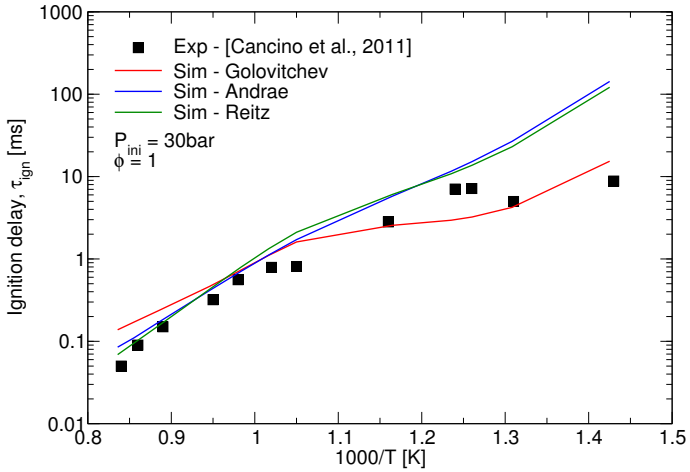

(b)

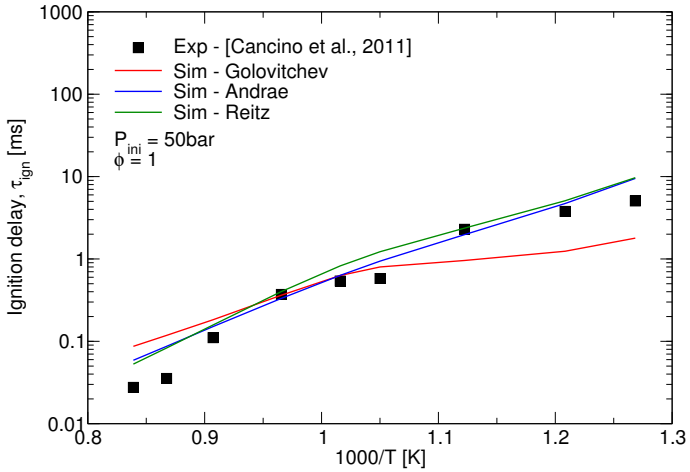

(c)

Figure 2.14: Comparison of predicted ignition delay times of the stoichiometric air mixture of surrogate comprising iso-octane 37.8%/n-heptane 10.2%/toluene 12%/ethanol 40% by volume, with its measurements by Cancino et al. [2009] at initial pressures of 10 bar (a), 30 bar (b) and 50 bar (c).

at high pressure has been done. Simulations of the surrogates made up of different components and compositions have been made and the results have been presented in Figures 2.13 and 2.14.

2.9 Gasoline surrogate formulation

The approach to surrogate formulation depends on its modelling application. A number of physical and chemical properties of the target fuel can be reproduced in the surrogate such as the distillation curve, RON, MON, stoichiometric air to fuel ratio, molecular weight, thermal conductivity and laminar burning velocity. At the same time, the number of components in gasoline surrogate is limited by the availability of chemical kinetic mechanisms. Since gasoline constituents can normally be classified into five or so classes, it seems natural to seek a surrogate with the same number of components. One mathematical constraint which must always be met while determining the composition of a surrogate is that the sum of the mole or volume fractions of its constituents must be one. This is shown mathematically for mole fractions as following:

$$\sum_{i=1}^{n} x_i = 1 \tag{2.29}$$

This means that for a *n* component surrogate, *n-1* properties can be used as constraints to optimise the surrogate composition. For most practical applications at least 4 properties of the target gasoline can be replicated in the surrogate and it is hoped that this will result in the simulation of various complex physicochemical behaviours which depend on these properties. For a correct prediction of the cumulative heat release the stoichiometric air to fuel ratio (AFR_s) and the calorific value of the surrogate must also be matched. The correct atomic proportions as well as the molar mass, *M*, will produce the desired AFR_s. In a quasi-dimensional combustion modelling approach for SI engines such as in this work, where the combustion rate is dependent on laminar burning velocity which is derived using empirical expressions, the surrogate oxidation in the end gas for autoignition prediction has no implications on the main combustion event. In such situations the surrogate calorific value in the vicinity of that of the gasoline should suffice and which is achieved by merely taking the atomic proportions as an optimisation constraint. However, the accurate reproduction of these properties as well as the laminar flame speed must be achieved when chemistry cou-

pled CFD modelling of the flame propagation is of interest. More demanding modelling applications such as spray combustion will require additional properties to be matched such as the distillation curve. For the quasi-dimensional combustion modelling in SI engine coupled with chemical kinetic modelling of surrogate autoignition in the end gas, the H/C and O/C ratios are crucial for a satisfactory translation of unburned species of the main combustion event (indolene, air and EGR) to the species in the chemical kinetic mechanism. Therefore these constraints are used in the determination of the surrogate composition and are mathematically given as:

$$\frac{\sum_{i=1}^{n} x_i H_i}{\sum_{i=1}^{n} x_i C_i} = H/C \tag{2.30}$$

$$\frac{\sum_{i=1}^{n} x_i O_i}{\sum_{i=1}^{n} x_i C_i} = O/C \tag{2.31}$$

Reproducing the correct autoignition behaviour in the surrogate is perhaps the biggest challenge in surrogate formulation. The realism of the surrogate in mimicking the autoignition characteristics of a gasoline is only partly dependant on the infallibility of the theoretical octane number model being used. A *true* surrogate for gasoline autoignition will show the same ignition delay as the gasoline at all conditions. It will show the emergence of similar ignition precursors at similar rates to that of the gasoline and therefore it will have, not only the same RON and MON as the gasoline but similar octane index (see Equation 1.2) no matter which engine the two are compared in. Matching just the RON and MON of the surrogate with that of the gasoline does not guarantee that the surrogate will reproduce the autoignition behaviour of the gasoline universally in all engines. To make matters worse, the empirical/theoretical octane number models are far from perfect. Detailed composition-based octane models such as [Ghosh et al., 2006], exist which account for the non-linear blending interactions of surrogate constituents. The Ghosh et al. [2006] model accounts for the paraffin-olefin and paraffin-naphthene interactions. The non-linear octane blending between ethanol and other gasoline constituents as shown by Foong et al. [2014] is a subject of ongoing research but no tried and tested octane number model exists at the time of the present work. Pera and Knop [2012] proposed a surrogate formulation approach which is purely based on matching the chemical and physical properties of surrogate to those of the target gasoline. However the approach suffers from weaknesses in the empirical octane number blending rules. Pera and others such

as Anderson et al. [2010] advocated the use of a linear by moles additivity rule for the TRF blends which was shown to perform better than the non-linear model of Morgan et al. [2010] and the composition-based octane model of Ghosh et al. [2006]. They proposed an improvement to the linear by moles expression for TRFs by suggesting blend octane numbers for toluene (RON 116 / MON 101.8) and demonstrated that their expression yielded the lowest absolute errors in comparison to 7 other octane number models [Knop et al., 2014]. Their approach has been found to produce appreciable octane numbers in the present work and due to its accuracy and simplicity, it has been adopted in the calculation of TRF octane numbers as well as blends containing olefins and ethanol.

$$\sum_{i=1}^{n} ON_i x_i = ON \tag{2.32}$$

Equations 2.29 to 2.32 provide five constraints for the determination of a so called properties-based surrogate. As opposed to this; a composition-based surrogate can also be formulated by simply translating the composition of the major constituents of gasoline to a representative surrogate of that particular family. The resulting surrogate will be expected to have different properties from that of the target gasoline as the surrogate components do not correctly represent all of the molecules in that family. It will be shown in this work that a surrogate whose composition is faithful to the proportions of the actual gasoline may perform better in replicating the autoignition behaviour than a purely properties-based surrogate containing unrealistic amounts of aromatics and oxygenates.

2.10 Summary

- **Chemical Kinetics Solver**, a Fortran code for the chemical kinetics calculations was successfully developed and validated against simulations of well-known commercial packages.
- **Chemical kinetic mechanisms**, after a literature survey of mechanisms of various sizes, it was concluded through numerical simulations that reduced and semi-detailed mechanisms of the order of about 600 reactions and 100 species offer pathways for key gasoline components, appreciable autoignition predictions and computational feasibility. Hence, three such mechanisms, Andrae, Golovitchev and the Reitz (MultiChem) models were selected to be used in this work.

- **Autoignition predictions**, the three models generally tend to perform better at high $p - T$ conditions than at low conditions. The Andrae model appears to predict autoignitions consistently with appreciable accuracy, however, the Reitz model appears to have a more accurate PRF mechanism.

- **Gasoline surrogate formulations**, the gasoline surrogates typically studied in the literature are either TRFs or multi-component blends whose compositions do not comply with the EN-228 specifications. It is therefore that gasoline specific surrogates are to be formulated which are composed of such compounds which represent the major constituents of the gasoline. The surrogate composition can either be determined by optimising the blend properties to match those of the target gasoline, an approach referred to as the properties-based approach, or if the composition of the gasoline is known than it can be assigned to the representative surrogate compounds, an approach named here as composition-based approach. Both of these approaches will be used in the subsequent chapters.

Chapter 3

Hydrocarbon oxidation chemistry

3.1 Introduction

During combustion process, hydrocarbon compounds undergo a particular sequence of interdependent elementary chemical reactions until their constituent carbon and hydrogen are fully oxidized. This sequence of intermediate chemical reactions, lays down the mechanism of oxidation for that particular hydrocarbon at those conditions. Different types of hydrocarbons have different oxidation mechanisms due to differences in the molecule size, geometry, constituent elements and nature of chemical bonds. Some compounds exhibit similar mechanisms and involve similar intermediate reactions. For example, the higher alkanes tend to decompose into lower olefins, e.g. C_2H_4, at high temperatures and therefore the subsequent reactions are similar to those of the olefin oxidation. Hence, a general understanding of hydrocarbon oxidation has been developed over the years; this may be applied to ignition/combustion of different hydrocarbon fuel molecules. Such mechanisms will be discussed in the following paragraphs.

Some of the hydrocarbon fuels have been the focus of research studies more than the others because of their significance and some times for their simpler molecular structure. For example, very widely studied is methane, which is the simplest hydrocarbon of great significance because of its use as a domestic fuel. Other examples are the primary reference fuels (PRF) i.e. iso-octane and n-heptane, which are used to characterise the knock resistance of gasoline in SI

engines.

It is primarily the temperature and the fuel to oxidiser ratio and to some extent the pressure which determine that which elementary reactions will dominate the others. The type of reactions at different temperatures may differ greatly and therefore different phases of oxidation chemistry can be defined for different temperature intervals. Historically, these temperature regimes have been divided into three; low, less than 800 K, intermediate, 800 - 1100 K and high, greater than 1100 K. A generic illustration of these distinct oxidation pathway regimes is shown in Figure 3.1, which has been adapted from [Miller et al., 2005]. This demarcation of temperature ranges is pressure dependent and by no means rigid. A change in temperature from one range to the other does not imply that the reactions of the first range completely cease to occur. Miller et al. [2005] state that the boundary between the intermediate and high temperature regimes is the loci of points at which the reaction ($\mathrm{H} + \mathrm{O_2}$) is neutral. At higher temperatures i.e. above the line, the branching reaction, ($\mathrm{H} + \mathrm{O_2} \longrightarrow \mathrm{OH} + \mathrm{O}$), dominates, whereas, at low temperatures i.e. below the line, the termination reaction, ($\mathrm{H} + \mathrm{O_2} + \mathrm{M} \longrightarrow \mathrm{HO_2} + \mathrm{M}$), is dominant. The boundary between the two regimes is marked by the balance between the two types of reactions. The intermediate temperature regime is typically characterised by the so-called negative temperature coefficient (NTC) phase which manifests as the degenerate chain branching reactions start to dominate the chain branching reactions of the low temperature regime. The boundary between the low and the intermediate regimes can thus be attributed to the neutrality of the peroxy radical chemistry (to be explained later).

Based on the temperature and pressure conditions, a fuel-air mixture may exhibit four types of distinct combustion behaviours. Below 473 K the oxidation of hydrocarbon occurs through very slow reactions and it is considered irrelevant to internal combustion engines. Between 500 K and 700 K a small amount of fuel undergoes partial oxidation and a minute heat release occurs leading to a temperature rise of only tens of degrees [Heywood, 1988]. At higher temperatures, a single or a two-stage ignition may be observed. The accumulation of active radicals to critical concentrations leads to a thermal runaway at which accelerated exothermic reactions cause a substantial heat release. This process is especially expedited if there is a further increase in the temperature and pressure through compression such as in the unburned zone of a SI engine. Such an ignition behaviour in which a mild ignition is followed by a hot flame is called two stage ignition. At significantly high temperatures only a single-stage ignition is

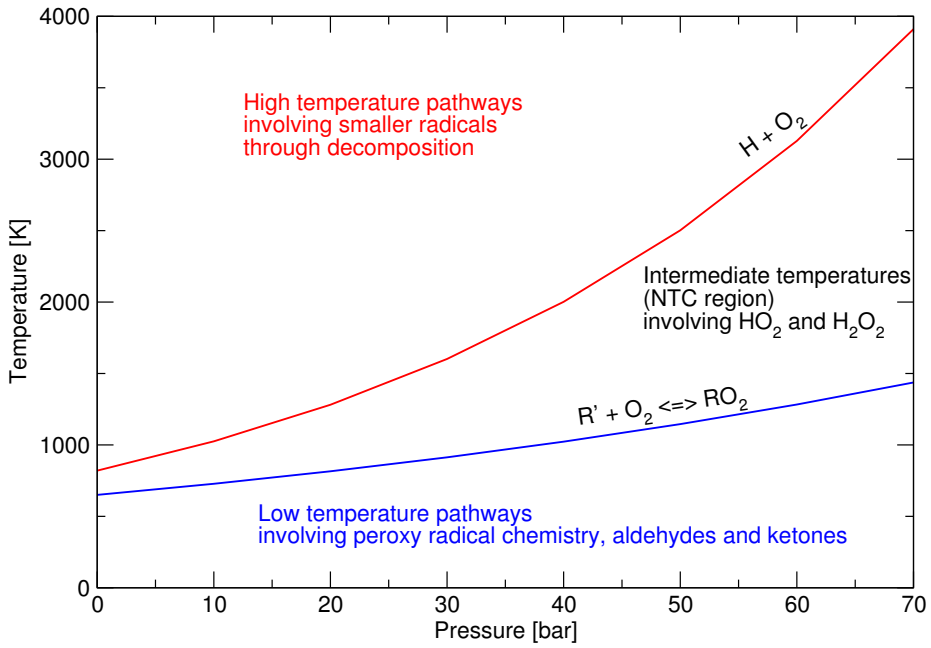

Figure 3.1: A generic illustration of the low, intermediate and high temperature pathway regimes for alkanes. Adapted from [Miller et al., 2005].

observed.

Hydrocarbon oxidation begins with the *initiation* reactions in which stable fuel molecules produce highly reactive radicals which further react with the fuel molecules and each other to form more radicals and stable molecules. The formation of stable molecules terminates that particular chain of reactions and therefore, such reactions are called *termination* reactions. The process in which radicals react to give off new active radicals is called *chain propagation*. If more radicals are formed than those being consumed then the propagation reactions are termed as *chain-branching* reactions. Chain propagation may lead to the formation of metastable radicals which survive longer than the others. These radicals may further go on to form either stable or active radicals and thus can result in a relatively slow increase in the number of radicals. Certain peculiar features of the hydrocarbon combustion such as two stage ignition, long ignition delays and NTC phase are explained by this type of reactions and these are known as *degenerate chain branching* reactions.

Since gasoline is a mixture of various different hydrocarbon molecules, its ignition behaviour is determined by complex interactions of these constituent molecules. In order to understand better the oxidation chemistry of gasoline; compounds belonging to the major constituent families of gasoline can be stud-

ied. The blends of these compounds can then be used as surrogates for gasoline.

In this work some of the key established features of hydrocarbon oxidation are presented and then the three reduced chemical kinetic schemes for gasoline surrogates presented in Section 2.5 are studied. The objectives of this study are

- to identify the key mechanisms employed in these models to determine if they are in accord with the established understanding of hydrocarbon oxidation
- to investigate the interactions of intermediate radicals formed during the oxidation of gasoline surrogates, in particular the effect of toluene and ethanol addition on the ignition precursors
- to investigate the reactivity exhibited by a gasoline surrogate in engine conditions and how they may lead to autoignition

3.2 General features of hydrocarbon oxidation

3.2.1 Low temperature oxidation

One of the main differences attributed to the low and high temperature oxidation pathways is the way the original carbon chain is broken down. At low temperatures the carbon chain is attacked by oxygen and various other active radicals, most important of which are H, O, OH and $\mathrm{HO_2}$. The resulting radicals undergo scission reactions which progressively shortens the carbon chain such as $\mathrm{C_4} \longrightarrow \mathrm{C_3} \longrightarrow \mathrm{C_2} \longrightarrow \mathrm{C_1}$. However, at higher temperatures the decomposition occurs through the breakage of the weakest bonds (typically the tertiary bonds) resulting in a shortening of the carbon chain such as $\mathrm{C_4} \longrightarrow 2\,\mathrm{C_2}$ [Griffiths, 1995]. Therefore, the differences in the carbon chain length of different alkanes have perceptible differences in the low temperature oxidation chemistry. However, at high temperatures, alkanes of different lengths quickly breakdown to similar smaller fragments and therefore size effects on the type of reaction pathways are negligible.

The selectivity of the initiation reactions is dependent on the oxygen concentration and the temperature. Consider the following two possibilities of initiation reactions:

$$\mathrm{RH} + \mathrm{O_2} \longrightarrow \mathrm{R^{\cdot}} + \mathrm{HO_2} \tag{3.1}$$

and

$$\mathrm{RH} \longrightarrow \mathrm{R_1} + \mathrm{R_2} \tag{3.2}$$

For typical alkanes, at temperatures higher than 1000 K, the reaction rate for the H atom abstraction reaction (3.1) is $1/1000^{\text{th}}$ of the decomposition initiation reaction (3.2). Therefore at temperatures higher than 1000 K, decomposition is the more significant pathway. Whereas at temperatures below 1000 K, the predominant initiation reaction is abstraction of H atom from the fuel molecule (3.1). At temperatures higher than 1400 K, decomposition is the sole initiation reaction [Griffiths and Barnard, 1995]. What follows at low temperatures from reaction (3.1) is the different ways in which its products react with its original reactants. One of the most important of these reactions is the alkyl/alkylperoxy radical equilibrium,

$$\mathrm{R^{\cdot}} + \mathrm{O_2} \longleftrightarrow \mathrm{RO_2} \tag{3.3}$$

The direction of reaction (3.3) has important implications on the reactions to follow. The activation energy for the forward reaction is negligible therefore at low temperatures more and more alkylperoxy radicals ($\mathrm{RO_2}$) are formed. The activation energy for the reverse reaction is considerable, about 30 kcal/mole for alkanes, therefore, the reverse reaction becomes dominant at high temperatures. This shift in equilibrium can be regarded as the transition from the low to intermediate temperature range. In addition to this, a temperature increase to the benefit of olefin formation through reaction (3.11) causes a reduction of the global reaction rate. This results in the manifestation of the NTC behaviour typical of most alkanes.

After the H atom abstraction reactions, the key radicals present in the system are $\mathrm{R^{\cdot}}$, $\mathrm{HO_2}$, OH and $\mathrm{RO_2}$. $\mathrm{HO_2}$ is inactive at low temperatures and therefore contributes little to the chain branching. From common initiation and initial propagation reactions, three types of degenerate branching involving alkyl peroxy may ensue [Sokolik, 1960]. At temperature less than 650 K, the chain is mainly propagated through a radical attack on the fuel molecules such as:

$$\mathrm{RO_2} + \mathrm{RH} \longrightarrow \mathrm{R^{\cdot}} + \mathrm{ROOH} \tag{3.4}$$

However, as the temperature increases the role of acyl hydroperoxides (see reaction 3.10) increases and finally, pathways involving formaldehyde become sig-

nificant. These pathways are given as follows.

$$\mathrm{RO_2} \longrightarrow \mathrm{R^{\cdot}CH_2CH_2OO} \longrightarrow \mathrm{R^{\cdot}O} + \mathrm{CH_3CHO} \tag{3.5}$$

$$\mathrm{RO_2} \longrightarrow \mathrm{R^{"}CH_2O^{\cdot}} \longrightarrow \mathrm{R^{"}} + \mathrm{CH_2O} \tag{3.6}$$

Reactions such as (3.7) which cause the build-up of alkyl hydroperoxide radicals are crucial to the early stages of heat release as the weak $\mathrm{O{-}O}$ bond easily breaks resulting in the formation of two active radicals:

$$\mathrm{ROOH} \longrightarrow \mathrm{RO} + \mathrm{OH} \tag{3.7}$$

The sudden accumulation of OH radicals results in further oxidation of the smaller fuel fragments and partially oxidized species through exothermic reactions signifying a first stage mild ignition. Sokolik [1960] cites Semenov on the assertion that decomposition of a peroxide radical can only occur once it has undergone internal isomerisation. This isomerisation of $\mathrm{RO_2}$ radicals occurs through the abstraction of an internal H atom from a location for which the *ring-strain energy* and the energy for H atom abstraction is the lowest [Westbrook et al., 1991]. Such a reaction can be depicted as:

$$\mathrm{RO_2} \longrightarrow \mathrm{QOOH} \tag{3.8}$$

The hydroperoxyalkyl radicals (QOOH) contain a vacant bond on one of the carbon atoms as well as the weak $\mathrm{O{-}O}$ bond as a result of which QOOH has a strong potential for undergoing four different chain branching reactions depending on the temperature. Its dissociation in low and intermediate temperature regime forms another important pathway as it produces smaller olefins and oxygenated species such as aldehydes. Aldehydes undergo oxidation much quicker due to the weak aldehydic $\mathrm{C{-}H}$ bond. They also have the potential to carry on chain branching and produce ROOH radicals as following; [Kolaitis and Founti, 2010].

$$\mathrm{RCHO/CH_2O} + \mathrm{RO_2} \longrightarrow \mathrm{RC^{\cdot}O/CHO} + \mathrm{ROOH} \tag{3.9}$$

Reaction (3.9) not only contributes to the ROOH chain branching route but forms acyl radicals ($\mathrm{RC^{\cdot}O}$), upon further oxidation of which, acyl hydroperoxy radicals, ($\mathrm{RCO(OO^{\cdot})}$), are formed. These radicals are more stable than alkylper-

oxy radicals and therefore may become important as the rate determining pathway [Koert et al., 1994]. An H atom abstraction as shown in the following reaction, produces acyl hydroperoxide or peracid.

$$\mathrm{RCO(OO^{\cdot})} + \mathrm{RH} \longrightarrow \mathrm{RCO(OOH)} + \mathrm{R^{\cdot}} \tag{3.10}$$

Koert et al. [1994] reports that although the formation and decomposition of acyl hydroperoxide provides a low temperature pathway, it is generally regarded unimportant, possibly because acyl hydroperxide is formed through addition of molecular oxygen to an acyl radical, this oxygen is only abundantly available for fuel lean conditions and since the reactions has a high activation energy, this pathway is only important for fuel lean and high temperature conditions.

Further addition of oxygen to QOOH can also occur forming hydroperoxyalkylperoxy radicals ($\mathrm{O_2QOOH}$). This pathway contributes substantially to the radical pool as $\mathrm{O_2QOOH}$ isomerises and subsequently dissociates to form ketohydroperoxy ($\mathrm{OQ^{'}OOH}$) and OH radicals. Further decomposition results in diketone ($\mathrm{OQ^{'}O^{\cdot}}$) as well as OH. At relatively higher temperatures QOOH may form through different reactions: cyclic ethers, ketones, $\mathrm{HO_2}$ and OH [Kolaitis and Founti, 2010].

This pathway, the isomerisation of ROO, followed by double $\mathrm{O_2}$ addition, has been found to be crucial in producing the NTC phase observed in alkanes and particularly the straight chained alkanes in which case the isomerisation is favoured for reasons described in later sections. Due to this significance of the so-called peroxy radical isomerisation and decomposition (PRID) pathway, it is central to almost all of the PRF mechanisms. Further details on this pathway and its reaction rate parameters can be found in [Curran et al., 1998a].

As the temperature increases, the reversibility of the reaction (3.3) starts to play its key role. The decomposition of $\mathrm{RO_2}$ causes a scarcity of this radical and this in turn starves the formation of peroxide radicals. This process intensifies as the temperature increases and more and more $\mathrm{RO_2}$ radicals vanish. This slowing down of the degenerate chain branching gives way to the non-branching reactions which cause a decrease in the global reaction rate. As the temperature increases beyond the low/intermediate temperature regime, the H atom abstraction reaction is not the only initiation channel. The fuel molecules undergo pyrolytic decomposition and form molecules of smaller molecular weights, including alkanes and olefins. But this is not the only source of smaller fuel molecules. From the reverse of reaction (3.3), more and more $\mathrm{R^{\cdot}}$ radicals are available to in-

teract with oxygen for further H atom abstraction,

$$\mathrm{R}^{\cdot} + \mathrm{O}_2 \longrightarrow \text{olefin} + \mathrm{HO}_2 \tag{3.11}$$

also, HO_2 radicals are active at high temperatures in reactions such as:

$$\mathrm{RH} + \mathrm{HO}_2 \longrightarrow \mathrm{R}^{\cdot} + \mathrm{HOOH} \tag{3.12}$$

These alternate reactions start to compensate for the NTC phase reduction of RO_2 radicals. HO_2 radicals formed in reaction (3.11) establish a $\mathrm{H}_2\mathrm{O}_2$ formation channel through reaction (3.12). At higher temperatures $\mathrm{H}_2\mathrm{O}_2$ is unstable and further decomposes to form two OH radicals. At intermediate to high temperatures HO_2 and $\mathrm{H}_2\mathrm{O}_2$ functionally replace RO_2 and ROOH.

3.2.2 High temperature oxidation

At high temperatures, the chain initiation reactions are predominantly the decomposition reactions in addition to the H atom abstraction reactions. Hydrocarbon fragments thus formed are short lived and undergo α or β scission, or polymerisation. β scission is thermodynamically favoured over α scission and it is the dominant reaction. In β scission reactions, the bond at a distance of two from the free radical breaks forming an ethene. Curran et al. [1998a] classified elementary reactions for n-heptane and iso-octane into 25 major classes encompassing the whole low to high temperature regimes. They demonstrated that high temperature oxidation can be simulated by means of 9 classes of reactions. Those reaction classes are not discussed here in detail, however, it is summarised that the decomposition of not only fuel molecules but the alkyl, alkenyl and olefins is a major branching mechanism. Internal H atom isomerisation carries on at high temperatures. Other smaller oxygenated species such as $\mathrm{CH}_2\mathrm{O}$ and CO along with olefins and smaller alkanes take over as the main participants of the subsequent oxidation reactions. H atom and CO oxidation is therefore central to any chemical kinetic mechanism. Participation of HO_2 radicals is increased due to their higher reactivity at these temperatures.

Important species	Andrae Model	Golovitchev Model	Reitz Model
RO_2	$C_8H_{17}OO$	$R_1C_8H_{17}OO$, $R_2C_8H_{17}OO$	$C_8H_{17}OO$
Oxygenated species			
Ketones, Ketohydroperoxides	$OC_8H_{15}O$ (diketone)	$C_7H_{14}CHO(OOH)$	Octyl ketohydroperoxide
Aldehydes:	CH_2O, CH_3CHO	CH_2O, CH_3CHO	CH_2O, CH_3CHO
Olefins	C_2H_4, C_4H_8, C_8H_{16} (DIB)	C_2H_4, C_3H_6, C_4H_8	C_2H_4, C_3H_4, C_3H_6

Table 3.1: Key intermediate species for iso-octane oxidation identified in the three reduced mechanisms during the low/intermediate temperature regimes.

3.3 Numerical predictions of oxidation pathways

Three reduced chemical kinetic mechanisms relevant to gasoline surrogates, introduced in Section 2.5, have been further studied. The concentrations of species which are known to act as active centres, as discussed in Section 3.2, have been monitored. The pathways involved in the emergence of these species have been discussed in the light of the accepted understanding of hydrocarbon oxidation. The chemical kinetics has been modelled as a $0 - D$ constant volume adiabatic system at initial conditions of 40 bar pressure and 700 K temperature for a stoichiometric mixture of the fuel being studied, with air. These $p - T$ conditions have been chosen as it is the low temperature and relatively high pressures which occur in the preflame gas of a SI engine.

3.3.1 Iso-octane

For the studied $p - T$ condition (i.e. 700 K and 40 bar), Fieweger et al. [1997] have shown the autoignition delay time of the stoichiometric iso-octane and air mixture to be 10 ms in their shock tube experiments. All three models are found to predict ignition delay times with appreciable accuracy for various fuels under different conditions, however, some models produce better results than the others. At the present operating condition, Reitz model predicts the closest ignition delay time (9.6 ms) to the shock tube, Andrae and Golovitchev models over predict by as much as 5 ms to 15 ms, respectively (Figure 2.11a).

Lenhert et al. [2009] and Vanhove et al. [2006] experimentally investigated the chemical interactions of various hydrocarbons and their intermediates at low and intermediate temperature regimes. Lenhert et al. [2009] observed in their pressurized flow reactor experiments that at a pressure of 8 atm, stoichiometric iso-octane starts to show a weak NTC behaviour at 665 K at which point only 20% of the iso-octane is converted into intermediate species. They found ethers to be the most abundant radicals comprising of 11% of the initial carbon atoms. Significance of ethers was also observed by Vanhove et al. [2006] in their RCM studies. The three kinetic models however do not replicate this observation (Figures 3.2, 3.3 & 3.4). The three models assume the disintegration of the alkane chain into smaller species through a ketohydroperoxy channel. Dihydroperoxyalkyl (O_2QOOH) are the most abundant radicals formed. There are no alkyl hydroperoxides ($ROOH$); the alkylperoxy radicals (RO_2) isomerise to form $QOOH$, followed by further O_2 addition. The difference between the three models is in the level of reduction applied to these steps. There is a clear similarity between the three models in terms of the selectivity of these intermediate functional groups which have been summarised in Table 3.1. However, the reaction coefficients for these elementary reactions are different and so are the predicted induction times as well as the extent of NTC region. After the ketohydroperoxide, olefins constitute most of the initial carbon atoms, particularly in the case of Andrae model, see Figure 3.2. Predicted amounts of other oxygenated species such as the aldehydes and ketones are minute. This was also observed by Lenhert et al. [2009] that aldehydes comprised of the 2% of the initial carbon atoms and ketones 1%. Species which are relatively stable accumulate to higher concentrations and their significance is because of their role in degenerate chain branching and the rate determination of the global reaction.

As described in Section 3.2, according to the 'classical' understanding of the hydrocarbon oxidation pathways, olefin formation is significant at higher temperatures and normally low temperature oxidation is attributed to the peroxy radical chemistry. The models do not include any $ROOH$ radicals. Steps are included for one isomer of octylperoxy in Andrae and two in the Golovitchev model; which internally isomerise to form $QOOH$. These steps have been lumped together into a single step in the Reitz model which predicts minute amounts of RO_2 radicals and most of the activity takes place through an octyl ketohydroperoxide radical and olefins. Significant amount of olefins is predicted before the first stage of ignition, however their amounts remain constant until a second stage ig-

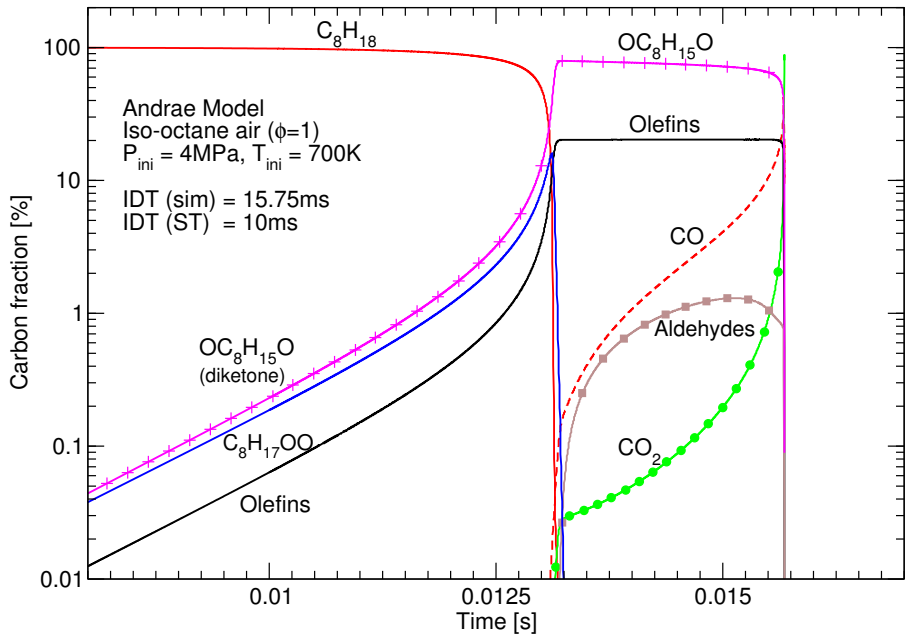

Figure 3.2: Predicted carbon fraction of the key intermediate species produced. See Table 3.1 for grouped species.

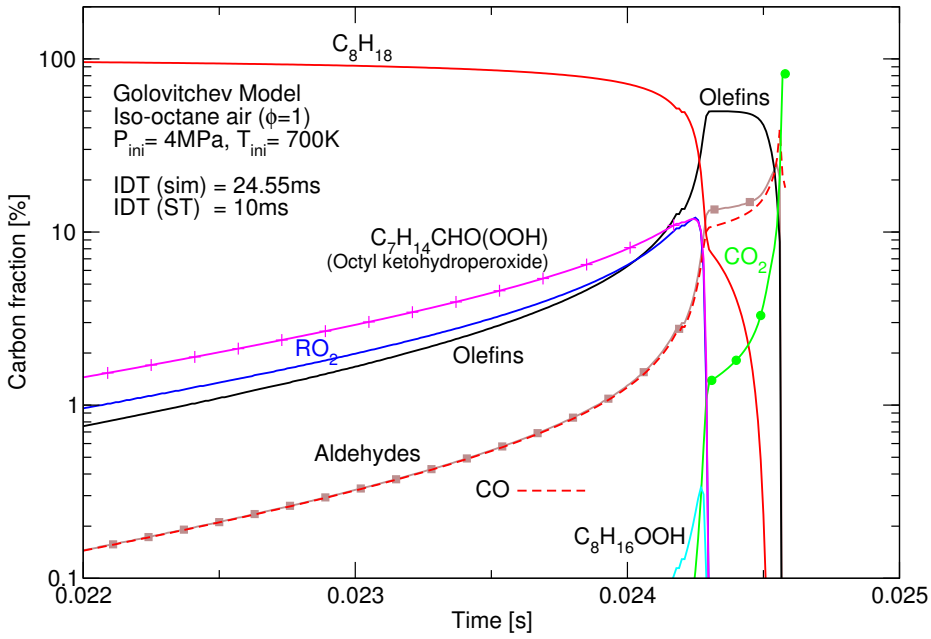

Figure 3.3: Predicted carbon fraction of the key intermediate species produced.

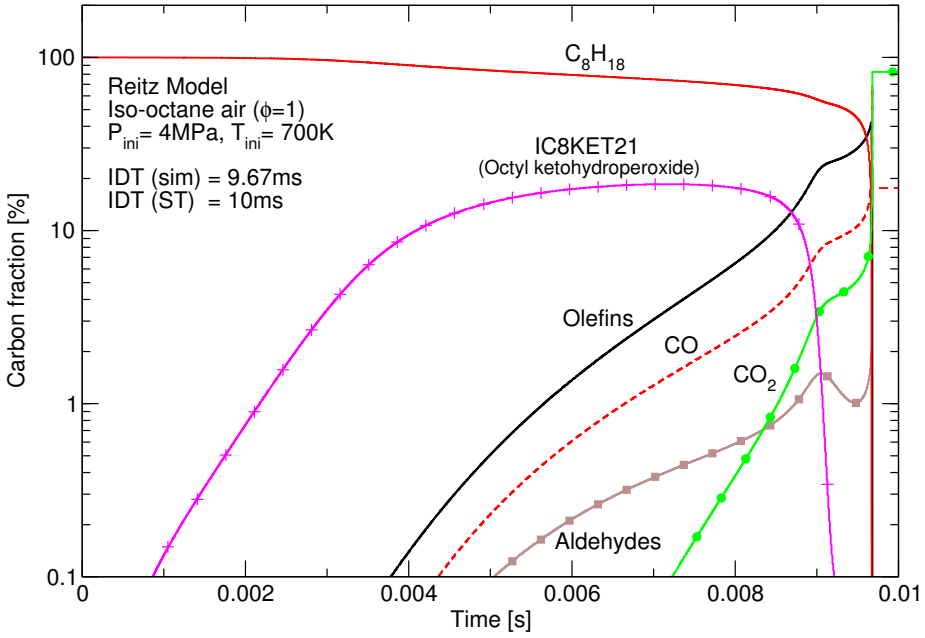

Figure 3.4: Predicted carbon fraction of the key intermediate species produced.

nition takes place which is when the smaller species are oxidised to form CO and CO_2. Andrae model constitutes a submodel for diisobutylene (DIB, JC_8H_{16}) oxidation and DIB constitutes most of the olefins during iso-octane oxidation. In case of the Reitz and Golovitchev models, it is the smaller olefins which account for most of the olefins, see Table.3.1. Formation of CO starts before the first stage of heat release in all models except the Andrae model which starts to predict a noticeable amount of CO only after the first stage ignition.

3.3.2 N-heptane

Where the oxidation pathways are quite similar for different alkanes, their relative importance may be different and also the reaction rates which determine their different reactivities. The straight chain alkanes are more prone to radical attack and H atom abstraction because of a greater number of secondary bonding sites which offer a lower bond energy barrier than a primary bonding site. Moreover, the alkylperoxy radical isomerisation is favoured more by the long straight chained structure than a branched one due to the lower intermediate ring strain energy. The higher rate of heptylperoxy radical isomerisation, the subsequent breaking of the peroxy bond and the formation of OH radicals results in the shorter induction times and a lower octane rating than its branched isomers.

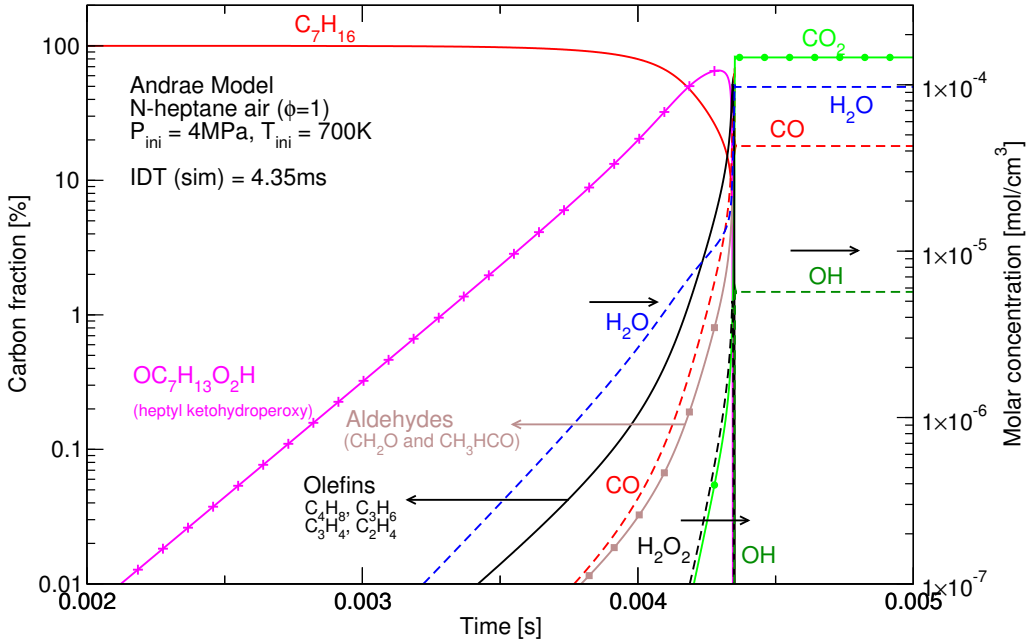

Figure 3.5: Carbon fraction of carbon containing key intermediates (left axis). Molar concentration of OH, hydrogen peroxide and water (right axis).

Such effects of the molecular size and structure on the autoignition chemistry and octane rating were studied by Westbrook et al. [1991].

Lenhert et al. [2009][1] observed significantly higher concentration of aldehydes for n-heptane than iso-octane. They explained this by the favoured double isomerisation and the decomposition of the QOOH radical. The aldehyde formation in case of iso-octane was said to take place through the formation of ethers from QOOH. The three reduced models; Andrae, Golovitchev and Reitz, predict the combined carbon fraction of $\mathrm{CH_2O}$ and $\mathrm{CH_3CHO}$ to be 1.3%, 15%, 1.5% respectively for iso-octane, and 7.3%, 11.5% and 5% for n-heptane, at the time of the first stage of ignition. The percentage carbon fraction is lower for iso-octane for Andrae and Reitz model just as observed by Lenhert et al. [2009]. Similar to iso-octane, olefins constitute the second most carbon atoms after the ketohydroperoxy radicals but their percentage is higher in the case of iso-octane. The reason being relatively slower isomerisation which results in other channels such as reaction (3.11), to compete with the isomerisation and form more olefins and $\mathrm{HO_2}$ radicals. Generally the most abundant olefins are ethene and propene but iso-butene and propadiene are also formed in considerable amounts.

One interesting difference between the three models is of the time span be-

[1]The n-heptane experimental conditions were: ϕ=0.51, 8 atm, 100 ms residence time.

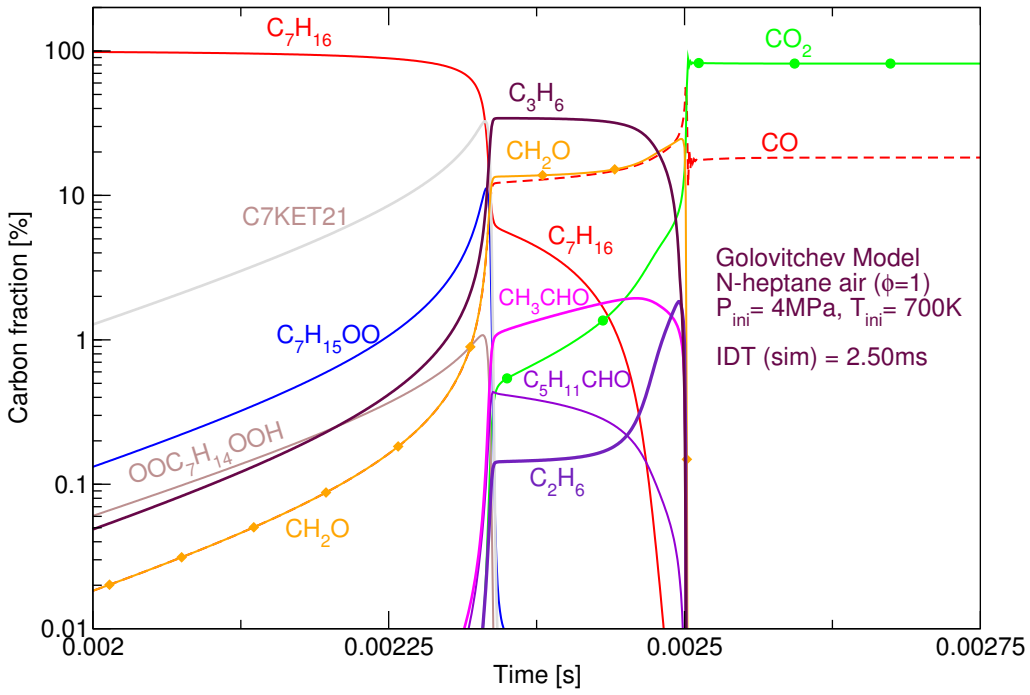

Figure 3.6: Carbon fraction of carbon containing key intermediates.

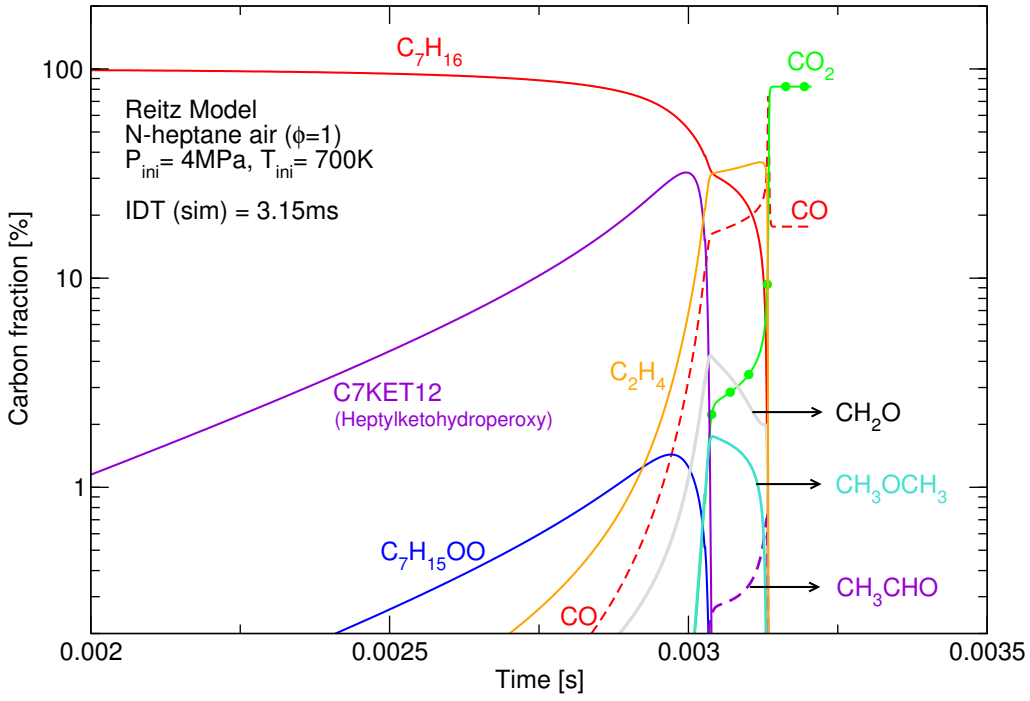

Figure 3.7: Carbon fraction of carbon containing key intermediates.

tween the 1st and 2nd stages of ignition. Andrae model predicts the longest ignition delay time ($\tau_{ign} = 4.35$ ms) to a single stage of ignition (Figure 3.5), however, the Golovitchev ($\tau_{ign} = 2.50$ ms) and Reitz models ($\tau_{ign} = 3.15$ ms) predict, although very close but two distinct heat release events i.e. an initial accumulation of radicals leading on to a thermal runaway causing a second stage of ignition, see Figures 3.6 & 3.7. At similar $p-T$ conditions of 41.4 bar and 695 K, Hartmann et al. [2011] have shown the ignition delay time of n-heptane and air mixture ($\phi = 1$) to be 2.69 ms as shown in Figure 2.11. N-heptane is known to exhibit the strongest NTC behaviour among typical gasoline surrogates. This delaying of the ignition due to NTC behaviour results in a pronounced separation of first stage or mild ignition from the second stage ignition. Ciezki and Adomeit [1993] showed in their shock tube experiments that as the initial temperature was decreased from 1030 K at pressures in the range of 12.3 - 15.1 bar, a pressure increase due to a first stage ignition appeared and started to become more pronounced and began to move closer to the second stage ignition and eventually merged into it when the temperature was low enough. From Figure 2.11b it can be seen that the NTC phase begins at a temperature of about 833 K. Therefore, at 700 K, n-heptane is expected to show a single stage ignition.

3.3.3 Toluene

Toluene exhibits negligible reactivity at low $p - T$ conditions and has been found difficult to ignite below 900 K and 17.0 bar, at which the ignition delay time is 218 ms [Roubaud et al., 2000]. At the time of this work, the lowest initial temperature measurement for toluene ignition in a shock tube was found to be 859 K (P =41.75 bar, τ =4.91 ms) made by Hartmann et al. [2011]. All three reduced models significantly over-predict the ignition delay time for these conditions. Although this temperature condition is higher than the 700 K temperature studied in the case of PRFs, a study of toluene oxidation pathways in the three reduced models at this condition is warranted as the objective is to identify key pathways and those intermediate species which take part in them.

The foundation studies of the oxidation of aromatics such as toluene and benzene at low temperatures were done by Burgoyne [1940] who identified the formation of benzyl alcohol, benzaldehyde, benzoic acid and phenolic compounds. Developing on this, Barnard and Ibberson [1965] laid out one of the earliest frame works of the low temperature toluene oxidation pathways using analogies to the aliphatic hydrocarbon oxidation. Using chromatographic analyses they identi-

fied intermediates as the products of extensive disintegration of the aromatic ring. Abstraction of the benzylic hydrogens forming benzyl radicals was proposed as the initiation reaction:

$$C_6H_5CH_3 + O_2 \longrightarrow C_6H_5CH_2 + HO_2 \tag{3.13}$$

The side chain is removed by an initial addition of O_2 forming benzylperoxy ($C_6H_5CH_2OO$) radicals which go on to dissociate rather than isomerise which is the case for alkanes. These dissociation rections are given as:

$$C_6H_5CH_2OO \longrightarrow C_6H_5O + HCHO \tag{3.14}$$

$$C_6H_5CH_2OO \longrightarrow C_6H_5CHO + OH \tag{3.15}$$

However, an elongation of the side chain can result in the formation of alkylperoxy radicals which can isomerise in pathways similar to those of the alkanes (Griffiths and Mohamed [1997]).

The works of Brezinsky [1986] provided a detailed understanding of the oxidation pathways of aromatics at high temperatures (875 - 1500 K) and the elementary reactions proposed in their mechanism are still used in toluene mechanisms including the three reduced models studied in this work. The initial generation of a radical pool comprising of HO_2, H, O and OH takes place either pyrolitically or through H atom abstraction. The type of initiation reactions normally has a negligible kinetic effect and it is the chain propagation reactions involving the initial radical pool and the fuel which determine the global reaction rate [Griffiths and Barnard, 1995]. The most aggressive attack on toluene is of the OH radicals followed by the H atoms. These reactions result in the formation of benzyl radicals, however this retards the chain propagation since the benzyl radicals are less reactive than OH and H radicals. This is because the benzene ring is resonance stabilised and in the case of alkyl benzenes (e.g. toluene) this has a dual effect of promoting the abstraction of benzylic hydrogen and then an inhibiting effect on the further oxidation of the benzyl radical [Roubaud et al., 2000]. Therefore benzyl radicals accumulate to considerable concentration and are highly susceptible to combining with H atoms and forming toluene and thus results in the slow conversion of toluene.

One of the key intermediates, benzaldehyde, is formed through more than one channels, e.g. reaction (3.15) or through reactions of benzyl with O_2 which

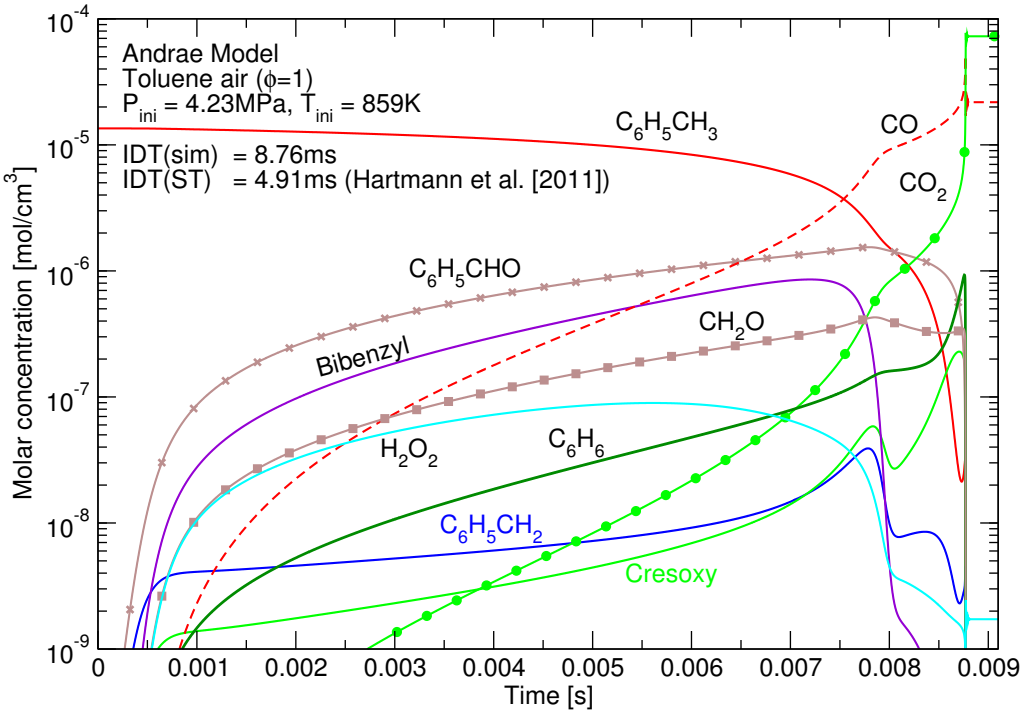

Figure 3.8: Molar concentration of the key intermediates formed during the pre-ignition reactions of toluene as predicted by the Andrae model.

also produces an OH radical:

$$C_6H_5CH_2 + O_2 \longleftrightarrow C_6H_5CH_2O{-}O \longrightarrow C_6H_5CHO{-}OH \longrightarrow C_6H_5CHO + OH \tag{3.16}$$

Reaction with HO_2, also produces benzylhydroperoxide ($C_6H_5CH_2O{-}OH$) which breaks to form benzaldehyde, OH and H radicals [Vanhove et al., 2006]. Benzaldehyde can further undergo H atom abstraction to form benzoyl through the following reaction.

$$C_6H_5CHO + X \longrightarrow C_6H_5CO + XH \tag{3.17}$$

where, X can be O_2, OH, H, O, CH_3 or HO_2. Benzoyl decomposes to form phenyl (C_6H_5) and CO. The final ignition is attributed to the degenerate branching caused by H_2O_2.

The toluene mechanism in the Reitz model is based on the TRF mechanism by Andrae et al. [2007] and comprises a primary set of channels for the oxidation of toluene to benzene and benzaldehyde. The toluene mechanism in the three reduced models includes a benzene submodel which offers channels for

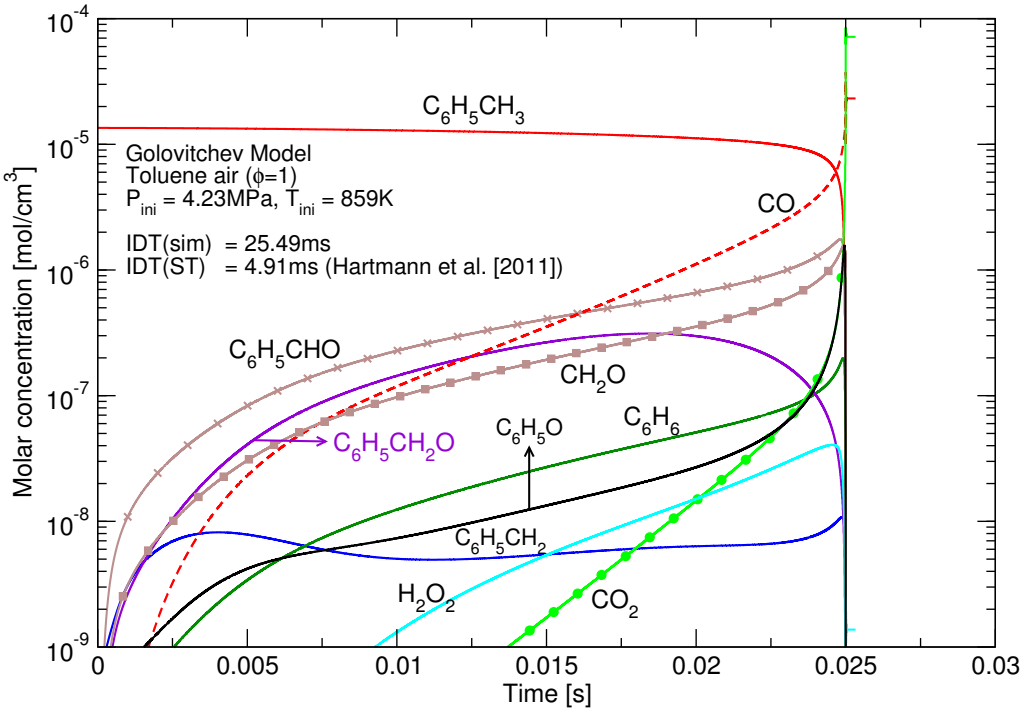

Figure 3.9: Molar concentration of the key intermediates formed during the pre-ignition reactions of toluene as predicted by the Golovitchev Model.

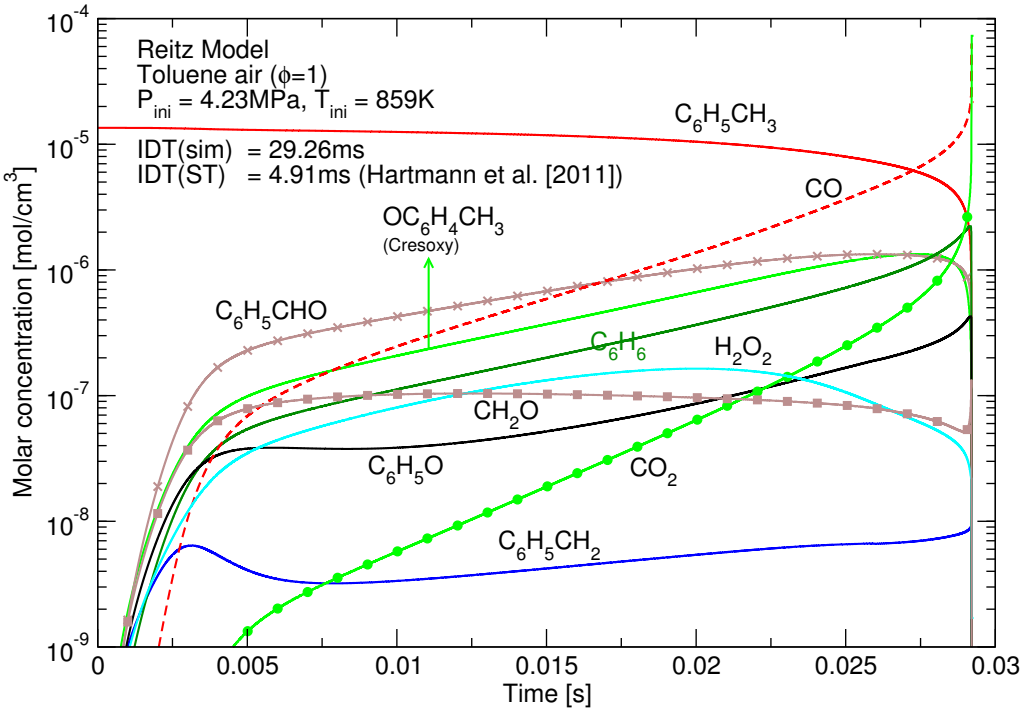

Figure 3.10: Molar concentration of the key intermediates formed during the pre-ignition reactions of toluene as predicted by the Reitz Model.

the oxidation of the phenyl radicals through smaller hydrocarbon molecules. It is not surprising to see a great similarity in the toluene oxidation pathways of three reduced models as the toluene oxidation is not so well understood as is the aliphatic oxidation and due to the limited sources of validation, most of the reduced models are based on similar mechanisms albeit different elementary reaction coefficients.

As proposed by the earlier studies; reduced models reveal that the most abundant intermediate species soon after the initiation reactions is benzaldehyde (Figures 3.8, 3.9 & 3.10). Its formation from the benzyl radicals occurs through reactions of zero activation energy (E_a). The Andrae model includes a reversible combination reaction of benzyl radicals to form bibenzyl in substantial concentration through a zero E_a reaction (Figure 3.8). Since there are no other reactions involving bibenzyl, it essentially withholds the benzyl radicals until the reverse reaction intensifies with temperature rise and it decomposes to from benzyl radicals. This can be seen as the increase in benzyl concentration during the time span of 7 to 8 ms in Figure 3.8. Formation of CH_2O is also substantial from reactions of benzyl with O_2 or HO_2 forming phenyl, CH_2O and an additional OH in case of HO_2. Although there are more elementary reactions for the formation of phenyl radicals than CH_2O, phenyl radical concentration is minute because of its quicker consumption in reactions with radicals such as H, OH, O and HO_2 leading to the formation of phenoxy radicals (C_6H_5O) and phenol (C_6H_5OH). Considerable amounts of cresoxy radicals ($OC_6H_4CH_3$) are predicted by the Andrae and Reitz models through the addition of O to toluene giving off a H atom. Decomposition of $OC_6H_4CH_3$ to form benzene, H and CO contributes substantially to the overall heat of reaction.

3.3.3.1 Effect of doping on toluene oxidation

A comparison of the heat release of elementary reactions in Andrae model reveals that most of the heat is released from the reactions involving the breaking of the H_2O_2 radical and the termination reactions of OH resulting in the formation of water. It is therefore postulated that in a blend, an early presence of the H_2O_2 radicals resulting from the oxidation of another blend component should promote toluene oxidation. This has been demonstrated in Figure 3.11, which shows the autoignition simulation results of a stoichiometric mixture of toluene and air and when H_2O_2 is added to it in amounts of 1% and 5% by mole of toluene. The effect of an initial presence of H_2O_2 radicals on the ignition delay time is non-

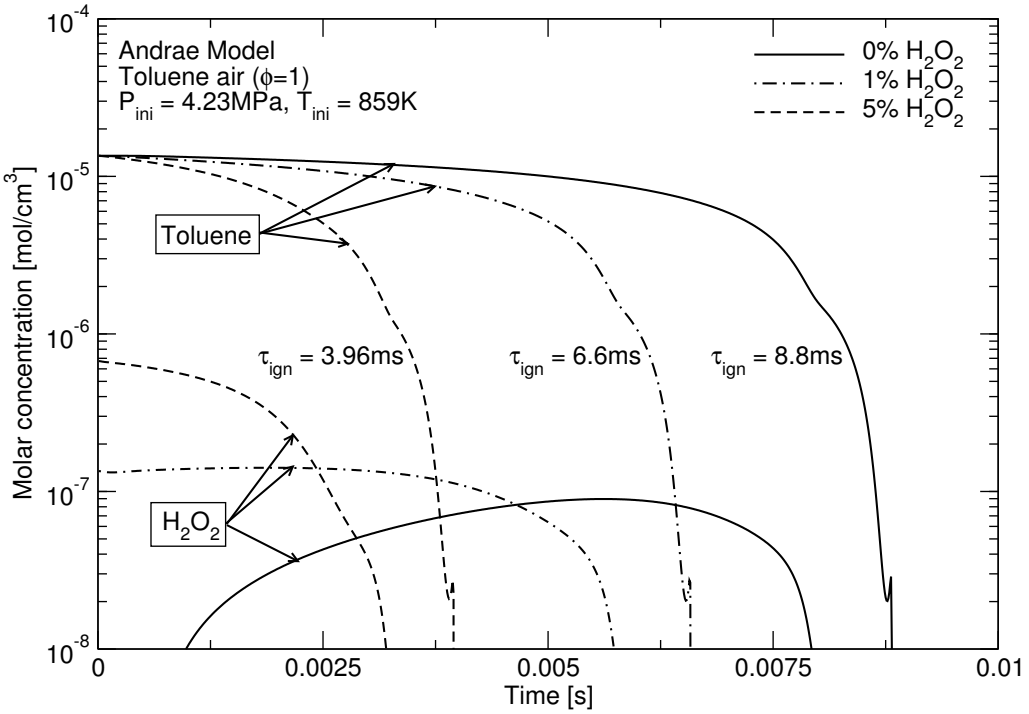

Figure 3.11: Effect of hydrogen peroxide doping on induction time of toluene as predicted by the Andrae model.

linear i.e. addition of 1% of H_2O_2 substantially reduces the ignition delay time, by 25%, and a further increase in its concentration decreases the ignition delay time by only about 15%. The possible reactions involving H_2O_2 are its $O-O$ breaking and the chain propagation reactions with the other active radicals. H_2O_2 decomposition to form OH radicals occurs at temperatures around 1000 K and therefore this pathway is not expected to contribute to the OH concentration in the early phases of oxidation. That is why no additional OH radicals are observed with doping, however, there is a quicker emergence of the HO_2 radicals. The reactions involving the production of the HO_2 radicals in Andrae model should produce the same number of H_2 and OH radicals in each cycle of reactions. OH radicals are consumed as soon as they are formed in the initiation reactions. This is seen as a sharp increase in the benzyl radicals in case of doping, rather than a more gradual and delayed increase as seen in Figures 3.8 to 3.10. Water is also formed in two of the reactions involving H_2O_2 which terminates the chain. It is thought that an increase in the initial concentration of H_2O_2 is counter balanced by the resonance stabilisation of benzyl radicals and higher rates of termination reactions which starts to diminish its effects on the ignition delay time.

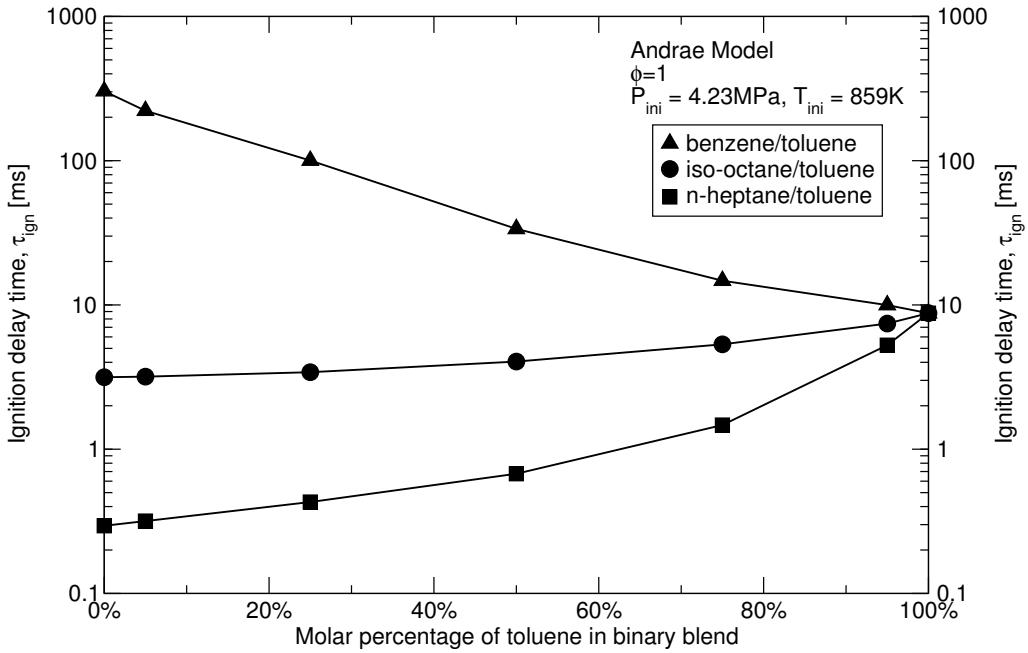

Figure 3.12: Ignition delay times of binary blends of toluene with benzene, iso-octane and n-heptane for stoichiometric mixtures with air.

3.3.3.2 Effects of binary blending on toluene ignition delay time

Ignition delay times for binary blends of toluene with benzene, iso-octane and n-heptane at the same $p - T$ condition of 42.3 bar and 859 K have been predicted using the Andrae model and presented in Figure 3.12. Blending two fuels may result in interaction of two sets of intermediate species creating new pathways and forming new intermediates. However, there may not be a mechanism change merely a thermal effect from the more reactive blend component. To the best of the authors knowledge, gas sampling studies of TRFs in the literature so far do not show any formation of new intermediates which were absent during the oxidation of the individual components. The mechanism of oxidation essentially remains the same, however, certain pathways may proceed at different rate depending on how the component fuels affect the active radical pool. Vanhove et al. [2006] studied the autoignition chemistry of the toluene-n-heptane and toluene-iso-octane blends at low $p - T$ conditions. For n-heptane and toluene blend, they observed that the mixture oxidation rate was mainly governed by the fast n-heptane chemistry. The effect of toluene was merely to retard the chemical activity by scavenging the active radicals leading to the formation of benzyl, benzaldehyde and ethyl benzene. The resulting shape of the ignition delay curve on an Arrhenius plot, showed similar NTC phase for pure n-heptane and the 50/50 blend

of n-heptane and toluene. However, in case of a 35/65 toluene-iso-octane blend they observed that the ignition delay sensitivity to temperature is dependent on the toluene content. Ignition delay times are more sensitive to temperature at higher values when toluene is present. More interestingly, they observed that at an initial temperature of about 856 K the ignition delay of a blend containing upto 60% by mole of toluene was weakly sensitive to the percentage of toluene. However, the ignition delay increased dramatically when the toluene percentage was increased from 60% to 80%. Autoignition simulations of iso-octane and toluene blends as shown in Figure 3.12, show no such behaviour. In fact, the ignition delay time predictions of all the binary blends show a non-linear but a gradual change as the toluene content is changed. Toluene also diminishes the already weak NTC behaviour of pure iso-octane. This suggests a strong interaction of the radical pools of iso-octane and toluene.

3.3.4 Ethanol

Ethanol oxidation is quite different from that of the hydrocarbons, however, most alcohols behave in a similar way to each other. Ethanol oxidation is initiated through following reactions:

$$\mathrm{C_2H_5OH} \longrightarrow \mathrm{CH_3} + \mathrm{CH_2OH} \tag{3.18}$$

$$\mathrm{C_2H_5OH} + \mathrm{X} \longrightarrow \{\mathrm{CH_2CH_2OH}\ \textit{or}\ \mathrm{CH_3CHOH}\ \textit{or}\ \mathrm{CH_3CH_2O}\} + \mathrm{XH} \tag{3.19}$$

Reaction (3.19) shows the formation of the three possible isomers after the H atom abstraction from ethanol. The 15 reactions involving these active radicals leading to the formation of the three isomers are identical in the Andrae and Golovitchev models which are based on the works of Marinov [1999] and the two models produce the similar ignition delay times as can be seen in Figure 2.11d. The reactions are present in the Reitz model but with different Arrhenius parameters. The Golovitchev model has a duplicate specie ($\mathrm{C_2H_5O}$) for one of the isomers namely $\mathrm{CH_3CH_2O}$ and is formed in three similar reactions to those of $\mathrm{CH_3CH_2O}$. The model also has two H atom abstraction reactions of ethanol with molecular oxygen which the two other models lack. The rate coefficient ratios of these abstraction reaction are crucial as the subsequent secondary reactions are

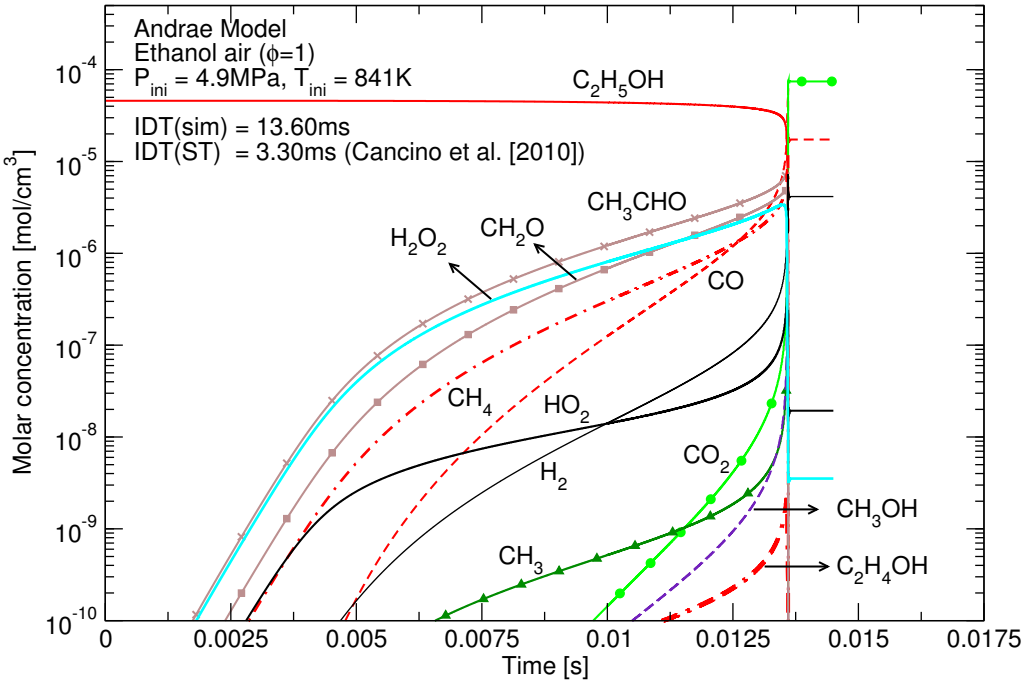

Figure 3.13: Molar concentration of the key intermediates formed during the pre-ignition reactions of ethanol as predicted by the Andrae model.

determined by the concentrations of these isomers. Limited information on these reaction coefficients has been reported in the literature and most of the mechanisms use the values proposed by Marinov [1999] with slight enhancements. Chain propagation involves reactions of the C_2 radicals with the active species. An important intermediate is CH_3CHO and therefore a mechanism for its oxidation is also included in any ethanol mechanism. CH_3CHO may dissociate to form CH_3 and HCO or react with O_2 to form acetyl (CH_3CO) and HO_2 radicals. Acetyl dissociates rapidly to form CH_3 and CO.

Ethanol exhibits long ignition delay time and like toluene is difficult to ignite at low $p-T$ conditions. Moreover, there are fewer ignition delay time measurements for pure ethanol in the literature. Cancino et al. [2010] were unable to ignite stoichiometric ethanol-air mixture at and below $p-T$ conditions of 47 bar - 781 K, 29 bar - 789 K and 10.1 bar - 900 K. Since the interest is in studying the oxidation pathway at high pressures and low temperatures which are relevant to engine operation, constant volume autoignition simulations have been done for a $p-T$ condition of 49 bar and 841 K, at which the ignition delay time is 3.30 ms. The Andrae and Golovitchev models show similar specie concentration profiles, however the C_1 and C_2 species appear slightly earlier in case of Golovitchev model. The species profiles of the Reitz model are also similar to the two other models

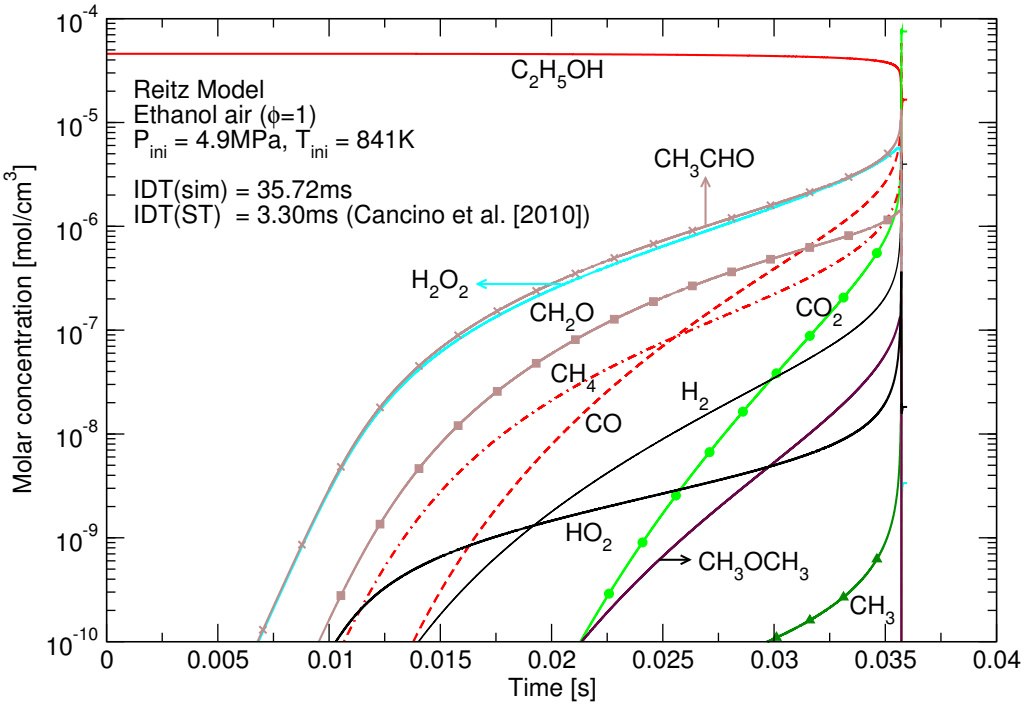

Figure 3.14: Molar concentration of the key intermediates formed during the pre-ignition reactions of ethanol as predicted by the Reitz Model.

however it predicts much delayed ignition delay time (Figures 3.13 and 3.14). Since the Reitz model was reduced to a greater degree some otherwise important pathways were neglected. It does not differentiate between the H atom abstraction from the two carbon atoms of ethanol and it does not include the ethanol dissociation pathway shown in reaction (3.18). Moreover, the reaction coefficient to one of the fall-off reactions involving the dissociation of ethanol is lower than that of the Andrae and Golovitchev models. Reitz model predicts considerable amounts of dimethyl ether (DME) as shown in Figure 3.14, therefore, a small number of carbon atoms are oxidised through DME oxidation pathways. Considerable amounts of C_2 radicals and stable molecules are also predicted by the three models but these have not been shown.

3.3.5 Effect of toluene on PRF oxidation

Summarising from the discussion laid out in Section 3.3.3.2, it can be said that toluene presence in a TRF should have different effects on iso-octane and n-heptane. The obvious cumulative effect of toluene on the blend reactivity is to delay the induction time as its content increases as can be seen in Figure 3.15, which shows ignition delay times of stoichiometric mixtures of PRF90 and its

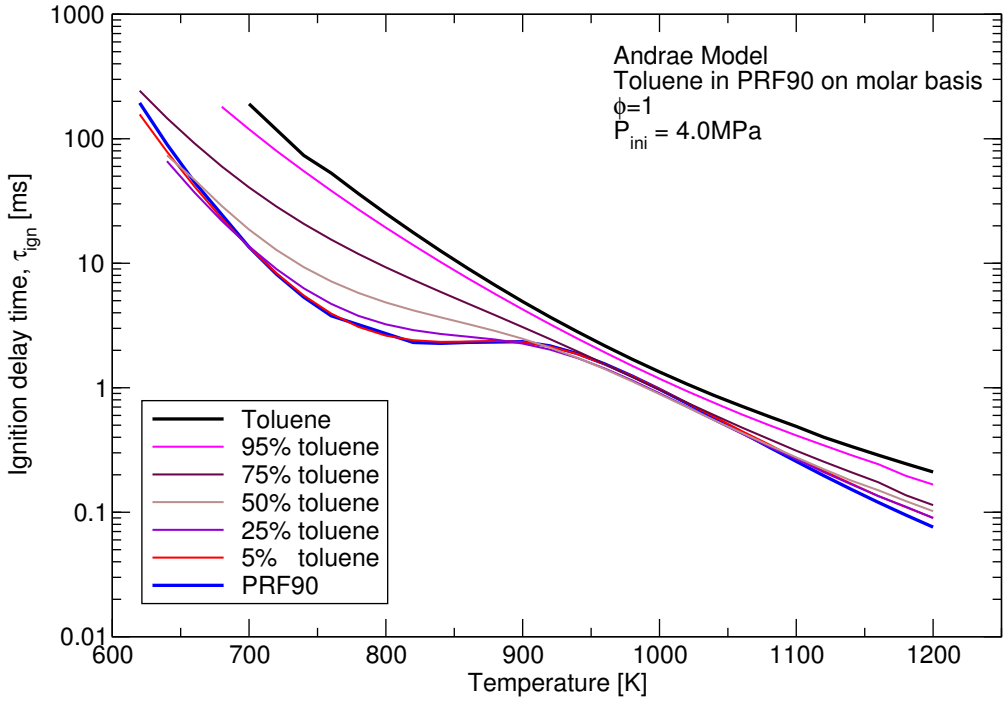

Figure 3.15: Ignition delay times of various blends of PRF90 and toluene.

blends with various molar amounts of toluene. A closer examination of the temperature profiles predicted by the Andrae model in Figure 3.16a shows that an initial 25% by mole toluene content in PRF90 accelerates the low temperature chemistry and advances the first stage ignition but it has a retarding effect on the intermediate temperature phase reactivity and therefore causes it to prolong. This is contrary to what is predicted by the Golovitchev and Reitz models (Figure 3.16b & c). The ignition delay times of the neat fuels and the blends are also predicted differently by the three models.

A higher toluene content starts to diminish the distinction between the two stages of ignition and reduces the NTC behaviour. Figure 3.17 shows an early emergence of the active centres as the toluene content increases. At low temperatures, H_2O_2 is formed as a consequence of the H atom abstractions by the HO_2 radicals. Therefore, an early appearance of the H_2O_2 is indicative of a higher concentration of the HO_2 radicals formed in the initiation reactions. But owing to its relative inertness, H_2O_2 concentration stabilises during the intermediate temperatures but it eventually decomposes at temperature around 1000 K to form OH radicals and causes a second stage ignition.

In order to assess the effect of toluene content in a TRF, the carbon fractions of key intermediates which are peculiar to each constituent fuel are determined

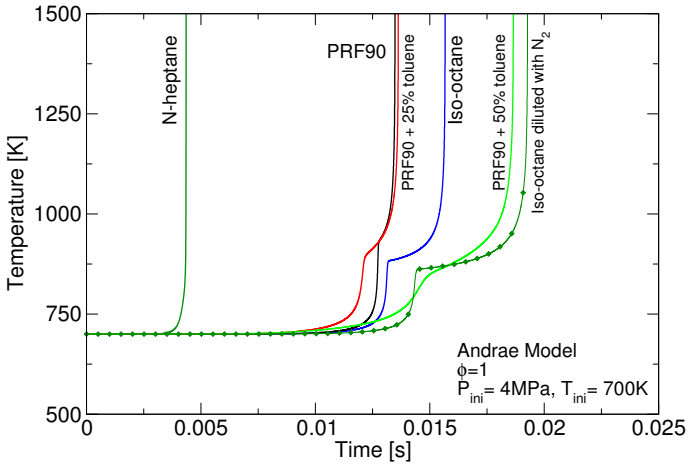

(a)

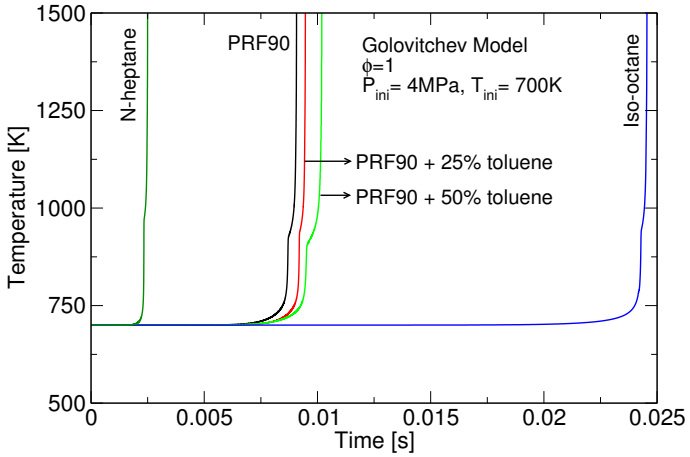

(b)

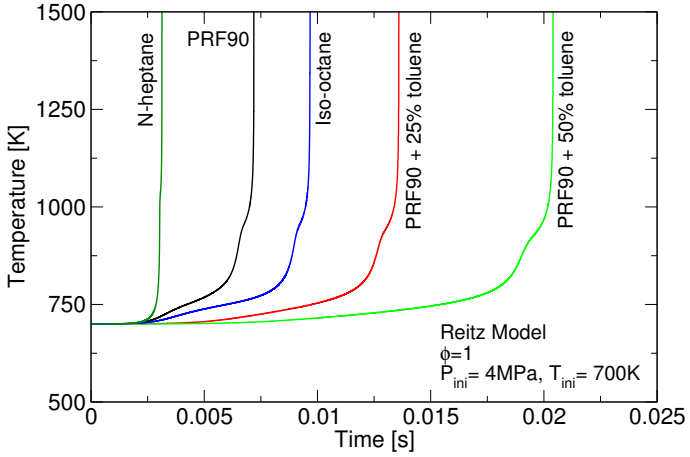

(c)

Figure 3.16: Temperature profiles of neat iso-octane, n-heptane, PRF90, PRF90 + 25% toluene and 50% toluene by moles as predicted by Andrae model (a), Golovitchev model (b) and Reitz model (c).

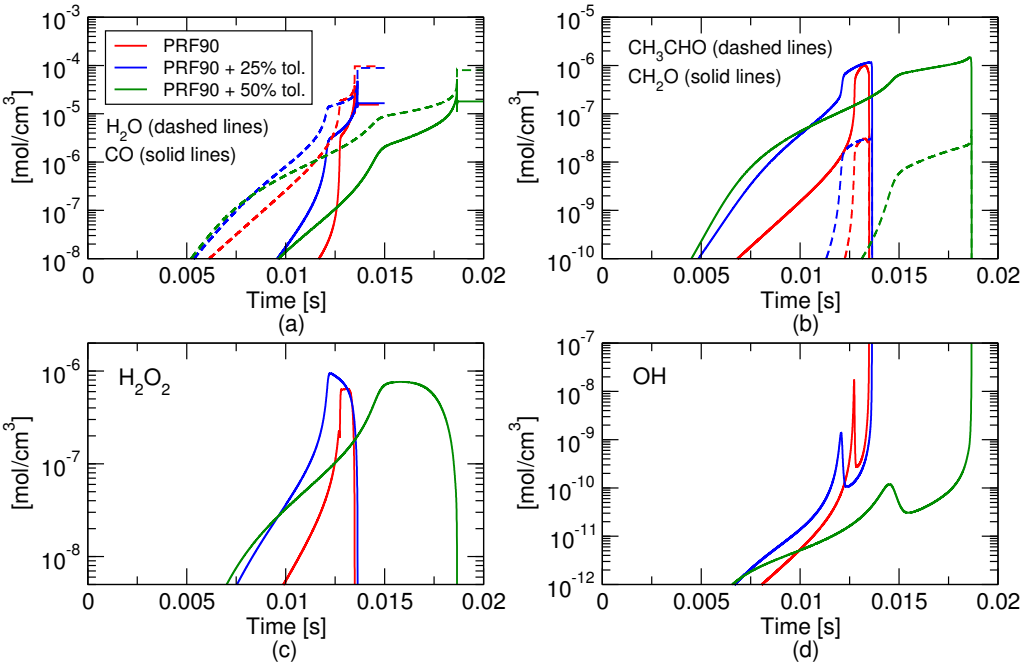

Figure 3.17: Variation in the concentration profiles of the key species and active centres of PRF90 due to the presence of an increasing molar content of toluene as predicted by the Andrae model.

based on the initial number of carbon atoms contributed by the respective fuel. These are then plotted against the temperature in Figures 3.18, 3.20 &3.19. Thus, a comparison can be made of the reactivity of the three component fuels when they are neat, in PRF90 or in the TRF (PRF90 + 25% by mol toluene). Carbon fractions for blends containing 25% ethanol have also been presented but are discussed in the later section. The conversion of the three fuels into their intermediates is driven by the system temperature and the reactant concentration. Blending fuels of different reactivites results in complex physicochemical interactions which can be separated into four categories on the basis of which the simulation results have been discussed. These are:

- Reduction of the initial concentration of each component due to blending and a resulting decreased reactivity at a given temperature, e.g. rate $= k[A]^n$ for $\mathrm{A} \longrightarrow \mathrm{B} + \mathrm{C}$.
- Components and their intermediates acting as heat energy sinks to undergo elementary reactions, i.e. fulfilling their activation energy needs by absorbing the heat released by another component.
- Components and their intermediates acting as heat energy sinks without

undergoing any reactions. This is the role played by a diluent such as N_2.

- Chemical interaction of blend components and their intermediates opening up new pathways and also activating or deactivating the radical pool.

The almost instantaneous increase in the temperature in Figures 3.16 marks the moment of ignition which is also coincident with the complete conversion of the fuel molecules into intermediate species. Therefore, the advanced ignition for PRF90 and PRF90 + 25% toluene from that of neat iso-octane is synonymous to an earlier conversion of iso-octane (not shown here), however, the percentage of iso-octane when blended is correspondingly higher than neat iso-octane at a given temperature, see Figure 3.18a. This means that although iso-octane converts quicker in time but its reactivity is reduced at any given temperature. The reason for this may seem to be a decrease in the concentration of iso-octane due to blending and its faster conversion is simply brought about due to an earlier heat release from the oxidation of more reactive component of the blend i.e. n-heptane in this case. However, the reduced reaction rate due to reduced concentration is not the sole consequence of blending. Interactions between the blend components also occur and may affect the reactivity of individual components. E.g. in Andrae model, heptyl radicals abstract H atoms from iso-octane and toluene to form n-heptane (thus explaining the decrease in n-heptane's reactivity) but these H atom abstractions from iso-octane are not enough to compensate for its reduced reactivity. The effect of reduced concentration of iso-octane due to blending can be separated from the presence of other reactive components by replacing them with N_2. Simulation has been done for a stoichiometric iso-octane air mixture diluted with N_2 such that the total number of moles are the same as in the case of PRF90 + 25% by mole toluene. Therefore, the same initial concentration of iso-octane is achieved as in the case of PRF90 + 25% toluene. The resulting carbon fraction of iso-octane is presented in Figure 3.18a and its temperature profile is presented in Figure 3.16a. It can be seen that although due to dilution the ignition is further delayed but the conversion rate of iso-octane at any given temperature is the highest when it is diluted, even more so than the stoichiometric mixture of neat iso-octane and air. This indicates that the reduced reactivity of iso-octane in blended form is not caused by a reduction in its concentration but mainly due to a scarcity of the active radicals because of a higher demand for them from various fuel fragments resulting in lower reaction rates. These fuel fragments thus formed scavenge the active radicals bringing the whole system to a bottle neck

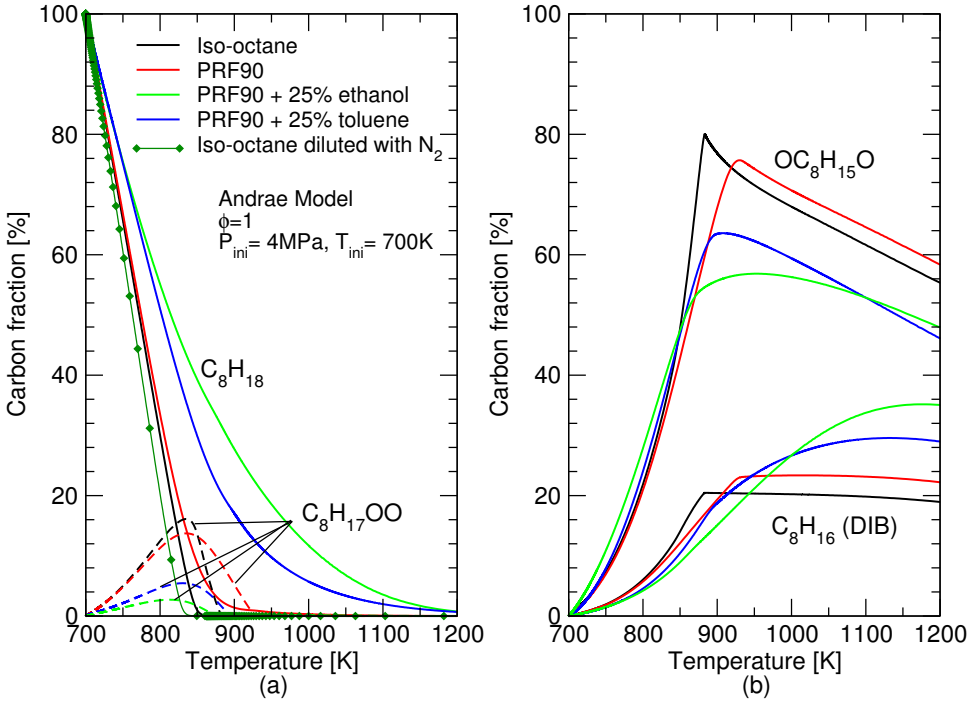

Figure 3.18: Carbon fractions of iso-octane and intermediates specific to it for four fuels; pure iso-octane (black lines), PRF90 (red lines) and PRF90 + 25% by mole toluene (blue lines) and PRF90 + 25% by mole ethanol (green lines).

which is then governed by the conversion of the component which was acting as a radical source.

Toluene converts quicker when blended with PRF90 but interestingly this speeding up of its conversion is due to both, an earlier heat release and also its scavenging of the active radicals produced mainly by n-heptane but also by iso-octane. This is evident by a lower percentage of toluene at any given temperature in Figure 3.19a. Even though in blended form the initial concentration of toluene is lower than in the pure case, the reactions involving its conversion are accelerated due to the availability of active radicals. Due to the stable nature of toluene intermediates, the radical scavenging effect of toluene is dominant over its contributory effect. A regeneration of toluene to minute concentrations can also be seen due to H atom addition to still surviving molecules containing a benzene ring.

The behaviour of n-heptane is completely opposite to that of the iso-octane and toluene. Its conversion is delayed in blended form, however, its conversion rate at a given temperature is sped up in an irregular way. Figure 3.20 shows that when in PRF90, the conversion rate of n-heptane is faster than when it is neat indicating that its reactive nature gives it a competitive edge on the scavenging

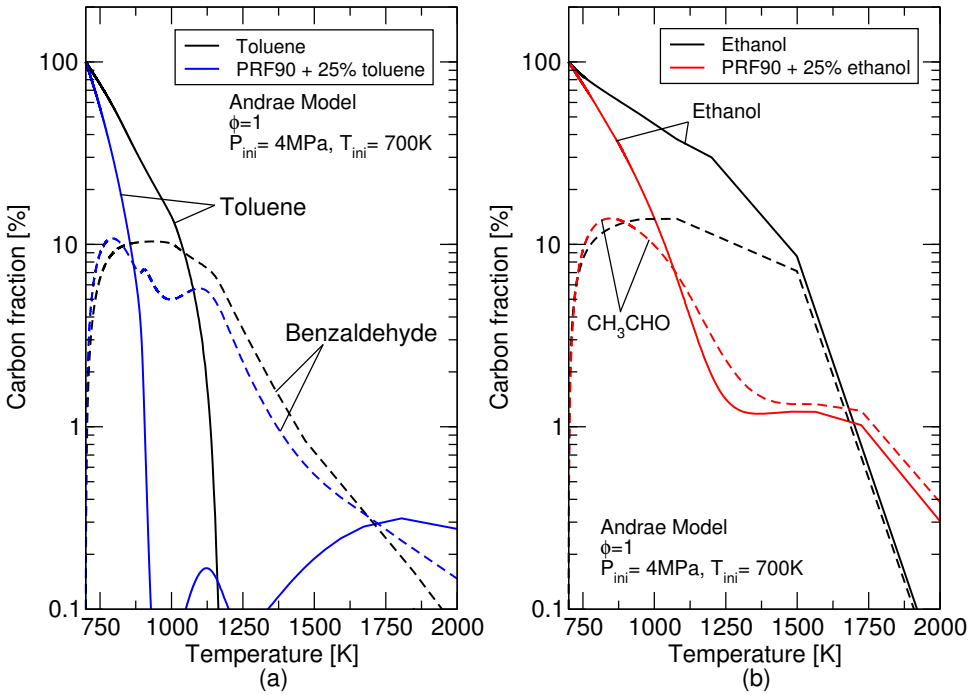

Figure 3.19: Predicted benzaldehyde carbon fraction of toluene (a) and acetaldehyde carbon fraction of ethanol (b) when in pure form and when blended with PRF90 by 25% by moles.

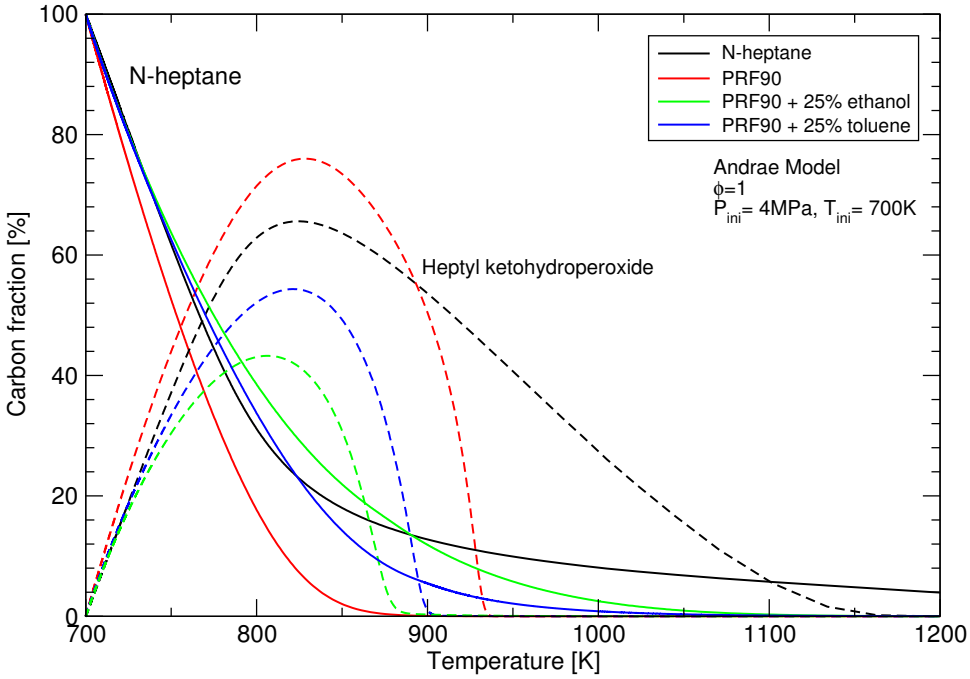

Figure 3.20: Carbon fractions of n-heptane and its ketohydroperoxide as predicted for four fuels; pure n-heptane (black lines), PRF90 (red lines) and PRF90 + 25% by mole toluene (blue lines) and PRF90 + 25% by mole ethanol (green lines).

of the active radicals produced by itself as well as iso-octane. The relationship between n-heptane and iso-octane is of n-heptane acting primarily as a source of radicals for initiation reactions and activation energy and iso-octane, primarily a source of radicals for the chain propagation of n-heptane. It appears that in a TRF, the reactivity of n-heptane is initially slowed down upto a temperature of about 830 K indicating the greater radical scavenging effect of toluene. At higher temperatures the conversion of n-heptane is quicker possibly due to the contribution of otherwise stable components to the active radical pool. From these observations, it can be hypothesised that in a TRF blend, n-heptane owing to its reactive nature acts as a source of activation energy and an initial radical pool for the less reactive fuels which then breakdown and become a source of active radicals to be scavenged by more reactive fuel fragments of n-heptane and toluene.

3.3.6 Effect of ethanol on PRF oxidation

In order to identify the effect of ethanol presence in a PRF, constant volume adiabatic simulations have been performed for mixtures of 5%, 25% and 50% by moles ethanol in PRF90 using the three reduced mechanisms. The temperature profiles for each blend and the neat fuels show the global reactivity and also the possible presence of a first stage mild ignition as shown in Figure 3.21. As previously seen in the case of toluene presence in PRF90, the three mechanisms simulate the effect of ethanol addition differently. The ignition delay time predictions of the three models for a blend containing 40% ethanol by moles in PRF77 (Fuel-B in Fikri et al. [2008]) show that the models predict poorly at low temperatures i.e. $<$833 K (Figure 2.13b). At higher temperatures Andrae and Reitz models predictions are appreciably accurate. The inaccuracies at low temperatures and the lack of experimental data for ethanol-PRF blends makes it difficult to state which model predicts the correct blending effect. Experimental ignition delay times in Figure 3.22 show that neat ethanol ignites at very similar times to that of iso-octane. Measurements in [Cancino et al., 2011] also show that the ignition delay times of a 25% ethanol and 75% iso-octane by volume blend are comparable to those of iso-octane. This suggests that ethanol addition in iso-octane does not increase the ignition delay time drastically. This is also reinforced by the RON/MON tests of Foong et al. [2014] which show that about 30% by moles ethanol in PRF90 will bring the RON of the resulting blend to 100 i.e. equal to iso-octane. However, these observations do not lend any credence to the simulated blending effects. Some similarity is observed between the Andrae and the Reitz models in that the

ignition occurs for 25% and 50% by mole addition of ethanol later than iso-octane and roughly at similar times.

Carbon fractions of iso-octane, n-heptane and ethanol during their oxidation in their pure form, in PRF90 and in a PRF90 + 25% by mole ethanol blend are also presented in Figures 3.18, 3.20 &3.19. The effect of ethanol presence on the reactivity of all three components are similar to those of toluene but more pronounced indicating a stronger radical scavenging effect of ethanol.

3.3.7 Discussion of chemical kinetics modelling

The $0-D$ ignition delay time predictions of the four major gasoline surrogate components; iso-octane, n-heptane, toluene and ethanol, show an appreciable general agreement with the experimental measurements. However, the models tend to deviate from measurements at lower temperatures and during the NTC phase of the fuels. The difficulty in validation of mechanisms at low temperatures arises from both the chemical complexities at these regimes as well as the shortcomings of the experimental apparatuses. It has been well known that the low/intermediate temperature chemistry is more complicated than the high temperature chemistry. The effects of molecular size and geometry on the pathways is much more pronounced at low/intermediate temperatures. Moreover, isomers of one compound may exhibit differing reaction coefficients and preference for pathways. This renders the generalisation of the chemical kinetics of one particular compound for others, difficult. One of the main objectives of mechanism reduction is therefore to find the right balance between generalisation and accuracy. This is much more difficult to achieve in multi-component mechanisms which comprise of pathways for the interaction of intermediate species of different fuel molecules. The reduced mechanisms studied presently, produce good predictions for iso-octane and n-heptane with the Reitz model having the most accurate PRF submodel but it is only the Andrae model which predicts well for toluene and ethanol at high pressure (Figure 2.11). The models predict acceptable ignition delay times for a TRF blend (Figure 2.13a), however, the low temperature predictions for an ethanol-PRF blend (Figure 2.13b) are poor.

The uncertainty of experimental measurements cannot be ignored, particularly at low temperatures where the ignition delay times are much longer and the effects of heat loss and charge non-homogeneity are pronounced. Since shock tube is a wave reactor, it is more suitable for measurements at high temperatures when the ignition delay times are shorter. The temperature increase is achieved

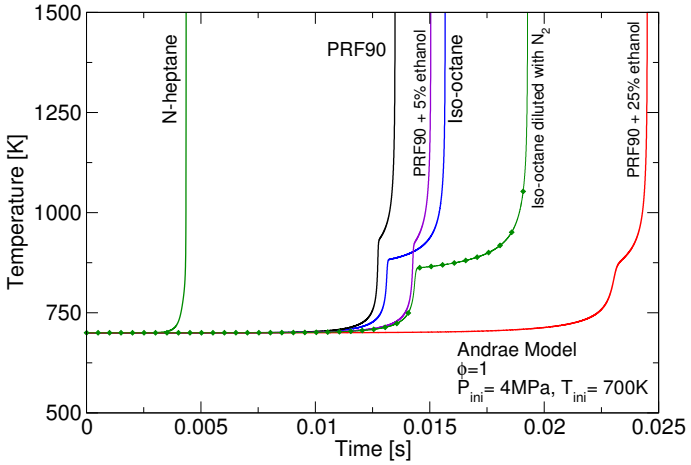

(a)

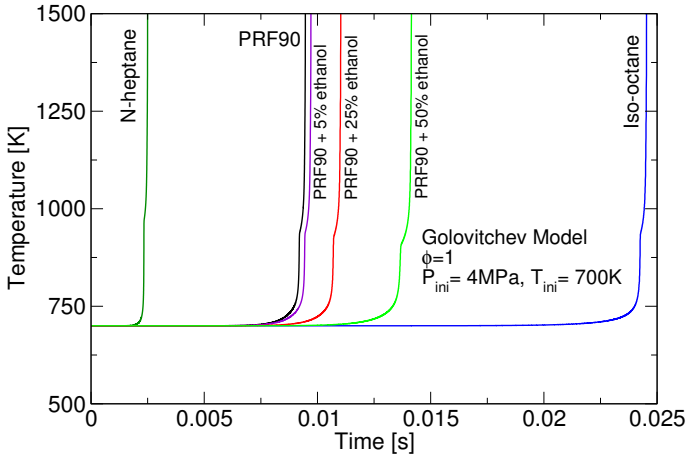

(b)

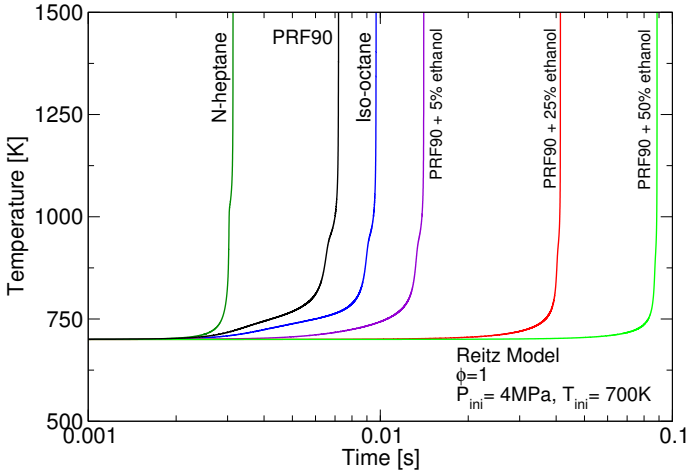

(c)

Figure 3.21: Temperature profiles of iso-octane, n-heptane, PRF90 and its blends with ethanol by molar percentages of 5%, 25% and 50% as predicted by the Andrae model (a), Golovitchev model (b) and the Reitz model (c) at 40 bar and 700 K.

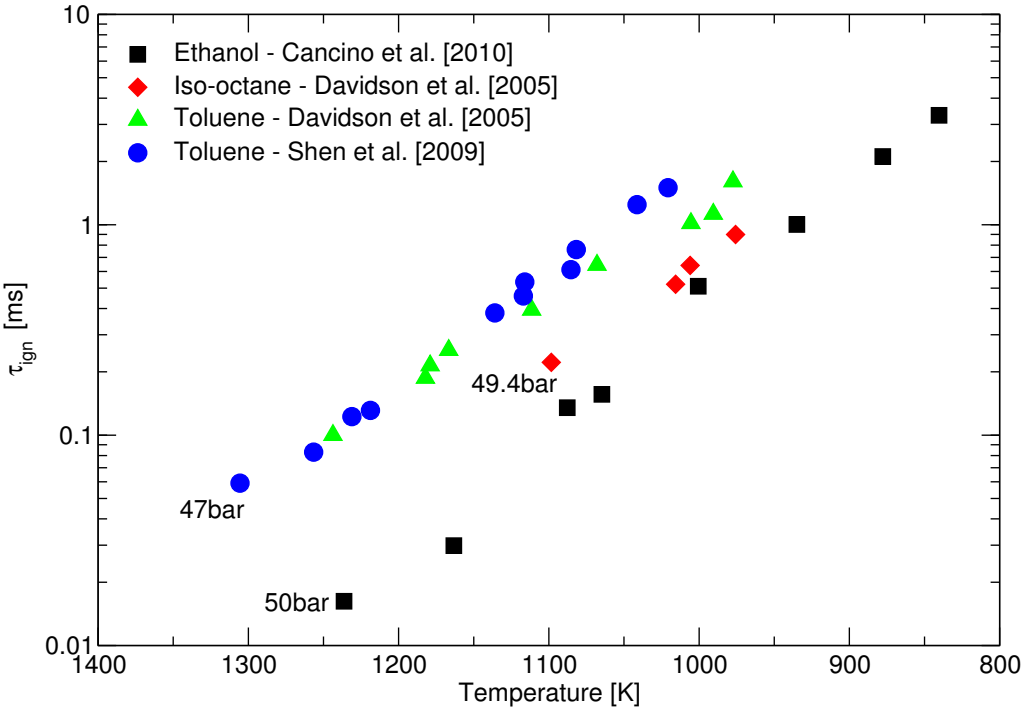

Figure 3.22: Experimentally measured ignition delay times from the literature for neat iso-octane, toluene and ethanol with air (ϕ=1) at similar pressures.

in very short times; around $< 10^{-7}$ s [Fernandes, 2010]. Measurements of different apparatuses at high temperatures agree well as compared to low temperatures. Similarly, the numerical predictions of short ignition delay times by different mechanisms differ less. At low temperatures, rapid compression machines are preferred as the charge can be kept at a sustained pressure and temperature for longer durations. However, this results in a greater deviation from the ideal behaviour.

Application of reduced chemical kinetic mechanisms to the modelling of practical combustion phenomena requires a preliminary study of the fidelity of the pathways included in these mechanisms to the established understanding of the oxidation pathways. Numerical modelling using these mechanisms allows the most significant species and reactions to be identified. For iso-octane; the low temperature activity takes place through the QOOH route followed by its double isomerisation. The formation of ROOH is omitted in most current reduced models. The models predict realistic concentrations of aldehydes and significant concentration of olefins is also predicted. Andrae model predicts a substantial amount of diisobutylene, however, it is the smaller olefins which are expected to be formed in more prevalent β scission reactions. The mechanism for n-heptane is

similar to iso-octane and the higher propensity for n-heptane to undergo double isomerisation after an initial H atom abstraction is correctly predicted. The most significant intermediate during toluene oxidation is predicted to be benzaldehyde as observed is experiments. The models do not differ greatly in ethanol pathways and predict acetaldehyde and formaldehyde to be the most significant species. The interaction of the intermediate species of different components occurs mainly in the secondary channels involving the smaller intermediates. Few reactions have been included in the primary channels in which relatively larger intermediates interact with each other.

Chemical kinetic modelling of the blends of toluene and ethanol in a PRF using the Andrae mechanism, reveals the mutual effects on the reactivity of each blend component. Toluene and ethanol reactivity is enhanced as they consume the active radicals produced by the more reactive blend components, mainly n-heptane but iso-octane as well. Ethanol has a stronger scavenging effect than toluene. Due to an earlier breakdown of n-heptane, an active radical pool is formed along with a heat release which helps in the breakdown of iso-octane. The radicals thus formed are more favourably consumed by n-heptane, toluene or ethanol intermediates starving the iso-octane conversion pathways.

Chapter 4

Description of SI engine combustion processes

4.1 Introduction

Combustion and its manifestation as flames is a complex phenomenon which primarily depends on the initial state of the fuel-oxidiser mixture; i.e. temperature, pressure and composition and also on the flow characteristics and the geometry of the system. All the above factors affect the nature of the flame and can be used to classify them in different categories. The principal mode of combustion in an SI engine is a propagating turbulent flame. In this chapter, the fundamentals of turbulence and combustion have first been presented followed by various engine related models used in this work.

4.2 Turbulence

Most flows encountered in nature are turbulent and combustion flows are no exception. In fact, combustion characteristics are highly dependent on the nature of the flow-field. An understanding of turbulence in engines and its quantification is crucial to understanding engine combustion.

Defining turbulence precisely is not straight-forward, however, it can be attempted by describing the statistical characteristics of a turbulent flow [Tennekes

and Lumley, 1972]. It manifests itself as three-dimensional random fluctuations of velocity and pressure when the inertial forces are orders of magnitude larger than the viscous forces, i.e. for large Reynolds numbers. The resulting flow pattern comprises vortices of varying sizes which are dissipative as the viscous shear stresses damp their kinetic energy by converting it into internal energy. Since turbulent fluctuations occur both in space and time, precise quantification at each point and at all times is rather cumbersome. Therefore, simpler analyses are statistical in nature. However, special cases of turbulence can be studied theoretically by assuming the fluctuations to be statistically steady and independent of some of the spatial dimensions. This allows for a simpler mathematical analysis of turbulence. Such assumptions have also been made during the course of this work; the in-cylinder turbulence is considered to be isotropic and homogeneous, i.e. independent of spatial coordinates and without any preferential direction.

4.2.1 Statistical quantification of turbulence

Some way of averaging the velocities of mean flow and the vortices and the size of the latter should be devised to quantify turbulence as simply as possible. The two key quantities are the turbulent velocity and a length scale. These are discussed below.

4.2.1.1 Turbulent velocity and turbulence intensity

Velocity fluctuations can be represented by the Reynolds decomposition of the instantaneous velocity as follows. Consider, for example, a case of steady turbulent flow where the instantaneous velocity measured at a fixed location is $U(t)$. The flow is statistically steady i.e. although the instantaneous velocity fluctuates, it does so about a time-independent mean value (Figure 4.1a) which is given as follows:

$$\bar{u} = \lim_{T\to\infty} \frac{1}{T} \int_0^T U(t)dt \tag{4.1}$$

The fluctuating component of the turbulent velocity can therefore be obtained as:

$$u(t) = U(t) - \bar{u} \tag{4.2}$$

Magnitude of turbulent fluctuations is best represented by the root-mean-square (rms) of the fluctuating component.

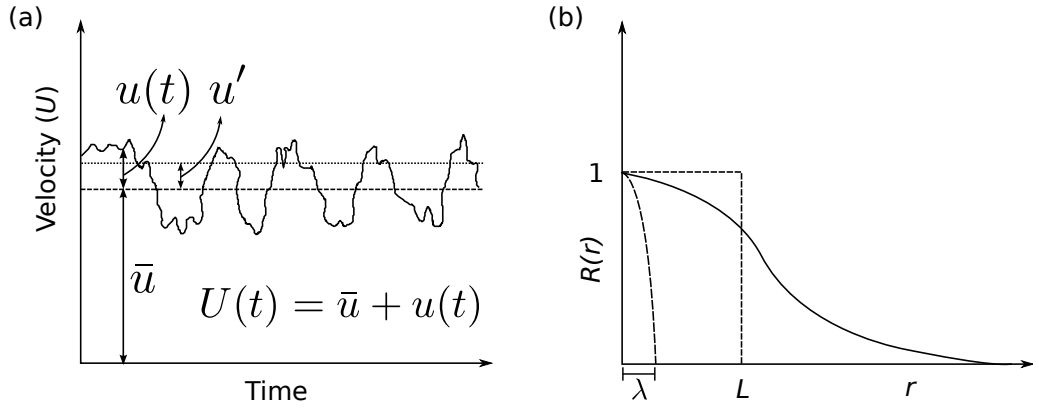

Figure 4.1: (a) An illustration of velocity fluctuations at a fixed point in a steady turbulent flow-field. (b) A typical autocorrelation function and the definition of the integral (L) and Taylor (λ) length scales.

$$u' = \sqrt{\overline{u^2}} \tag{4.3}$$

The rms velocity, u', is commonly used as a measure of the intensity of turbulent fluctuations. It is the characteristic speed with which the largest of the eddies rotate. The ratio of the rms velocity to the mean velocity, $u'/\bar{u}$, is termed as the 'turbulence intensity'. For a non-isotropic case, the other components of the turbulent fluctuations, v' and w', can be obtained in a similar way. The kinetic energy of turbulence can then be obtained separating the three orthogonal components of the velocity as,

$$k = \frac{1}{2}(u'^2 + v'^2 + w'^2) \tag{4.4}$$

For an isotropic flow, the rms velocities are the same in all directions and therefore the turbulent kinetic energy is simply

$$k = \frac{3}{2}u'^2 \tag{4.5}$$

4.2.1.2 Turbulent length scales

In addition to the rms velocity, the definition of a representative size of the eddies is necessary to define the complete state of turbulence. An average size of the eddies can be determined by considering the autocorrelation of velocity fluctuations at two neighbouring points, x and $x + r$. The change in the product of

velocities at these two points, $\overline{u(x)u(x+r)}$, as the distance r is increased gives an indication of the correlation between the local velocity fluctuations. The maximum distance, upto which the two velocities are well correlated, gives a measure of the size of the largest eddies. A normalised spatial autocorrelation function $R(r)$ can be defined as:

$$R(r) = \frac{\overline{u(x)u(x+r)}}{u'^2} \tag{4.6}$$

The area under the autocorrelation function is given by the following integral and gives a quantitative measure of the largest eddies and is known as the integral length scale, L [Tennekes and Lumley, 1972]. It is equal to the width of a rectangle of the same size as the area under the autocorrelation curve; see Figure 4.1b.

$$L = \int_0^\infty R(r)dr \tag{4.7}$$

Determining the integral length scale by making a series of two simultaneous velocity measurements at increasing distances by using methods such as the two-point LDV is rather difficult. A related quantity, the integral time scale, τ_L, can be determined in a similar manner by making measurements at a single point at different times if the Taylor hypothesis of frozen turbulence applies[1]. Thus an autocorrelation function in terms of time can be obtained as,

$$R(t) = \frac{\overline{u(t_0)u(t_0+t)}}{u'^2} \tag{4.8}$$

and the associated time scale known as the integral time scale can obtained as,

$$\tau_L = \int_0^\infty R(t)dt \tag{4.9}$$

The integral time scale is the time taken by an eddy of size L to complete one rotation. Dimensional analysis provides the following relationship between integral length scale and the integral time scale.

$$\tau_L \sim \frac{L}{u'} \tag{4.10}$$

[1]According to Taylor's hypothesis, when the turbulence intensity ($u'/\bar{u}$) is very small in a steady flow, multiple simultaneous measurements at various locations are equivalent to measurements taken at a single location at different times as the eddy advects through the probe along the flow.

As stated earlier, one of the definitive characteristics of turbulence is that it is dissipative due to viscous shear stresses. However, viscous forces play their role at small scales across which the velocity gradients are large [Lipatnikov, 2013]. Large vortices, of scale L, carry most of the kinetic energy and are largely unaffected by these viscous effects. They eventually break down to smaller eddies in which kinetic energy is dissipated to heat through viscous action at a rate given by

$$\epsilon \sim \frac{u'^3}{L} \tag{4.11}$$

The length of these smaller eddies is given by the following expression due to Kolmogorov [1941] and is known as the Kolmogorov microscale.

$$\eta = C_\eta \left(\frac{\nu^3}{\epsilon}\right)^{1/4} \tag{4.12}$$

where, C_η is a constant, of the order of unity [Borghi and Destriau, 1998] and ν is the kinematic viscosity. Substituting for ϵ from equation (4.11) in the above equation, the expression can be written in terms of the Reynolds number as:

$$\eta = C_\eta \frac{L}{Re^{3/4}} \tag{4.13}$$

and

$$Re = \frac{u'L}{\nu} \tag{4.14}$$

A length scale between the integral length scale and the Kolmogorov scale can be defined by expanding the autocorrelation function, $R(r)$, into a Taylor series and neglecting the higher order terms in the expansion. The remaining series gives a parabolic approximation of R as shown in Figure 4.1b and the distance at which the parabola intersects the abscissa gives a characteristic length scale known as the Taylor microscale, [Taylor, 1915]. The Taylor microscale is given by the expression:

$$\lambda = C_\lambda \frac{L}{Re^{1/2}} \tag{4.15}$$

Where, C_λ is a dimensionless constant whose value is suggested to be $\sqrt{40.4}$ [R. G. Abdel-Gayed and Bradley, 1984].

From the discussion so far, it can be seen that the integral length scale and the

rms velocity provide a great deal of information about the state of turbulence. Therefore, a number of mathematical models have been proposed over the years for their calculation. One such model is the $k - \epsilon$ model which is widely used for modelling turbulence in a variety of flows. It has also been employed in this work and is discussed in some detail in Section 4.7.1.

4.3 Background to combustion and flames

Combustion is an exothermic ensemble of reactions of a fuel and an oxidiser. A *flame* is the region to which the combustion reactions are confined; often but not always, the flame is luminous and in a premixed gaseous fuel-oxidiser mixture, it is self-propagating. This self sustained propagation of a flame usually occurs at speeds much lower than the local sonic speed, such a flame is termed as a *deflagration wave*. A flame which propagates at supersonic speeds is a *detonation*. Deflagration occurs through a gradual thermal and mass diffusion, whereas a detonation is a shock wave which is sustained by the energy liberated from combustion at a location through which the shock wave had passed.

The fuel-oxidiser contact necessary for the reactions to occur may take place before or after the ignition. If the fuel and oxidiser are premixed as in an SI engine, then the flame propagation is governed by the equilibrium between the chemical reactions and molecular transport. If no mixing of the fuel and oxidiser occurs before the ignition then the flame is anchored to the boundary between the fuel and oxidiser and the heat release is governed by rate of mixing. Such flames are referred to as diffusion flames and are relevant to diesel engines. The fuel and oxidiser may also be partially premixed – diffusion and partially premixed flames have not been considered as they are out of the scope of this work.

The nature of the flame is greatly affected by interactions of flow-field and the reaction zone. The flame may be *laminar* or *turbulent* depending on the state of turbulence. Turbulent flames are found in most of the practical applications such as combustion engines, gas turbines, furnaces etc. Laminar flames have very limited practical application, however, they are extensively studied for the insight it offers into the burning characteristics of various fuels. In practical combustion devices where turbulent flow conditions exist, the flame is distorted due to its interaction with the various turbulent eddies resulting in a propagation velocity which is not only a function of the laminar burning velocity, but the turbulence characteristics as well. Study of laminar premixed flames is therefore a prerequi-

site to the study of turbulent premixed flames and its concepts are discussed in the following section.

4.3.1 Laminar premixed flames

A flame which propagates in a premixed combustible mixture through the intermolecular transfer of heat and active radicals is a laminar premixed flame. The two fundamental characteristic properties of such a flame are the unstretched laminar burning velocity (u_l) and the adiabatic flame temperature (T_a), flame stretching is described below. The adiabatic flame temperature is achieved in an ideal adiabatic burning of the mixture. The laminar burning velocity is the speed at which a flat flame propagates in an infinite quiescent unburned mixture when there is no heat loss [Matalon, 2009]. In case of a stationary or stabilised flame, it is equal in magnitude to the velocity at which the unburned mixture moves towards it.

The thermo-diffusive process across a flame can be described with the help of a sketch for the planar $1-D$ laminar flame as shown in Figure 4.2. Four zones can be identified based on the temperature and concentration of the reactants and products. The cold unburned reactants at temperature T_u reside in a reactant zone from where they diffuse towards the reaction zone. As the heat is diffused away from the reaction zone, the oncoming reactants are preheated before they break down to form active radicals in the reaction zone. The luminous part of the reaction zone contains radicals such as CC, CH, CN, OH and NH (for hydrocarbon fuels), in their electronically excited states which cause their definitive chemiluminiscence upon deexcitation. The relatively slower recombination or termination reactions form the final products, $\mathrm{CO_2}$, $\mathrm{H_2O}$, CO as well as aldehydes etc., accompanied by the emission of infrared radiations. The fully burned product zone contains the final combustion products at temperature T_b.

The temperature and concentration profiles across a flame are non-linear which means that the demarcation of unburned and burned zones and the definition of the flame thickness is not straightforward. In literature, there are various ways of defining the flame thickness, e.g. as discussed in [Gillespie et al., 2000]. Mass diffusion length ($\delta_D = D_{ij}/u_l$) can be defined to represent flame thickness; where, D_{ij} is the mass diffusivity of the deficient reactant i with respect to the abundant reactant j. Similarly a thermal diffusion length can also be defined, as $\delta_T = \kappa/u_l$; where, κ is the thermal diffusivity of the unburned mixture. Generally, a hydrodynamic length, given as $\delta_l = v_u/u_l$ is used; where, v_u is the kinematic viscosity

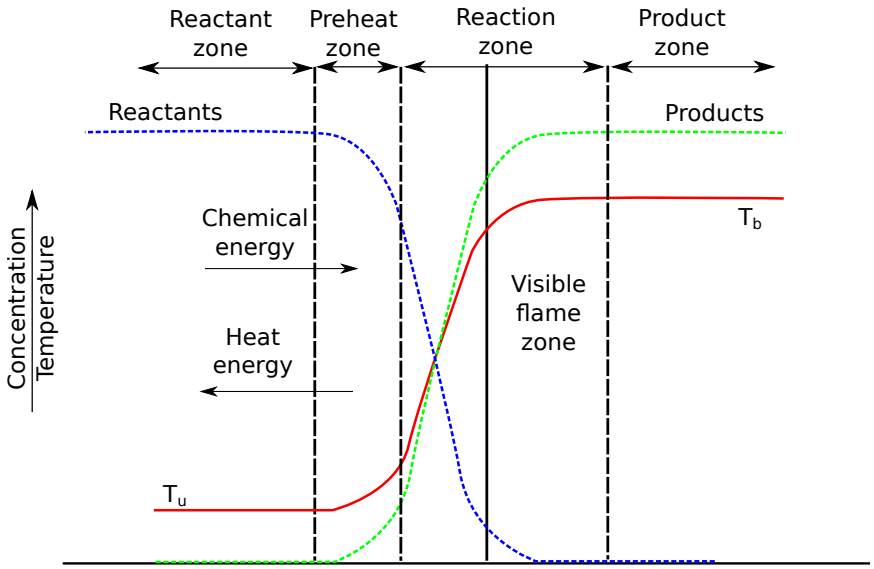

Figure 4.2: Schematic showing temperature and concentration profiles associated with a $1-D$ premixed adiabatic flame; adapted from Griffiths and Barnard [1995].

of the unburned mixture. For an infinitesimally thin planar flame front as shown in Figure 4.3, the conservation of mass dictates:

$$\rho_u u_n = \rho_b S_n = \dot{m} \tag{4.16}$$

where, the subscripts u and b represent the unburned and burned quantities, respectively, ρ is gas density and S represents the flame speed relative to the products. The same holds for an ideal planar flame with finite thickness for which the characteristic laminar burning velocity, u_l, is self determined by the rate at which the active radicals are formed and diffused towards the unburned gas as well as the rate at which heat is diffused towards the unburned gas. The thermal expansion of the burned gas induces an expansion velocity u_g. The flame speed, S_n, is given as:

$$S_n = u_n + u_g \tag{4.17}$$

A real flame is however, subject to stretch. Departure from adiabatic conditions and compositional inhomogeneity results in a non-uniform diffusion of active species and a non-uniform heat loss. As a result the flame propagates at uneven speeds and takes a cellular form. The resulting curvature stretches the flame and in effect tend to thin it out. In addition to being caused by the flame curvature, stretch is also induced due to aerodynamic strain. The stretch rate act-

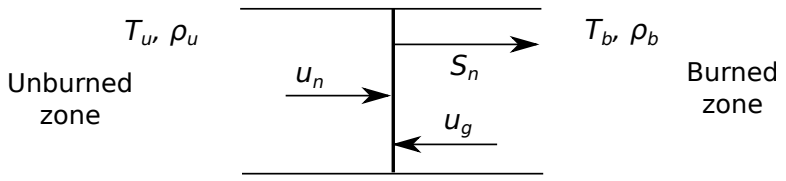

Figure 4.3: Schematic showing a $1-D$ planar flame and its associated burning speeds.

ing at a given point on the flame surface due to Williams [1985] is mathematically given as:

$$\alpha = \frac{1}{A}\left(\frac{dA}{dt}\right) \tag{4.18}$$

4.3.1.1 Instabilities in laminar premixed flames

Flame instability arises in the form of cells or wrinkles in the flame surface even when it is propagating in a quiescent mixture, in the absence of any turbulence. Instabilities may be intrinsic to the combustion process or they may arise due to an interaction between combustion and the acoustics of the system. The first type consists of Darrieus-Landau hydrodynamic instability and the thermo-diffusive instability. The second type consists of thermo-acoustic instability.

Hydrodynamic instability was first explained by Darrieus [1938] and Landau [1944] and has its origins in the presence of pressure gradients upstream and downstream of the flame front due to the deviation of the streamlines from their original path as they cross the flame front at an angle. The deviation of streamlines is depicted in Figure 4.4a which illustrates how the increase in burned gas velocity (S_b) due to density decrease is accompanied by a deviation of direction towards the surface normal. As no two streamlines can intersect, the streamlines curve to eventually become parallel further downstream. The deviation of streamlines in the downstream is accompanied by a deviation of upstream streamlines in the same direction. This causes the streamlines to converge when the flamelet is concave towards the unburned gas (Figure 4.4a) and diverge when the flamelet is convex. As a result the flow must accelerate into concave flamelets and deccelerate into convex flamelets. As a consequence the flame cellularity is to increase with time [Searby, 2008].

Thermo-diffusive effects arise when the diffusion of heat and species is not along parallel streamlines due to the presence of wrinkling as shown in Fig-

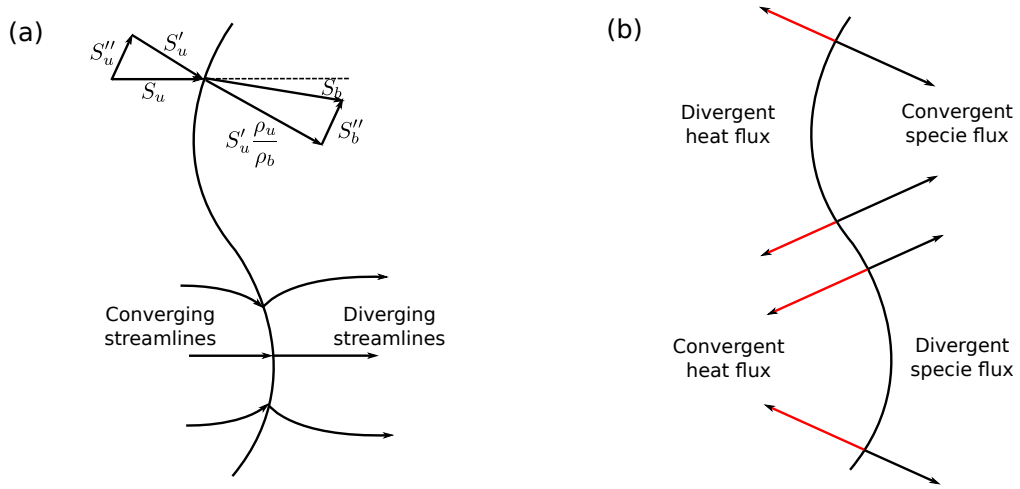

Figure 4.4: Schematics showing (a) the Darrieus-Landau hydrodynamic instability and (b) thermo-diffusive effects in a wrinkled laminar premixed flame.

ure 4.4b. When the flame thickness is comparable to the wavelength of wrinkling, the heat flux will converge to a smaller volume where the flamelet is concave towards the unburned gas. As a result the local temperature will increase and consequently the burning velocity as well. Opposite happens when the flamelet is convex in relation to the unburned gas. Similarly, the active species will diffuse and diverge for a concave flamelet resulting in a reduced chemical activity and hence the burning velocity. The correct balance of these two can have a stabilising effect on the wrinkled flame. The ratio of the two fluxes is called Lewis number, Le, which can be given as the ratio of the thermal and mass diffusivity coefficients as:

$$Le = \frac{\kappa}{D_m} \tag{4.19}$$

A larger than unity Lewis number indicates that the effects of heat diffusion are dominant and the flame is thermo-diffusively stable.

4.3.2 Turbulent premixed flames

A flame which develops in a turbulent medium will experience deformation. This increases the surface area of the flame and hence the burning velocity. The turbulence is typically characterised as the root-mean-square velocity, u', of the underlying flow-field. Turbulent eddies of various scales are also defined. The turbulent flame speed and flame brush thickness, which is a characteristic measure of

the transition zone between the unburned and burned gases of a wrinkled turbulent flame, are dependent on u', the turbulent length scales as well as the chemical and molecular quantities of the mixture [Borghi et al., 2008].

In an SI engine, as the flame originates from the spark kernel, its size in terms of a representative radius, is small enough to allow an initial smooth laminar like growth. At this stage the flame simply resides with in the bigger eddies which are represented by the integral length scale (L); and the flame is merely convected as a whole. As the flame grows, it is able to interact with a larger portion of the turbulence spectrum which results in its wrinkling. However, it is not just the size of the turbulent eddies which affects the degree of wrinkling but also the time which the flame spends interacting with the eddy. The time taken by a laminar flamelet of thickness, δ_l, to pass through a point is known as the laminar chemical time scale; $\tau_c = \delta_l/u_l$. An integral time scale can be defined based on the integral length scale such as, $\tau_L = L/u'$, which primarily is a qualitative measure of time taken by the eddy to turn. It can also be regarded as the time for which the eddy remains intact. The ratio of the integral time scale to the chemical time scale gives a dimensionless number which is named after Damköhler.

$$Da = \frac{L}{\delta_l}\frac{u_l}{u'} = \frac{\tau_L}{\tau_c} \tag{4.20}$$

A large value of Damköhler number indicates weak turbulence and vice versa. A dimensionless expression for strain rate can be obtained by normalising the chemical time scale with the Taylor eddy time scale ($\tau_\lambda = \lambda/u'$) which is known as the Karlovitz stretch factor.

$$Ka = \frac{u'}{\lambda}\frac{\delta_l}{u_l} = \frac{\tau_c}{\tau_\lambda} \tag{4.21}$$

When the flame thickness is smaller in relation to the turbulent eddies, the flame surface is prone to wrinkling. However, eddies, smaller than the flame thickness reside with in the flame and affect the local thermo-diffusive balance.

4.3.2.1 Regimes of premixed combustion

The relative magnitudes of the above mentioned quantities can be used to identify various regimes of premixed combustion. Two dimensionless quantities; u'/u_l and L/δ_l can be plotted on a so called Borghi diagram [Borghi and Destriau, 1998] as shown in Figure 4.5. The solid lines on the diagram mark the boundaries between the different regimes of combustion as described below:

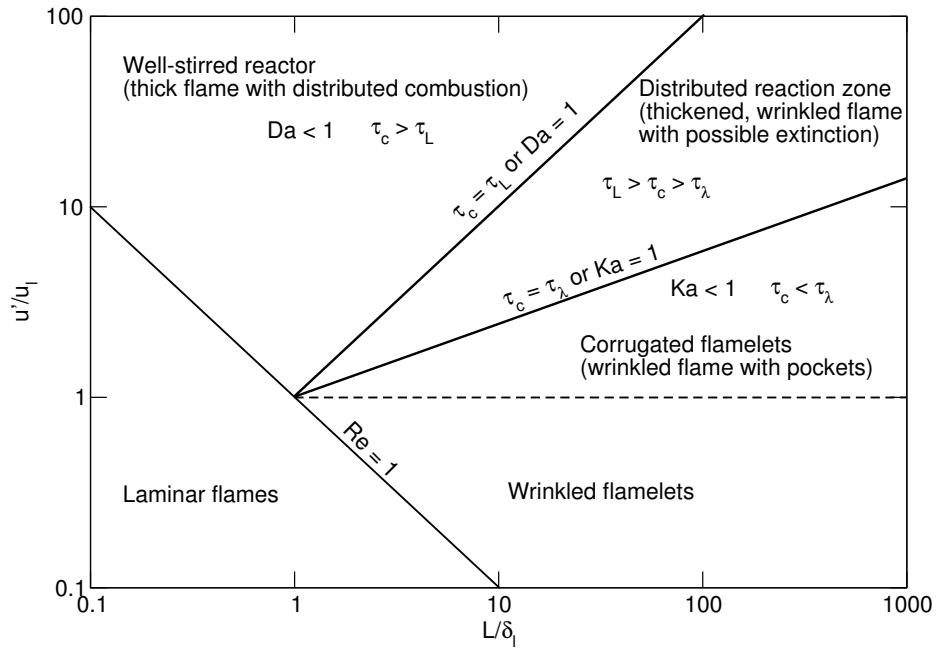

Figure 4.5: Borghi diagram

- **Laminar flames** ($Re < 1$): The flame is laminar as the turbulence is weak and the size of eddies is smaller than the flame thickness and therefore does not cause any wrinkling of the flame.

- **Wrinkled flamelet regime** ($Re > 1$, $Ka < 1$, $u' < u_l$): These conditions pertain to a wrinkled flamelet regime. The integral length scale, L, is larger than the flame thickness and causes the flame to wrinkle. However, the turbulence is not strong enough to cause any folding or stretching of the flame surface. The chemical time scale is shorter than the Taylor eddy time scale which means that the smaller eddies are able to burn before they break down. As a result each flamelet or cell burns in a similar way as a laminar flame. It has also been widely argued that a turbulent flame can be treated as an array of laminar flamelets within which no turbulence structures exist [Bradley, 1992] and considerable experimental evidence in support of this view has been produced, see [Warnatz et al., 2001, p. 204] but this holds true for conditions when the Damköhler number is large as in this wrinkled flamelet regime. This clearly is irrelevant to combustion in SI engines where a simplification assumption like that of the laminar flamelets will not explain the flame perturbations caused by the smaller turbulent length scales.

- **Corrugated flamelet regime** ($Re > 1$, $Ka < 1$, $u' > u_l$): Turbulence intensity is higher in comparison to the local laminar flame speed. As a result the flame is not only wrinkled but folded on itself resulting in the formation of pockets of unburned mixture on the burned side and vice versa. Flames in SI engines tend to be in this wrinkled-corrugated regime.

- **Distributed reaction zone** ($Re > 1$, $Ka > 1$, $Da > 1$): As $\tau_c > \tau_\lambda$, there is insufficient time for the eddies to burn. This results in a greater stretching and breaking up of the flame resulting in distributed reaction zones. The resultant flame is also much thickened.

- **Thickened flames, well-stirred reactor** ($Re > 1$, $Ka > 1$, $Da < 1$): The chemical life time is longer than the life time of even the biggest eddies. The flame is continuously stretched and broken up resulting in localised extinctions.

4.4 Modelling of combustion in SI engines

The prime objective of engine combustion modelling is to be able to predict the mass burning rate of the air-fuel charge on which the engine performance calculations rely. Several approaches exist for the simulation of the combustion process and are generally classified as zero, multi-zone and multi-dimensional. Burluka [2010] presented an overview of the thermodynamic modelling approach which is the approach taken in the present work and forms the basis for The University of Leeds engine modelling code 'Leeds University Spark Ignition Engine' or LUSIE for short. Zero dimensional representation of the combustion process neglects the spatial details and therefore the thermodynamic state of the in-cylinder gases is only a function of time. Multi-zone approach builds on the same principle but differentiates between a burned and an unburned zone by defining a thin reaction zone or a flame front separating the two zones each characterized by its own thermodynamic state and composition. Multi-dimensional models account for the detailed fluid dynamics and its interaction with the combustion chemistry and therefore the governing equations are a function of space and time making the solution computationally expensive. Where the importance of multi-dimensional modelling is incontestable, the development of models for the multi-zone approach is of considerable importance as it allows a fast analysis of the effects of various engine design parameters on engine performance.

4.5 Zero/multi-zone thermodynamic modelling

Over the years, thermodynamic models governing various SI engine phenomena have been implemented in a Fortran code at The University of Leeds as a library referred to as LUSIE, the groundwork for which was laid out in [Hynes, 1986]. Models comprised in LUSIE are described in detail later in Section 4.6; for a brief history of LUSIE development, the interested reader is directed to [Conway, 2013]. Hattrell [2007] combined the combustion routines of LUSIE which is a closed cycle code with GT-Power which offers versatile capabilities of 1-D modelling of the gas exchange process. The resulting hybrid modelling environment is referred to as GT-LU. The present work is the continuation of the development of predictive modelling tools for engine design, particular emphasis here is on modelling autoignition in the end gas with realistic hydrocarbon oxidation reaction kinetics. The significant contribution of the present work to LUSIE and GT-LU is the development of subroutines for the chemical reaction kinetics.

4.5.1 Zero dimensional thermodynamic modelling

The zero dimensional approach assumes the conversion of the air-fuel charge to final combustion products in a single step. The reaction rate is given by an empirical expression often containing adjustable parameters. The so-called Wiebe function, i.e. a zero-dimensional model proposed by Ivan Wiebe in 1954 was based on the assumption that the detailed chemical reaction kinetics can be reduced to a generic macroscopic reaction rate expression for engineering applications. The Wiebe function is still very often used in engine modelling as it offers unrivalled convergence and computational speed. But the same nature which makes its use advantageous is the cause of its inherent weakness. The Wiebe function is an empirical one which is defined for one particular engine condition and its extrapolation to other conditions is difficult. A review on the subject has been presented by Ghojel [2010]. Multi-zone thermodynamic modelling of the SI engines may offer a better accuracy of burn rate predictions at feasible computational speeds.

4.5.2 Two-zone thermodynamic modelling

Two-zone modelling is the simplest of the zonal modelling approaches as it assumes the in-cylinder charge to have been divided into a burned and an unburned zone. This implies that the zonal boundary is an infinitesimally thin

reaction zone which separates the two zones. The burned zone is assumed to be composed of the burned products of the air-fuel mixture at chemical equilibrium. The rate at which the unburned mixture burns is governed by the rate at which this infinitesimally thin flame advances into the unburned zone which is quantified as a turbulent burning rate, u_{tr}. Thus the amount of fuel that burns in a single time-step, dt, is given as:

$$\Delta m_b = \rho_u A_{fb} u_{tr} dt \tag{4.22}$$

where, ρ_u is the density of the unburned mixture and A_{fb} is the effective area of the infinitesimally thin flame. A two-zone model available in LUSIE has been investigated in the past and discussions on its strong and weak points may be found in Hattrell [2007]. Since the turbulent flame has a finite thickness, the rate at which the fresh mixture is entrained into the flame brush is unequal to the mass burning rate, i.e. $\dot{m}_e \neq \dot{m}_b$. The two rates are determined separately in a three-zone modelling approach as described below.

4.5.3 Three-zone thermodynamic modelling

The three-zone model introduces a third zone, i.e. an entrainment zone in which the fresh unburned mixture burns according to a local chemical burn-up time scale. Earliest works on this approach were done by Blizard and Keck [1974]. The flame wrinkles and folds on itself encapsulating and entraining the unburned mixture and giving the flame brush a finite thickness. The rate at which the unburned mixture is entrained (dm_e) is given as:

$$\frac{dm_e}{dt} = \rho_u A_{fe} u_{te} \tag{4.23}$$

where, A_{fe} is the area of the leading edge of the flame brush and u_{te} is the entrainment velocity. The entrainment area is different from the surface area of the burned gases, A_{fb}. The entrained fresh charge converts to equilibrium products at a chemical burn-up time scale which depends on the local unstretched laminar burning velocity and the size of the turbulent eddies. The choice of either the integral length scale or the Taylor microscale results in the expressions:

$$\tau_b = C_b \frac{L}{u_l} \tag{4.24}$$

and

$$\tau_b = C_b' \frac{\lambda}{u_l} \tag{4.25}$$

where, C_b and C_b' are coefficients to which the burn rate is very sensitive. In this work, the calculation of τ_b has been done in GT-Power which uses the Taylor microscale based definition. The mass burning rate is then given by:

$$\frac{dm_b}{dt} = \frac{m_e - m_b}{\tau_b} \tag{4.26}$$

4.5.4 Turbulent burning velocity

Unlike laminar burning velocity, the turbulent burning velocity is not a fundamental property of the mixture. Its complex dependencies on flow details mean that development of theoretical models has been a difficult task. Numerous mathematical models have been proposed, see, e.g. [Lipatnikov, 2013], some at The University of Leeds, such as the Leeds Ka model proposed in [Abdel-Gayed et al., 1987] and the Bradley-Lawes $Ka - Le$ model [Bradley et al., 1992], however, the discussion of all of such models is out of the scope this thesis.

Perhaps the simplest and pioneering model for turbulent flame speed was proposed by Damkohler [1940] who proposed:

$$\rho_u v_T A_T = \rho_u v_L A_L \tag{4.27}$$

where, A_L is the overall area of the wrinkled flame surface, whereas, A_T is mean area of the flame front within the turbulent brush. The turbulent flame speed, v_T, is therefore given by:

$$v_T = v_L \left\langle \frac{A_L}{A_T} \right\rangle \tag{4.28}$$

Damköhler related v_T to the rms velocity, u', by proposing that $A_L/A_T = 1 + v'/v_L$ which results in the expression:

$$v_T = v_L + v' \tag{4.29}$$

The model produces reasonable u' dependency trends for v_T as the u' increases, as long as u' is not too high so that it causes extinction to occur, as clearly the model predicts an indefinitely increasing turbulent burning velocity as u' increases. Another deficiency is that the model produces non-physical trends for

mixtures which are outside the flammability limits, for which v_L is zero, however, the model gives a v_T equal to v' [Warnatz et al., 2001].

Zimont [1979] proposed that the mechanism of turbulence effects on the turbulent burning velocity can be treated based on the eddy size. In his model, the effect of the larger eddies of size comparable to the integral length scale is wrinkling of the flamelets increasing the entrainment area and the burning velocity. Mathematically, the enhancing effect of an increased entrainment area of the flame on the otherwise low laminar burning velocity can be given as,

$$u_t = u_{n,t} \left\langle \frac{\overline{A_t}}{A_o} \right\rangle \tag{4.30}$$

however, the ratio of the total area of the wrinkled, thickened flame, A_t, to the projected areas, A_o, is not used here to enhance the local laminar burning velocity, u_l, but rather a local quasi-laminar burning velocity, $u_{n,t} \propto u' Da^{1/2}$. The smaller eddies, i.e. $\eta < \delta_l$ affect the burning rate by penetrating the preheat zone which enhances the local mixing, as a result of this preheat zone perturbation, the flame is thickened. Zimont's assumptions cause a fully developed flame as the ratio $\overline{A_t}/A_o$ is assumed to be independent of the flame development time. The fully developed turbulent burning velocity was thus given as,

$$u_{t,\infty} = C_z u' Da^{1/4} \tag{4.31}$$

where, Da is the Damköhler number given by Equation 4.20, C_z is a model constant for which different values have to be taken based on whether a two-zone approach is considered or three-zone [Abdi Aghdam, 2003]. As the velocity by Equation 4.31 can either be the turbulent mass burning velocity, u_{tr}, as originally intended by Zimont, or the entrainment velocity, u_{te}, as intended here in a three-zone approach; the model constant, C_z, can be regarded as the ratio of the two velocities, i.e. u_{tr}/u_{te}, [Conway, 2013]. In an attempt to define this relationship and assign a single value to C_z, whether two-zone or three-zone approach is used; a density ratio, ρ_u/ρ_b, has been included in Equation 4.31.

$$u_{t,\infty} = C_z u' Da^{1/4} \frac{\rho_u}{\rho_b} \tag{4.32}$$

Equation 4.32 intends to capture the thermal expansion effects on flame. A value of 0.35 for C_z has been found reasonable for various naturally aspirated and turbocharged engines by Conway [2013], it has been adopted in this work too.

The assumptions in the Zimont model hold true for moderate turbulence, i.e. $u' < u'_m$, where, u'_m is the level of turbulence after which the turbulent burning velocity starts to decrease as the flamelets start to fold and merge decreasing the surface area. Moreover, for the wrinkling caused by larger eddies the condition $L >> \delta_l$ should hold true and for small-scale mixing the condition $\eta < \delta_l$. This is true for high Reynolds numbers and Damköhler numbers i.e. the wrinkled and corrugated flamelet regimes as shown earlier in Figure 4.5; these assumptions are very relevant to SI engine combustion, unlike the rather simpler laminar flamelet approach briefly touched in Section 4.3.2.1.

Lipatnikov and Chomiak [1997] pointed out the time dependency of the flame development, i.e. the time scale for the various convection, conduction and chemical processes equilibrate is longer than for the small-scale mixing processes and therefore the flame brush thickness depends on the flame development time. This is particularly true for flames in SI engines, as the flame originates from a small kernel and so its radius ranges from a very small value which is a few times of the large-scale eddies to a point where the condition $L >> \delta_l$ becomes true, to a point where the flame radius is much larger than the integral length scale. Optical observation of engine flames reveals that three distinct phases of flame development exist [Liu et al., 2013]. These are initial rapid flame acceleration, main propagation of the fully developed flame with an approximately constant velocity and finally a deceleration phase in the close proximity of the cylinder walls. The early flame kernel grows in a laminar-like manner, it wrinkles as it interacts with the turbulent eddies increasing the surface area and the brush thickness which increases the turbulent rate. This is physically observed as the rapid acceleration of the flame. Lipatnikov and Chomiak [1997] proposed a development factor, f_d, which encapsulates elapsed time since spark, t, and is given as,

$$f_d = \left\{1 + \frac{\tau_L}{t}[e^{\left(-\frac{t}{\tau_L}\right)} - 1]\right\}^{1/2} \tag{4.33}$$

Although the Lipatnikov model produces a decreasing flame acceleration however, it does not account for the flame deceleration when it is in close vicinity of the cylinder walls. This flame-wall interaction is a complex physicochemical phenomena and it is particularly difficult to study in engines even with a full-bore optical access due to light reflection from the chamber walls. As the flame approaches the walls, heat loss from the flame increases which decreases the reaction rates. Moreover, the wrinkled flame also gets truncated due to contact with the walls decreasing the entrainment area and the termination of radicals at solid

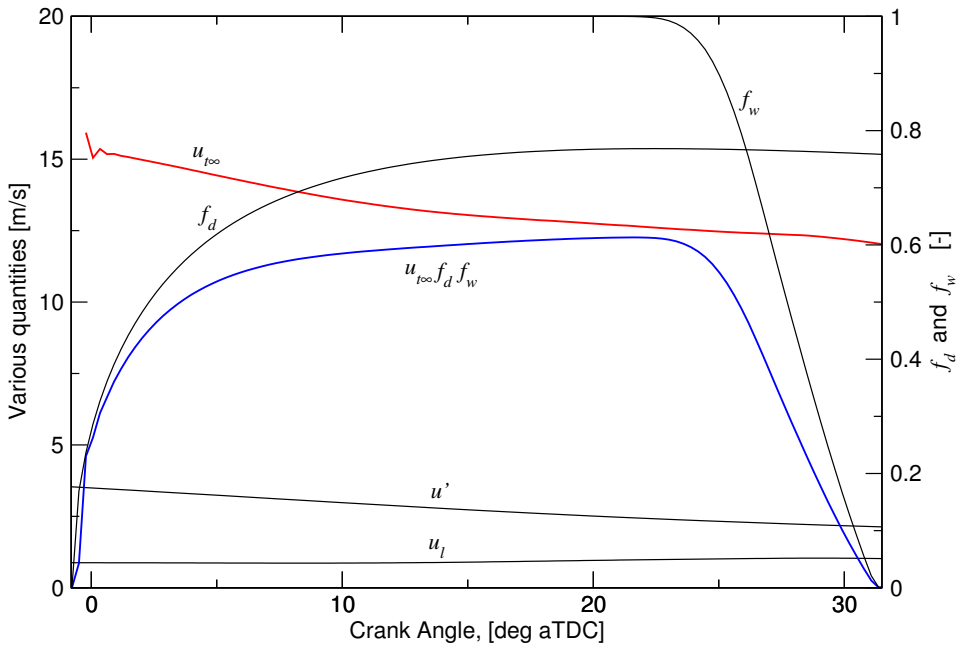

Figure 4.6: Typical behaviour of various Zimont-Lipatnikov model quantities. Calculations made for Di3 engine, see Section 4.10.2 for engine details, at 2000 rpm, 20 bar bmep. The u_l is determined for a stoichiometric mixture of indolene and air.

surfaces leads to flame extinction.

Abdi Aghdam [2003] observed in his optical observations of a disk chamber LUPOE[1] that the ratio of the active entrainment area of the flame to the total area (entrainment and the contact) is largely independent of the engine operating conditions, when plotted against the ratio, r_f/r_b; where, r_f is the flame radius and r_b is the bore radius. In earlier LUSIE versions, this ratio was multiplied with the burning velocity to account for flame deceleration. However, since this simpler approach did not account for the flame brush and the approach was based on observations of a disk shaped chamber, an expression was added to LUSIE by Hattrell [2007] derived on basis of the self-similar flame structure by Lipatnikov and Chomiak [2000] and applied to engine combustion by Aghdam et al. [2007]. Measurements of a progress variable representing the deceleration factor tends to collapse into a single curve, best represented by a function of the following form:

$$f_w = erf\left(\frac{R_w - r'}{\delta_t(t)}\right) \tag{4.34}$$

[1]LUPOE stands for Leeds University Ported Optical Engine. For details on LUPOE see Section 4.10.1.

Where R_w is the bore radius and r' is the current flame radius. The flame brush thickness, δ_t, is governed by turbulent diffusion and is given by Lipatnikov and Chomiak [2000] as:

$$\delta_t(t) = u'\tau_L \left\{ 2t' \left[1 - \frac{1}{t'}(1 - e^{-t'}) \right] \right\}^{1/2} \tag{4.35}$$

Where t' is a dimensionless time given by t/τ_L.

The entrainment velocity, u_{te}, required for the mass entrainment rate in equation (4.23) is given by the expression:

$$u_{te} = (u_l + u_{t,\infty} f_d) f_w \tag{4.36}$$

Figure 4.6 shows graphically various quantities which have been discussed so far. Since the flame which has a characteristic laminar burning velocity, u_l, is subjected to turbulence of intensity, u', consequentially its fully developed turbulent burning velocity, u_{t0}, is much higher than u_l and is shown by the red line. However, in an engine, this equilibrium velocity is not achieved instantaneously at the inception of the flame. The initial flame acceleration is accounted for by the development factor, f_d, and the final deceleration due to wall proximity by, f_w. These factors when multiplied to u_{t0} produce the expected three stages of flame propagation, shown in blue.

The Zimont-Lipatnikov model has been extensively studied in Lipatnikov and Chomiak [2002] as well as Abdi Aghdam [2003] who made a comparison with the Leeds Ka and $KaLe$ models and found that the models performed similarly well, however, the Zimont-Lipatnikov model performed better at different compression ratios, equivalence ratios and speeds of the naturally aspirated LUPOE. The model has previously been found to perform well for a variety of engines and operating conditions and it has been adopted in this work as well. However, most of the previous applications of this model have been to naturally aspirated engines and it must be pointed out that with extreme pressure charging of engines, there is a need for an investigation into the validity of the Zimont model to such modern turbocharged engines. In this work the model has been applied to a turbocharged SI engine.

4.6 Introduction to LUSIE

LUSIE is a collection of models which simulate the closed part of the engine cycle including the compression and expansion by modelling its various physicochemical processes in a sequential manner. This is done by dividing the whole duration of the firing cycle in small discrete time steps. For every incremental change in the time the piston movement is calculated and the corresponding volume and resulting pressure changes as well. Specialized routines calculate the flow characteristics, combustion rate, chemical equilibrium composition, heat transfer and blowby etc. An excellent description of the LUSIE models and its way of operation has been presented by Hattrell [2007] and Conway [2013]. A brief overview of these routines/models is presented in the following sections leading up to a description of GT-LU which is the main research tool used in the present work.

4.6.1 Motoring simulation

Each LUSIE simulation run begins by first performing a motoring simulation of the cycle. This is done by simply calculating the polytropic compression pressure and temperature as the combustion chamber volume changes because of the piston motion. The in-cylinder composition is assumed to be frozen. The heat loss to the walls is calculated and the mass lost due to blowby as well.

4.6.2 Heat transfer

The dominant mode of heat transfer between the combustion gases and the engine chamber walls in SI engines is convection. Heat flux varies from surface to surface and may reach values of $10\,\mathrm{MW/m^2}$ at the interface of the burned gas and the chamber walls, known as the wetted area, [Heywood, 1988]. Numerous formulas exist for instantaneous convective heat transfer coefficient which originate from the Nusselt-Reynolds relationships for turbulent flows in pipes. Correlations of Annand [1963] and Woschni [1967] are used in LUSIE as in many other engine simulation packages. Details on the implementation of these correlations in LUSIE can be seen in [Abdi Aghdam, 2003], [Liu, 2004], [Hattrell, 2007] and [Conway, 2013].

4.6.3 Blowby

Pressure in the crank case remains much lower than the compression and combustion pressures in the cylinder. The in-cylinder gases tend to leak through the gap between the piston and the liner. This flow is minimised by machining the piston and the liner to very close tolerances to achieve the tightest possible fit. Additional sealing is provided by installing a set of rings on the piston which provide even tighter seal without excessive friction and a dedicated oil scrapper ring also helps in maintaining a film of lubricant. Modern production engines have low levels of blowby and therefore a good prediction of the cylinder pressures can be achieved even in the absence of a blowby model. LUPOE2-D, see Section 4.10.1 for details on the engine, however, has considerable amount of blowby (about 10% from previous studies on LUPOE1 [Abdi Aghdam, 2003]) and therefore blowby is modelled for LUPOE2-D simulations only.

LUSIE includes a blowby model which simulates the leakage of in-cylinder gases by an expression for compressible isentropic flow of gas though an orifice. The derivation of the expression can be seen in Appendix C of [Heywood, 1988] and details on its implementation in LUSIE can be found in [Abdi Aghdam, 2003] and [Hattrell, 2007]. In LUSIE a distinction is made between the part of blowby mass which permanently escapes the combustion chamber and a portion which re-enters the combustion chamber during the late stages of combustion during the expansion stroke.

4.6.4 Laminar burning velocity

For SI engine modelling, the laminar burning velocity can be most accurately determined by using empirical correlations derived from experimental measurements in a spherical vessel of the flame radius and associated pressure rise as a laminar flame propagates radially outwards from a central spark [Heywood, 1988]. Measurements can be found in the literature for laminar burning velocities of methane, propane, iso-octane, gasoline and methanol, at various engine relevant pressures, temperature and compositions. A power law expression by Metghalchi and Keck [1982] has been used in LUSIE as well as GT-Power and is given as,

$$u_l = \left(B_m + B_\phi(\phi - \phi_m)^2\right)\left(\frac{T_u}{T_0}\right)\alpha\left(\frac{p}{p_0}\right)^{\beta}(1 - 2.06(Dilution)^{0.77}) \qquad (4.37)$$

where, B_m is the maximum velocity at an equivalence ratio ϕ_m. The in-cylinder equivalence ratio is ϕ, T_u is the unburned gas temperature and T_0 and p_0 are standard temperature and pressure, 300 K and 1 atm respectively. Dilution refers to the mass fraction of the residuals in the unburned zone. The temperature and pressure exponents, α and β, and the other model constants for gasoline which are used in this work are based on the works of Takashi and Kimitoshi [2006] and are given as:

B_m [m/s]	B_ϕ [m/s]	ϕ_m	α	β
0.350	-0.549	1.1	2.4 - 0.271 $\phi^{3.51}$	-0.357 + 0.14 $\phi^{2.77}$

4.6.5 Autoignition modelling

Autoignition modelling is key to the prediction of knock occurrence during the development phase of an engine design and this is one of the main objectives of this work. As discussed in Chapter 2, chemical reaction kinetics has been employed to predict the end gas autoignition. Prior to the use of detailed chemical kinetic mechanisms, an empirical expression and skeletal mechanisms have long been used in LUSIE and GT-LU. A widely used empirical model is by Douaud and Eyzat [1978], commonly known as the D&E model and it has been introduced earlier in Section 1.6. Among the skeletal models are the renowned 'Shell' model by Halstead et al. [1977] as well as the model by Chun et al. [1989] and its refinements, e.g. [Cowart et al., 1991] and [Nishiwaki et al., 2000], were previously used for autoignition with reasonable success. These mechanisms have been discussed in Chapter 2, discussion here is reserved only for the coupling of chemistry solver with LUSIE and GT-LU.

The autoignition modelling approach in this work involves modelling of the oxidation chemistry of the air-fuel mixture in the end gas by using the chemistry solver discussed earlier in Section 2.4. The chemistry calculations are performed at each time step (or the crank degree increment) of the main engine cycle simulation. The inputs required for the chemistry modelling are the pressure, temperature, volume and initial composition of the end gas. On every call to the autoignition subroutine, the change in concentration of each species and the new end gas temperature is determined. The new unburned zone temperature is fed back to the main cycle simulation and the species concentrations are saved for the next iteration, see Figure 4.7. Same procedure is carried out for subsequent time steps, however, the saved specie concentrations from the previous time step are

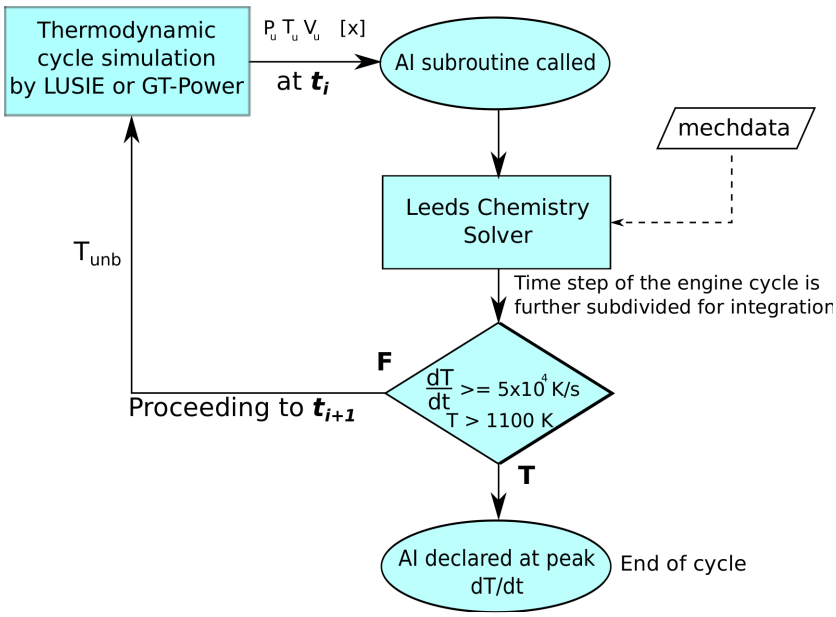

Figure 4.7: Flow of data and sequence of operations carried out in autoignition modelling. AI stands for autoignition.

used to advance the chemistry calculations. However, since the cylinder volume changes continuously so does the number of moles of the unburned gas as the flame advances and consumes a portion of it, the concentration of species within the autoignition subroutine needs to be adjusted at every time step.

4.6.5.1 Species translation between LUSIE/GT-LU and chemical kinetics mechanisms

Modelling of the main combustion event, i.e. flame propagation requires the knowledge of laminar burning velocity of the fuel. As in this work, an empirical expression, Equation 4.37, has been used to determine the laminar burning velocity of gasoline and since, a gasoline surrogate is to be used for the autoignition in end gas, the composition of the end gas as determined by the combustion routine must be translated into an equivalent surrogate-air mixture with the same equivalence ratio and total amount by mass.

The situation is much simpler if the fuel is a pure compound, e.g. iso-octane or n-heptane. In this case, the molar concentration of the unburned species i.e. fuel, O_2, N_2 and the burned residuals are simply assigned to the appropriate elements of the composition array in the autoignition subroutine. However, if gasoline is to be modelled, then typically indolene which is a standard gasoline, is

used to simulate the flame propagation event. It is common practice to adjust the calorific value and the stoichiometric air-to-fuel ratio of indolene to match that of the target gasoline. Translating the unburned gas composition, indolene, air and residuals, to the species in autoignition subroutine is not that straightforward.

Since we are simulating the autoignition behaviour of gasoline by means of a surrogate, the underlying assumption is that the surrogate *must* replace gasoline at the same equivalence ratio. Splitting the concentration or moles of gasoline in the unburned gas into the surrogate components based on its molar composition will only be acceptable if the C/H/O atomic proportion of indolene is the same as that of the surrogate. Or in other words, the surrogate has the same stoichiometric air-to-fuel ratio, A/F_{st}, as the target gasoline. It is for this reason that matching of A/F_{st} was emphasised in Section 2.9. However, it may not always be possible to formulate a surrogate with the same stoichiometric air-to-fuel ratio as the target gasoline. The best approach, and the one which is used in this work, is to recalculate the surrogate-air composition according to the prevailing equivalence ratio regardless of whether the A/F_{st} was matched or not while conserving the total mass of unburned charge.

4.6.5.2 Autoignition criteria

The instant at which autoignition is said to have occurred is when there is a sharp increase of temperature. Halstead et al. [1977] used an arbitrary threshold value of 10^7 K/s for the rate of temperature rise or the temperature value of 1100 K. A similar criteria of two conditions has long been used in LUSIE. A temperature rise up to 1100 K at a rate of 10^5 K/s has been used and this criteria has been kept for all skeletal models in the present version of LUSIE. However, it was observed that the same criteria did not produce sensible autoignition onset timings when detailed chemical kinetics was used.

A temperature threshold as low as 1100 K was attained at fairly similar times by different mechanisms as well as different surrogates resulting in a decreased sensitivity of the autoignition onset to different mechanisms or surrogates. For example, when PRFs of RON ranging from 0 to 100 were subjected to the same unburned zone $p-T$ conditions, the autoignition onset varied by only a few degrees. A more sensible autoignition criteria is the peak of the rate of temperature rise as this is the criteria used in the constant volume predictions of autoignition. Therefore, in detailed chemical kinetics modelling, the autoignition onset is taken to be the time at which the highest peak of the rate of temperature rise is achieved

and it is at least over $50000\,\mathrm{K/s}$ and the unburned temperature is at least 1100 K.

4.6.6 Cyclic variability

Engine processes are transient in nature even when the engine is operating at steady operating conditions, i.e. load and speed. A manifestation of this is that the cylinder pressure varies substantially between individual cycles, as much as 20 %. This variation is reflected in associated performance parameters, e.g. the mean effective pressure. The cyclic variability worsens the operating range of the engine as well as its performance. It has been previously claimed that as much as 10 % increase in the power can be achieved with same fuel consumption in the absence of cyclic variability [Ozdor et al., 1994]. Besides, at knock limited spark timing, it is the fastest burning cycles with high pressures which are more prone to knocking; they therefore determine the maximum compression ratio and the octane requirement of the engine. Another problem associated with cyclic variability is the emissions which may arise if the variability is likely to lead to a missfire.

In order to quantify cycle to cycle variability (ccv) normally a coefficient of variation or standard deviation of a fluctuating quantity is determined. This quantity may be the imep, combustion duration or the in-cylinder pressure, either its maximum value or one at a certain crank angle. The origins of cyclic variability may arise from a number of factors discussed in detail by Matekunas [1983] and Ozdor et al. [1994]. Some of the key factors which may cause cyclic variability have been summarised below.

- Variation in flow-field i.e. turbulence. This is marked by a fluctuation of rms velocity at a given angle from one cycle to another.
- Variation in overall equivalence ratio from one cycle to another owing to variation in injection characteristics or evaporation in case of port fuel injected or carburetted engines.
- The amount of burned gas residuals or recirculated exhaust gas.
- Spatial variation in equivalence ratio in the combustion chamber caused by imperfect mixing of fuel-air and residuals causing inhomogeneities.
- Variation in spark discharge characteristics which may affect the initial flame kernel growth.

Aghdam et al. [2007] suggest that the factors arising from the spark plug type and the orientation of the spark gap may affect the extent of cyclic variability but as they do not vary from one cycle to another they are not the primary cause of variability. Effects of spark discharge are minimal as well, as long as the spark energy exceeds the activation energy which is mostly the case. Hinze and Miles [1999] found that the spatial variation of the burned residuals decreases to less than 1 % of the rms value around the spark plug region towards the end of the compression stroke rendering it insignificant. Various studies suggest that variability in turbulence intensity and the charge composition (charge dilution) are the most significant causes of cyclic variability, see [Burluka et al., 2012; Johansson, 1996; Lipatnikov and Chomiak, 1998; Shen et al., 1996].

Various modelling approaches have been adopted to investigate cyclic variability in engines. These range from simpler phenomenological models up to Direct Numerical Simulations (for pros and cons of CFD modelling, interested reader is referred to Chapter 3 in [Conway, 2013]). If the objective of cyclic variability modelling is to study its effect on engine performance and knocking tendency, then a simpler phenomenological approach is preferred. Aghdam et al. [2007] successfully simulated cyclic variability by varying ϕ and u' in LUSIE. This approach was applied to naturally aspirated and heavily turbocharged engines by Conway [2013] and good agreement was found with the experiments. Same approach has been implemented in GT-LU by the author. Variation in ϕ and u' was made according to a Gaussian distribution of a mean value, μ, and standard deviation, σ. A variation in standard deviation of 5 % and 12.5 % for ϕ and u' was made in this work based on the works of Aghdam et al. [2007].

4.7 Introduction to GT-Power

GT-Power[1] is a versatile multiphysics package for engine performance modelling. It combines various models, most of which were primarily developed by Thomas Morel along with other researchers. Central to GT-Power is the 1-D wave dynamics of the complete intake and exhaust system. This is modelled by dividing the intake and exhaust systems into subvolumes to which the conservation of mass and energy is applied and the flow between subvolumes is calculated by using the momentum equation and the solution of such a system of equations is obtained on a "staggered mesh" [Morel et al., 1990; Sapsford et al., 1992]. Since

[1]Gamma Technologies, Inc. www.gtisoft.com

the length of 'plumbing' on an engine is much larger than the cross section, this 1-D discretisation allows for accurate flow modelling in flow objects of various geometries, e.g. pipes of different cross sections, tapers and bends, orifices, etc. Inclusion of in-cylinder processes, e.g. the thermodynamic cycle, combustion and heat transfer creates a complete engine modelling environment which offers fast parametric studies of the gas exchange process and its effects on engine performance. The accuracy of predictions of the gas exchange process through GT-Power has resulted in its wide spread use in the automotive industry; see also Figure 6.2 as an example of the predictions of gas exchange process made in this work by GT-Power.

For combustion, in addition to Wiebe function, a quasi-dimensional thermodynamic model is adopted which is similar in principle to LUSIE as described in Section 4.5.3, however, it differs from LUSIE in regards to the calculation of turbulent entrainment rate. Because the viability of the Zimont-Lipatnikov model in LUSIE has been demonstrated in the past at Leeds University and because it allows greater freedom of studying the effects of various model constants, it is used in this work rather than the one in GT-Power.

GT-Power offers a graphical user interface based platform which allows for a pictorial construction of an engine model as shown in Figure 4.8. In this section, some of the key models of GT-Power which have been employed in this work are presented.

4.7.1 In-cylinder flow models

The fresh charge motion during the intake stroke gives rise to a large-scale jet flow. A major portion of the in-cylinder turbulent kinetic energy is contributed from the large-scale motion of the inducted charge. In direct injection engines fuel injection during compression stroke creates additional kinetic energy. The geometry of the intake ports, valves and combustion chamber may often induce large-scale rotational flows such as swirl, squish and tumble. Moreover, the piston motion affects these flow characteristics by imparting velocity to the flow and also by compressing the charge. The inward piston motion causes a unidirectional i.e. axial compression of the charge. It may also be subject to radial compression due to the squish near the top dead centre. Due to this transient and inhomogeneous nature of in-cylinder flow the detailed 3-D description is a difficult undertaking. The description of turbulence requires solution of partial differential equations for the generation and dissipation of turbulent kinetic en-

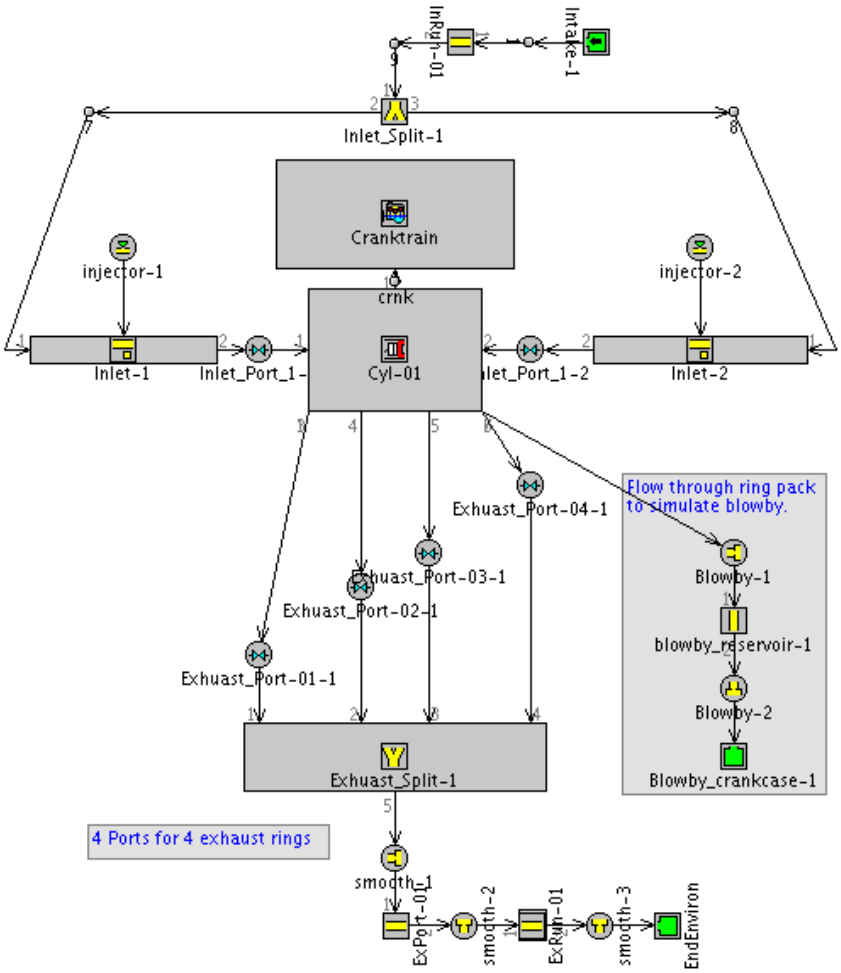

Figure 4.8: Graphical schematic of the LUPOE2-D GT-Power model employed in this work for GT-LU modelling studies of combustion, cyclic variability and autoignition.

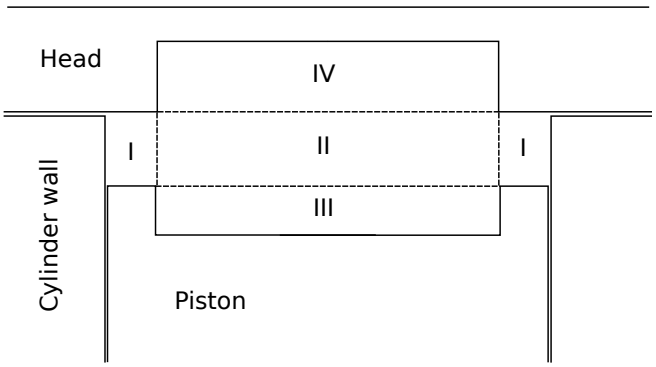

Figure 4.9: Illustration showing the combustion chamber divided in four regions for each of which a pair of turbulent kinetic energy and dissipation rate equations are solved.

ergy, e.g. as the widely used $k - \epsilon$ model. In computational fluid dynamics, the numerical solution of the 3-D Navier-Stokes equations and turbulence equations discretised over the whole cylinder volume is carried out. Such simulations are time consuming and computationally expensive.

A much simpler alternative to CFD is a zonal approach as proposed by Morel and Mansour [1982] by means of which the state of turbulence is determined in relatively larger regions or zones of the flow-field. In GT-Power, the combustion chamber is divided into four subvolumes as shown in Figure 4.9, in which the turbulence is assumed to be homogeneous and isotropic. The flow in each subvolume is defined by the calculation of radial and axial velocities, swirl, squish, turbulence kinetic energy and a turbulent length scale. Details on this subvolume approach to the application of $k - \epsilon$ model in engines can be found in Morel and Mansour [1982] and Morel and Keribar [1985].

4.7.1.1 Swirl, radial and axial velocities

The axial velocity component is determined from the piston kinematics which is the velocity of the piston relative to the liner. The radial velocity is due to squish and the reverse squish between subvolume I and II (Figure 4.9). Squish occurs as the piston reaches near the TDC and the subvolume I above the piston lip squeezes out the charge mass radially inwards in the form of a turbulent jet. The effects of squish on turbulence depends on the geometry of the piston bowl and the head but are generally weak. Squish intensifies the swirl but this happens for only a short span of time and has negligible effect on the burn rate [Lumley, 1999], however, it is accounted for in the model for swirl.

Swirl is determined by a model proposed in [Morel and Keribar, 1985] which assumes that the flow in each subvolume revolves with a constant angular velocity, magnitude of which is intensified as more mass enters the region either from the intake or a neighbouring region or it is reduced as the mass leaves. The angular velocity of the swirl gradually decreases due to the viscous friction acting on the surrounding walls.

4.7.1.2 Turbulence model

Morel and Mansour [1982] extended the standard $k-\epsilon$ model for engines following the proposition made by Reynolds [1980] on the limitations of the standard energy dissipation equation to capture the behaviour of homogeneous turbulence in engines. Morel pointed out that in addition to Reynolds proposition of a spherical compression in engines, the compression is axial as well as radial. Use of original model was found to produce an unrealistic increase in the turbulent length scale as the charge was compressed. This problem was eliminated by modifying the kinetic energy production term by defining the local strain-rate tensor for the three types of compressions i.e. pure spherical, axial and radial. The resulting transport equations are presented here for reference. For kinetic energy:

$$(m_j k_j)' = \sum \dot{m}_{ij} k_{ij} + \sum \rho U_{diff}(k_i - k_j)A + m_j S_k + \dot{m}_{int} k^*_{int} - \dot{m}_{exh} k^*_{exh} + \dot{m}_{inj} k^{**}_{inj} + \dot{m}_{sq} k^{**}_{sq} \tag{4.38}$$

and for energy dissipation:

$$(m_j \epsilon_j)' = \sum \dot{m}_{ij} \epsilon_{ij} + \sum \rho U_{diff}(\epsilon_i - \epsilon_j)A + m_j S_\epsilon + \dot{m}_{int} \epsilon^*_{int} - \dot{m}_{exh} \epsilon^*_{exh} + \dot{m}_{inj} \epsilon^{**}_{inj} + \dot{m}_{sq} \epsilon^{**}_{sq} + \frac{k_j^2}{L_j^2} \tag{4.39}$$

Where the superscript * indicates that the terms be applied to region I and IV and ** applies to region II, III and IV only. The subscript j refers to the region under consideration, i refers to the adjacent region. Subscript ij refers to the situations where the subscript can either be i or j depending on the direction of flow between the two regions. Various kinetic energy source terms are: k_{int}, due to the charge inducted through the intake; k_{exh}, due to the mass leaving to the exhaust; k_{inj}, due to the fuel injection; k_{sq}, due to squish. Further details on those

can be found in [Morel and Mansour, 1982].

The two $k - \epsilon$ coupled partial differential equations are solved for all four regions along with the equations for swirl and squish. The quasi-dimensional modelling of combustion results in a division of the charge in two zones, a burned and an unburned zone. An assumption of a spherical flame which is truncated by the chamber walls and the knowledge of the amount of mass burned helps in determining the size and shape of the burned zone. The solution of the $k - \epsilon$ model for all four regions results in the knowledge of total kinetic energy of each region which can then be used to determine specific kinetic energy of the burned and unburned zone.

4.8 Introduction to GT-LU

GT-LU, which is formed by the coupling of GT-Power and LUSIE was first developed by Hattrell [2007]. The description of the earlier version can be found in [Hattrell et al., 2006]. For the current version of GT-LU, the relevant models of LUSIE were migrated to the newer user-templates of GT-Power v 7.2 and v 7.3 with necessary restructuring of the subroutines to allow efficient simulation of multiple cases for multicylinder engines with cyclic variability and autoignition modelling. Some of the new modifications to GT-LU are listed below:

- In the older version, an empirical expression for the determination of u' was incorporated which correlated u' to the mean piston speed. In the current version, for the in-cylinder flow description, provision has been made to either employ the models available in GT-Power for swirl, tumble and the $k - \epsilon$ model for turbulence or to input spatially averaged u' and L obtained by CFD modelling of cold flow i.e. without combustion.

- The autoignition subroutine comprising of the previous empirical and skeletal models of LUSIE have been retained while the newly developed chemical kinetics solver has been added to GT-LU.

- Subroutines to model cyclic variability in combustion by using the approach outlined in Section 4.6.6 were retained with appropriate restructuring in the current version of GT-LU.

The operation of GT-LU is such that GT-Power controls the overall execution of the code and provides the user with the graphical user interface. The engine

model is constructed by the selection of appropriate submodels for engine geometry, fluid flow, heat transfer, combustion etc; an example of which is presented in Figure 4.8. Figure 4.10 shows a flowchart of sequence of operations carried out by GT-LU. Details on the use of GT-LU can be found in AppendixA.1.

4.9 CFD modelling of turbulence

The multi-zone approach to combustion modelling abandons the geometric details of the flow-field i.e. it assumes homogeneous and isotropic turbulence. To accompany this approach the nature of in-cylinder flow is simplified and described by quantities such as u' and L obtained after averaging. Intensive and detailed CFD modelling approaches such as Direct Numerical Simulation (DNS) and even the relatively simplified approaches such as Large Eddy Simulation (LES) and the solution of Reynolds Averaged Navier-Stokes (RANS) equations are not justifiable when a multi-zone combustion model is to be used as the superfluity of 3-D details of the flow are to be eventually averaged into a single representative quantity for the whole volume. Moreover, the computational power and time required for such simulations are of the order of a few days to weeks. The $k-\epsilon$ turbulence model makes an *a priori* assumption that the turbulence is isotropic and therefore the turbulence intensity and length scales can be taken as scalars. This major simplification of the $k-\epsilon$ model results in its ease of use and due to which it is widely popular. Its implementation in a simpler domain (subvolume approach as discussed in Section 4.7.1.2) has also seen great use. However, typically during the engine development process, CFD modelling of the flow from the intake runners, through the ports and into the cylinder is carried out to optimise geometries for better bulk flow characteristics such as swirl and tumble. Normally, revised $k-\epsilon$ models are used such as the RNG $k-\epsilon$ model; i.e. obtained by using the Re-Normalisation Group methods. This model was used in support of this work. From such simulations, the mass averaged kinetic energy of the charge can be obtained as well as an integral length scale and can be used for multi-zone combustion modelling. It is of interest to compare the turbulence calculations of the subvolume approach to the $k-\epsilon$ model in GT-Power and the CFD modelling results from a RNG $k-\epsilon$ model. This comparison is presented in Chapter 6.

The CFD modelling in support of this work was carried out with the package, Star-CD, at Mahle Powetrain Ltd. The kinetic energy averaged over the whole

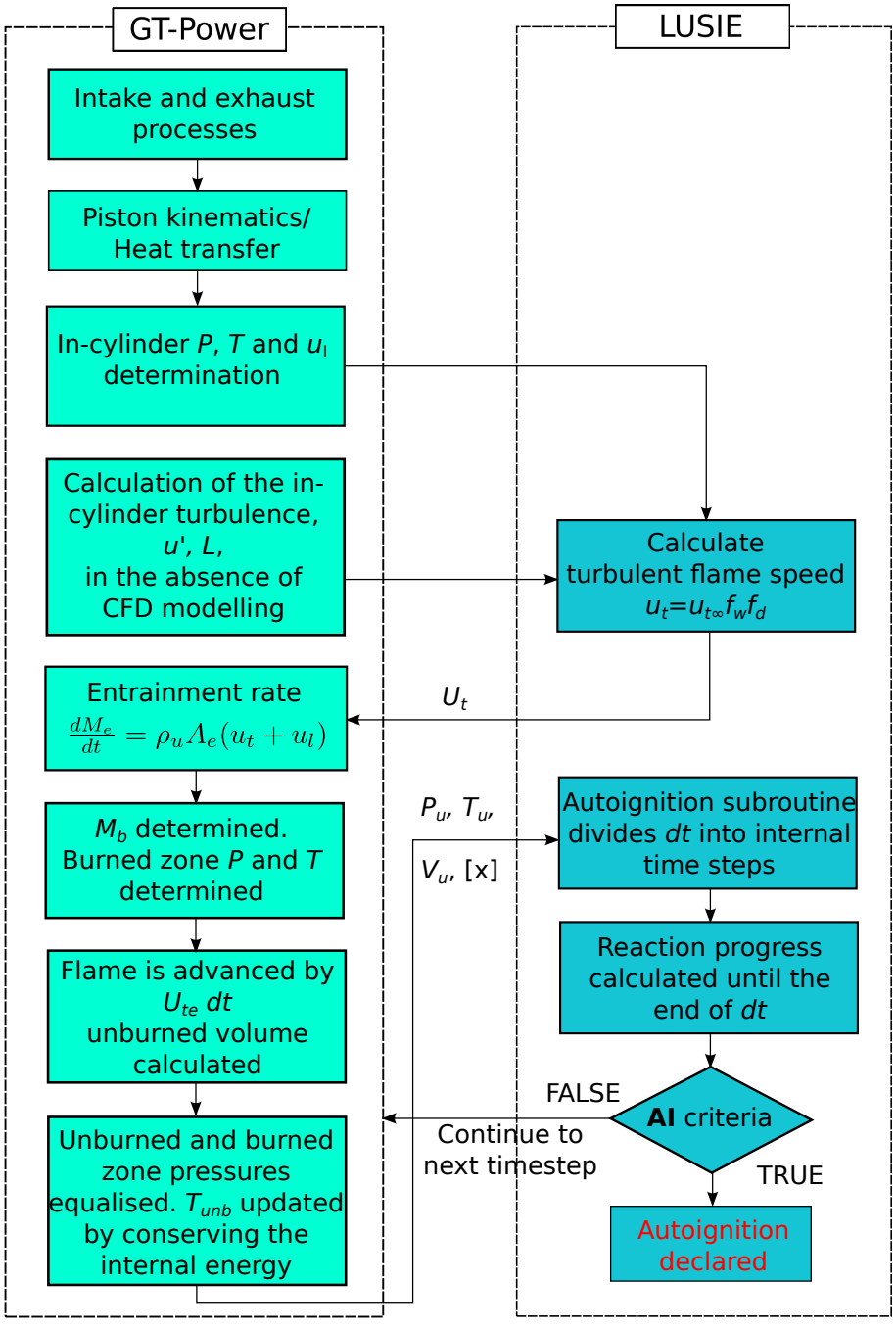

Figure 4.10: Flow of data and sequence of operations carried out by GT-LU

cylinder charge for cold flow, i.e. without combustion, and is used as an input to the entrainment model. This makes the turbulence generated from CFD different from the subvolume approach in which only the unburned mass is used in the averaging. The subvolume approach tends to over predict the turbulence intensity because of large sized subvolumes on which the transport equations are applied. Mass transfer between these subvolumes is accounted for in the bulk flow whereas the motion of the mass which stays with in one region constitutes turbulence.

4.10 Description of the test cases

No experimental work was undertaken by the author, however, the modelling work has been supported by measurements from two research engines. One, LUPOE2-D which is a bespoke optical research engine at the University of Leeds and the second engine, a 3-cylinder downsized, technology demonstrator engine designed and built at Mahle Powertrain Ltd. It is referred here as the Mahle Di3 engine. The description of these engines is given in following sections.

4.10.1 LUPOE2-D

LUPOE is the acronym for Leeds University Ported Optical Engine constructed on top of a single cylinder agricultural diesel engine made by Lister-Petter which donated the crank assembly on which bespoke piston, head and liner were installed. Modifications were also made to the intake and exhaust system. The name LUPOE is followed by a number indicating the generation and an alphabet which indicates the combustion chamber or head geometry; such as LUPOE2-D, which has a disk shaped combustion chamber i.e. a flat head and piston. LUPOE2-D experiments performed by Roberts [2010] have been analysed in this work and used in support of the combustion and autoignition modelling. The experimental setup is shown in Figure 4.12 and the design specifications of LUPOE2-D are presented in Table 4.1.

Modifications to the intake and exhaust system were made with the intention to reduce large-scale mean flow as much as possible. This was attempted by orienting the two diametrically opposed intake ports at a certain angle to the cylinder axis that minimal bulk flow motion is achieved in the cylinder (see Figure 4.11). The liner was designed to have four staggered rings of exhaust ports as

Bore (mm)	80
Stroke (mm)	110
Conrod length (mm)	232
Clearance height (mm)	7.5
Geometric swept volume (cm^3)	552.9
Effective swept volume (cm^3)	361.4
Geometric compression ratio	15.7
Effective compression ratio	10.6
Intake port close (° CA aTDC)	-107.8
Exhaust port open (° CA aTDC)	101.0

Table 4.1: Design specifications of the LUPOE2-D as used in experiments by Roberts [2010].

can be seen in Figure 4.11 to enhance the scavenging process and reduce burned residual. This was done to reduce any ambiguity in the charge composition at the beginning of a new cycle. This was further enhanced by operating the engine in a skip-fired mode i.e. the engine was motored for multiple cycles between two fired cycles to purge any left over burned products. The fuel was mixed with air well upstream of the intake ports (about 350 mm) via a bespoke fuel injector located in the throat of a venturi. The fuel supply was pressure regulated and its mass flow rate was carefully controlled to achieve correct mixture composition. The intake runners were heated using band heaters to assist evaporation and mixing to achieve a homogeneous mixture. The engine is air cooled and cylinder barrel and the head temperature was regulated by means of heaters and thermocouples. The engine can be run in both SI and HCCI mode.

The engine can be operated with a metallic head or a head with a full-bore window fitted with a quartz disc to allow high speed filming. However, since the objective of this work and of that of Roberts [2010] was the study of autoignition, the metallic head was used as the optical head is prone to breaking due to high cylinder pressures in knocking regime. The in-cylinder pressure was recorded using two pressure transducers. One Kistler piezoelectric pressure transducer Type 601A was mounted flush to the cylinder wall such that the diaphragm was exposed to the chamber surface. This transducer measured the gauge pressure which was referenced to an absolute pressure transducer mounted lower in the barrel where it was shielded from high compression and combustion temperatures. The use of the reference transducer was to accurately measure the cylinder pressure at the exhaust port closure to allow a precise calculation of the end gas pressure and temperature. Detailed information on the measurement of vari-

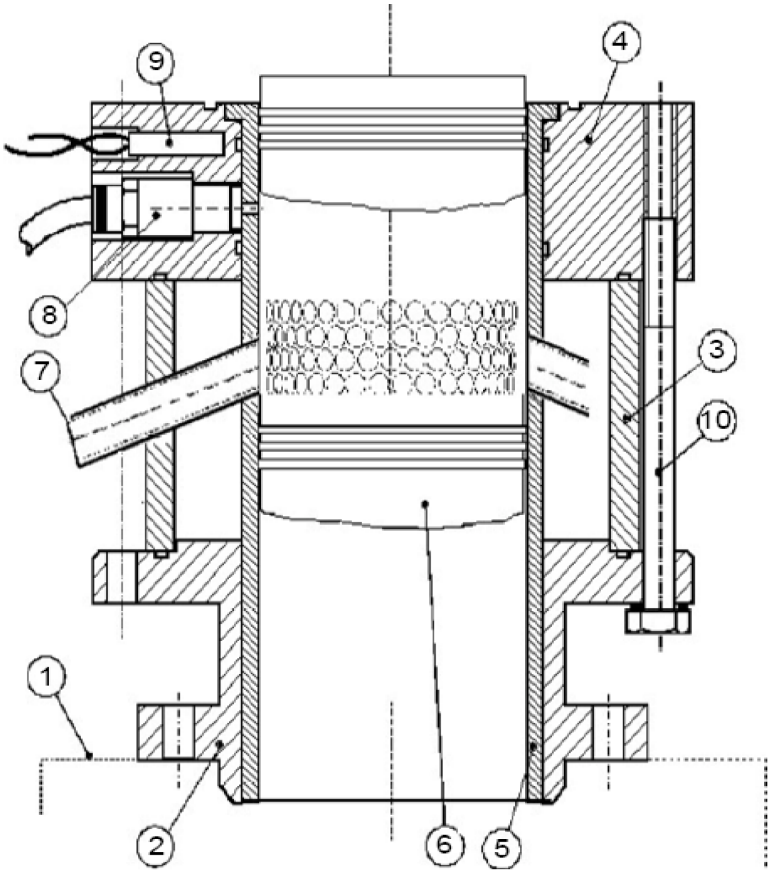

Figure 4.11: An annotated cross-section view of LUPOE2-D [Abdi Aghdam, 2003].

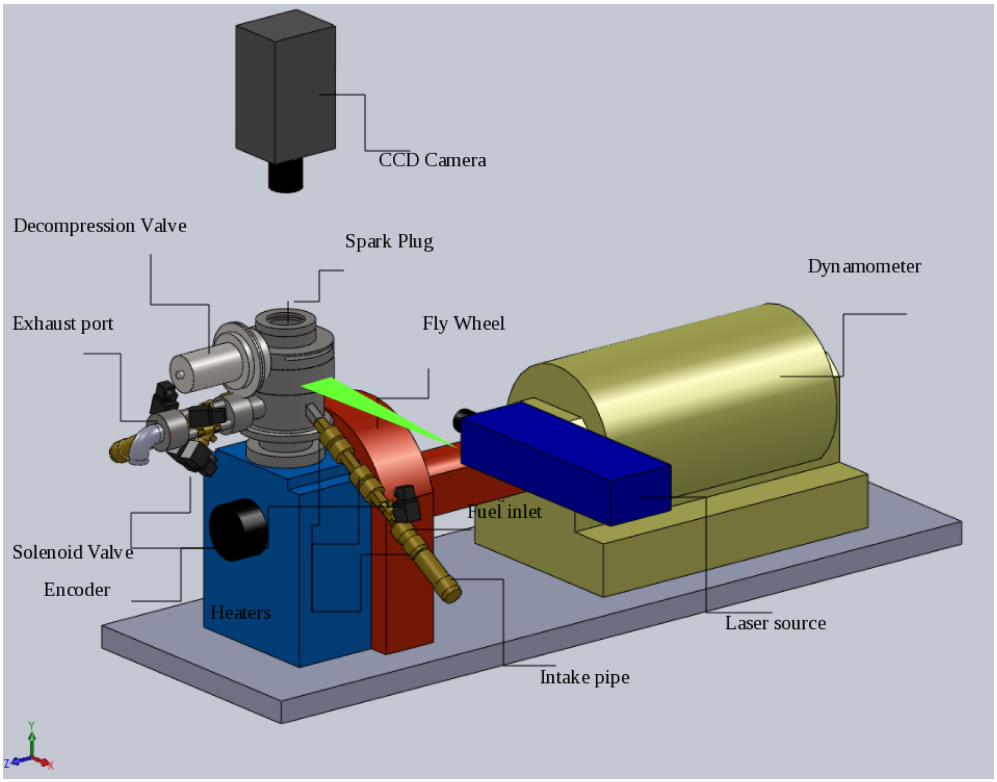

Figure 4.12: An annotated CAD drawing of LUPOE2-D and its auxiliaries. Also shown is the top and side optical access and laser positioning for LDV and PIV experiments [Ling, 2011].

ous other quantities and experimental methodology can be found in Chapter 3 of [Roberts, 2010].

Recent modifications to LUPOE2-D made by Ling [2014] have given it the name 'LUPOE2-D boosted'. These modifications include 1) reduction of the exhaust port rings from four to two to increase the effective compression ratio and 2) independently controlled solenoid valves in exhaust runners which after a number of purging cycles are closed earlier to allow longer filling of the cylinder so that a higher initial pressure is achieved. The engine is always fed with air from a regulated steady supply of compressed air at 4 bar pressure. This arrangement has been developed to study combustion regimes which occur at higher pressures. However, naturally aspirated LUPOE2-D has been studied in this work. For studies at higher intake pressures, the Mahle turbocharged downsized engine which is described below was used.

4.10.2 Mahle Di3 engine

This engine was developed by Mahle Powertrain Ltd. to demonstrate advantages of the aggressive downsizing and turbocharging strategy, presented in Chapter 1. The engine is shown in Figure 4.13 and its key specifications are presented in Table 4.2. For further details on design, turbocharging strategy and performance characteristics of the engine, interested reader is referred to [Lumsden et al., 2009]. The engine was put to extensive experimental tests at Mahle to study the limits to which the engine can be taken to achieve these benefits. Expectedly, knocking was found to be a limiting problem for fuels of low octane quality, and especially at low speeds and high loads. That is why, one of the main objectives of this work has been to demonstrate the role of chemical kinetics in autoignition predictions while paying attention to the fuel composition and properties. This was difficult to achieve with the previous skeletal models in LUSIE.

A complete GT-Power engine model was supplied by Mahle which was extensively validated by the author to the test data for a range of operating conditions. The model was modified to run with GT-LU submodels. Before running the model predictively with GT-LU, it was made sure through simulations with a pre-determined combustion rate, that correct volumetric efficiency, indicated and brake mean effective pressures etc. were predicted. This made it easier to discern inaccuracies in predictive combustion from other factors.

Since the engine was designed to meet high performance targets and emission restrictions; its combustion chamber shape is far from the simplified disk shape,

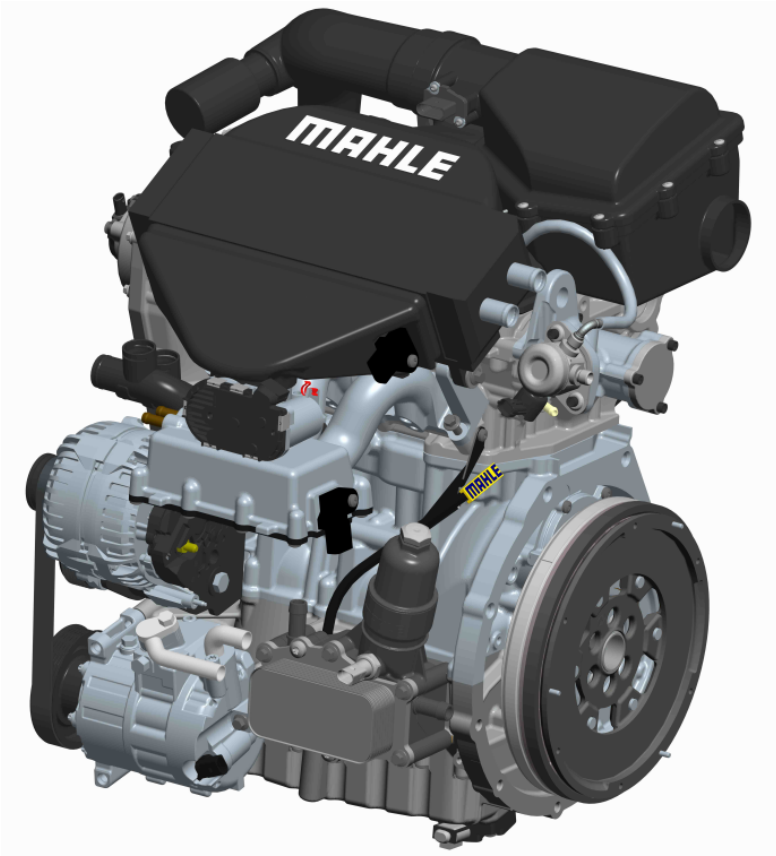

Figure 4.13: A CAD generated view of the Mahle Di3 engine.

Bore (mm)	83
Stroke (mm)	73.9
Stroke-bore ratio	0.89
Cylinder displacement (dm^3)	0.4
Cylinder number and arrangement	3 in-line
Displacement (dm^3)	1.2
Bore spacing (mm)	91
Conrod length (mm)	123
Compression ratio	10.2, 11.2, 12.2 (based on piston design)
Firing order	1-3-2

Table 4.2: Main cylinder and cranktrain design specifications of the Mahle Di3 turbocharged downsized engine.

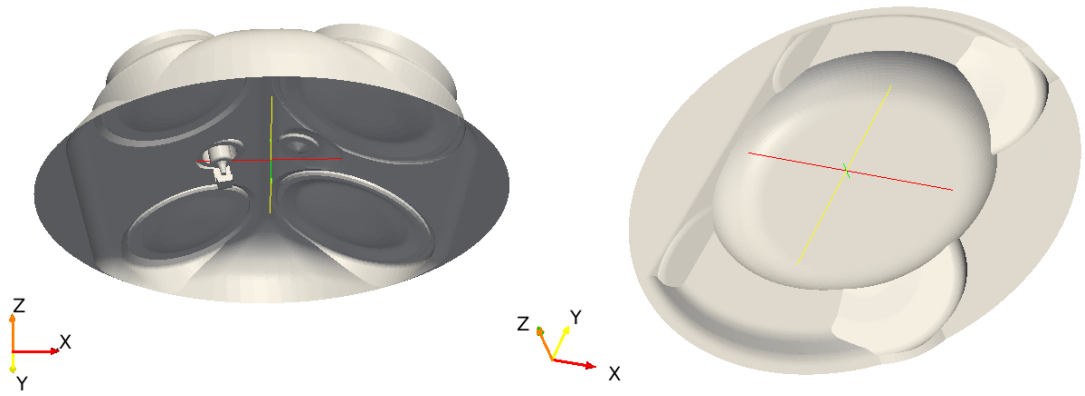

Figure 4.14: Views of the cylinder head (left) and the piston crown (right) of the Mahle Di3 engine.

it is shown in Figure 4.14. Owing to the complex shape of the head and more so of the piston crown, determining the recess volumes to be used for turbulence calculations in GT-Power was not so straightforward. However, volumes were determined by means of a CAD software (SolidWorks) and necessary approximations were made where determining subvolumes directly was not possible.

Chapter 5

Autoignition in LUPOE2-D

5.1 Introduction

Numerous studies have demonstrated that autoignition in HCCI and controlled autoignition (CAI) engines can be reliably predicted using multi-component gasoline surrogate mechanisms, e.g. [Andrae and Head, 2009; Knop et al., 2013]. However, autoignition occurs in HCCI and CAI engines at in-cylinder pressures and temperatures typically much lower than in an SI engine, especially if the latter is supercharged. Furthermore, as stated earlier, chemical kinetic mechanisms are routinely validated against shock tube and rapid compression machine measurements of the ignition delay times, τ_{ign}, of various gasoline surrogate fuels. The conditions for these laboratory measurements are similar to those which prevail before ignition in an HCCI or CAI engine, and the recent kinetic mechanisms, e.g. Andrae and Head [2009]; Huang et al. [2010]; Ra and Reitz [2011], perform remarkably well at these regimes as shown in various Arrhenius plots in Chapter 2, e.g. Figures 2.10 and 2.11. Yet, in an SI engine the propagating premixed flame induces higher end gas pressure and temperature and the question arises of whether the reduced chemical mechanism will perform equally well. This Chapter covers the application of the three reduced chemical kinetic mechanisms studied in Chapters 2 & 3, to the prediction of autoignition in LUPOE2-D.

A review of practical gasoline surrogates was presented in Section 2.8 and the approaches to gasoline surrogate selection were presented in Section 2.9. In this Chapter these approaches have been employed to formulate surrogates to model

Engine speed (rpm)	1500
Equivalence ratio (ϕ)	1.0
Mass flow rate of air (g/s)	13.8
Intake and cylinder head temperature (K)	343
EGR content (% by mass)	0

Table 5.1: LUPOE2-D operating conditions at which ULG90, PRF90, TRF90 and iso-octane were tested.

the autoignition of an unleaded gasoline of RON 90, named here ULG90[1], in LUPOE2-D. Autoignition predictions for iso-octane, PRF90 and a TRF90 composed of 71.5% by volume toluene and the rest n-heptane, have also been made.

5.2 Supporting experiments

Experiments were performed on LUPOE2-D[2] by Roberts [2010]. The engine was operated in skip-fired mode with a non-fired to fired cycle ratio of 9:1. This was done to achieve complete expulsion of the burned gases so that the charge composition at the beginning of a new cycle is unambiguously known. The engine was ran at a standard operating condition presented in Table 5.1.

Iso-octane, as well as three fuels of very different compositions, a commercial gasoline, a PRF and a TRF, but all with the same RON of 90 were tested in the knocking regime to assess the differences in their auto-ignition behaviour. For all the fuels, stoichiometric mixtures were tested. TRF90 was blended with toluene and n-heptane only, as most of the octane quality of ULG90 came from its branched paraffin content. Difference in the reactivity of the two fuels due to different constituents was expected to manifest as different knock onsets regardless of the equivalent RON. However, TRF90 produced a similar knock onset as ULG90, in a contrast to PRF90, discussed later.

5.2.1 Normal burning rates and cyclic variability

All experiments showed considerable cyclic variability in cylinder pressure, as is shown in Figure 5.1 for ULG90. The raw in-cylinder pressures were analysed in this work to make comparisons with each other as well as the simulations. The overall extent of cyclic variability seems to be the same for the four fuels,

[1] See Table 5.2 for the composition of ULG90
[2] For details on LUPOE2-D, see Section 4.10.1

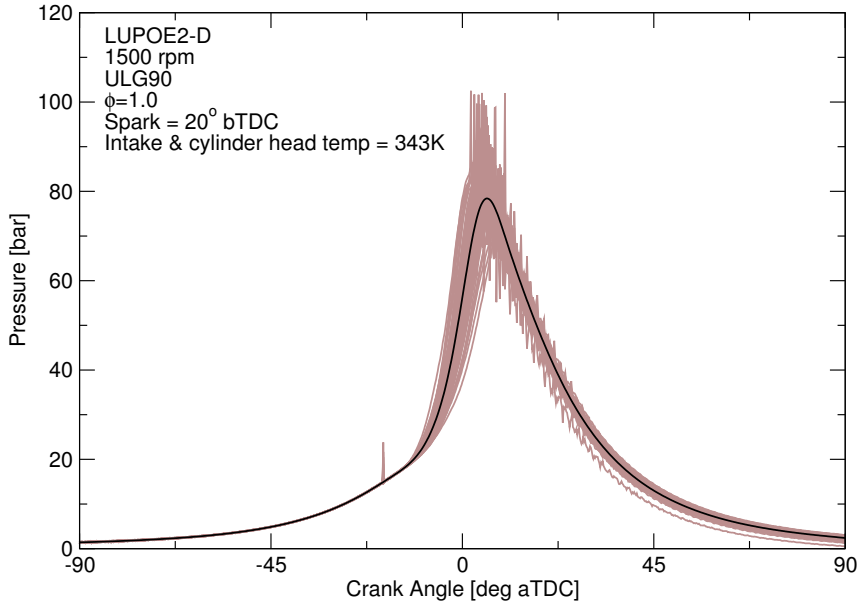

Figure 5.1: A set of 100 fired cycles for ULG90 shown by grey lines. Black line shows the ensemble average of smoothed firing cycles.

however, the mean normal, i.e. pre-knock burn rate forms two groups; iso-octane and PRF90 are slightly slower burning with lower peak pressures compared with the relatively fast burning ULG90 and TRF90. Roberts [2010] corroborated this observation with the works of Smallbone [2004] who conducted experiments on similar ULG and TRF blends in a similar engine. Recent laminar burning velocity, u_l, measurements of Al-Mughanam [2013] in a constant volume spherical bomb show that, at same conditions,[1] toluene and iso-octane consistently have a lower u_l as compared to n-heptane, ethanol and 1-hexene. Particularly, at $\phi = 1$, u_l for toluene and iso-octane is about 0.43 m/s and for n-heptane and ethanol, it is roughly 0.49 m/s. Slower burning of PRF90 and iso-octane can thus be explained with their lower u_l, whereas the relatively faster burning of TRF90 and ULG90 is because of the presence of 28.5% n-heptane in TRF90 and in case of ULG90, due to the presence of olefins.

5.2.2 Fuel effects on knock onset and its statistical variation

Although ULG90 and TRF90 produce higher and earlier peak pressures, they knock slightly later than PRF90, see Figure 5.2. This indicates that the octane quality of PRF90 has depreciated at the prevailing unburned zone $p - T$ conditions of LUPOE2-D from those of the RON test at which the three RON 90 fuels

[1] T = 360 K, P = 0.1 MPa, $\phi = 0.9 - 1.2$

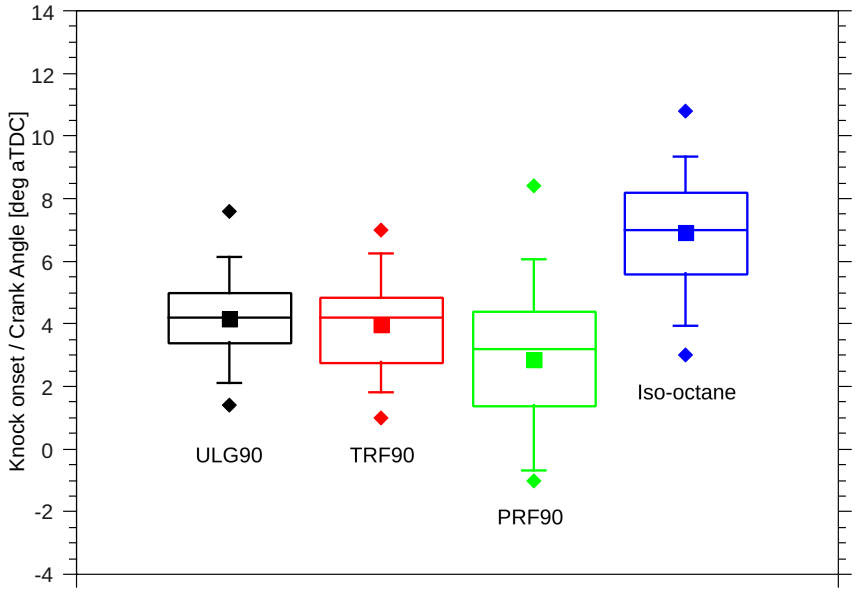

Figure 5.2: Statistical variation of experimental knock onsets for the four tested fuels. Squares: mean knock onset, diamonds: earlier and latest knock onsets, box: 25/75 percentile, whiskers: 5/95 percentile.

(must) have the same knock onset. Iso-octane knocks the latest as expected, however, what is interesting to note is the spread of knock onsets of the four fuels in Figure 5.2. The spread is markedly greater for PRF90 and iso-octane even though their composition is much simpler than ULG90. This suggests that, at the prevailing unburned $p-T$ conditions, the ignition delay times of iso-octane and PRF90 are much more sensitive to variation in pressure and temperature as compared to ULG90 and TRF90. This has implications on the suitability of a fuel for an engine as it is the fastest burning cycles which knock at the earliest and determine the knock limited spark advance (KLSA). Thus a fuel with a greater variability in knock onsets will be more likely to limit a more beneficial spark advance. This will be further investigated by computing reactivity carpet plots of these fuels in the subsequent sections.

PRF90 and TRF90 can be regarded as surrogates for ULG90 due to their same RON and therefore ULG90 is considered to be the reference for in-cylinder thermodynamic state and knock onset. The mean knock onsets shown in Figure 5.2 were obtained by averaging all the cycles. In order to compare the knocking tendency of the four fuels under the same $p-T$ history, experimental cycles with similar pre-knock pressure to that of ULG90 were selected (see Figure 5.3). Because the fuel composition has only a small effect on the heat loss, matching pressure effectively means matching the temperature of the gas ahead of the flame. The

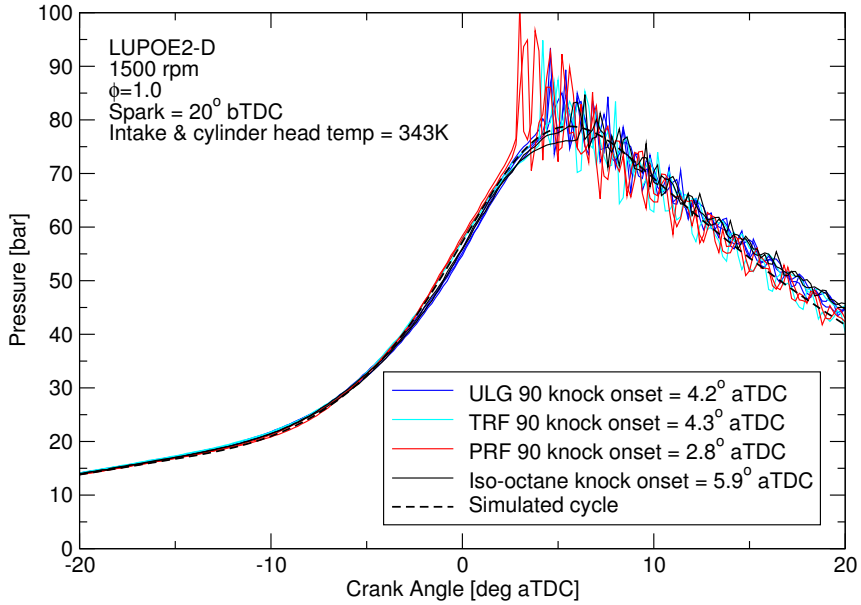

Figure 5.3: Knocking experimental cycles of the four fuels with similar pressures to that of the pre-knock pressure of the mean ULG90 cycle.

knock onsets of the selected cycles were then averaged for each fuel, as presented in Figure 5.3. These mean knock onsets reflect the overall averages of Figure 5.2.

5.3 LUPOE2-D modelling

Since the main objective was to study the effects of fuel composition on engine autoignition, it was of utmost importance to eliminate any differences between the simulated in-cylinder thermodynamic state and that in the experiments as well as differences between various fuels, so that all the fuels were subjected to the same $p - T$ history in the unburned zone. Therefore, instead of using the predictive combustion model of GT-LU (described in Chapter 4 and used later in Chapter 6) a non-predictive "empirical" approach was taken for combustion modelling. The fuel mass burning rate for the mean ULG90 cycle was determined by doing a rate of heat release analysis in GT-Power based on the cylinder pressure for engine conditions shown in Figure 5.1. The same GT-Power model as shown in Figure 4.8 was employed for this reverse analysis as was later used for the autoignition simulations. This kept the essential submodels, such as those of the heat transfer and the gas exchange process the same, while performing the heat release analysis and the forward simulations involving autoignition predictions. Since LUPOE2-D was operated in skip firing mode, an ideal scavenging

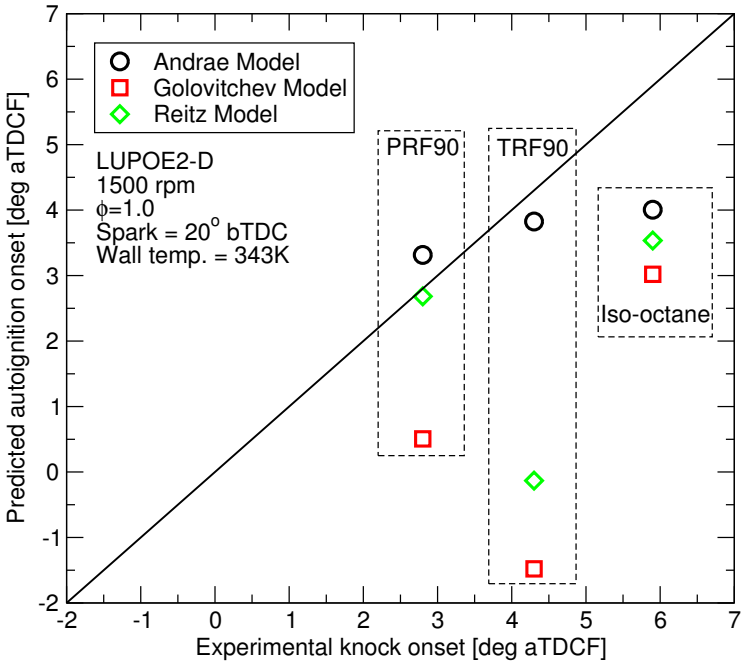

Figure 5.4: Comparison of the predicted and experimental autoignition onsets for PRF90, TRF90 and iso-octane.

was assumed in the modelling which meant that all burned residuals were expunged. The resulting differences in the predicted autoignition times is expected to be caused solely by differences in the autoignition chemistry of the fuels. The simulated cylinder pressure is presented in Figure 5.3 in the dashed line.

5.4 Results and discussion

The chemical activity which takes place in the in-cylinder charge is modelled from the beginning of the compression process. At the moment of spark discharge, the burned and unburned zones are formed and the chemistry modelling is carried on in the unburned zone. As the three reduced chemical kinetics models studied in this work, namely, Andrae, Golovitchev and Reitz models comprise pathways for iso-octane, n-heptane and toluene, autoignition modelling of PRF90, TRF90 and iso-octane can be performed. Predicted autoignition onsets for these fuels under the same engine operating conditions of Table 5.1 have been compared to the observed knock onsets in Figure 5.4. The Andrae model appears to perform consistently better than its competitors, however, the Reitz model produces very accurate autoignition prediction in the case of PRF90. Golovitchev model consistently predicts shorter delays as was seen earlier in the

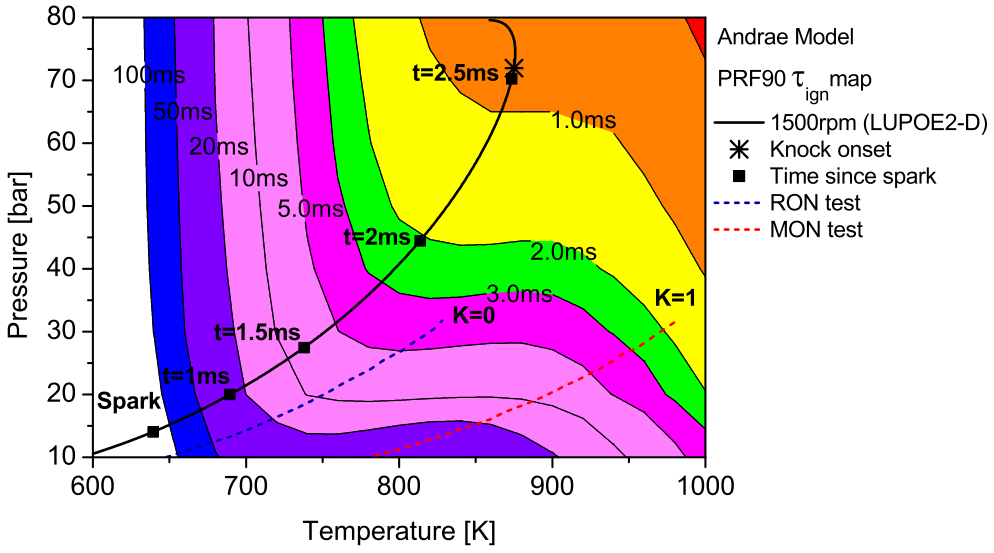

Figure 5.5: The τ_{ign} contour map of PRF90 as predicted by the Andrae model superimposed with the unburned zone $p-T$ history of LUPOE2-D and typical RON/MON tests.

constant volume calculations in Chapter 2. An inspection of ignition delay times upto 850 K or 1000 K/T of 1.1 in Figure 2.11a shows that the Golovitchev model tends to predict shorter delays for iso-octane during the NTC phase which explains the earlier autoignition prediction for iso-octane and PRF90 in LUPOE2-D. Although, toluene ignition delay times at 50 atm are overpredicted, it can be seen that the model predicts shorter delays at lower pressure, see Figure 2.10c. Figure 2.13a also shows that the Golovitchev model predicts shorter ignition delays when toluene is present which explains the earlier autoignition onset for TRF90 in LUPOE2-D. Figure 5.4 thus highlights the importance of the fact that for a chemical kinetics mechanism to correctly predict autoignition in an engine it is crucial to produce the correct ignition delay times at all the $p-T$ conditions leading up to the autoignition.

The relationship between the end gas thermodynamic state and the autoignitive tendency of a fuel can be presented as ignition delay time (τ_{ign}) contours on a $p-T$ carpet plot as shown in Figures 5.5, 5.6 and 5.7. The end gas thermodynamic path in LUPOE2-D as well as the RON and MON tests are superimposed on the τ_{ign} maps for PRF90, TRF90 and iso-octane, which were calculated using Andrae model. The RON and MON trajectories are for iso-octane in a CFR engine taken from [Farrell and Bunting, 2006] and K is the engine dependent parameter in the

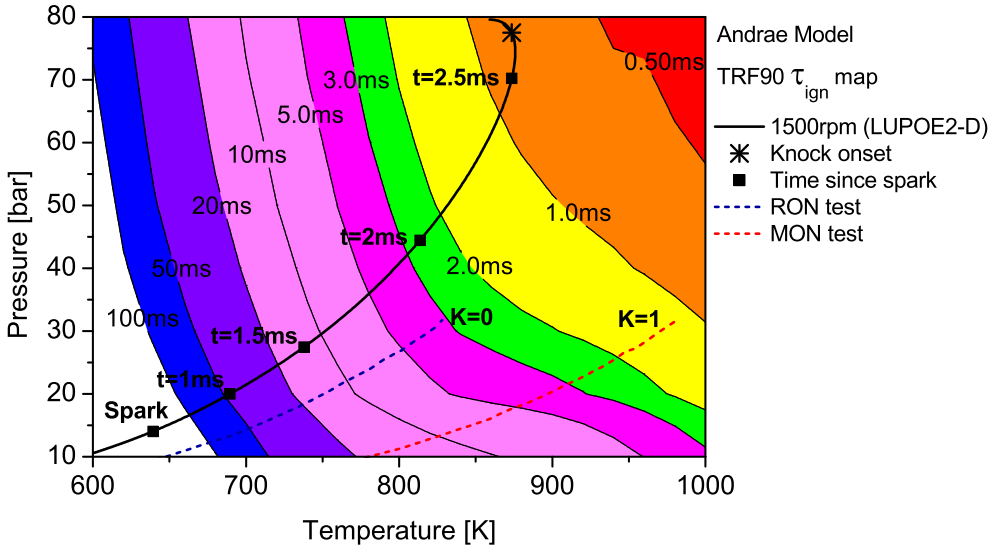

Figure 5.6: The τ_{ign} contour map of TRF90 as predicted by the Andrae model superimposed by the unburned zone $p-T$ history of LUPOE2-D and typical RON/MON tests.

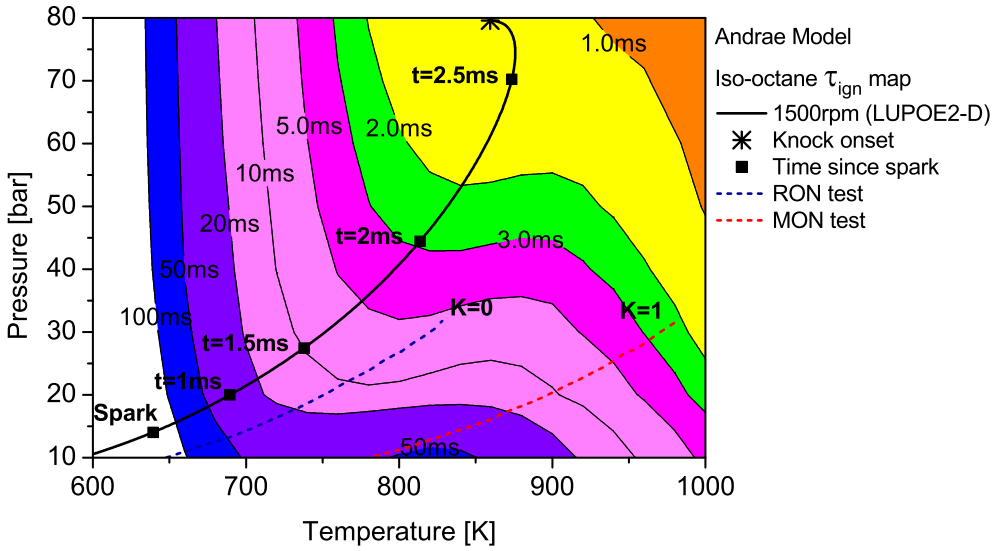

Figure 5.7: Unburned zone $p-T$ history of LUPOE2-D and typical RON/MON tests superimposed on the τ_{ign} contour map of iso-octane as predicted by the Andrae Model.

relation, $OI = RON - K(RON - MON)$, due to Kalghatgi [2001] as discussed in Section 1.4.1.2. The differences in fuel reactivity are shown by the shape of the contours and the extent to which the regions of different τ_{ign} span. The S-shaped contours on PRF90 and iso-octane plots show the NTC behaviour of the two fuels. The LUPOE2-D $p-T$ trajectory follows such a path that it is unable to take advantage of the NTC behaviour of iso-octane and PRF90. It takes a path just before the start of NTC phase when the regions of shorter τ_{ign} occur earlier. In case of iso-octane, however, since the ignition delay times are longer than TRF90 and PRF90 at a given $p-T$ condition, the knock takes places much later. A further comparison of the τ_{ign} contours of PRF90 and TRF90 shows that the regions of short τ_{ign} are situated at lower $p-T$ conditions for PRF90 and the LUPOE2-D trajectory lies in these critical regions bringing the knock onset to an earliest value of 2.8° CA aTDC among all the fuels studied.

The end gas thermodynamic path in RON test spends the same amount of time in regions of very similar τ_{ign} for both PRF90 and TRF90 which gives them the same RON values and therefore, PRF90 is by definition the surrogate for TRF90 and ULG90 yet at only the unburned zone $p-T$ conditions as offered by the RON test. Similarly, since ULG90 has a MON of 84.7, a PRF of the same ON can be regarded as its surrogate but only at $p-T$ condition of the MON test. However, a single multi-component blend with non-zero sensitivity can be used to reproduce the autoignition behaviour of a gasoline at both RON and MON test $p-T$ conditions. It is tempting to consider such a blend a surrogate for gasoline at all $p-T$ conditions but a blend which has been matched to the RON/MON of a gasoline will have the same reactivity for only a narrow region of the $p-T$ landscape. The fact that most modern SI engines operate with temperature and pressure history very similar to LUPOE2-D or at even higher pressures due to turbocharging, RON and MON are not sufficient to characterise autoignition of gasoline in such engines.

The constraints discussed in Section 2.9 have been optimised for ULG90 to formulate a properties-based surrogate. A composition-based surrogate is also studied whose composition is the same as that of the major gasoline constituent families. Table 5.2 lists the compositions of these ULG90 surrogates. A tri-component TRF with the same RON and MON as ULG90 has also been studied. The autoignition onsets of these ULG90 surrogates for the same ULG90 $p-T$ history have been simulated using the Reitz model only because it is the Reitz model which has pathways for a naphthene i.e. cyclohexane, a suitable surrogate com-

Gasoline components	ULG90 % vol.	Surrogate components	Comp. based	Props. based	TRF
Iso-paraffins	60.0	Iso-octane	60.0	54.51	54.81
N-paraffins	8.0	N-heptane	8.0	16.35	16.74
Aromatics	21.0	Toluene	21.0	27.89	28.45
Naphthenes	11.0	Cyclohexane	11.0	1.26	-
RON	90		94.38	90	90
MON	84.7		89.65	84.7	84.67
A/F_s	14.69		14.56	14.69	14.49
Knock (aTDCF)	4.2°	AI* (Reitz)	2.87°	1.52°	1.16°
		AI (Golov.)	-	-	-1.06°
		AI (Andrae)	-	-	3.2°

* AI: Autoignition onset

Table 5.2: Key properties and volumetric composition of ULG90 and its surrogates. Predicted surrogate autoignition onsets for the ULG90 $p-T$ condition of Fig. 5.3 have also been tabulated.

ponent. The autoignition predictions of the TRF have been made by the three mechanisms and the results have been presented in Table 5.2. It is found that it is the TRF with Andrae model which predicts the closest autoignition to that of the ULG90. A time difference between the predicted autoignition onset and the observed knock onset is expected due to the time taken by a pressure wave emanating from the autoigniting center to reach the pressure transducer. An upper estimate for such a time difference can be made as $Bore/a$, where, the speed of sound is given as, $a = \sqrt{\gamma RT}$ and at a unburned gas temperature of 800 K in LUPOE2-D at 2000 rpm, a maximum estimated delay of 1.4° can be expected in knock oscillations to appear after autoignition. Among the two 4-component surrogates, it is the composition-based surrogate which predicts closer to the observed knock onset although its theoretical RON and MON are much different from those of ULG90. Among all three surrogates, it is the TRF which predicts the closest autoignition using the Andrae model. This is not surprising as the chemical kinetic mechanisms for TRFs are studied and validated much more than other hydrocarbon groups. The difference in the autoignition onsets of the properties and composition based surrogates is not so large as to deduce whether anyone of two surrogate formulation approaches is superior. However, it is evident that optimising the RON, MON and other physical properties of the surrogate does not necessarily result in the surrogate with the same autoignition properties as the gasoline.

This study demonstrates that reduced chemical kinetics can feasibly be used

in the prediction of gasoline autoignition in an SI engine by approximating its properties by a surrogate. The choice of the mechanism and the surrogate affect greatly the prediction accuracy. The choice of the surrogate components is however limited by the availability of mechanisms for their oxidation. Surrogate composition may ideally be optimised by using target properties as constraints, however, weaknesses in the available empirical octane number models make this approach unreliable. Although the prediction of octane numbers is important in the formulation of a surrogate but matching of the RON and MON does not guarantee the correct reproduction of gasoline ignition behaviour in the surrogate as the modern SI engines operate at conditions much different form the RON and MON tests. Moreover, a compositional fidelity of the surrogate to that of the gasoline is also important in producing the correct autoignition behaviour in the surrogate.

The mechanisms generally over-predict the ignition delay time at low temperatures and pressure of about 40 bar. However, earlier autoignition onsets in an engine have been predicted by the three models; in particular the Golovitchev and Reitz models, indicating shorter ignition delay time predictions at lower pressures.

Chapter 6

Combustion and autoignition modelling in a turbocharged SI engine

6.1 Introduction

As the main objective of this project was to develop combustion and autoignition modelling tools and test their viability for a highly turbocharged downsized SI engine, the combustion, cyclic variability and chemical kinetics models discussed in Chapters 2 & 4 were used to model the Di3[1] engine at various operating conditions. Recent notable application of the LUSIE/GT-LU to engine modelling has been done by Conway [2013] and Hattrell [2007]. Conway [2013] found through his modelling of six engines, both naturally aspirated and turbocharged, that the combustion models were not capable of predicting combustion accurately for different intake pressures. An adjustment of the turbulent length scale had to be made through a multiplier in Equation 4.15 for the after-burning[2] expressions in order to achieve a good agreement with the experiments, however, this adjustment was kept to a minimum. It has been observed during the course of this work as well, that there is no single universal set of model constants for different engines and different load and speed points of a given engine. Previously, mod-

[1] See Section 4.10.2 for the engine details.
[2] See Section 4.5.3 for details on after-burning in a three-zone combustion model.

elling studies of LUPOE with both disc-shaped and pent-roof combustion chambers, [Hattrell, 2007], were done with appreciable accuracy with a fixed set of constants mostly optimised from constant volume bomb experiments (e.g. [R. G. Abdel-Gayed and Bradley, 1984]) and LUPOE itself. But LUPOE has been limited to low crankshaft speeds (up to 1500 rpm) and it has only recently been upgraded to operate at boosted pressures (up to 2 bar). At these conditions the combustion model in LUSIE/GT-LU performs fairly well, however, model predictions deviate from measurements for high load, high speed conditions of production engines; in many cases the latter use special intake arrangements to induce very high turbulence, highly directional mean flow patterns and heavy pressure charging. Effects of pressure charging on pre-mixed turbulent combustion is an on-going research interest and has also been studied in this work. Modelling of cyclic variability in conjunction with chemical kinetics modelling of autoignition has been carried out to determine if this approach predicts a reasonable percentage of knocking cycles and if this can be used to predict the knock limited spark advance (KLSA). The aims of studies presented in this Chapter are summarised in the following:

- Assess combustion modelling for a variety of load-speed points.
- Compare the in-cylinder turbulence calculations of CFD modelling and the $k - \epsilon$ model of GT-Power for Di3 engine.
- Study the effect of load and speed variation on the turbulent flame structure.
- Assess the viability of the simple cyclic variability model for prediction of in-cylinder pressure variation at high boost pressures.
- Assess the accuracy of autoignition predictions in relation of the mean knock onsets at various operating points.
- Simulate knocking frequency by modelling the effect of cyclic variability on autoignition.
- Simulate knocking frequency for a range of spark timings, to determine a knock limited spark advance.

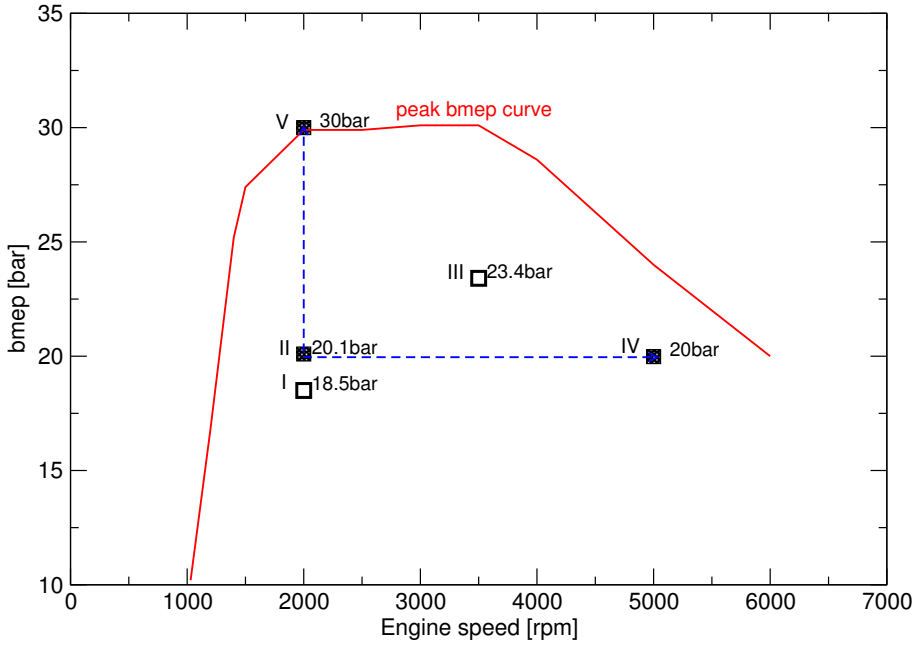

Figure 6.1: Peak bmep curve of the Di3 engine, showing the operating points studied in this Chapter.

6.2 Di3 engine operating conditions

The peak bmep curve of the Di3 engine is shown in Figure 6.1 where are also shown the five operating points which have been studied in this Chapter. Autoignition studies were made for the three points (I, III and IV) which lie under the peak bmep curve as comprehensive experimental data was only available for these points in the knocking regime. Typically, low speed and high load points are of interest as there is a higher propensity of knock at these conditions. However, for the objectives of this work, i.e. to demonstrate the viability and accuracy of autoignition modelling and effects of surrogate composition on autoigntion onsets, the low load points were sufficient. Three of the five operating points were chosen such that only either the speed or the load, i.e. boost pressure was changed; these are points II, IV and V in Figure 6.1. This allowed a modelling study of effect of variation in speed and load on the flame structure. CFD modelling for all the five points was done at Mahle Powertrain Ltd and University of Leeds with contribution from Silvano [2013].

Engine tests were performed with two fuels as detailed in Table 6.2 to assess the engine knock behaviour at these operating conditions and compression ratios with the aim of determining the most efficient combination of fuel, compression

	Speed (rpm)	P_{plen} (bar)	bmep (bar)	Spark (deg aTDC)
I	2000	1.82	18.52	-0.77
II	2000	1.72	20.09	-1.14
III	3500	2.05	23.41	-5.11
IV	5000	1.77	19.98	-6.6
V	2000	2.64	30	-3.41

Table 6.1: Five Di3 operating conditions studied in this work. These conditions are referred here onwards to by the corresponding roman numeral.

	E5-95/85	102RON
RON	95	101.9
MON	85	88.6
Density (at 15°C) [kg/L]	0.7539	0.7574
Net calorific value [MJ/kg]	42.54	41.93

Table 6.2: Specifications of the two fuels used in Di3 engine tests.

ratio and operating conditions. For this work only one compression ratio, i.e. 10.2, was studied. For the baseline conditions in Table 6.1, E5-95/85 was used and the combustion and cyclic variability modelling in subsequent sections pertains to this fuel. The other fuel, 102RON, has briefly been considered later during the autoignition modelling in Section 6.7.

6.3 GT-Power model validation

Before any predictive modelling could be done, the GT-Power model of this engine was thoroughly validated against experimental measurements [Neumeister and Oudenijeweme, personal communication]. Heat release analysis of the measured cylinder pressures provided the fuel mass burning rates which were used in an initial set of simulations to accurately reproduce the in-cylinder pressure. This allowed various other flow related, thermodynamic and performance quantities to be validated against measurements. Prediction of the correct instantaneous mass flow rate of air into each cylinder is of key importance as various other engine parameters are dependent on it. Moreover, the predicted pressures and flow rates in the intake and exhaust runners were used as boundary conditions for the CFD modelling to predict the in-cylinder turbulence. The model correlation to the engine test data can best be depicted by log-log plots of cylinder

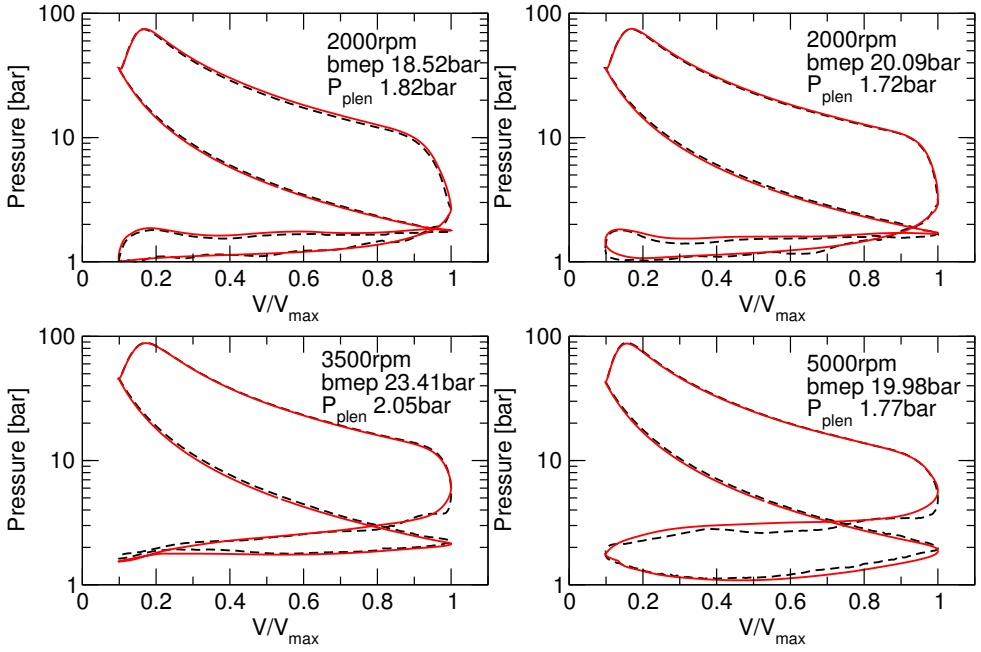

Figure 6.2: log-log charts showing the in-cylinder pressure and volume at the conditions studied. Black dashed line represents the engine test measurements. Solid red lines represent simulation results using non-predictive combustion model.

volume and pressure as e.g. shown in Figure 6.2. The GT-Power model is able to correctly predict the gas exchange process thereby reproducing the correct volumetric efficiency.

The adopted procedure made it certain that with the use of predictive GT-LU combustion model, any deviation of cylinder pressure was due to combustion model and not due to the initial and boundary conditions in various other sub-models of GT-Power, e.g. the intake and exhaust systems and model for heat transfer.

6.4 In-cylinder turbulence

The rms velocity, u', averaged over the whole cylinder mass, and the integral length scale for the five operating points shown in Figure 6.1 have been presented in Figure 6.3. The increase in engine speed expectedly increases the turbulence intensity as the latter relates to the intake jet velocity. In addition to this, as the initial bulk flow or the mean flow is set up by the interaction between the intake jet and chamber walls, differences can be seen in the integral length scale for different operating points during the intake and compression strokes owing

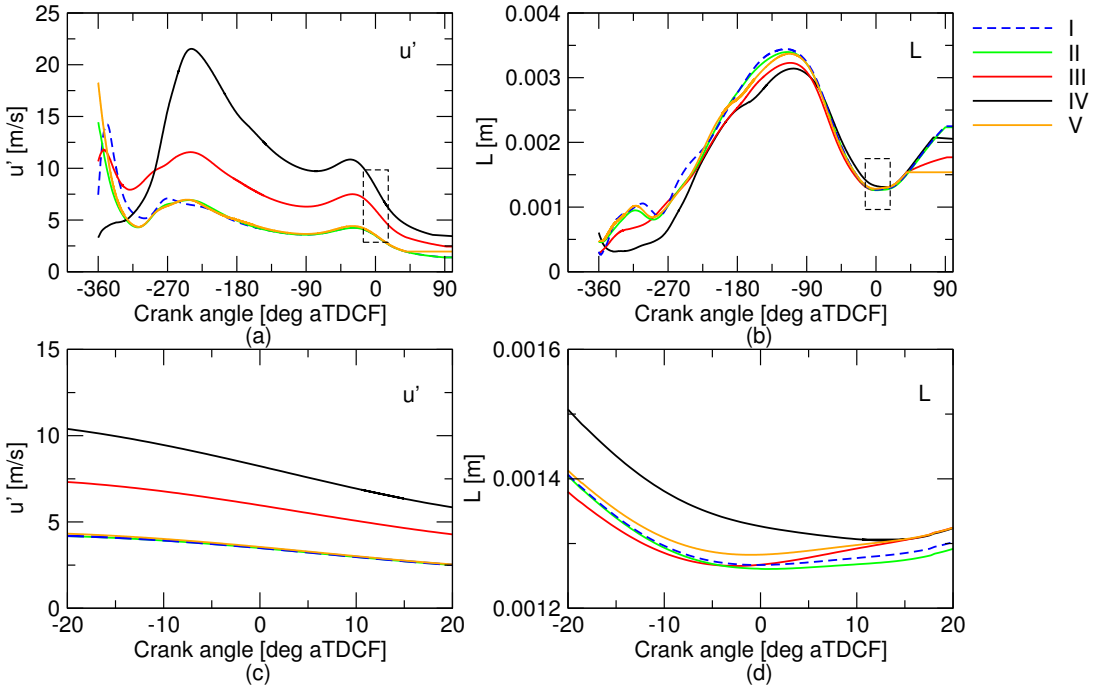

Figure 6.3: CFD modelling results showing u' and L for the five operating conditions. c & d show the close up for crank angles around TDCF.

to different valve timings. An earlier or a delayed valve timing will result in the intake jet interacting with the piston at a different position thereby affecting the size of the large scale flow pattern and hence the integral length scale. However, as the piston approaches TDC, the flow becomes unstable as it breaks into smaller and smaller eddies, the memory of the initial difference in large scale eddies during the intake and early parts of the compression stroke is lost. This can be seen as a convergence of the integral length scale to approximately the same value for all the operating points in Figure 6.3d. The simulations also reveal that an increase in the engine load and a corresponding increase in the boost pressure does not affect the rms velocity (see the 2000 rpm cases). However, the change in physical properties of the air fuel mixture due to turbocharging is expected to affect the turbulent burning velocity and the structure of the flame.

A comparison of the turbulence calculations by the CFD modelling and the $k-\epsilon$ model in GT-Power has been presented in Figure 6.4. GT-Power's turbulence model predicts much larger turbulent length scale and it must be pointed out that in the case of CFD modelling, the length scale pertains to the whole cylinder volume owing to the fact that cold flow was modelled, however, in the case of GT-Power's $k-\epsilon$ model, it is of the unburned zone only, see Section 4.7.1 for details.

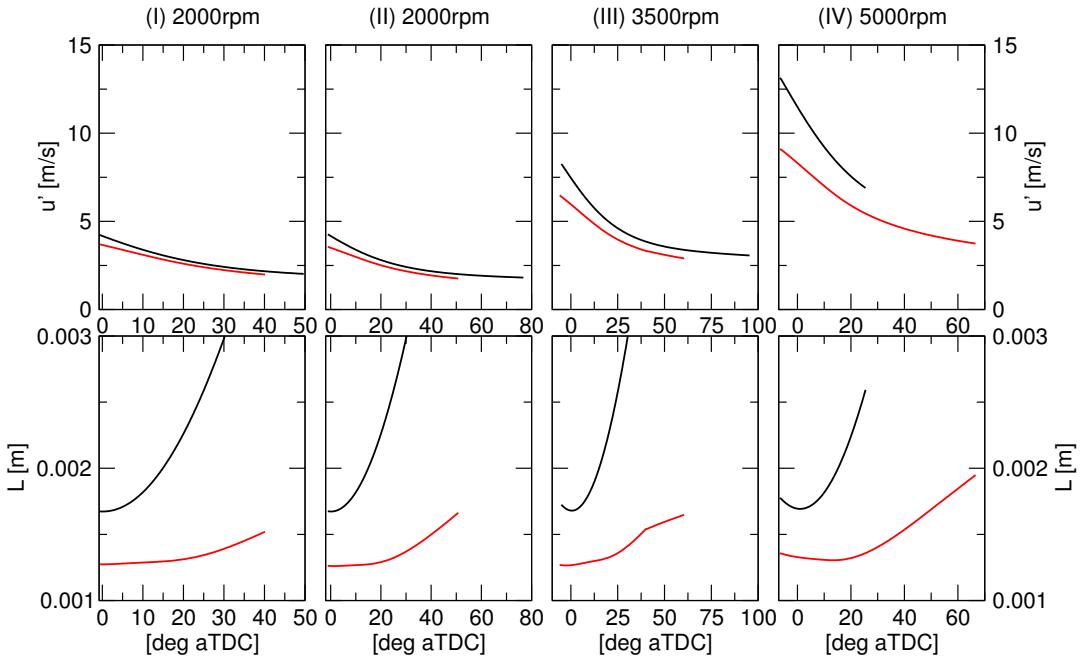

Figure 6.4: Comparison of u' and L obtained by CFD modelling and the GT-Power's $k-\epsilon$ model during the time of flame propagation. Black lines: $k-\epsilon$ model in GT-Power; red lines: CFD modelling.

At low engine speeds the rms velocity is only slightly larger than that of the CFD modelling results but the difference grows with the engine speed. Owing to this small difference in u' at lower speeds, the two turbulence data sources result in very similar combustion rates and hence the cylinder pressures.

6.5 Combustion modelling results

Ideally, a fixed set of constants should allow the correct prediction of combustion rate at all engine loads and speeds. However, as stated earlier, this was found unachievable by Conway [2013], his finding is confirmed by this work. The rate of 'burn-up' of entrained mass had to be adjusted to achieve an agreement between the experiments and simulations. As the eddy burn-up model, see Equation 4.26, in GT-Power was employed in this work, this adjustment was made by scaling up or down the Taylor microscale using a multiplier, C_λ, in GT-Power, see Equation 4.15. This in turn altered the chemical burn-up time scale given by Equation 4.25, thereby altering the fuel mass burning rate. Prediction of cylinder pressure was found to be very sensitive to the multiplier, C_λ, as can be seen in Figure 6.5. A large multiplier and therefore a large Taylor microscale results in

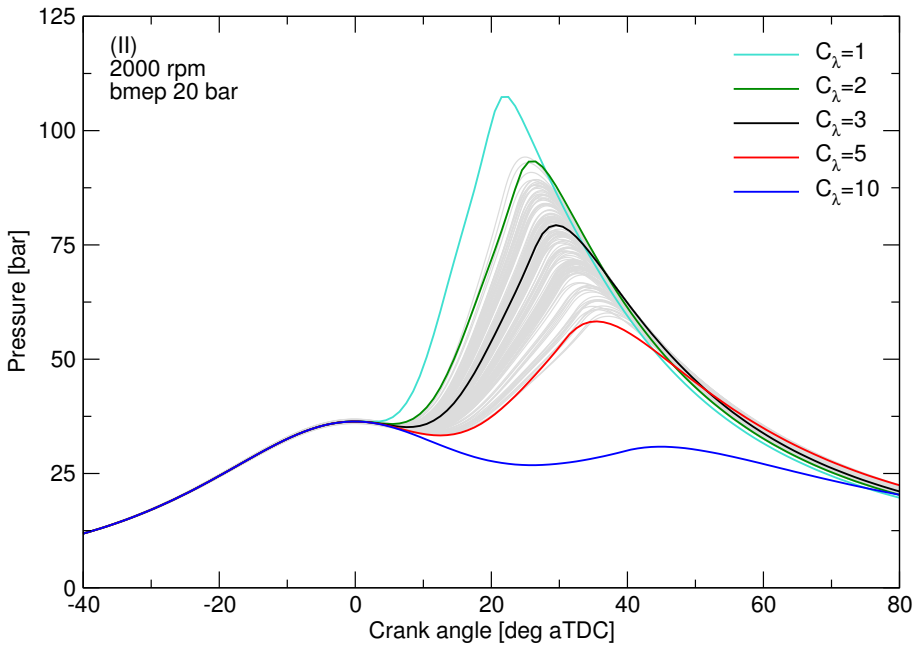

Figure 6.5: Effect of Taylor microscale variation in the eddy burn-up model, on cylinder pressure. Grey lines show simulated cyclic variation.

a longer chemical burn-up timescale and consequently slower increase in cylinder pressure. Simulations with a C_λ of 3 predicts cylinder pressure which agrees with the mean of all cycles for this particular operating condition, i.e. No. II. Different multipliers were needed to predict the mean cycle correctly for the other load-speed points, these multipliers are presented in Table 6.3.

The mean cycles simulated using the CFD modelled turbulence and from GT-Power's $k-\epsilon$ model have been presented in Figure 6.6. It can be seen that the relatively small difference between the rms velocity predicted by CFD and the $k-\epsilon$ model in GT-Power at 2000 to 3500 rpm leads to similar cylinder pressure using the same Taylor microscale multiplier. However, at 5000 rpm, the relatively stronger turbulence intensity predicted by the $k-\epsilon$ model in GT-Power results in higher cylinder pressure than the one calculated from CFD turbulence. One may choose to adjust C_λ to match either one of these cylinder pressures to the mean experimental pressure. However, the $k-\epsilon$ model in GT-Power tends to over-predict the turbulence intensity due to the division of the combustion chamber into fewer large subvolumes as described in Section 4.7.1.2. This model assumes that the gas flow which takes place across the boundary of these subvolumes constitutes the bulk flow, whereas the gas motion which stays with in a subvolume constitutes the turbulence intensity. As a result, for the larger subvolumes, tur-

	Speed (rpm)	P_{plen} (bar)	bmep (bar)	C_λ	Parametric study
I	2000	1.82	18.52	2	Spark
II	2000	1.72	20.09	3	-
III	3500	2.05	23.41	3	Spark
IV	5000	1.77	19.98	1	Charge temperature

Table 6.3: Taylor microscale multiplier, C_λ, used in this work to predict the mean cycles of the four engine load-speed points.

bulence intensity is over-predicted. GT-Power's $k-\epsilon$ model was also found to over-predict the turbulence in a naturally aspirated LUPOE2-D in comparison to the LDV measurements of rms velocity by Hussin [2012]; predictions were about 2 times higher than the measurements at spark i.e. -20° aTDCF. Since the GT-Power $k-\epsilon$ model makes very similar predictions to CFD at low speeds yet at a fraction of the computational cost, its use is desirable; particularly in the absence of a reliable knowledge of the in-cylinder flow field through experimental diagnostics. Yet in what follows, the CFD-derived turbulence was used as input to combustion routines because of the arguably better consideration of chamber geometry and swirl and tumble present in the Di3 engine.

Lipatnikov and Chomiak [2002] found the Zimont model to be superior among others at predicting the turbulent burning velocity. This has been seconded by Liu et al. [2013], who found the Zimont model to perform equally as well as the Leeds $KaLe$ model. However, researchers have always faced difficulty at narrowing down the range of values for the model coefficients. Abdi Aghdam [2003] was able to compare the turbulent entrainment rate predictions using the Zimont model to the entrainment rate determined from his natural light flame imaging in LUPOE; the model was found to be superior to the Leeds Ka and $KaLe$ models. Although not explicitly stated, it is thought that the proportionality constant, C_z, in the Zimont model was adjusted to achieve an agreement. A value of 0.35 for C_z in the Zimont-Lipatnikov model, see Equation 4.32, has been found reasonable by Conway [2013] and has been used in this work. It is argued in this work that it is the eddy burn-up model which offers greater uncertainty on account of difficulty in resolving various turbulent scales which interact with the flame and therefore an adjustment of the model coefficient in burn-up model is warranted over a relatively more reliable entrainment rate model, i.e. Zimont-Lipatnikov model.

Consider the three Di3 engine operating conditions namely, II, IV and V in

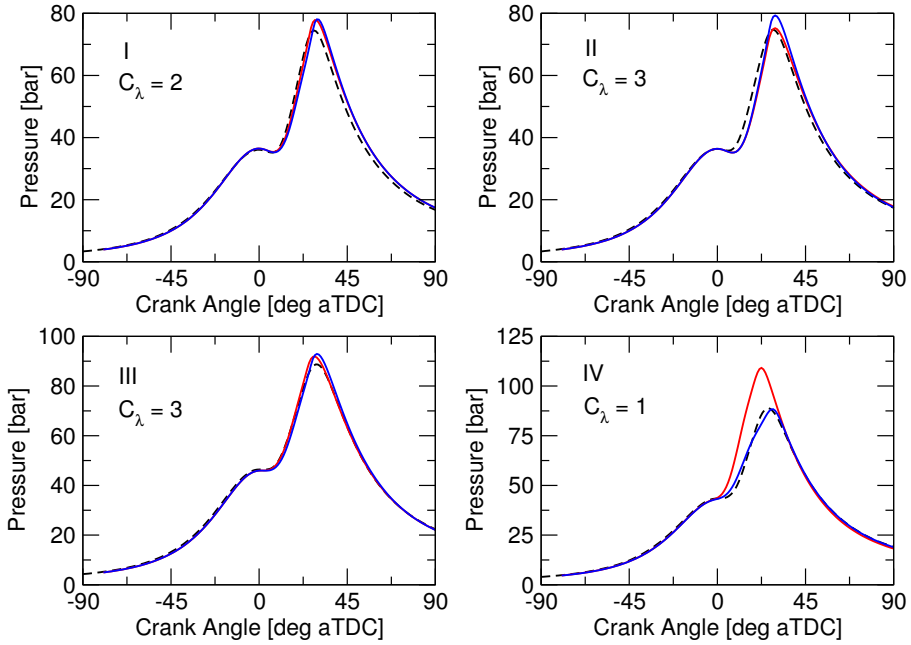

Figure 6.6: Comparison of the simulated mean cycles, using as an input, the turbulence from CFD modelling (blue lines) and the $k-\epsilon$ model in GT-Power (red lines). Black dashed lines represent engine test data.

Table 6.1 and shown as black squares in Figure 6.1. For these conditions, the engine speed or the load and correspondingly the plenum or boost pressure was varied. The spark timing was always kept at 1° of crank angle delayed from the borderline detonation timing (denoted as BLD+1°). This allowed to study the effects of speed and boost pressure variation on turbulence and combustion. It was seen earlier in Figure 6.3 that the rms velocity increases only with speed, whereas the integral length scale largely remains the same at all conditions. Studies such as [Peters, 1988] and [Borghi et al., 2008] show that in SI engines the degree of wrinkling i.e. the number and size of wrinkles on the flame front, increases as the ratio u'/u_l is increased while the integral length scale remains constant. Turbulent burning velocity is weakly dependent on the integral length scale which may not change much as the engine operating conditions change, however, a change in turbulence intensity affects eddies of sizes smaller than the laminar flame thickness which has implications on the flame structure. An increased u' increases the dissipation rate as well as the Reynolds number (Figure 6.7c) and thereby decreases the smaller turbulent length scales i.e. the Taylor and Kolmogorov scales. These are shown in Figure 6.8 and are calculated as:

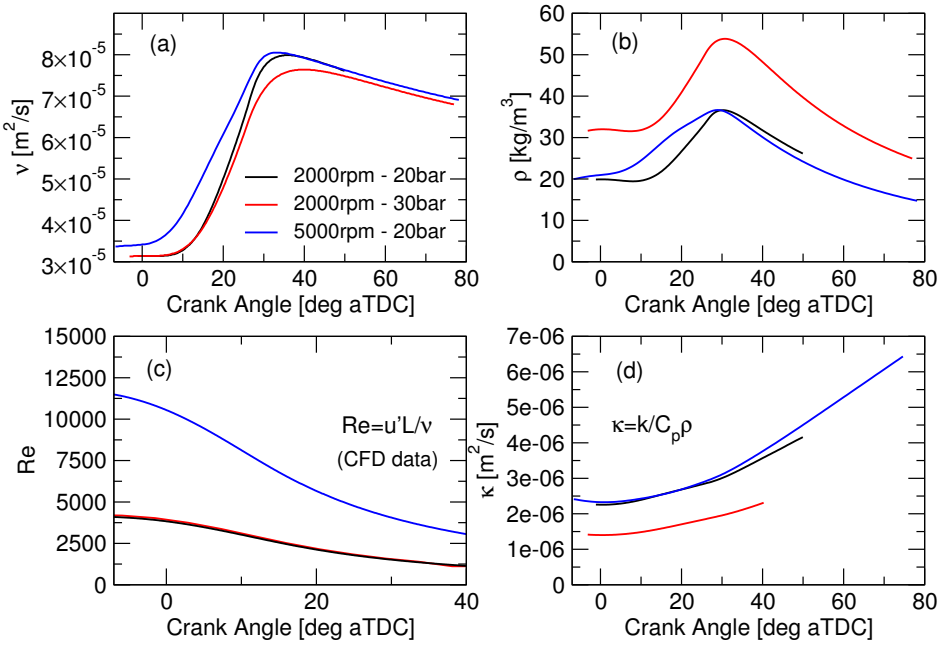

Figure 6.7: Effect of variation in engine speed and load (boost pressure) on (a) kinematic viscosity, ν, (b) unburned charge density, ρ, (c) Reynolds number, Re, and (d) Thermal diffusivity.

$$\lambda = \frac{L}{\sqrt{Re}} \qquad \text{and} \qquad \eta = \left(\frac{\nu^3}{\epsilon}\right)^{1/4}$$

without any proportionality coefficients which gives the lowest estimate of λ and η. The Gibson scale which by definition is the size of eddies which have a circumferential velocity equal to the local laminar burning velocity i.e. $u_G = u_l$, has also been calculated using the expression,

$$L_G = \frac{u_l^3}{\epsilon} \tag{6.1}$$

It must be noted at this stage that the Taylor microscale actually used in the calculation of eddy burn-up time scale was determined in GT-Power[1]. It was not possible to output the Taylor microscale from GT-Power. Although restrictive, this does not hamper the analysis made in this section. The simulated in-cylinder pressures have been shown to agree with the measurements (Figure 6.6) and correspondingly a correct amount of initial air-fuel charge and its composition is predicted in the cylinder. Based on these quantities, the laminar burning veloc-

[1]Personal communication with Gamma Technologies revealed that the Taylor microscale in GT-Power is determined by an unpublished proprietary expression of form as in equation 4.25.

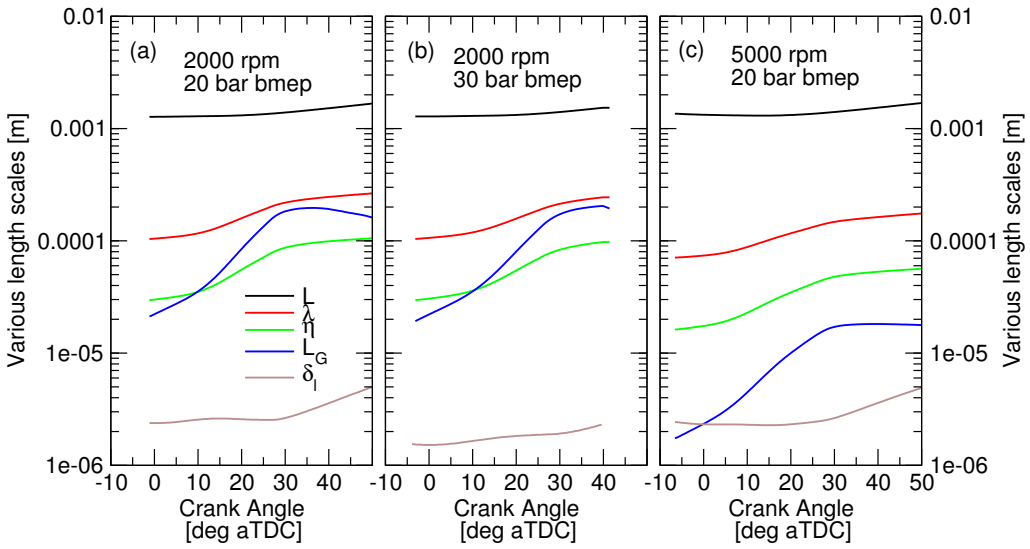

Figure 6.8: Effect of variation in engine speed and load (boost pressure) on various turbulent length scales and the laminar flame thickness.

ity, u_l, is calculated using the expression discussed in Section 4.6.4 and it offers a reasonable estimate of the Gibson scale.

The Gibson scale, L_G, for the three conditions for which the load and speed were varied has been presented in comparison to the integral, Taylor and Kolmogorov scales and the laminar flame reaction zone thickness given as, $\delta_l = \frac{\kappa}{u_l}$, in Figure 6.8. It can be seen that as the engine speed is increased, an increase in u' and ϵ causes the Taylor and Kolmogorov length scales to decrease. As the increase in dissipation rate dominates over changes in the laminar burning velocity in Equation 6.1, the Gibson scale decreases as well. The laminar flame thickness follows the same trend as the thermal diffusivity, κ, in Figure 6.7d and does not change as the speed is increased. As a result, now a greater spectrum of smaller eddies can penetrate the preheat zone; this can be seen on the Borghi diagram in Figure 6.9 as an upward shift towards thickened distributed flame regime. The Gibson scale being smaller than the Kolmogorov scale is physically meaningless as it is out of the inertial range of the turbulent eddies i.e. $\eta \ll l < L$.

For the two 2000 rpm cases, the Gibson scale starts smaller than the Kolmogorov scale at spark but soon increases and becomes comparable to the Taylor microscale, see Figures 6.8a & b. An increase in load at the same speed increases the charge density and decreases the laminar flame thickness caused by a decrease in the thermal diffusivity as shown in Figure 6.7d. The change in the turbulent flame regime is brought about by this change in flame thickness relative to the turbu-

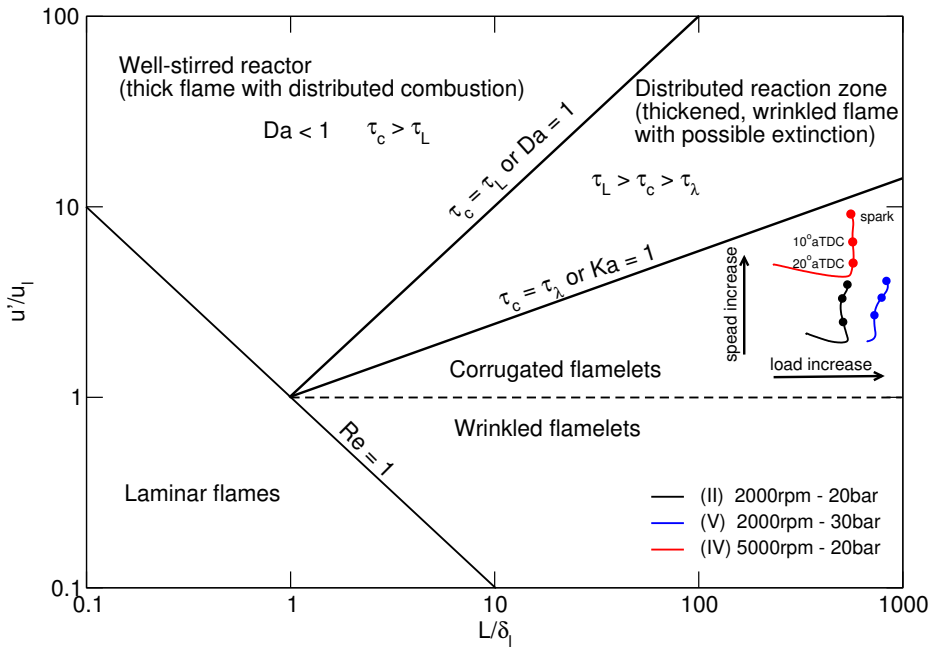

Figure 6.9: Effect of load (boost pressure) and speed variation on the flame regime on a Borghi diagram. See Table 6.1 and Figure 6.1 for details on the operating points.

lent eddies because a greater spectrum of eddies are able to wrinkle the flame rather than being able to perturb it. Since $L_G > \eta$ at 2000 rpm, $Ka < 1$ and the flame must remain in the corrugated flamelet regime and shifts towards a higher ratio L/δ_l on the Borghi regime diagram. The Taylor and Kolmogorov scales for the two 2000 rpm cases are very similar as expected, since the turbulent properties have been shown earlier to not change with load; the Gibson scale is only slightly different because of changes in u_l. Laminar burning velocity decreases as the pressure increases however, reduced burned residuals tend to offset this and as a result u_l does not vary much, hence the very similar Gibson scales. Similar trends were observed by Linse et al. [2009] in their CFD and quasi-dimensional modelling of a turbocharged engine. Their interpretation of the effect of boost pressure and speed is based on a Peters-Borghi diagram after Peters [1988], which considers a thin reaction regime for $Ka > 1$ however, this does not change the inference that a speed increase causes a greater spectrum of smaller eddies to penetrate the preheat zone causing the flame brush to increase.

The ultimate effect of adjusting the Taylor microscale multiplier, C_λ, is to alter the turbulent flame brush thickness which can be approximated as the difference of entrainment radius and burned gas radius. This thickness is not the same as the

one given by Equation 4.35 which is dependent only on the large scale turbulence and mathematically independent of any modification of the Taylor microscale. A larger multiplier results in a thicker flame brush. The simulations show that as the engine speed is decreased and/or the load is increased, there is a requirement for the Taylor multiplier to be increased i.e. the flame brush should be thicker. This seems contradictory to the flame regime analysis in preceding paragraphs. The requirement for Taylor microscale adjustment in the burn-up model in an apparently contradictory manner to the expected changes in flame structure can be caused by a number of reasons. The experimentally determined quantities are thought to be reliable and an unlikely source of model disagreement as widely used tried and tested techniques are employed in measuring such quantities. The other possible sources can be, the CFD data, u' and L, the smaller scales of turbulence which are determined using expressions presented in Section 4.2.1.2 and a similar proprietary expression in GT-Power, an inaccurate estimate of the laminar burning velocity, or the entrainment model itself. The CFD data, although possibly inaccurate, cannot cause this as in such a case a single Taylor microscale multiplier will be expected to work for all the engine conditions i.e. if the CFD predictions are wrong by the same magnitude for all the conditions.

The expression for u_l, Equation 4.37, as presented in Section 4.6.4 has been shown by Sileghem et al. [2013] to use a higher value of the power exponent for temperature dependence than observed in their experiments for a commercial gasoline. Also, it is likely that the combustion instability behaviour of the E5-95/85 gasoline in this work is different from the gasoline for which the expression for laminar burning velocity, Equation 4.37, was derived. Moreover, the effects of flame stretch and thermo-diffusive instability are carefully avoided during measurements of laminar flame speed, on basis of which the empirical expressions for u_l are then determined. So any flame instability which may actually be present in the engine is neglected in the analysis presented above introducing uncertainties. Any inaccuracies in u_l will have significant effect on the after-burning as the chemical eddy burn-up time is calculated as $\tau_b = \lambda/u_l$. Validation of the burning velocity expressions at high $p-T$ conditions of engines such as the Di3 engine is not possible owing to insufficient u_l measurements and particularly the onset of instabilities at those conditions.

The calculation of Taylor microscale in GT-Power and the entrainment model may also be significant sources of inaccuracies. The Zimont model treats the turbulent eddies of size smaller than the laminar flame thickness to affect the local

thermo-diffusive balance by enhancing the local mixing, thereby increasing the burning rate. The perturbation of the inner reaction layer, whose thickness is δ_l, has not been observed in engine flames and is thought to be not possible as increased kinematic viscosity in the preheat zone would dissipate entrained eddies [Lipatnikov, 2013].

The present simulation work indeed raises questions on possible deficiencies in the Zimont-Lipatnikov model applied to turbocharged engines. It is worth revisiting briefly the main premise of Zimont-Lipatnikov model. It is, that the scales of turbulence larger than δ_l increase the turbulent burning (entrainment) velocity by increasing the surface area. This wrinkling increases both the instantaneous front and average flame brush thickness which is a time dependent phenomenon given by Equation 4.35 which encapsulates well the self-similarity of a developing turbulent flame. The interaction of eddies smaller than δ_l however, is much more complex and not fully understood. Zimont postulated that smaller eddies enhance the turbulent burning velocity or entrainment in this approach, by enhancing the mixing. This process achieves an equilibrium in a short duration of time because of the shorter timescales associated with the Kolmogorov scales. These assumptions hold true for moderate turbulence i.e. $u' < u'_m$; where, u'_m is the turbulence intensity level at which the turbulent burning velocity starts to decrease due to a decrease in entrainment area as the flamelets increasingly fold and merge; localised quenching may also occur at very high u' values. The value of u'_m is fuel specific and depends on ϕ and $p - T$ of the mixture. It is not possible to say it with certainty that the turbulence intensity in the Di3 engine falls within this range as to the best of author's knowledge, no studies have been reported on the u' dependence of the turbulent burning velocities of gasoline or its surrogates at more intense engine like conditions. The need for increasing the Taylor microscale multiplier to decrease the burn-up time may be due to an over-prediction of the entrainment rate by the Zimont-Lipatnikov model due to wrongly over-estimating the effects of smaller eddies on thermo-diffusive mixing. One may ask, if this is true then this should be even more amplified at higher engine speeds and high values of u' because then Kolmogorov eddies penetrating the flame will have higher kinetic energy and will be less susceptible to complete dissipation causing even greater mixing and perturbation hence increasing the burning rate. But it could simply be that the model is able to correctly predict the entrainment rate and burn-up time as u' is increased but is deficient when the charge density is increased at any given speed.

The various sources of uncertainly require further study both numerically and experimentally. For the sake of this work, further simulations have been carried out with optimised Taylor microscale, however, no adjustment is made to Taylor microscale or any other model constants when spark timing and charge temperature sweeps are performed.

6.5.1 Spark timing and charge temperature sweeps

The Di3 operating conditions, I to IV, presented earlier in Table 6.3 were then taken as baseline conditions and parametric simulations were done. While keeping all the other operating parameters constant, only the spark timing was varied for the two of the conditions and charge temperature was varied for the other two conditions. Since the valve timing was kept the same for each spark advance sweep, the in-cylinder turbulence predicted for the baseline conditions was used for all other parametric simulations.

In order to assess the correctness of the combustion model, crank angles at which 10%, 50% and 90% of the fuel mass is burned have been compared to the experimental values, this comparison is shown in Figure 6.10. It can be seen that once a correct baseline operating point is modelled, a correct trend of fuel mass fraction burned (MFB) points is predicted for a variation in spark timing or the charge temperature. This is one advantage which the predictive combustion model offers over the non-predictive Wiebe function, for which the knowledge of the Wiebe constants is a prerequisite at all conditions. At the same time the combustion model in GT-LU allows a faster yet reliable modelling of the effects of variation in parameters such as spark timing and intake charge temperature on the engine performance. These effects on the engine performance have not been discussed here as it is out of the scope of this work. Subsequent work deals with combining these parametric simulations with cyclic variability and autoignition modelling.

6.6 Cyclic variability modelling results

Cyclic variability in the combustion process has been modelled on the assumption that it is the random variation of turbulence intensity, u', and the charge composition, ϕ, from one cycle to another which are the major sources of cyclic variation. This variation in u' and ϕ is brought about by generating separate

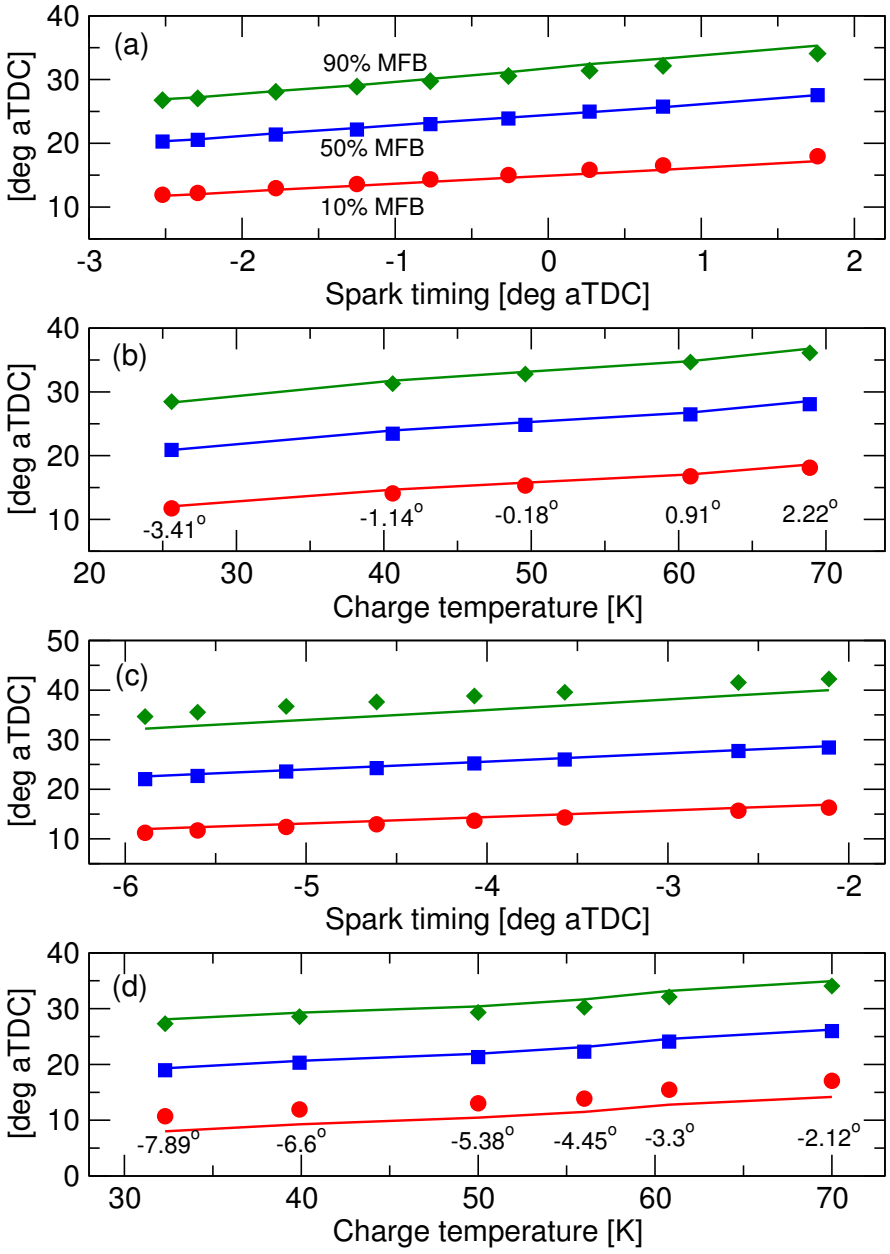

Figure 6.10: 10%, 50% and 90% fuel mass fraction burned (MFB) points for spark timing and inlet charge temperature sweeps for Di3 engine operating conditions: (a) I, (b) II, (c) III, (d) IV as in Table 6.1. Simulations are represented by lines. Spark timing for charge temperature sweeps have also been shown.

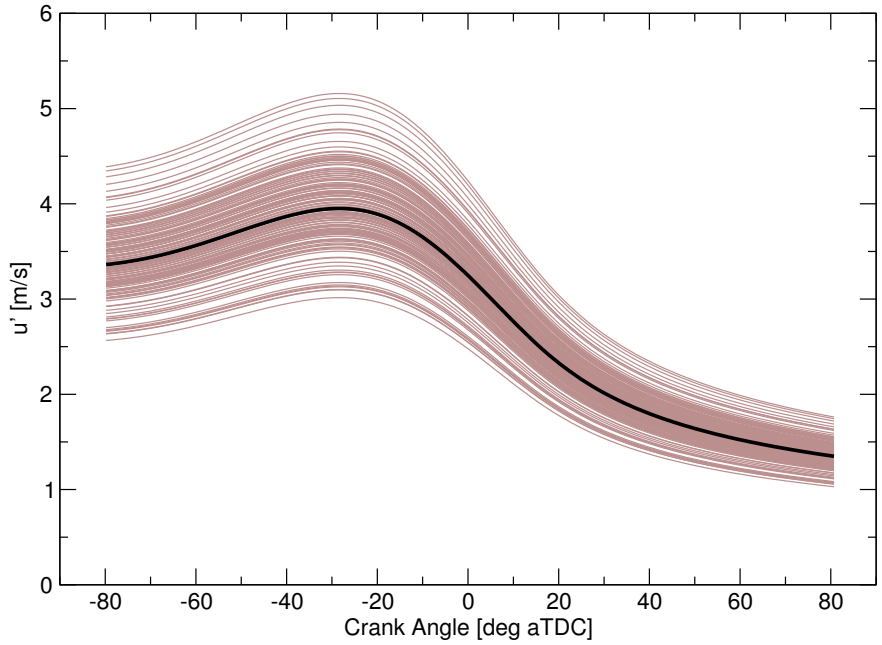

Figure 6.11: 144 perturbed cycles of rms velocity according to a Gaussian distribution. The black line represents the mean rms velocity.

multipliers according to a Gaussian distribution as described in Section 4.6.6 and using them to perturb u' and ϕ in the beginning of each new cycle, see e.g. Figure 6.11 for u'. This differs from the earlier implementation of this approach by Conway [2013] in which the rms velocity was perturbed at spark and its dissipation was determined by a 0-D $k-\epsilon$ model. Currently, since cold flow turbulence was calculated beforehand, this was not possible and the end result is of the rms velocity being varied about its mean value according to the Gaussian distribution. An example of these multipliers is presented in Figure 6.12 which are the quantile-quantile plots comparing the generated or expected values with those of a normal distribution. The closeness of the generated multipliers to the reference line of a normal distribution indicate that the multipliers do in fact form a Gaussian distribution and lie with in the specified standard deviation percentage i.e. 12.5% for u' and 5% for ϕ.

The results from cyclic variability modelling are dependent on how well the mean cycle is modelled. This is evident for the 2000 rpm case shown in Figure 6.13 as the clusters of simulated and experimental peak pressures, P_{max}, are non-overlapping and this expectedly results in a difference in the mean peak pressures, $\bar{P}_{max}$. However, the spread of P_{max} is determined by how well the cyclic variability is accounted for by the modelling approach. The spread of the

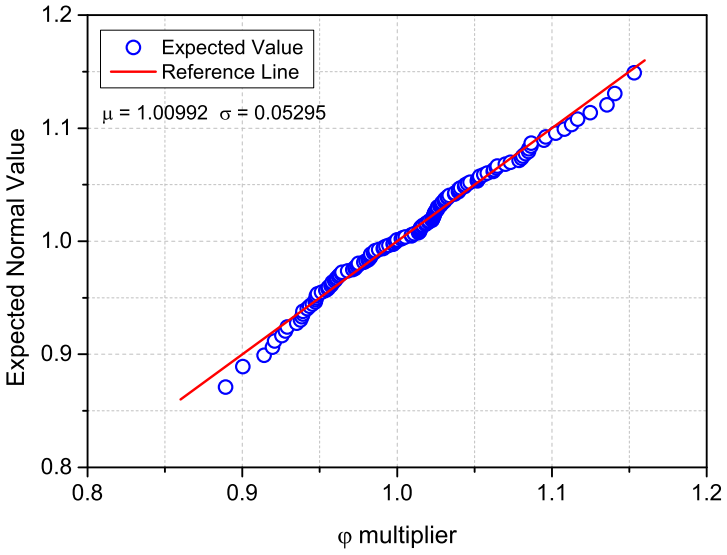

(a)

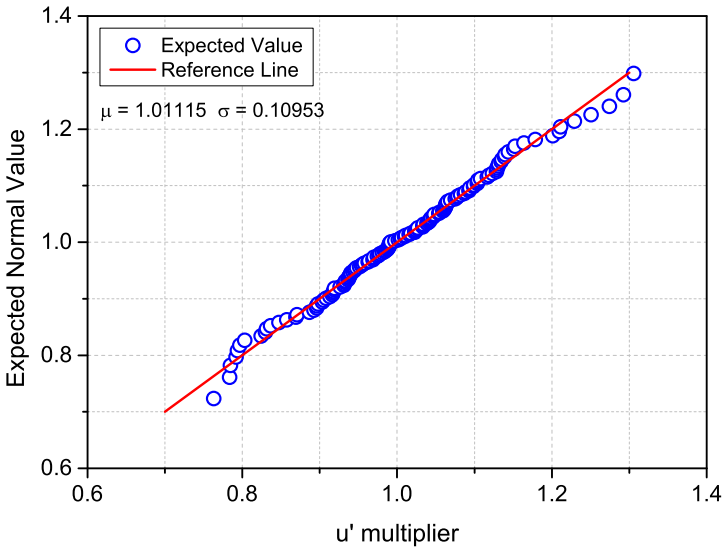

(b)

Figure 6.12: Quantile-quantile plots comparing the generated (expected) Gaussian multipliers for (top) ϕ and (bottom) u', to a reference Gaussian distribution.

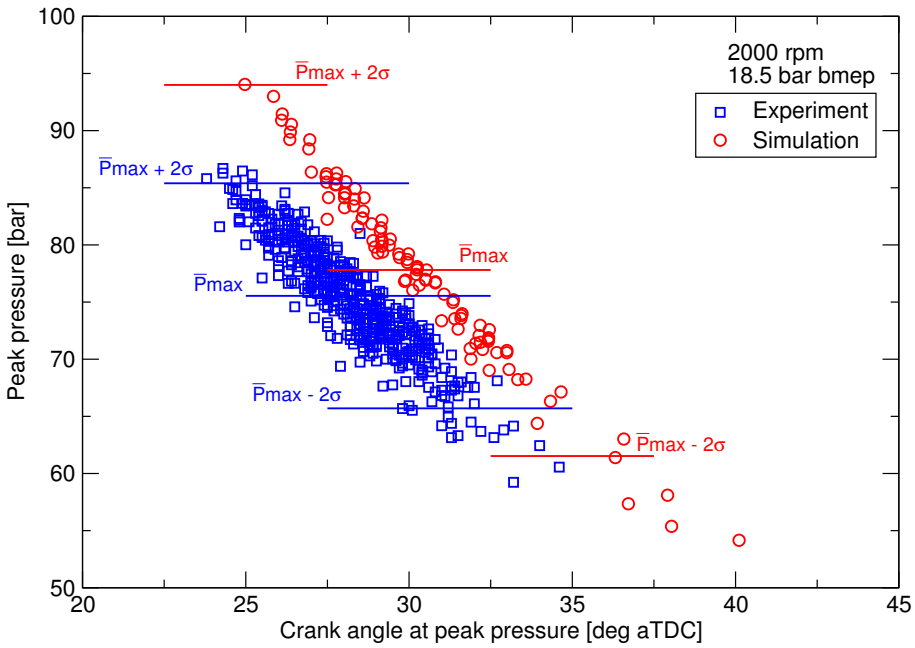

Figure 6.13: Comparison of simulated and actual peak cylinder pressure at corresponding crank angle. The mean peak pressure, $\bar{P}_{max}$, and pressures at $\pm 2\sigma$ have also been indicated.

simulated P_{max} is clearly more than the experimental spread evidenced by the difference in $\bar{P}_{max} \pm 2\sigma$ in Figures 6.13 and 6.14.

Conway [2013] has shown in the modelling of the naturally aspirated LUPOE2-D and its boosted version as well as various turbocharged production engines that the simulated standard deviation of P_{max} for LUPOE2-D was 1.3 times that of the actual engine whereas, it was roughly twice in case of turbocharged production engines. The same is observed for the Di3 engine, possibly because of closed feedback control strategy employed in running the production engines and the Di3 engine in this case, which may have altered the operating conditions i.e. spark timing to prevent knock from occurring; with a secondary effect of reducing variability. The difference in standard deviation of P_{max} can also be attributed to the fact that the modelling approach does not fully reproduce the 2-D scatter of P_{max} for the middle cycles[1]. Since a large number of cycles were recorded during engine tests i.e. about 3000 cycles; there are a large number of cycles with P_{max} close to the $\bar{P}_{max}$, their standard deviation is much lower as compared to only hundred or so simulated cycles.

Frequency histograms for P_{max} shown in Figure 6.15 show that the test data is

[1]Middle cycles are the cycles which have P_{max} closest to the mean peak pressure, $\bar{P}_{max}$.

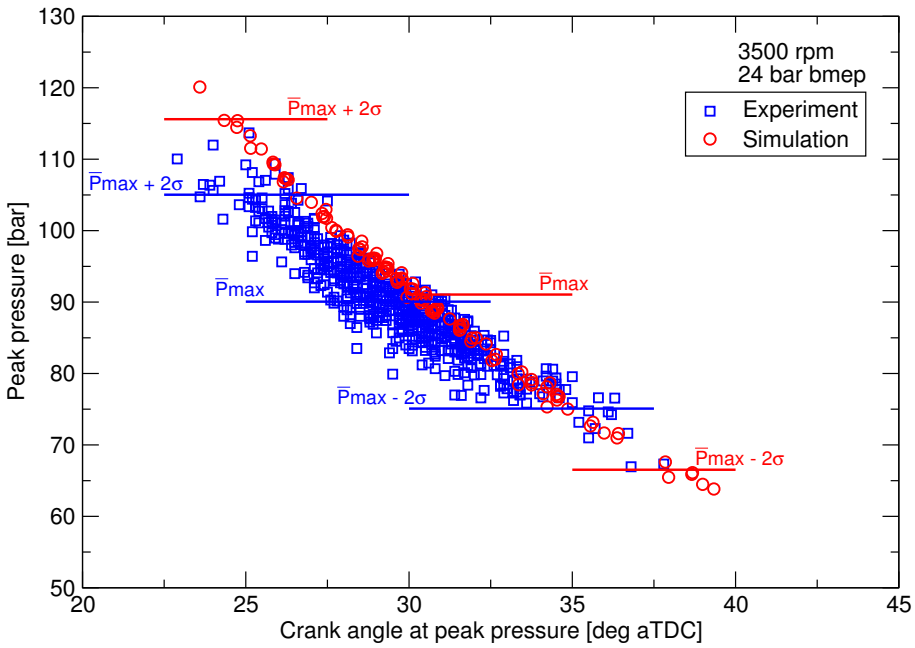

Figure 6.14: Comparison of simulated and actual peak cylinder pressure at corresponding crank angle. The mean peak pressure, $\bar{P}_{max}$, and pressures at $\pm 2\sigma$ have also been indicated.

very slightly skewed towards high P_{max} values whereas the simulations tend to predict a few more slow burning cycles i.e. low P_{max} values (see e.g. Figure 6.13). The distribution of the actual P_{max} and θP_{max} (Figure 6.16) are much more closer to a normal distribution than the simulated ones which still apparently follow the bell curve. For our autoignition modelling, the slow cycles are of lesser importance as they are less prone to knocking so the excessively slow burning cycles in simulations do not cause great concern as they are automatically ignored while calculating the percentage of autoigniting cycles, as will be described in subsequent sections.

Similar cyclic variability results have been seen for the modelling of the other two conditions (II and IV, Table 6.1). As stated earlier, given that the mean cycles agrees well, a reasonably good spread of fast to middle cycles can be predicted with this fairly simple modelling approach. The wider horizontal and vertical scatter seen for the middle cycles in engine test data can be attributed to the spatial variation in turbulence intensity which cannot be accounted for in a homogeneous assumption of turbulence as in this case.

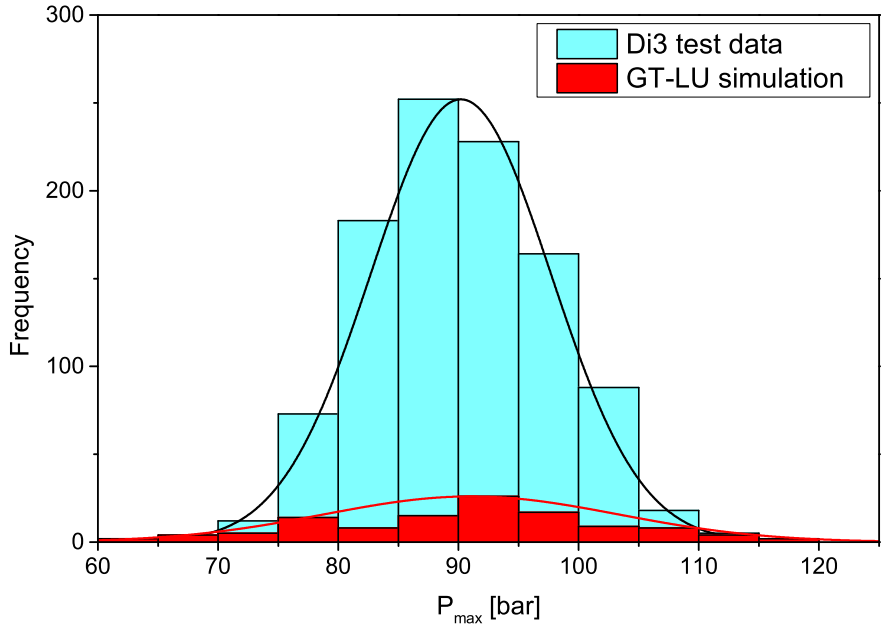

Figure 6.15: Comparison of simulated and actual $\bar{P}_{max}$ frequency. Corresponding normal distribution curves scaled to the maximum have also been shown.

6.7 Autoignition modelling results

Past research on engine knock at Leeds University has mainly focused on experimental investigations such as recording of the natural light and Schlieren images of knocking centres as well as pressure oscillations. Autoignition modelling has been limited to the use of empirical models such as the D&E model described in Chapter 1, or the relatively simpler skeletal chemical kinetics e.g. the Shell model and the skeletal Keck model, described in Chapter 2. Previous modelling studies such as [Smallbone, 2004], [Roberts, 2010] and [Conway, 2013] show that the original D&E model generally predicts poorly as newer engines operate at much different $p - T$ conditions than the CFR engine which Douaud and Eyzat [1978] used to determine their model constants. Moreover, the gasoline composition has changed since, this means that even when the octane index of a gasoline based on the Kalghatgi K factor, is used in the D&E model rather than the RON and MON, model results will still not be accurate. The skeletal Keck model, although better than D&E, was found to have inconsistent behaviour for different engines, generally it had a tendency of predicting late autoignition for naturally aspirated

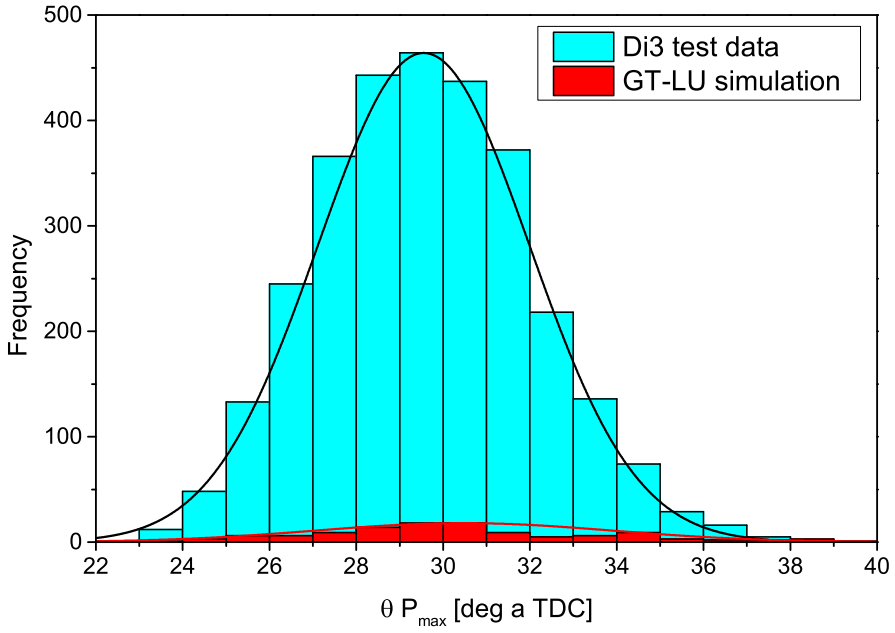

Figure 6.16: Comparison of simulated and actual $\theta\bar{P}_{max}$ frequency. Corresponding normal distribution curves scaled to the maximum have also been shown.

engines and early autoignition for boosted engines [Conway, 2013]. Application of chemical kinetics for gasoline surrogates is expected to overcome issues of accounting for complex chemistry of the gasoline, automatically accounting for the effects of the thermodynamic state of the end gas owing to turbocharging and intercooling as well as the effect of burned residuals on autoignition.

6.7.1 Gasoline surrogates

Two notions central to the application of chemical kinetics for autoignition modelling are (a) the use of a reliable chemical kinetics mechanism and (b) the use of the correct surrogate for gasoline under consideration. The mechanisms used in the course of this work have been discussed earlier in Chapter 2 and two surrogate formulation approaches were discussed in Section 2.8. It was learned through autoignition modelling of LUPOE2-D in Chapter 5 that the composition of a properties based surrogate obtained by optimising its properties to match those of the gasoline may not reflect accurately the gasoline composition. In such cases, it is the composition based surrogates which tend to have a higher fidelity

Gasoline components	E5-95/85 % vol.	Surrogate components	Prop. based A/G	Prop. based R	Comp. based A/G	Sur95o*
Saturates	56.1	Iso-octane	28.42	39.81	41.48	43.85
	-	N-heptane	16.33	10.74	14.66	17.92
Aromatics	31.9	Toluene	33.07	30.36	31.9	34.81
Olefins	6.7	Olefin**	16.84	13.53	6.96	-
Ethanol	5.3	Ethanol	5.35	5.57	5.03	3.42
Benzene	0.4	None	-	-	-	-
RON	95	-	95	95	95	95
MON	85	-	85	85	86.7	85
H/C	1.786	-	1.786	1.786	1.883	1.801
O/C	0.0176	-	0.0176	0.0176	0.007	0.011

* [Pera et al., 2012]

** IC_4H_8 for Andrae and Golovitchev models. Cyclohexene for the Reitz model.

Table 6.4: Key properties and volumetric composition of E5-95/85 fuel and its surrogates. A, G, and R indicate the Andrae, Golovitchev and Reitz models.

to the autoignition behaviour of a gasoline as was observed in Chapter 5. Properties based surrogates may suffer from approximations in empirical octane number models and do not always simulate the oxidation behaviour of a gasoline even though their key physical properties are matched.

The fuel, E5-95/85, was simulated using surrogates obtained by applying both, the properties-based and composition-based approaches as well as a surrogate proposed by Pera and Knop [2012], referred to as Sur95o, for a very similar French gasoline which conforms to the EN 228 specifications. These surrogates are presented in Table 6.4.

Another gasoline, referred here to as 102RON, was a premium forecourt fuel which contained substantial amounts of methyl tertiary butyl ether (MTBE). As MTBE was not present in the three reduced mechanisms employed in this work, the MTBE content was substituted by ethanol in the surrogate, as ethanol like MTBE is an oxygenate and both have similar RON and MON. It is however not purported that the two are alike in terms of their oxidation behaviour. The resulting composition of the surrogate representing it is shown in Table 6.5.

6.7.2 Knock in Di3 engine

Before autoignition predictions can be compared to knock observations in Di3 engine, knocking cycles need to be separated from the non-knocking ones and their knock onset timing be determined. The recorded cylinder pressures were

Gasoline components	102RON % vol.	Surrogate components	Comp. based
Saturates	41	Iso-octane	30.66
	-	N-heptane	10.34
Aromatics	35	Toluene	35.0
Olefins	12	DIB, C_8H_{16}	12.0
Ethanol	0.8	Ethanol	12.0
MTBE	11.4		NA
RON	102		100.2
MON	88.6		90
H/C	1.798		1.802
O/C	0.021		0.038

Table 6.5: Key properties and volumetric composition of 102RON fuel and its surrogate. The surrogate is a composition based surrogate containing high octane components; diisobutylene and ethanol which replaces MTBE.

subjected to a high-pass Butterworth filter (order 9, cut-off frequency 1.5kHz). After an initial visual inspection of the cylinder pressures and corresponding filtered pressures a threshold value of oscillation amplitude of 1 bar was set for 2000 rpm cases to distinguish the knocking cycles. An example of a normal and a knocking cycle is shown in Figure 6.17; one can see an almost instantaneous appearance of pressure oscillations in the cylinder. As knock is a consequence of autoignition, the actual chemical kinetic ignition occurs slightly before its onset. The appearance of the first pressure spike after autoignition depends on the location of the autoigniting centre relative to the pressure transducer, cylinder bore, engine speed and the speed of sounds at the prevailing temperature. The time difference between the two events is the time taken by an acoustic wave to reach the pressure transducer. This introduces an uncertainty, although not large, in the perceived autoignition onset which in this work is taken to be base of the first pressure spike.

It becomes more important to discern between the background noise due to engine vibrations and knock at high engine speeds as is evident by the presence of an oscillation of amplitude of roughly 1 bar for an otherwise normal cycle in Figure 6.18 shown by the black line. A threshold higher than 1 bar would, however, result in a knock onset much later than the original autoignition. It is therefore that a double criteria is used for high engine speeds; first knocking cycles were segregated based on a threshold of 2 bar and the onset was taken to be the instant when the oscillations of magnitude 1 bar first occurred.

The amplitude of pressure oscillations during knocking gives an indication

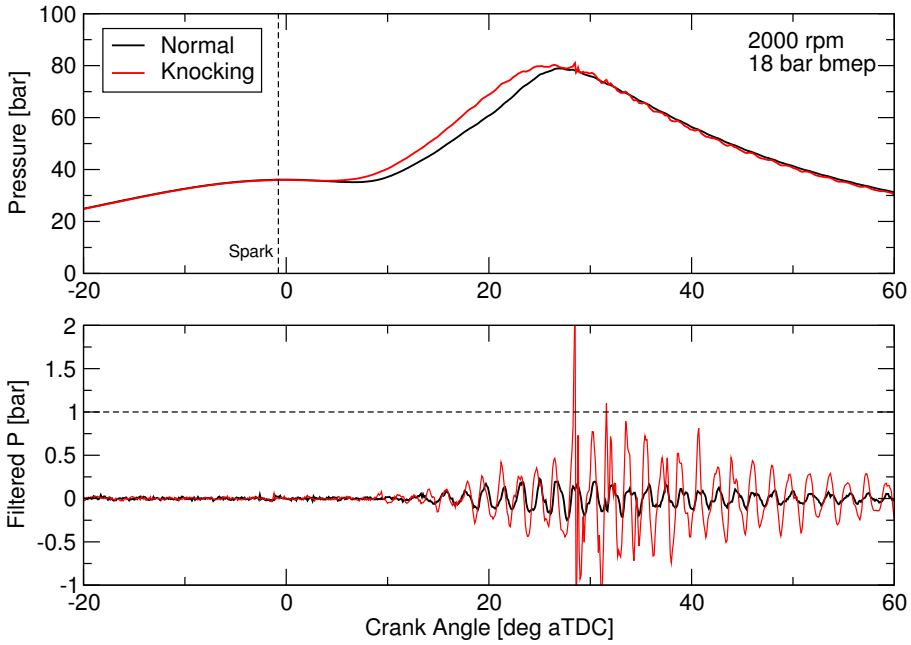

Figure 6.17: Examples of a normal (non-knocking) cycle and a knocking cycle at low engine speed with corresponding filtered pressure oscillations indicating the knock onset.

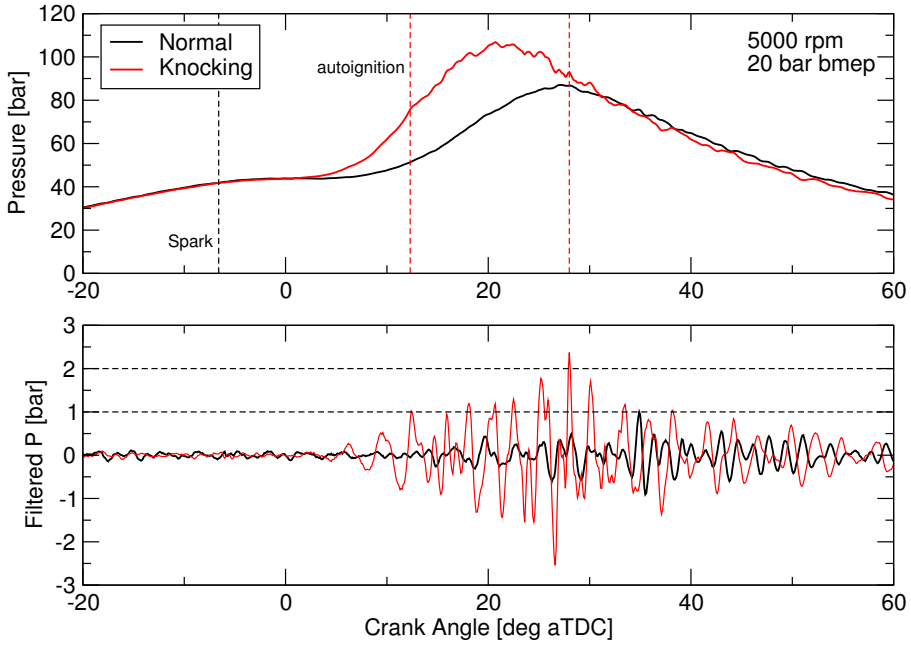

Figure 6.18: Examples of a normal (non-knocking) cycle and a knocking cycle at high engine speed with corresponding filtered pressure oscillations indicating the knock onset in dashed red lines.

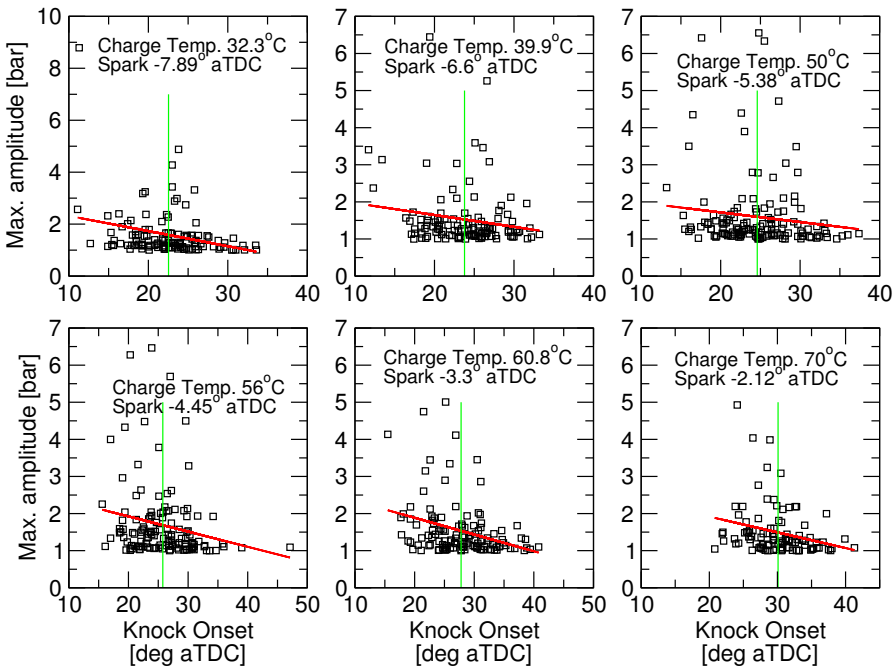

Figure 6.19: Maximum amplitude of pressure oscillations vs. corresponding knock onset for the six charge temperatures at 5000 rpm, shown as symbols. Red lines: linear best fit; green lines: average knock onset.

of its intensity. The maximum amplitude of these oscillations have been plotted against the corresponding knock onset in Figure 6.19 for the 5000 rpm cases for which the charge temperature was varied; the spark timing was varied as well so that the end gas temperature for all the cases was similar. The result was that roughly the same percentage of knocking cycles was detected for all cases; the percentage of knocking cycles ranged from 34% of the cycles for hottest charge yet most delayed spark timing, to 40% for the coldest charge yet most advanced timing. From the linear best fit to the data shown in Figure 6.19, there seems to be a correlation between the intensity of the knock and how soon it occurs. An earlier knock onset implies that there still is a substantial amount of unburned charge left in the cylinder whose spontaneous ignition is more likely to cause severe knock. Similar trend was found for the cases for which only the spark timing was varied (not shown here graphically). This idea is later used in autoignition modelling to attempt to quantify the knock likelihood after a predicted autoignition event.

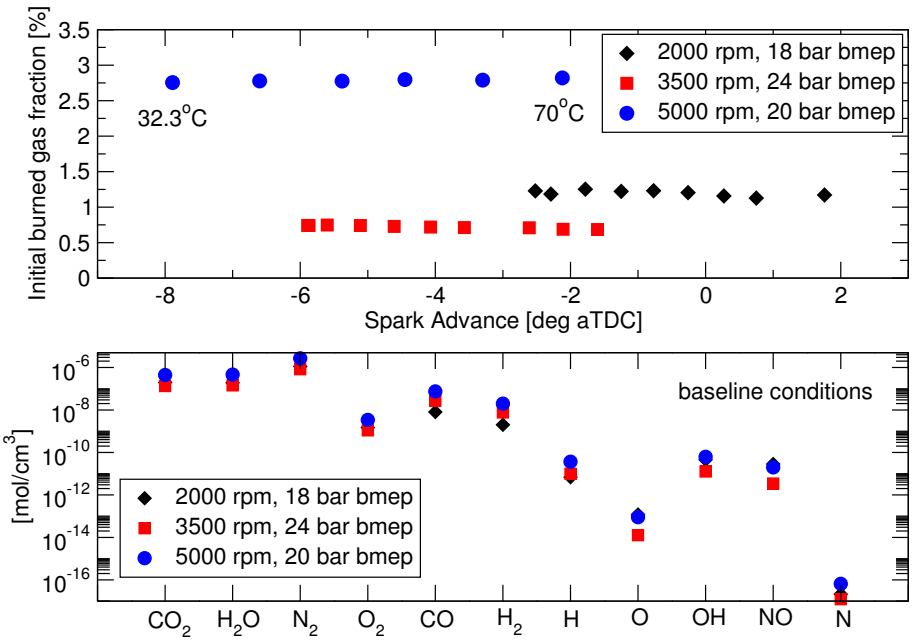

Figure 6.20: Top: simulated burned gas residuals as percentage by mass of the total charge at cycle start; bottom: molar concentration of burned residual species.

6.7.3 Autoignition modelling for the mean cycles

So far combustion modelling for the mean cycles at various conditions has been achieved with appreciable accuracy. With this, the thermodynamic state and its composition is also defined providing input into the autoignition subroutines. Concentrations of the species in the unburned charge, i.e. the fuel and air, are passed onto the species in the chemical kinetics mechanism as discussed in Section 4.6.5.1; as well as the burned gas residuals[1], the fractions of which is presented in Figure 6.20. The simulated effect of burned gas residuals on the autoignition onset is usually advancing the latter by a few degrees but it must be noted that when the residuals were ignored, the end gas $p - T$ conditions were still the same and the concentration of the unburned species were unchanged too. So the advancing of the autoignition by the EGR is purely due to the initiation of pathways involving burned species.

In order to assess the correctness of the predicted autoignition onsets, they should be compared to an experimental benchmark. The average knock onset of all the recorded experimental cycles is not a good candidate for such a benchmark when it is only the mean cycle being modelled. The reason is that the fast

[1]Burned gas species in GT-Power comprise of CO_2, H_2O, N_2, O_2, CO, H_2, H, O, OH, NO, N and Ar.

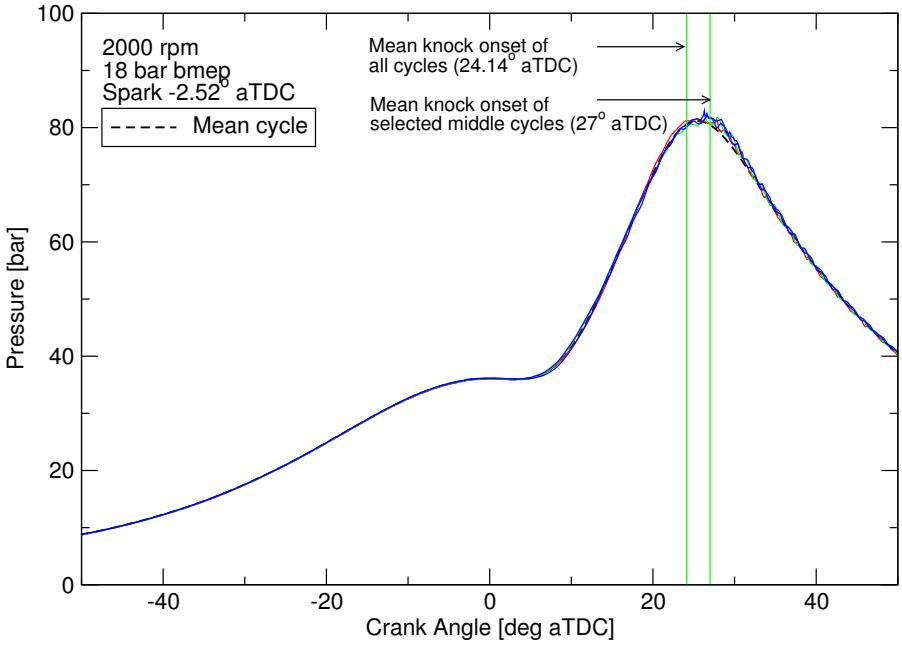

Figure 6.21: Selected middle cycles which are within 1.5% of the mean cycle upto 15° aTDC. Mean knock onsets for all cycles and selected mean cycles have also been shown.

burning cycles are more likely to knock, the average knock onset will be representative of the fast cycles and not the mean cycle or the middle cycles. Since a cycle to cycle comparison is not possible, the middle cycles which are very close to the mean cycle are chosen for knock onset averaging as shown in Figure 6.21. Those cycles are chosen which are within 1.5% of the mean cycle pressure upto 15° aTDC; which allows a direct comparison of the predicted autoignition onset for the mean cycle to mean knock onset of selected middle cycles.

Autoignition predictions made with the use of surrogate fuels presented in Table 6.4 have been compared to the observed knock onsets in Figure 6.22. The middle cycles are found to knock only at three most advanced spark timings which implies that it is the fast burning cycles which have a greater knocking propensity. The surrogates generally agree well with the mean knock onset of the middle cycles (red squares). The Golovitchev model predicts autoignition sooner as was seen earlier in the case of LUPOE2-D (see Figure 5.4). The Andrae and Reitz model predictions are remarkably good, Andrae model with both composition-based and properties-based surrogates whereas, the Reitz model only with Sur95o. The Reitz model could not be used for surrogates containing iso-butene as it is not present in the mechanism, however, the surrogate suitable

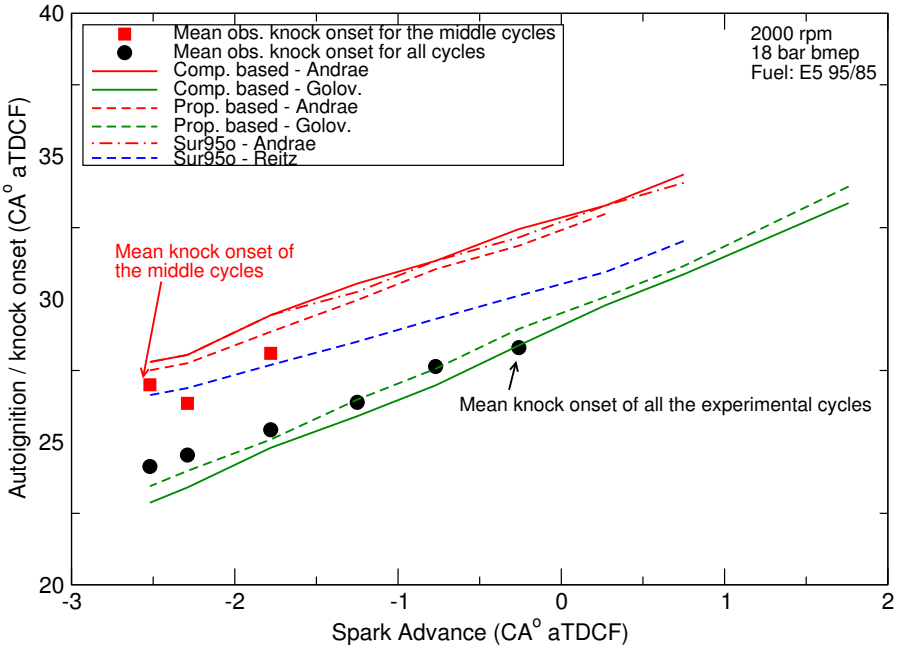

Figure 6.22: Comparison of predicted autoignition onsets to mean knock onsets for all the cycles and those of the selected middle cycles.

for Reitz model i.e. the one containing cyclohexene, did not predict any autoignition. This was surprising as cyclohexene has a much lower RON and MON than iso-butene and yet its presence in the blend resulted in much longer ignition delays.

The composition based surrogate in this work has a composition very similar to that of Sur95o by Pera and Knop [2012] and produces very similar autoignition onsets. Andrae model predictions have an average percentage error of about 5% for Sur95o and composition based surrogate; and about 3% for the properties based surrogate. Predictions of Reitz model with Sur95o have an average percentage error of 0.3%. However, the trend predicted by the Reitz-Sur95o combination seems to produce earlier autoignition as the spark timing is retarded.

The sensitivity of the chemical kinetics mechanisms can be assessed by subjecting PRFs of starkly different composition to the same unburned zone $p-T$ conditions. This has been done for the spark timing of -2.52° aTDC in Figure 6.23. For this simulation, the fuel effect on burning rate is neglected and the underlying assumption is that all the fuels burn at the same rate resulting in same $p-T$ conditions in the unburned zone. The Andrae and Golovitchev models predict a trend which is expected of these fuels, e.g. n-heptane autoignites earlier than other PRFs. The Andrae model does not differentiate greatly between PRF50 and

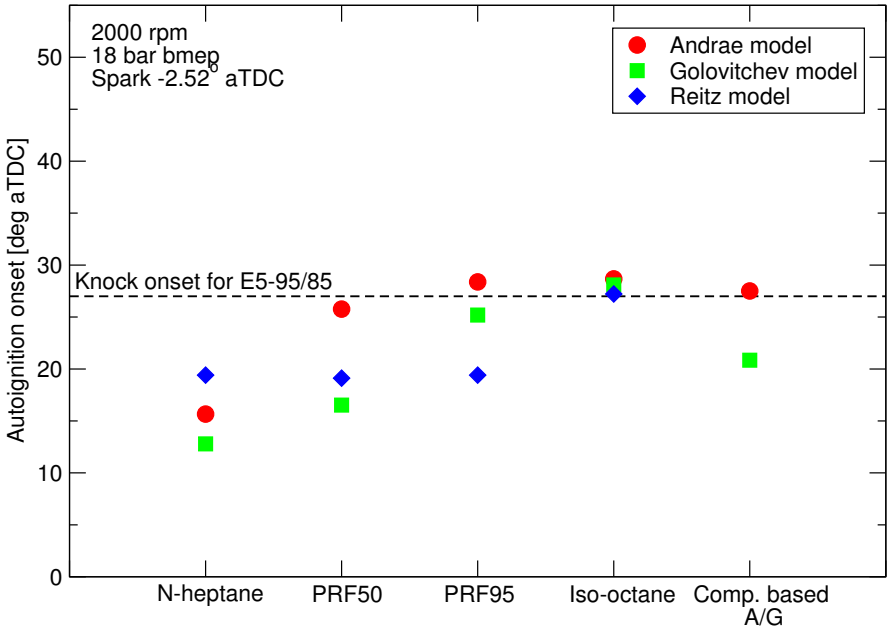

Figure 6.23: Autoignition onsets predicted for various fuels of different compositions at the same unburned $p-T$ conditions using three chemical mechanisms.

PRF95, the difference in autoignition onset is only 2.6° of crank angle. Although Golovitchev model which seemingly predicts a reasonable trend, predicts very early autoignition. The models produce similar trend as was seen in LUPOE2-D modelling in Chapter 5, see Figure 5.4. The Reitz model which was seen to have the most accurate PRF submodel does not seem to differentiate between various PRFs. Initially it was thought to be caused by the presence of burned residuals however, a simulation without residuals resulted in slightly late autoignition yet still very similar for all three PRFs.

Similar autoignition onsets of surrogates with slightly different compositions can be explained by the fact that the ignition delay times of different fuels tend to be of the same magnitude when the temperature and pressure is very high. It is tempting to borrow the concept from the Livengood-Wu integral that it is the small ignition delay times which contribute the most to the integral (cumulative induction time) and thus contribute towards the autoignition however, when chemical reaction kinetics is solved continuously for changing $p-T$ and composition, the autoignition onset is equally dependent on reaction rates at low and high $p-T$ conditions. The reason for similar autoignition onsets for surrogates of slightly different composition is that the pressure and temperature eventually reaches very high values.

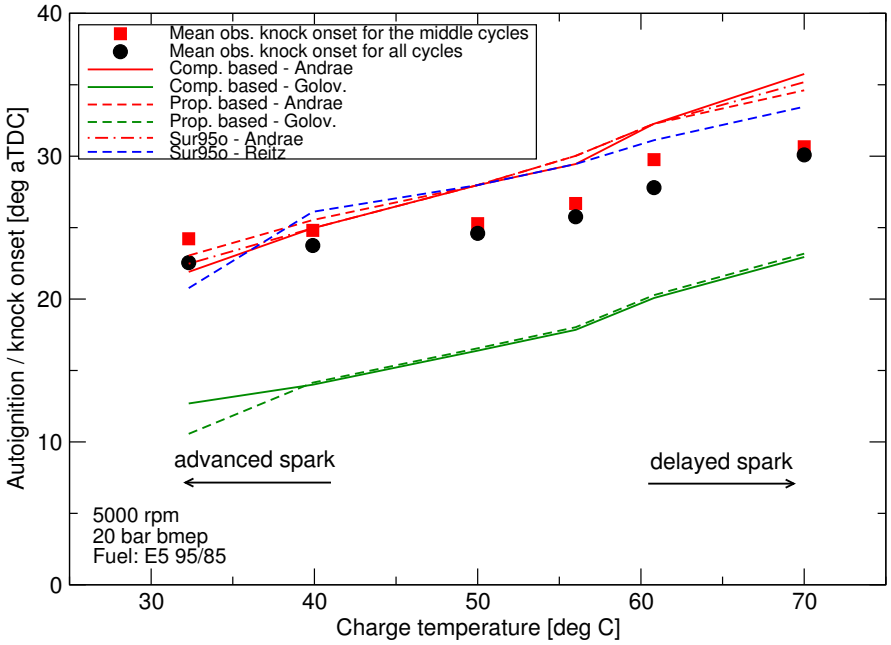

Figure 6.24: Comparison of predicted autoignition onsets to mean knock onsets for all the cycles and those of the selected middle cycles.

Similar results are obtained for the 3500 rpm and 5000 rpm cases however, results for the 5000 rpm case only have been presented in Figure 6.24; in this case the intake charge temperature and spark timing were varied. Since a greater percentage of cycles is knocking (i.e. 34 to 40% depending on operating conditions), the mean knock onset of the middle cycles is very close to the mean of all the cycles. All surrogates predict reasonably good autoignition onsets with the use of Andrae model. The Sur95o and Reitz model combination predicts well however, it still did not predict autoignition for surrogates containing cyclohexene. From these observations it can be concluded that the Andrae model makes more accurate predictions of the autoignition onsets and the trend as the spark timing and/or charge temperature is varied. For further simulations with cyclic variability in autoignition, the Andrae model with the properties based surrogate is employed.

6.7.4 Cyclic variability and autoignition

As it has been seen that quite accurate autoignition predictions can be achieved for the mean cycle, however, this is not sufficient when the optimum operating conditions are very close to the knocking conditions as is the case with most mod-

ern engines. In such cases, prediction of a knock-limited spark advance can be beneficial, particularly during the development phase. Prediction of autoignition for the full range of cyclic variability and some means of indicating the severity of predicted autoignition can indicate if an operating condition would be infeasible.

The issue of determining whether an autoignition event will lead to knock is of deflagration to detonation transition (DDT) which can be analysed by means of thermal explosion theories [Radulescu et al., 2013]. However, most of DDT models are based on a single step reaction or a double Arrhenius expression to account for the two stage heat release. However, such models are fuel specific; in addition, a spatial resolution of temperature gradient may also be required. Due to such limitations DDT modelling has not been attempted in this work, however, its inclusion will greatly enhance any future modelling work.

Presently, two knock indices are defined based on various observed relationships between knock intensity and engine operating conditions based on the analysis of knock in Di3 engine presented in Section 6.7.2. These can be summarised as following:

- The detonability of an autoigniting center increases with temperature and pressure.
- The knock intensity is higher when a large portion of charge is still unburned.
- The knock intensity at same $p-T$ conditions and fraction of unburned fuel yet different engine speeds will be lower at high speeds due to a rapid rate of expansion.

A phenomenological expression based on the above assumptions has been used for a qualitative appraisal of the knock intensity through a non-dimensional knock index, KI given as:

$$KI = \frac{60^6}{N}(1 - m_b)e^{(\frac{-6000}{T_u})} \tag{6.2}$$

An arbitrary, experience based threshold value of 5 for the knock index was found reasonable in the past for the LUPOE2-D engine which operates at much lower speeds (up to 3000 rpm when naturally aspirated), however, the knock index decreases drastically as the engine speed increases (see Figure 6.25b) and the threshold of 5 does not differentiate between possibly knocking and non-knocking cycles as the knock index becomes smaller than 5 for engine speeds

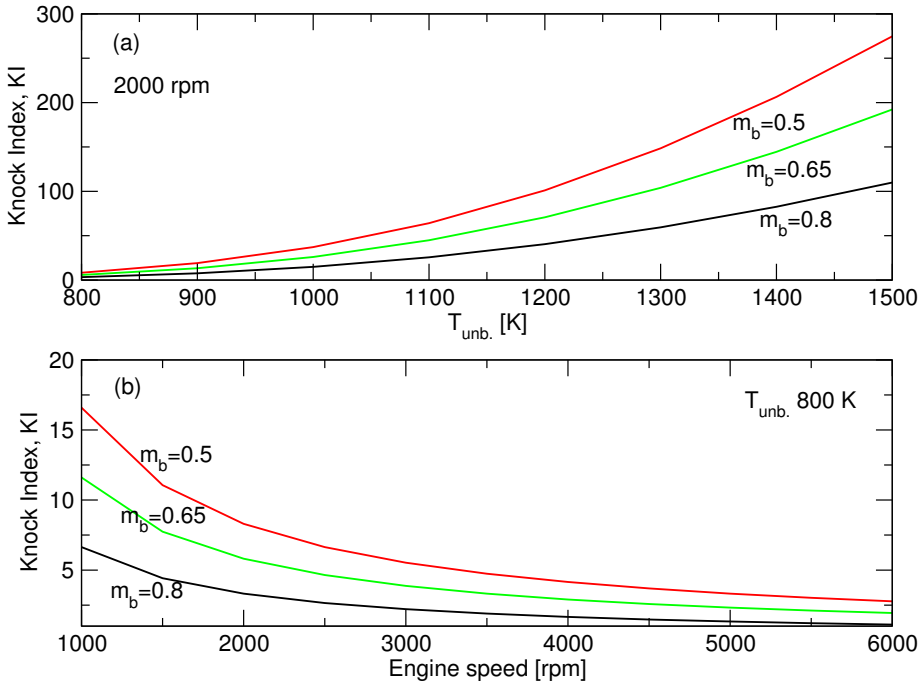

Figure 6.25: Variation in Knock Index, KI, for typical range of values of $T_{unb.}$, m_b and engine speed.

higher than about 2000 rpm, as was the case for Di3 engine. Another indicator was devised to attempt to quantify knock intensity by means of determining the pressure rise which may be caused due to the spontaneous ignition of the unburned charge using the relation,

$$\frac{\Delta P_{ai}}{P} = \left(\frac{1 - m_b}{m_b}\right)\left(\frac{P - P_{mot}}{P}\right) \tag{6.3}$$

A similar knock intensity can also be derived from the experimental knocking cycles as a ratio of the maximum amplitude of knock, P_{ampl}, to the pressure at the base of that knock, P i.e. pressure which would have existed, had the knock not taken place. This has been determined here as following:

$$\frac{\Delta P_{ai}}{P} = \frac{P_{ampl}}{P_{max} - P_{ampl}} \tag{6.4}$$

The pressure ratio, $\frac{\Delta P_{ai}}{P}$, and the corresponding knock onset times have been determined for all the experimental knocking cycles at the three studied conditions and the corresponding linear best fits have been presented in Figure 6.26. The knock intensity remains the same at the same load even when the engine speed has been increased from 2000 rpm to 5000 rpm. An increase in load (3500 rpm

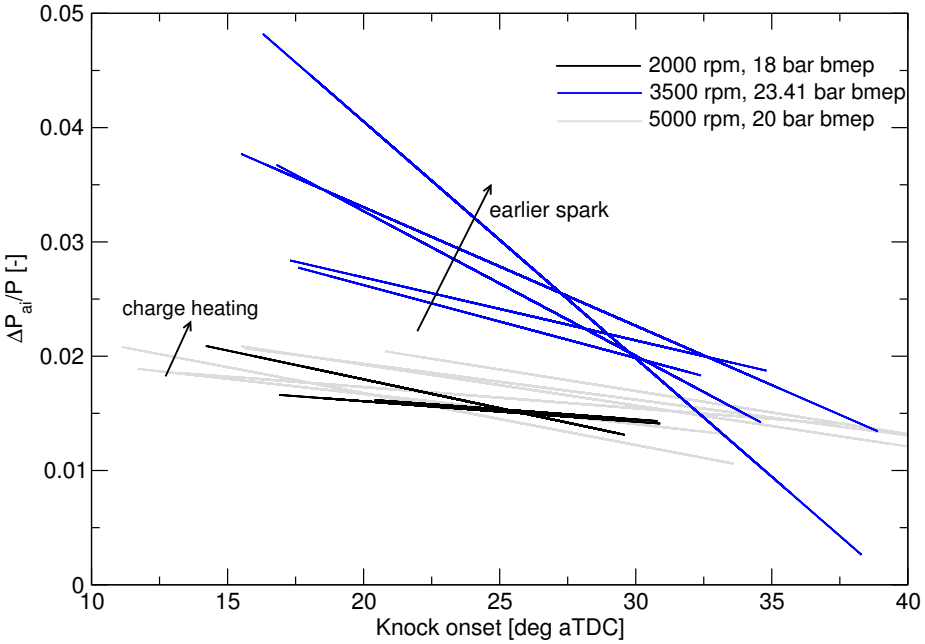

Figure 6.26: Effect of charge heating and spark advance on knock intensity, $\Delta P_{ai}/P$, at different speed and load conditions of the Di3 engine tests.

case) and further spark advance causes knock of greater amplitude. It can be seen that a minimum threshold of 0.015 can be chosen as a boundary between knocking and non-knocking cycles, N.B. experimental knocking and non-knocking cycles were initially differentiated based on a threshold set after a careful visual inspection of cycles at various conditions as described earlier. What Figure 6.26 shows is that such a visually determined threshold actually leads to a common criteria for different operating conditions. The pressure ratio determined experimentally and through modelling can then easily be compared to determine the percentage of knocking cycles.

Autoignition predictions were made coupled with cyclic variability and the pressure ratio, $\frac{\Delta P_{ai}}{P}$, was determined according to equation 6.3. This has been shown graphically in Figure 6.27 for a decremental spark advance at 2000 rpm. All the points in the figure represent predicted autoignition onsets which occur sooner as the spark is advanced and the knock intensity can be seen to increase as well. Equation 6.3 tends to overpredict knock amplitude as it assumes instantaneous consumption of the unburned charge and it is therefore that the calculated pressure ratios is higher than the experimental ones. An arbitrary threshold of 0.15 is chosen and the percentage of the cycles with the pressure ratio, $\frac{\Delta P_{ai}}{P}$, higher than 0.15 has been compared to the knocking frequency observed in the

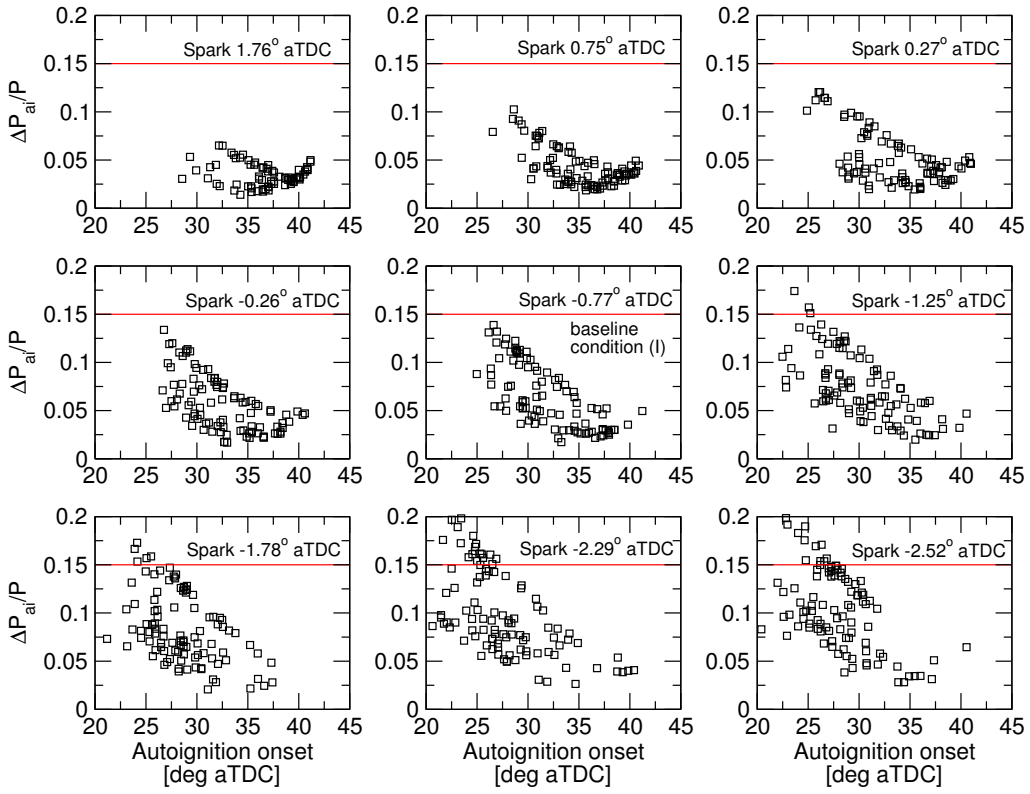

Figure 6.27: Plots showing P_{ai}/P vs. corresponding predicted autoignition onset for full range cycles at various spark timings.

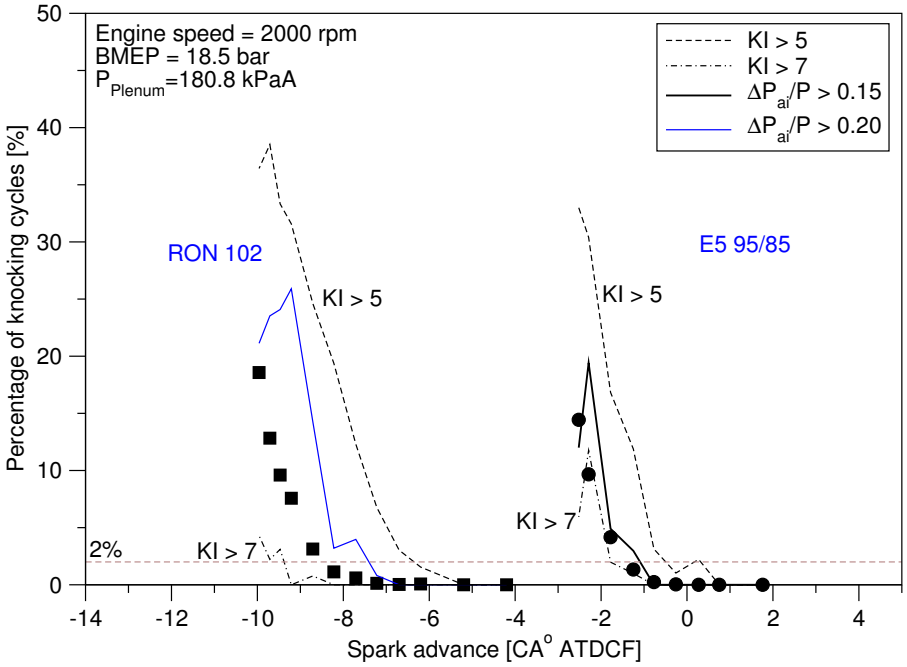

Figure 6.28: Comparison of computed knock frequencies based on various knock indices to the experimental knock frequency shown as symbols.

engine tests, see Figure 6.28. For experimental knocking cycles, pressure oscillation of magnitude of 1 bar was taken as an indicator of knock at 2000 rpm. A reasonably good agreement is obtained between the experimental and modelled frequency for the E5-95/85 fuel, however, the same knock index thresholds do not necessarily produce the correct knocking frequency trend for a RON 102 fuel. Both knock indices are imperfect and require an experience based threshold value to be chosen, however, even with these discrepancies, the spark timing at which knocking frequency become considerable i.e. about 2%, can be predicted with an accuracy of 2° of crank angle.

6.8 Fuel-engine interaction

Modelling of reactivity maps of various gasoline surrogates in Chapter 5 helped illustrate the interaction between fuel reactivity and the unburned zone $p - T$ history of the naturally aspirated LUPOE2-D. Figures 5.5 to 5.7 revealed that the two gasoline surrogates of the same RON as the target gasoline, showed different reactivity at the unburned zone $p - T$ conditions of LUPOE2-D and therefore autoignited at different times, both in experiments and in simulations. This

demonstrated the diminished relevance of RON to autoignition characterisation of fuels in engines different from the CFR engine. This notion is reinforced for a turbocharged engine such as the Di3 engine when the unburned zone $p-T$ histories at different conditions of the Di3 engine are plotted, see Figure 6.29 which also shows the τ_{ign} contour map computed for a five-component surrogate for the E5-95/85 gasoline, see the properties-based surrogate in Table 6.4. Two key observations can be made which are that the Di3 engine operates further afar from the $p-T$ trajectories of the RON and MON tests shown in Chapter 5. Owing to intercooling, the temperature at any given pressure is lower than that of the LUPOE2-D or the CFR engine. This results in a negative K-value at the three Di3 engine conditions as given by Equation 1.3; -1.22 for 2000 rpm and 30 bar bmep, -0.89 for 2000 rpm and 18 bar bmep and -0.72 for 5000 rpm and 20 bar bmep. The second observation is that the gasoline surrogate does not show a NTC behaviour and that for high enough pressures, i.e. higher than 40 bar, the autoignition delay times do not seem to be sensitive to pressure change for temperatures upto about 750 K. As a result, an increase in load as e.g. at 2000 rpm does not increase the predicted autoignition propensity, in fact autoignition is predicted at lower load as $p-T$ trajectory enters shorter ignition delay times when a higher pressure trajectory stays in longer ignition delay times.

An increase in engine speed increases the K-value, also shown by Kalghatgi [2014] and even though the $p-T$ trajectory passes through regions of short ignition delay times, the autoignition onset is much delayed as the times spent by the end gas at these short ignition delay times is smaller.

6.9 General discussion and conclusions

The quasi-dimensional thermodynamic modelling approach, although sensitive to the inaccuracies of underlying flow-field definition, predicts remarkably well the fuel burning rates for different operating conditions after optimisation of the turbulent length scale which governs the burning of eddies entrained into the flame brush. This results in a fast and reliable prediction of cylinder pressure when spark timing and intake charge temperature is varied without the need for any further optimisation of the length scale. The combustion models employed in this work have been applied to their limits in terms of the engine operating conditions. Past modelling studies at Leeds University using LUSIE/GT-LU of low speed simple geometry engines such as LUPOE, did not require a great deal of

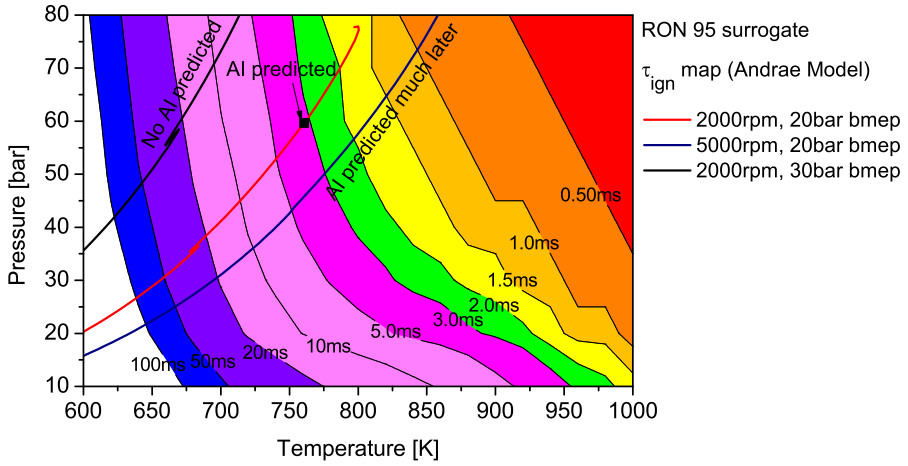

Figure 6.29: The τ_{ign} contour map of the RON 95 properties based surrogate of composition, iso-octane 28.42%/n-heptane 16.33%/toluene 33.07%/ethanol 5.35%/iso-butene 16.84% by volume, computed using the Andrae model. The cylinder pressure and unburned zone temperature histories of Di3 engine have been superimposed.

change in the constants as the models were very well correlated to such regimes. The application of these models to high specific weight, turbocharged engines by Conway [2013] and in this work reveals their weaknesses. It is thought that the main sources of inaccuracy are the turbulence and in particular its resolution to smaller eddies which interact with the flame and secondly possible deficiencies in the Zimont-Lipatnikov model at high pressures. Turbulence inaccuracies manifest as the wrong eddy size to be assumed to entrain the flame front. The size of these eddies determines the burn-up timescale and therefore the mass burning rate. The deficiencies in Zimont-Liptanikov model may possibly arise due to an excessive model sensitivity to smaller eddies increasing the burning rate due to an exaggerated mixing in the preheat zone. Besides the need for Taylor microscale adjustment, the modelling approach is able to predict combustion rates at different spark timings and charge temperature, remarkably well. This allowed further simulations on cyclic variability and autoignition.

The application of reduced chemical kinetic mechanisms results in superior autoignition predictions as demonstrated for three engine speeds and various spark timings and charge temperatures. For the same conditions, the previously used skeletal Keck model predicts earlier onsets, see Figure 6.30. Expectedly, the accuracy of autoignition predictions is greatly affected by the accuracy of chemi-

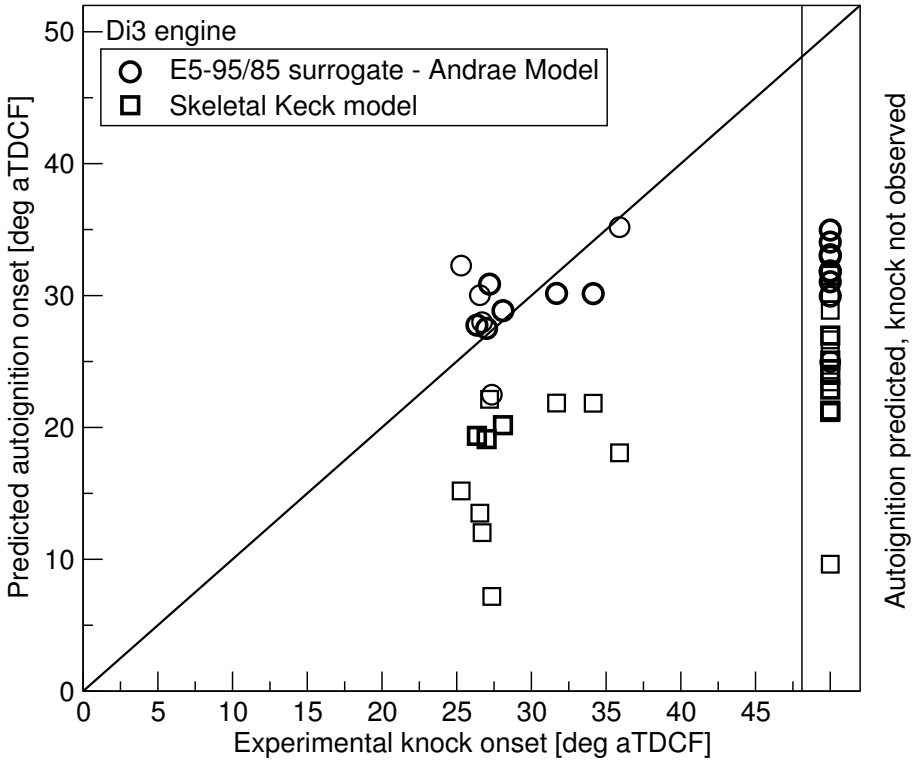

Figure 6.30: Autoignition onsets predicted using the properties based surrogate with Andrae model and the skeletal Keck model at Di3 engine speeds of 2000, 3500 and 5000 rpm.

cal kinetic mechanisms however, surrogates of slightly different compositions do not differ much and can be treated as gasoline surrogates as long as their composition is reflective of that of the gasoline. From modelling of LUPOE2-D it was found that a surrogate which is obtained by optimising its properties was not necessarily a true representative of the autoignition chemistry of gasoline and that is why the composition based surrogate was found to perform better. However, for the E5-95/85 gasoline the properties based surrogate performed slightly better than the composition based surrogate as the two were not starkly different.

It is pointed out that the correct fraction of toluene in the surrogate is more important than the rest as it is the less reactive surrogate components which determine the global reaction rate, (see Section 3.3.7), and since the fraction of ethanol, another high RON component, is mostly fixed around 5% by volume, it is toluene fraction which is crucial to the correct reproduction of the autoignition behaviour of gasoline. There is no sufficient agreement on the suitability of a representative olefin as pointed out earlier in Section 2.8. The three chemical kinetics mechanisms studied in this work do not have the same olefins and the Reitz model

which has one of the more suitable olefins, cyclohexene, predicts excessively long ignition delay times with it. It is for this reason that surrogates with olefin have not performed well in this work. For surrogates containing four components, iso-octane, n-hetpane, toluene and ethanol, the relative proportion of iso-octane and n-heptane can be adjusted to optimise RON and MON. However, the gasoline composition analyses presented in [Pera and Knop, 2012], [Bradley and Head, 2006] and [Mehl et al., 2011] reveal that the branched to straight chained alkanes ratio is approximately 3.5:1. This proportion is used in cases when the composition breakdown of alkanes in the target gasoline is unknown. Surrogates with PRF proportions different from this value do not necessarily produce very different autoignition onsets. The properties based surrogate for ULG90 has much higher toluene content than the gasoline and too low a cyclohexane fraction to cause longer delays, hence the greater observed difference between the simulated and actual autoignition onsets. The surrogates for E5-95/85 have similar toluene content and yet the PRFs and olefin in the surrogates are much different, the autoignition onsets are not so much. This is also partly because the Di3 engine is able to achieve much higher $p - T$ conditions at which the induction times of different fuels converge to similar values.

To conclude, attempting to optimise a gasoline surrogate with the given levels of accuracy in chemical kinetic mechanisms and octane number models, is rather an unproductive endeavour as slight differences in surrogate composition do not cause much difference in autoignition onsets. The chemical kinetics modelling of autoignition will in fact benefit the most through more fundamental research on the determination and improvement of chemical kinetics for surrogate components at high pressures. Studies into theoretical octane number models bear secondary importance as RON and MON have diminished relevance to modern turbocharged engines.

Chapter 7

Conclusions and future recommendations

7.1 Introduction

This work comprises development of a Fortran code for chemical kinetics calculations of autoignition in the end gas of SI engines (Chapter 2). The code was combined with an existing quasi-dimensional thermodynamic combustion modelling code named LUSIE. The resulting LUSIE code was then coupled with the commercial packages, GT-Power (Chapter 4). This allowed fast parametric simulations of the engine process allowing to study the effects of different operating conditions on combustion and autoignition. This was done to address the issue of predictability of autoignition event particularly in turbocharged, downsized SI engines (Chapters 5 & 6). The use of chemical kinetics also allowed a study of the interactions of key gasoline surrogate components, iso-octane, n-heptane, toluene and ethanol; during autoignition reactions (Chapter 3).

Key conclusions from the various studies done in this work have been summarised in the following section. Recommendations on the further improvement of the tools developed in this work and areas of study are presented as well.

7.2 Conclusions

- Reduced or semi-detailed chemical kinetic mechanisms such as the Andrae, Golovitchev and Reitz/MultiChem models, are an attractive choice for autoigntion modelling in quasi-dimensional engine combustion codes, as accurate predictions can be made in reasonable computational times. This also offers the benefit of modelling different fuel compositions without the need for any model adjustments.

- The accuracy of autoignition predictions in an engine is sensitive to the model accuracy. Since the unburned zone $p-T$ in an engine is continuously changing, the mechanism must predict the correction $p-T$ dependence of the various elementary reaction rates. The three mechanisms studied in this work tend to perform better mostly at high $p-T$ conditions than at lower values which results in deviation of the autoignition predictions from the observed knock onsets in the engines. The Andrae model seems to perform consistently well for various engine conditions and fuel blends.

- Autoigntion behaviour of gasoline can be simulated by using a surrogate as it reduces the compositional complexity of gasoline. As PRFs have zero sensitivity by definition, multi-component surrogates are therefore used which comprise of compounds which represent the major constituents of a gasoline, e.g. iso-octane, n-heptane, toluene, ethanol and some times an olefin. Through modelling in Chapter 3 of the oxidation pathways of the first four compounds, it was revealed that the four components affect each other differently. N-heptane which is the more reactive blend component breaks down sooner and acts as a source of active radicals for the otherwise less reactive blend components which breakdown faster in its presence, these are, toluene and ethanol. Iso-octane on the other hand seems to convert slower at any given temperature when it is blended with other components. This is possibly due to the scavenging of active radicals by other blend components. The radical scavenging effect of ethanol appears to be stronger than toluene as it causes even slower conversion of iso-octane and n-heptane as compared to toluene.

- The surrogate composition can be determined by optimising the key surrogate properties, e.g. octane numbers, to match those of the gasoline as demonstrated by Pera and Knop [2012]. However, such a 'properties-based'

approach does not guarantee the correct simulation of gasoline autoignition behaviour as shown through LUPOE2-D modelling in Chapter 5. This is because the empirical octane number models used to determine the blend ONs may be deficient, moreover, a single compounds belonging to a certain chemical group does not necessarily represent the autoignition behaviour of all the compounds in that group. E.g. the autoignition delay times of o-xylene are shorter than m- and p-xylene [Shen and Oehlschlaeger, 2009], and a typical gasoline may have various C_8H_{10} aromatics in amounts comparable to or more than toluene [Kalghatgi, 2014, p.35]. Autoignition modelling of LUPOE2-D and Di3 engine shows that it is more important for a surrogate to reflect the actual composition of the gasoline than to have the same RON and MON.

- Minute differences in the composition of different surrogates do not cause a considerable difference in the autoignition predictions because at high $p-T$ conditions, different fuels tend to have similar autoignition delay times, see, e.g. 2.13.

- The quasi-dimensional thermodynamic approach to combustion modelling was only able to predict the combustion rates for a turbocharged SI engine after an optimisation of the Taylor microscale of turbulence in the eddy burn-up model. This may have been caused by the oversimplifying assumption of homogeneous turbulence or possibly due to inaccuracies in resolving the large scale turbulence into small scale turbulence which in this work was done in GT-Power. This was made difficult due to the obscurity of the expressions used in GT-Power. The Zimont-Lipatnikov model which is used in this work to determine the turbulent entrainment velocity may also be exaggerating the effects of smaller eddies on the flamelets causing an overprediction of the entrainment, thereby, arising the need for a thicker flame to decrease the burning rate. This is why the chemical burn-up time was increased by increasing the Taylor microscale multiplier, C_λ, in GT-Power.

- The approach to modelling cyclic variability in combustion from [Aghdam et al., 2007], by perturbing u' and ϕ according to a Gaussian distribution of standard deviations of 12.5% and 5% resulted in wider scatter of maximum cylinder pressure as compared to the measurements. The model was also unable to capture fully the horizontal and vertical spread of maximum

cylinder pressures for middle cycles possibly due to the assumption that the underlying turbulence is homogeneous. A coupling with autoignition modelling demonstrated that with the inclusion of an empirical knock index, a reasonable estimate of the knocking frequency and knock-limited spark advance can be made.

7.3 Future recommendations

- **Turbulent burning velocity**: This work suggests that a dedicated investigative study of the various turbulent burning velocity expressions, including the Zimont-Lipatnikov model, is warranted at the high pressure and high turbulence conditions of modern engines. Recent optical measurements by Ling [2014] of combustion in boosted LUPOE2-D are expected to allow a greater understanding of combustion in such regimes and an associated numerical study of various combustion models will be greatly beneficial.

- **GT-LU**: In the current version of GT-LU, v7.3, the after-burning expressions in GT-Power are used which use an internally determined Taylor microscale. This restricts the indepth analysis of these quantities and an assessment of their accuracy. It is proposed that the expressions for the calculation of Taylor and Kolmogorov length scales as well as the after-burning expressions from LUSIE be incorporated into GT-LU in the user-template '$\mathrm{EngCylinder_{C}ombustion.F}$'. This will allow greater flexibility to study different turbulent burning velocity models.

- **ckinterp.f**: In this work, the Chemkin II interpreter, ckinterp.f, was employed for a preliminary parsing of the chemical kinetics mechanisms to generate a formatted text file, mechdata, containing the mechanism information. This dependency on ckinterp.f can be eliminated by developing a parser preferably in Python language which offers built-in functionalities well suited to an application as such.

- **Chemical kinetics solver**: The solver in its current state is able to perform a constant volume autoignition calculation in 10 s to 1 minute depending on the fuel and operating conditions[1]. A complete engine cycle simulation in

[1]For n-heptane air mixture of $\phi = 1$ at 40 bar and 800 K, the simulation time is 11 s for a Dual Core 3 GHz desktop machine.

GT-LU with autoignition calculations is of the order of upto one minute. These computational times, although not excessively long can be further improved through further optimisation of the code structure.

The capabilities of the code as a chemical kinetics research tool can be further enhanced by developing routines for sensitivity analyses.

- **Cyclic variability and autoignition modelling**: The current approach to modelling the cyclic variability in autoignition is rather computationally inefficient as in order to generate a statistically significant sample, roughly 100 to 150 engine cycles are simulated with cyclic variability. This results in computational times of a few hours for a single engine condition. It is proposed that perhaps only the limiting cases of autoignition in the slowest and fastest burning cycles can be modelled and based on the predicted knock intensity for the limiting cases, the overall knocking cycle frequency can be interpolated.

- **Empirical knock index**: The two knock indices employed in this work required different threshold values to distinguish knocking cycles from non-knocking for two different fuels. A more theoretical approach to the deflagration to detonation transition prediction may result in better prediction of knock as a consequence of kinetically predicted autoignition.

Appendix A

A.1 User guide (GT-LU v7.3)

GT-LU v7.3 is a collection of various user written models in the user-subroutine templates (Fortran files) which accompany GT-Power v7.3. These models and the user-subroutine template they are written in are presented in Table 1. The GT-LU user is provided the compiled GT-LU library named GTIusr73_dp.dll.

A.1.1 Migrating from a non-predictive GT-Power model to a predictive GT-LU model

A non-predictive engine model lacks necessary prerequisites to a completely predictive GT-LU engine model. These are:

1. A flow object to calculate the in-cylinder flow characteristics for the calculation of the turbulent flame speed or the read the turbulence information from an external file.

2. A flame object to specify the combustion chamber geometry which is used for the calculation of the flame surface area. The chamber geometry is specified by providing STL files for the piston fireface and the head. This geometry is not used in any of the flow or heat transfer calculations but it must tally with the geometry specified in EngCylGeom. It is also stressed that care should be taken while exporting the STL files from the CAD models

No.	Name of the user-subroutine template (FORTRAN filename)	Name of subroutine within the FORTRAN file)	Calling Template from GT-Power
1	EngCylFlow.F	TURBULENCE_USER reads external turbulence data from an ASCII file. Perturbs u' if cyclic variability is activated	From the flow object in EngCylFlow
2	EngCylCombSITurb.F	TURBFLSPEEDUSER Contains the turbulent flame speed expressions	From TRBSPEED in EngCylCombSITurb
3	EngCylinder_Combustion_Knock.F	KNOCKUSRMOD Contains the skeletal keck and the detailed chemical kinetics programme	From the 'knock model object in the 'advanced' tab in EngCylCombSITurb
4	XYFunction.F	XYGUNC_USER contains code for the perturbation of air to fuel ratio when cyclic variability is invoked	TimeFunction Function type is set to user and a UserModel is specified

Figure 1: Details of the GT-Power user templates which have been used to incorporate various LUSIE submodels.

such that there is no unit miss-match between GT-Power and the original CAD model.

The procedure to call various GT-LU models from UserModels in GT-Power is described below.

A.1.1.1 Burn rate

For burn rate calculations, an EngCylCombSITurb object is to be made. This object will require following other objects to be added to it in various of its tabs. These are:

Main: A flame object which has been described earlier.

LamSpeed: Appropriate fuel is selected for laminar flame speed calculation. Other setting are typically set to default.

TrbSpeed: A UserModel is to specified for turbulent flame speed model and turbulent flame speed model type is set to user.

Advanced: A UserModel can be specified to use the chemical kinetics solver subroutines of LUSIE to perform autoignition calculations. This will require the user to provide the ASCII mechanism file named mechdata.

Input type	Description	Integer Values
Integers	Turbulence source	[turb_source]
	Cyclic variability switch. 1 means ON, 2 means OFF	[CTC_switch]
Real Numbers	Not in use	1.0
Strings	Name of the turbulence text file	[turb_file]
RLT Variables	Cycle No. Case No. Flow Pressure	period icase dfmax dpmax
Plots (9 available)	-	-

Figure 2: Inputs to the UserModel for turbulent flame speed model.

A.1.1.2 UserModel for turbulent flame speed

The inputs to the UserModel for turbulent flame speed are provided in Table 2.

A.1.1.3 UserModel for autoignition

The inputs to the UserModel for autoignition predictions are provided in Table 3. The chemical kinetics mechanism parameters are provided in an ASCII file named 'mechdata' which should be placed in the same directory as the GT-Power model. The second integer value in the UserModel refers to the three mechanisms which have been provided, namely, 1. Andrae, 2. Golovitchev and 3. Reitz. More detail on the chemical kinetic mechanisms is presented in section 3. The composition of the surrogate needs to specified as molar fraction. The skeletal Keck model can be chosen by entering 1 as the 1^{st} integer however, the warranty for skeletal Keck model stands as it was for earlier GT-LU versions.

A.1.1.4 Flow object (EngCylFlow)

The flow object which is made using the EngCylFlow object is required to determine the in-cylinder turbulence which is an input to the flame development calculations in the EngCylCombSITurb. The in-cylinder turbulence may be calculated using the GT-Power's k-epsilon model or it may be read from an external turbulence text file. In case the internal k-epsilon model is to be used then all the settings in the flow object are to be left to default except the necessary geometry inputs in the geometry tab. In case external turbulence is to be read, a UserModel

Input type	Description	Integer Values
Integers	Detailed kinetics or skeletal keck model	1 for skeletal keck. 2 for detailed chemical kinetics
	Chemical kinetics model	1 – Andrae Model 2 – Golovitchev Model 3 – Reitz Model
	Cyclic variability switch. 1 mean ON	[CTC_switch]
Real Numbers	RON MON IOCTANE NHEPTANE TOLUENE ETOH MTOH IC4H8 DIB or IC8H16 BENZENE CYCHEXENE CYCHEXANE	95 85 0.343 0.158 0.423 0.076 0 0 0 0 0 0
Strings	Not in use	abc
RLT Variables	Cycle No. Case No. Flow Pressure	period icase dfmax dpmax
Plots (2 available)		

Figure 3: Inputs to the UserModel for autoignition subroutines.

object is to be made and called from the User Routine tab. Since GT-LU reads only the in-cylinder root-mean-square velocity (u') and the integral length scale (L), the flow model type needs to be set to use:trb. The inputs to the UserModel are provided in the following table.

A.1.2 External turbulence file format

An ASCII file containing the in-cylinder rms velocity and integral length scale in SI units must be provided in the same directory as the GT-Power model. The file should be structured such that the crank angles are in 1^{st} column, rms velocity in 2^{nd} and the integral length scale in 3^{rd} with spaces as delimiters. The format is shown below as an example.

-179.5	9.0344995323	0.0116081259
-178.5	8.9840826669	0.011727627
-177.5	8.9161701618	0.0118287205
...	...	...

The total number of data points (rows) must not be more than 2000. A file larger than 2000 rows would result in a run-time error. Although GT-LU flow subroutine is able to adjust for a non-zero TDCF but it is highly recommended to format/adjust the crank angle in the turbulence text file from either -360° to +360° or -180° to +180° depending on whether the engine is 4 stroke or 2 stroke, with TDCF at 0°.

A.1.3 Chemical kinetic mechanisms

GTLU v7.3 offers a provision of the use of three semi-detailed chemical kinetic mechanisms which have been discussed in Chapter 2. Each mechanism comprises of atleast four key surrogate compounds for gasoline namely, iso-octane, n-heptane, toluene and ethanol. Care should be taken while entering the composition of the surrogate in the real numbers tab of the userknock object (UserModel for autoignition). The RON and MON specified in the real numbers tab of the userknock are only needed by the older skeletal Keck model and are irrelevant to the detailed chemistry solver.

A.1.4 Cyclic variability in GT-LU

GT-LU cyclic variability is based on a Gaussian perturbation of the in-cylinder rms velocity and equivalence ratio from one cycle to another. Through research on the Leeds University ported engines and various other production engine, it has been found that a standard deviation of 12.5% for the rms velocity and a value of 5% for the equivalence ratio produces a realistic spread in the in-cylinder pressure about its mean value. The GT-LU cyclic variability is designed to work in such a way that when invoked, each case in the GT-Power model will run for a pre-set number of cycles. The in-cylinder pressures for only those cycles will be written which converge based on the minimization of the mass flow rates and pressures from one cycle to another cycle. The in-cylinder pressures are written in text files which are named in a format as e.g. CTC_CYLP01_1. Where CTC mean 'cycle to cycle', CYLP01 means 'cylinder number 1' and the integer at the end refers to the case number. The cyclic variability parameters are also written in a file named CTC_METRICS which contains the numbers of the cycles which are perturbed and also the multipliers for the rms velocity and the equivalence ratio. The metrics for each case are separated by a header.

A.1.4.1 Setting cyclic variability in a GT-LU model

The steps to setting up cyclic variability are given as follows:

STEP 1 (The cyclic variability switch) The universal integer switch for cyclic variability is to be entered in all four UserModels i.e. the userturbspeed, user-knock, the UserModel in the flow object and UserModel in the TimeFunction which is described subsequently. An integer value of 1 means that the cyclic variability is invoked and any value other than 1 would turn off the cyclic variability.

STEP 2 (Time function for air to fuel ratio) A 'TimeFunction' object needs to be created to invoke cyclic variability for the equivalence ratio or the air to fuel ratio. A UserModel is to be specified in user model object name whose inputs are provided in Table 4. All the other inputs in the TimeFunction should be set to 'ign'. When the TimeFunction is made correctly and called from 'Fuel Ratio' in the 'Rate' tab of the injectors, a run-time message should appear indicating:

GTLU v7.3 - AFR perturbed

Input type	Description	Integer Values
Integers	Cyclic variability switch. 1 mean ON, 2 mean it is OFF	[CTC_switch]
Real Numbers	Mean AFR or phi	A real number
Strings	Not in use	abc
RLT Variables	Cycle No. Case No. Flow Pressure	period icase dfmax dpmax
Plots (None available)	None	None

Figure 4: Inputs to the UserModel induce fluctuations in air to fuel ratio or equivalence ratio.

A.1.4.2 Convergence control and number of cycle to be ran

Since each case is to be run for a fixed number of cycles (normally 500 - 600) the automatic shut-off option is to be turned off in the Run Setup. When cyclic variability is invoked properly the user should see a message for the perturbation of the rms velocity (u′) and the equivalence ratio (phi) separately. The message will look like as following:

GTLU: Perturbing rms velocity

A.1.5 GT-LU outputs

All but one UserModel for GT-LU write results which can be seen in the GT-Post. These GT-Post results are only for cylinder no. 1. Other output files which GT-LU writes are given below.

KNOCK01: Contains autoignition related information. The integer at the end of the file name represents the case number. Autoignition information for all the cylinders is written in the same file. CTC_METRICS: Contains cyclic variability related parameters. CTC_CYLP01_1: Contains the in-cylinder pressures and cylinder temperatures for all the converged cycles.

References

Abdel-Gayed, R. G., Bradley, D., and Lawes, M. (1987). Turbulent burning velocities: A general correlation in terms of straining rates. *Proceedings of the Royal Society of London. A. Mathematical and Physical Sciences*, 414:389–413.

Abdi Aghdam, E. (2003). *Improvement and validation of a thermodynamic S.I. engine simulation code*. PhD thesis, School of Mechanical Engineering, The University of Leeds.

Aghdam, A. E., Burluka, A. A., Hattrell, T., Liu, K., Sheppard, C. G. W., Neumeister, J., and Crundwell, N. (2007). Study of cyclic variation in an SI engine using a quasi-dimensional combustion model. *Society of Automotive Engineers*, SAE Technical Paper 2007-01-0939.

Al-Mughanam, T. (2013). *Fundamental characterisation of the flame propagation of synthetic fuels*. PhD thesis, School of Mechanical Engineering, The University of Leeds.

Anderson, J. E., Kramer, U., Mueller, S. A., and Wallington, T. J. (2010). Octane numbers of ethanol and methanolgasoline blends estimated from molar concentrations. *Energy & Fuels*, 24(12):6576–6585.

Andrae, J. (2008). Development of a detailed kinetic model for gasoline surrogate fuels. *Fuel*, 87(1011):2013 – 2022.

Andrae, J., Bjrnbom, P., Cracknell, R., and Kalghatgi, G. (2007). Autoignition of toluene reference fuels at high pressures modeled with detailed chemical kinetics. *Combustion and Flame*, 149(12):2 – 24.

Andrae, J. and Head, R. (2009). HCCI experiments with gasoline surrogate fuels modeled by a semidetailed chemical kinetic model. *Combustion and Flame*, 156(4):842 – 851.

Annand, W. J. D. (1963). Heat transfer in the cylinders of reciprocating internal combustion engines. *Proceedings of the Institution of Mechanical Engineers*, 177(1):973–996.

Attard, W. P., Toulson, E., Watson, H., and Hamori, F. (2010). Abnormal combustion including mega knock in a 60turbocharged pfi engine. SAE Technical Paper 2010-01-1456.

Barnard, J. and Ibberson, V. (1965). The gaseous oxidation of toluene {II} the analytical results. *Combustion and Flame*, 9(2):149 – 157.

Bedoya, I. D., Cadavid, F., Saxena, S., Dibble, R., Aceves, S., and Flowers, D. (2012). A sequential chemical kinetics-cfd-chemical kinetics methodology to predict hcci combustion and main emissions.

Blizard, N. C. and Keck, J. C. (1974). Experimental and theoretical investigation of turbulent burning model for internal combustion engines. SAE Paper No. 740191.

Borghi, R. and Destriau, M. (1998). *Combustion and flames: chemical and physical principles*. Editions Technip, Paris, 1st edition.

Borghi, R., Mura, A., and Burluka, A. A. (2008). Turbulent premixed flames: Experimental studies over last decades. *Combustion phenomena*, CRC Press.

Bounaceur, R., Da Costa, I., Fournet, R., Billaud, F., and Battin-Leclerc, F. (2005). Experimental and modeling study of the oxidation of toluene. *International Journal of Chemical Kinetics*, 37(1):25–49.

Bozza, F., Siano, D., and Torella, E. (2009). Cycle-by-cycle analysis, knock modeling and spark-advance setting of a downsized spark-ignition turbocharged engine. *SAE Int. J. Engines*, 2:381–389.

Bradley, D. (1992). How fast can we burn? *Symposium (International) on Combustion*, 24(1):247 – 262. ¡ce:title¿Twenty-Fourth Symposium on Combustion¡/ce:title¿.

Bradley, D. and Head, R. (2006). Engine autoignition: The relationship between octane numbers and autoignition delay times. *Combustion and Flame*, 147(3):171 – 184.

Bradley, D., Lau, A. K. C., and Lawes, M. (1992). Flame stretch rate as a determinant of turbulent burning velocity. *Philosophical Transactions of the Royal Society : Physical and Engineering Sciences*, 338(1650):359–387.

Brezinsky, K. (1986). The high-temperature oxidation of aromatic hydrocarbons. *Progress in Energy and Combustion Science*, 12(1):1 – 24.

Burgoyne, J. H. (1940). The combustion of aromatic and alicyclic hydrocarbons. v. the products of combustion of benzene and its monoalkyl derivatives. *Proceedings of the Royal Society of London. Series A. Mathematical and Physical Sciences*, 175(963):539–563.

Burluka, A. (2010). Combustion in a spark ignition engine. *Handbook of Combustion*, Volume 3: Gaseous and Liquid Fuels.

Burluka, A., Hussin, A. E.-D., Ling, Z.-Y., and Sheppard, C. (2012). Effects of large-scale turbulence on cyclic variability in spark-ignition engine. *Experimental Thermal and Fluid Science*, 43(0):13 – 22. Seventh Mediterranean Combustion Symposium.

Burluka, A. A., Liu, K., Sheppard, C., Smallbone, A. J., and Woolley, R. (2004). The influence of simulated residual and no concentrations on knock onset for prfs and gasolines.

Cancino, L., Fikri, M., Oliveira, A., and Schulz, C. (2009). Autoignition of gasoline surrogate mixtures at intermediate temperatures and high pressures: Experimental and numerical approaches. *Proceedings of the Combustion Institute*, 32(1):501 – 508.

Cancino, L., Fikri, M., Oliveira, A., and Schulz, C. (2011). Ignition delay times of ethanol-containing multi-component gasoline surrogates: Shock-tube experiments and detailed modeling. *Fuel*, 90(3):1238 – 1244.

Cancino, L. R., Fikri, M., Oliveira, A. A. M., and Schulz, C. (2010). Measurement and chemical kinetics modeling of shock-induced ignition of ethanolair mixtures. *Energy & Fuels*, 24(5):2830–2840.

Cash, J. (1983). The integration of stiff initial value problems in odes using modified extended backward differentiation formulae. *Computers & Mathematics with Applications*, 9(5):645 – 657.

Chun, K. M., Heywood, J. B., and Keck, J. C. (1989). Prediction of knock occurrence in a spark-ignition engine. *Symposium (International) on Combustion*, 22(1):455 – 463.

Ciezki, H. and Adomeit, G. (1993). Shock-tube investigation of self-ignition of n-heptane-air mixtures under engine relevant conditions. *Combustion and Flame*, 93(4):421 – 433.

Conway, G. T. (2013). *Cyclic variability of flame propagation and autoignition in supercharged and naturally aspirated SI engines*. PhD thesis, School of Mechanical Engineering, The University of Leeds.

Cowart, J., Keck, J., Heywood, J., Westbrook, C., and Pitz, W. (1991). Engine knock predictions using a fully-detailed and a reduced chemical kinetic mechanism. *Symposium (International) on Combustion*, 23(1):1055 – 1062. ¡ce:title¿Twenty-Third Symposium (International) on Combustion¡/ce:title¿.

Cox, R. and Cole, J. (1985). Chemical aspects of the autoignition of hydrocarbonair mixtures. *Combustion and Flame*, 60(2):109 – 123.

Curran, H., Gaffuri, P., Pitz, W., and Westbrook, C. (1998a). A comprehensive modeling study of n-heptane oxidation. *Combustion and Flame*, 114(12):149 – 177.

Curran, H., Gaffuri, P., Pitz, W., and Westbrook, C. (2002). A comprehensive modeling study of iso-octane oxidation. *Combustion and Flame*, 129(3):253 – 280.

Curran, H., Pitz, W., Westbrook, C., Callahan, G., and Dryer, F. (1998b). Oxidation of automotive primary reference fuels at elevated pressures. *Symposium (International) on Combustion*, 27(1):379 – 387. Twenty-Seventh Sysposium (International) on Combustion Volume One.

Dahnz, C. and Spicher, U. (2010). Irregular combustion in supercharged spark ignition engines pre-ignition and other phenomena. *International Journal of Engine Research*, 11(6):485–498.

Damkohler, G. (1940). Der einfluss der turbulenz auf die flammengeschwindigkeit in gasgemischen. *Z Elecktrochem*, 46:601.

Darrieus, G. (1938). Propagation d'un front de flamme: Assai de théorie des vitesses anomalies de déflagration par developpment spantané de la turbulencel. *Presented at the 6th int. Cong. Appl. Mech.*, Paris.

Davidson, D., Gauthier, B., and Hanson, R. (2005). Shock tube ignition measurements of iso-octane/air and toluene/air at high pressures. *Proceedings of the Combustion Institute*, 30(1):1175 – 1182.

Douaud, A. M. and Eyzat, P. (1978). Four-octane-number method for predicting the anti-knock behaviour of fuels and engines. *Society of Automotive Engineers*, SAE Technical Paper 780080.

Farrell, J. and Bunting, B. (2006). Fuel composition effects at constant RON and MON in an HCCI engine operated with negative valve overlap. SAE Technical Paper 2006-01-3275.

Fernandes, R. (2010). Combustion chemistry. *Handbook of Combustion*, Volume 3: Gaseous and Liquid Fuels.

Fieweger, K., Blumenthal, R., and Adomeit, G. (1997). Self-ignition of s.i. engine model fuels: A shock tube investigation at high pressure. *Combustion and Flame*, 109(4):599 – 619.

Fikri, M., Herzler, J., Starke, R., Schulz, C., Roth, P., and Kalghatgi, G. (2008). Autoignition of gasoline surrogates mixtures at intermediate temperatures and high pressures. *Combustion and Flame*, 152(12):276 – 281.

Foong, T. M., Morganti, K. J., Brear, M. J., da Silva, G., Yang, Y., and Dryer, F. L. (2014). The octane numbers of ethanol blended with gasoline and its surrogates. *Fuel*, 115(0):727 – 739.

Gardiner, W. (2000). *Gas-Phase Combustion Chemistry*. Springer-Verlag New York, Inc.

Gauthier, B., Davidson, D., and Hanson, R. (2004). Shock tube determination of ignition delay times in full-blend and surrogate fuel mixtures. *Combustion and Flame*, 139(4):300 – 311.

Ghojel, J. (2010). Review of the development and applications of the wiebe function: A tribute to the contribution of ivan wiebe to engine research. *International Journal of Engine Research*, 11(4):297–312. cited By (since 1996)14.

Ghosh, P., Hickey, K., and Jaffe, S. (2006). Development of a detailed gasoline composition-based octane model. *Industrial & Engineering Chemistry Research*, 45(1):337–345.

Gillespie, L., Lawes, M., Sheppard, C. G. W., and Woolley, R. (2000). Aspects of laminar and turbulent burning velocity relevant to SI engines. SAE Technical Paper 2000-01-0192.

Gordon, S. and BcBride, B. (1971). *Computer Program for Calculation of Complex Chemical Equilibrium Compositions, Rocket Performance, Incident and Reflected Shocks and Chapman-Jouguet Detonations, NASA SP-273*.

Griffiths, J. (1995). Reduced kinetic models and their application to practical combustion systems. *Progress in Energy and Combustion Science*, 21(1):25 – 107.

Griffiths, J. and Mohamed, C. (1997). Chapter 6: Experimental and numerical studies of oxidation chemistry and spontaneous ignition phenomena. In Pilling, M., editor, *Low-Temperature Combustion and Autoignition*, volume 35 of *Comprehensive Chemical Kinetics*, pages 545 – 660. Elsevier.

Griffiths, J. F. and Barnard, J. A. (1995). *Flame and Combustion*. Blackie Academic & Professional.

Halstead, M., Kirsch, L., and Quinn, C. (1977). The autoignition of hydrocarbon fuels at high temperatures and pressuresfitting of a mathematical model. *Combustion and Flame*, 30(0):45 – 60.

Han, D., Han, S.-K., Han, B.-H., and Kim, W.-T. (2007). Development of 2.0l turbocharged disi engine for downsizing application. SAE Technical Paper 2007-01-0259.

Hartmann, M., Gushterova, I., Fikri, M., Schulz, C., Schiel, R., and Maas, U. (2011). Auto-ignition of toluene-doped n-heptane and iso-octane/air mixtures: High-pressure shock-tube experiments and kinetics modeling. *Combustion and Flame*, 158(1):172 – 178.

Hattrell, T. (2007). *A computational and experimental study of spark ignition combustion*. PhD thesis, School of Mechanical Engineering, The University of Leeds.

Hattrell, T., Sheppard, C. G. W., Burluka, A. A., Neumeister, J., and Cairns, A. (2006). Burn rate implications of alternative knock reduction strategies for turbocharged si engines. SAE Technical Paper 2006-01-1110.

H.E.Avery (1974). *Basic Reaction Kinetics and Mechanisms*. MacMillan Eduation Ltd.

Heywood, J. (1988). *Internal combustion engine fundamentals*. McGraw-Hill, Inc.

Hinze, P. C. and Miles, P. C. (1999). Quantitative measurements of residual and fresh charge mixing in a modern si engine using spontaneous raman scattering. SAE Technical Paper 1999-01-1106.

Hoepke, B., Jannsen, S., Kasseris, E., and Cheng, W. K. (2012). EGR effects on boosted SI engine operation and knock integral correlation. *SAE Int. J. Engines*, 5:547–559.

Hu, H. and Keck, J. (1987). Autoignition of adiabatically compressed combustible gas mixtures. SAE Technical Paper 872110.

Huang, C., Golovitchev, V., and Lipatnikov, A. (2010). Chemical model of gasoline-ethanol blends for internal combustion engine applications. SAE Technical Paper 2010-01-0543.

Hussin, A. E. (2012). *New and Renewable Energy: Renewable Fuels in Internal Combustion Engines*. PhD thesis, School of Mechanical Engineering, The University of Leeds.

Hynes, J. (1986). *A Computational and Experimental Study of Spark Ignition Combustion*. PhD thesis, Department of Mechanical Engineering, The University of Leeds.

Jia, M. and Xie, M. (2006). A chemical kinetics model of iso-octane oxidation for {HCCI} engines. *Fuel*, 85(1718):2593 – 2604.

Johansson, B. (1996). Cycle to cycle variations in s.i. engines - the effects of fluid flow and gas composition in the vicinity of the spark plug on early combustion. SAE Technical Paper 962084.

Kalghatgi, G. (2001). Fuel anti-knock quality - part i. engine studies. SAE Technical Paper 2001-01-3584.

Kalghatgi, G. (2014). *Fuel/Engine Interactions*. SAE International. DOI 10.4271/R-409.

Knop, V., Loos, M., Pera, C., and Jeuland, N. (2014). A linear-by-mole blending rule for octane numbers of n-heptane/iso-octane/toluene mixtures. *Fuel*, 115(0):666 – 673.

Knop, V., Pera, C., and Duffour, F. (2013). Validation of a ternary gasoline surrogate in a CAI engine. *Combustion and Flame*, 160(10):2067 – 2082.

Knox, J. (1967). *Photochemistry and Reaction Kinetics*. Cambridge University Press.

Koert, D., Miller, D., and Cernansky, N. (1994). Experimental studies of propane oxidation through the negative temperature coefficient region at 10 and 15 atmospheres. *Combustion and Flame*, 96(12):34 – 49.

Kolaitis, D. I. and Founti, M. A. (2010). Cool flames. *Handbook of Combustion*, Volume 1: Fundamentals and Safety (2010) WILEY-VCH Verlag GmbH & Co. KGaA.

Kolmogorov, A. N. (1941). English translation (1991): The local structure of turbulence in incompressible viscous fluid for very large reynolds numbers. *Proceedings: Mathematical and Physical Sciences*, 434(1890):pp. 9–13.

Kukkadapu, G., Kumar, K., Sung, C.-J., Mehl, M., and Pitz, W. J. (2013). Autoignition of gasoline and its surrogates in a rapid compression machine. *Proceedings of the Combustion Institute*, 34(1):345 – 352.

Landau, L. D. (1944). On the theory of slow combustion. *Acta Physiochim URSS*, 90:77–85.

Lenhert, D. B., Miller, D. L., Cernansky, N. P., and Owens, K. G. (2009). The oxidation of a gasoline surrogate in the negative temperature coefficient region. *Combustion and Flame*, 156(3):549 – 564.

Leppard, W. R. (1990). The chemical origin of fuel octane sensitivity.

Lewis, B. and von Elbe, G. (1987). *Combustion Flames and Explosions of Gases*. Harcourt Brace Jovanovich, Publishers.

Lindemann, F. A., Arrhenius, S., Langmuir, I., Dhar, N. R., Perrin, J., and McC. Lewis, W. C. (1922). Discussion on "the radiation theory of chemical action". *Trans. Faraday Soc.*, 17:598–606.

Ling, Z. (2011). *Characterization of Knock and Autoignition in a Boosted Spark Ignition Engine*. PhD thesis, Transfer Report. Department of Mechanical Engineering, The University of Leeds.

Ling, Z. (2014). *Characterization of Knock and Autoignition in a Boosted Spark Ignition Engine*. PhD thesis, Department of Mechanical Engineering, The University of Leeds - *in preparation*.

Linse, D., Hasse, C., and Durst, B. (2009). An experimental and numerical investigation of turbulent flame propagation and flame structure in a turbo-charged direct injection gasoline engine. *Combustion Theory and Modelling*, 13(1):167–188.

Lipatnikov, A. and Chomiak, J. (1997). A simple model of unsteady turbulent flame propagation. *SAE Technical Paper*, (972993).

Lipatnikov, A. N. (2013). *Fundamentals of Premixed Turbulent Combustion*. CRC Press, Boca Raton, Florida, 1st edition.

Lipatnikov, A. N. and Chomiak, J. (1998). Randomness of flame kernel development in turbulent gas mixture. SAE Technical Paper 982617.

Lipatnikov, A. N. and Chomiak, J. (2000). Modeling of pressure and non-stationary effects in spark-ignition engine combustion: A comparison of different approaches. *Society of Automotive Engineers*, SAE Technical Paper 2000-01-2034.

Lipatnikov, A. N. and Chomiak, J. (2002). Turbulent flame speed and thickness: phenomenology, evaluation and application in multi-dimensional applications. *Progress in Energy and Combustion Science*, 28:1–74.

Liu, C. and Karim, G. A. (2008). A 3d-simulation with detailed chemical kinetics of combustion and quenching in an hcci engine.

Liu, K. (2004). *LUSIE Manual*. PhD thesis, School of Mechanical Engineering, The University of Leeds.

Liu, K., Burluka, A., and Sheppard, C. (2013). Turbulent flame and mass burning rate in a spark ignition engine. *Fuel*, 107(0):202 – 208.

Livengood, J. and Wu, P. (1955). Correlation of autoignition phenomena in internal combustion engines and rapid compression machines. *Symposium (International) on Combustion*, 5(1):347 – 356.

Lumley, J. (1999). *Engines An Introduction*. Cambridge University Press.

Lumsden, G., OudeNijeweme, D., Fraser, N., and Blaxill, H. (2009). Development of a turbocharged direct injection downsizing demonstrator engine. *SAE Int. J. Engines*, 2:1420–1432.

Machrafi, H., Cavadias, S., and Amouroux, J. (2009). The development and experimental validation of a reduced ternary kinetic mechanism for the auto-ignition at {HCCI} conditions, proposing a global reaction path for ternary gasoline surrogates. *Fuel Processing Technology*, 90(2):247 – 263.

Marinov, N. M. (1999). A detailed chemical kinetic model for high temperature ethanol oxidation. *International Journal of Chemical Kinetics*, 31(3):183–220.

Matalon, M. (2009). Flame dynamics. *Proceedings of the Combustion Institute*, 32(1):57 – 82.

Matekunas, F. A. (1983). Modes and measures of cyclic combustion variability. SAE Technical Paper 83033.

Mehl, M., Chen, J. Y., Pitz, W. J., Sarathy, S. M., and Westbrook, C. K. (2011). An approach for formulating surrogates for gasoline with application toward a reduced surrogate mechanism for cfd engine modeling. *Energy & Fuels*, 25(11):5215–5223.

Mehl, M., Faravelli, T., Ranzi, E., Giavazzi, F., Scorletti, P., Terna, D., D'Errico, G., Lucchini, T., and Onorati, A. (2005). Kinetic modelling study of octane number and sensitivity of hydrocarbon mixtures in CFR engines. SAE Technical Paper 2005-24-077.

Metcalfe, W. K., Pitz, W. J., Curran, H. J., Simmie, J. M., and Westbrook, C. K. (2007). The development of a detailed chemical kinetic mechanism for diisobutylene and comparison to shock tube ignition times. *Proceedings of the Combustion Institute*, 31(1):377 – 384.

Metghalchi, M. and Keck, J. C. (1982). Burning velocities of mixtures of air with methanol, isooctane, and indolene at high pressure and temperature. *Combustion and Flame*, 48:191–210.

Miller, J. A., Pilling, M. J., and Troe, J. (2005). Unravelling combustion mechanisms through a quantitative understanding of elementary reactions. *Proceedings of the Combustion Institute*, 30(1):43 – 88.

Morel, T., Flemming, M., and LaPointe, L. (1990). Characterization of manifold dynamics in the chrysler 2.2 s.i. engine by measurement and simulation. *SAE Technical Paper*, (900679).

Morel, T. and Keribar, R. (1985). A model for predicting spatially and time resolved convective heat transfer in bowl-in-piston combustion chambers. *SAE Technical Paper*, (850204).

Morel, T. and Mansour, N. (1982). Modeling of turbulence in internal combustion engines. *SAE Technical Paper*, (820040).

Morgan, N., Smallbone, A., Bhave, A., Kraft, M., Cracknell, R., and Kalghatgi, G. (2010). Mapping surrogate gasoline compositions into ron/mon space. *Combustion and Flame*, 157(6):1122 – 1131.

Neumeister, J. and Oudenijeweme, D. Mahle powertrain Ltd. Personal communication.

Nishiwaki, K., Yoshihara, Y., and Saijyo, K. (2000). Numerical analysis of the location of knock initiation in S. I. engines. SAE Technical Paper 2000-01-1897.

Ogink, R. (2004). *Computer Modelling of HCCI Combustion*. PhD thesis, Division of Thermo and Fluid Dynamics, Chalmers University of Technology.

Ogink, R. and Golovitchev, V. (2002). Gasoline HCCI modeling: An engine cycle simulation code with a multi-zone combustion model. SAE Technical Paper 2002-01-1745.

Ozdor, N., Dulger, M., and Sher, E. (1994). Cyclic variability in spark ignition engines a literature survey. SAE Technical Paper 940987.

Pera, C. and Knop, V. (2012). Methodology to define gasoline surrogates dedicated to auto-ignition in engines. *Fuel*, 96(1):59–69.

Peters, N. (1988). Laminar flamelet concepts in turbulent combustion. *Symposium (International) on Combustion*, 21(1):1231 – 1250. Twenty-First Symposuim (International on Combustion).

Piperel, A., Montagne, X., and Dagaut, P. (2007). Hcci engine combustion control using egr : Gas composition evolution and consequences on combustion processes. SAE Technical Paper 2007-24-0087.

R. G. Abdel-Gayed, K. J. A.-K. and Bradley, D. (1984). Turbulent burning velocities and flame straining in explosions. *Proceedings of the Royal Society of London. Series A, Mathematical and Physical Sciences*, 391(1801):393–414.

Ra, Y. and Reitz, R. D. (2008). A reduced chemical kinetic model for {IC} engine combustion simulations with primary reference fuels. *Combustion and Flame*, 155(4):713 – 738.

Ra, Y. and Reitz, R. D. (2011). A combustion model for ic engine combustion simulations with multi-component fuels. *Combustion and Flame*, 158(1):69 – 90.

Radulescu, M. I., Sharpe, G. J., and Bradley, D. (2013). A universal parameter quantifying explosion hazards, detonability and hot spot formation: The χ number. *Proc. of the Seventh International Seminar on Fire & Explosion Hazards (ISFEH7)*.

Reynolds, W. (1980). Modeling of fluid motions in engines: An introductory overview. *Symposium on Combustion Modeling in Reciprocating Engines*, pages 131–155.

Roberts, P. (2010). *Fuel and residual effects in spark ignition and homogeneous charge compression ignition engines*. PhD thesis, School of Mechanical Engineering, The University of Leeds.

Roberts, P. and Sheppard, C. (2013). The influence of residual gas NO content on knock onset of iso-octane, PRF, TRF and ULG mixtures in SI engines. *SAE Int. J. Engines*, 6:2028–2043.

Roubaud, A., Minetti, R., and Sochet, L. (2000). Oxidation and combustion of low alkylbenzenes at high pressure: comparative reactivity and auto-ignition. *Combustion and Flame*, 121(3):535 – 541.

Sapsford, S., Rischards, V., Amlee, D., Morel, T., and Chappell, M. (1992). Exhaust system evaluation and design by non-linear modeling. *SAE Technical Paper*, (920686).

Searby, G. (2008). Instability phenomena during flame propagation. *Combustion phenomena*, CRC Press.

Shen, H., Hinze, P. C., and Heywood, J. B. (1996). A study of cycle-to-cycle variations in si engines using a modified quasi-dimensional model. SAE Technical Paper 961187.

Shen, H.-P. S. and Oehlschlaeger, M. A. (2009). The autoignition of c8h10 aromatics at moderate temperatures and elevated pressures. *Combustion and Flame*, 156(5):1053 – 1062.

Shen, H.-P. S., Vanderover, J., and Oehlschlaeger, M. A. (2009). A shock tube study of the auto-ignition of toluene/air mixtures at high pressures. *Proceedings of the Combustion Institute*, 32(1):165 – 172.

Sileghem, L., Alekseev, V., Vancoillie, J., Geem, K. V., Nilsson, E., Verhelst, S., and Konnov, A. (2013). Laminar burning velocity of gasoline and the gasoline surrogate components iso-octane, n-heptane and toluene. *Fuel*, 112(0):355 – 365.

Silke, E. J., Curran, H. J., and Simmie, J. M. (2005). The influence of fuel structure on combustion as demonstrated by the isomers of heptane: a rapid compression machine study. *Proceedings of the Combustion Institute*, 30(2):2639 – 2647.

Silvano, P. (2013). *MSc project*. PhD thesis, School of Mechanical Engineering, The University of Leeds.

Smallbone, A. (2004). *Fuel and residual effects on knock onset in spark ignition engines*. PhD thesis, School of Mechanical Engineering, The University of Leeds.

Sokolik, A. (1960). *English translation (Jerusalem, 1963): Self-Ignition, flame and detonation in gases*. USSR Academy of Sciences-Institute of Chemical Physics.

Stenls, O., Gogan, A., Egnell, R., Sundn, B., and Mauss, F. (2002). The influence of nitric oxide on the occurrence of autoignition in the end gas of spark ignition engines. SAE Technical Paper 2002-01-2699.

Stewart, P., Larson, C., and Golden, D. (1989). Pressure and temperature dependence of reactions proceeding via a bound complex. 2. application to $2CH_3 \longrightarrow C_2H_5 + H$. *Combustion and Flame*, 75(1):25 – 31.

Stone, R. (1999). *Introduction to Internal Combustion Engines*. MACMILLAN Press Ltd.

Takashi, H. and Kimitoshi, T. (2006). Laminar flame speeds of ethanol, n-heptane, iso-octane air mixtures. *2006 Fisita Conference, 3-7th April, 2006, Detroit*.

Taylor, A. M. (2008). Science review of internal combustion engines. *Energy Policy*, 36(12):4657 – 4667. Foresight Sustainable Energy Management and the Built Environment Project.

Taylor, G. I. (1915). Eddy motion in the atmosphere. *Philosophical Transactions of the Royal Society of London. Series A, Containing Papers of a Mathematical or Physical Character*, 215(523-537):1–26.

Tennekes, H. and Lumley, J. L. (1972). *A First Course in Turbulence*. MIT, Cambridge, MA, 1st edition.

Troe, J. (1974). Fall-off curves of unimolecular reactions. *Berichte der Bunsengesellschaft fr physikalische Chemie*, 78(5):478–488.

Vanhove, G., Petit, G., and Minetti, R. (2006). Experimental study of the kinetic interactions in the low-temperature autoignition of hydrocarbon binary mixtures and a surrogate fuel. *Combustion and Flame*, 145(3):521 – 532.

Wang, Y., Yao, M., and Zheng, Z. (2013). A semi-detailed chemical kinetic model of a gasoline surrogate fuel for internal combustion engine applications. *Fuel*, 113(0):347 – 356.

Warnatz, J., Maas, U., and Dibble, R. W. (2001). *Combustion: Physical and chemical fundamentals, modeling and simulation, experiments, pollutant formation*. Springer, Heidelberg, 3rd edition.

Westbrook, C. K., Pitz, W. J., and Leppard, W. R. (1991). The autoignition chemistry of paraffinic fuels and pro-knock and anti-knock additives: A detailed chemical kinetic study. SAE Technical Paper 912314.

Williams, F. (1985). *Combustion Theory*. Addison-Wesley, California.

Woschni, G. (1967). A universally applicable equation for the instantaneous heat transfer coefficient in the internal combustion engine. SAE Technical Paper 670931.

Zhen, X., Wang, Y., and Zhu, Y. (2013). Study of knock in a high compression ratio {SI} methanol engine using {LES} with detailed chemical kinetics. *Energy Conversion and Management*, 75(0):523 – 531.

Zhong, B.-J. and Zheng, D. (2014). A chemical mechanism for ignition and oxidation of multi-component gasoline surrogate fuels. *Fuel*, 128(0):458 – 466.

Zimont, V. (1979). Theory of turbulent combustion of a homogeneous fuel mixture at high reynolds numbers. *Combustion, Explosion and Shock Waves*, 15(3):305–311.